A FLUID INCLUSION AND TRACE ELEMENT GEOCHEMICAL STUDY OF THE GRANITE-HOSTED, ST. LAWRENCE FLUORSPAR DEPOSITS AND RELATED HOST ROCKS

CENTRE FOR NEWFOUNDLAND STUDIES

TOTAL OF 10 PAGES ONLY
MAY BE XEROXED

(Without Author's Permission)

CELESTINE JAMES COLLINS

National Library of Canada
Acquisitions and Bibliographic Services Branch
395 Wellington Street
Ottawa Ontario
K1A 0N4

Bibliothèque nationale du Canada
Direction des acquisitions et des services bibliographiques
395 rue Wellington
Ottawa Ontario
K1A 0N4

NOTICE

The quality of this microform is heavily dependent upon the quality of the original thesis submitted for microfilming. Every effort has been made to ensure the highest quality of reproduction possible.

If pages are missing, contact the university which granted the degree.

Some pages may have indistinct print especially if the original pages were typed with a poor typewriter ribbon or if the university sent us an inferior photocopy.

Reproduction in full or in part of this microform is governed by the Canadian Copyright Act, R.S.C. 1970, c. C-30, and subsequent amendments.

AVIS

La qualité de cette microforme dépend grandement de la qualité de la thèse soumise au microfilmage. Nous avons tout fait pour assurer une qualité supérieure de reproduction.

S'il manque des pages, veuillez communiquer avec l'université qui a conféré le grade.

La qualité d'impression de certaines pages peut laisser à désirer, surtout si les pages originales ont été dactylographiées à l'aide d'un ruban usé ou si l'université nous a fait parvenir une photocopie de qualité inférieure.

La reproduction, même partielle, de cette microforme est soumise à la Loi canadienne sur le droit d'auteur, SRC 1970, c. C-30, et ses amendements subséquents.

Canada

A Fluid Inclusion and Trace Element Geochemical Study of the Granite-hosted, St. Lawrence Fluorspar Deposits and Related Host Rocks

by

Celestine James Collins, B.Sc./B.Ed.

A thesis submitted to the School of Graduate Studies

in partial fulfillment of the requirements for

the degree of

Master of Science

Department of Earth Sciences

Memorial University of Newfoundland

August 1992

St. John's Newfoundland

Abstract

The St. Lawrence Fluorspar Deposits, on Newfoundland's south coast, are vein-type deposits hosted by and genetically related to the Devonian St. Lawrence Granite. The alkaline to peralkaline granite was emplaced to high crustal levels in a post-tectonic, extensional regime that followed a major Silurian orogenic event. In the late stages of a protracted cooling history, this relatively dry, hypersolvus granite magma evolved the F-rich fluids from which the veins were formed.

The fluorspar veins are structurally controlled, occurring as open-space filling in fracture systems that developed in response to both regional stress regimes and localized regimes generated by the cooling and crystallizing of the granite pluton. The vein mineralogy is dominated by fluorite, with lesser amounts of quartz, calcite, barite and minor sulphides. The fluorite is highly variable in colour and primarily coarse grained and delicately banded, although fine grained varieties and breccia zones are common in the larger veins. The vein contacts are mostly sharp with little or no evidence of intense wall-rock alteration along the vein margins.

The chemical and physical conditions that prevailed during the deposition of the veins were investigated using geochemical and fluid inclusion studies of growth-zoned, brecciated and other more homogenous samples from various veins. The zones and growth directions were defined by macroscopic and microscopic examination of hand specimens, combined with field observations where possible. Growth zones, in the vein samples, range in thickness from 100 to 1 mm, with the majority ranging from 10 to 5 mm.

Microthermometric investigations of fluid inclusions in fluorite and other vein minerals indicate homogenization temperatures ranging from 500°C to 50°C and fluid salinity ranging from 30 to 0 equivalent weight percent NaCl. As a consequence of the high-level, relatively low-pressure environment in which the veins were formed, it is inferred that homogenization temperatures closely approximate formation temperatures. Variations between growth zones indicate that fluorite precipitation took place through a wide range of fluid temperatures and salinity. The cyclic nature of these variations can be related to individual fluid pulses, which in turn reflect changing fluid conditions within larger evolutionary cycles. The temperature and salinity variations can be accounted for by the unmixing of a supercritical magmatic fluid into a low salinity vapour and a high salinity liquid at near magmatic temperatures. These fluids were further modified by condensation, boiling and mixing as they migrated through the higher levels (low pressure/temperature) of the conduit system. Fluorite precipitation appears to have been primarily in response to the increasing pH of the fluid, caused by boiling or incursion of lower pH ground waters.

High precision trace element analyses of fluorite, calcite and host rocks were conducted utilizing inductively coupled plasma-mass spectrometric analysis (ICP-MS), supplemented by whole rock analysis by X-ray fluorescence spectrometry (XRF). The fluorite is relatively enriched in Y and REE with the former averaging 660 ppm and the latter 240 ppm. Systematic changes in REE concentrations in fluorite are interpreted to reflect changing fluid conditions from early to late stages of mineralization. The early-stage fluorite is characterized by LREE enrichment and HREE depletion while the late-stage fluorite is characterized by LREE depletion and MREE to HREE enrichment.

The systematic variations of REE concentrations in fluorite reflect dramatic changes in fluid composition with progressive evolution. Such REE behavior may be a result of reversals in the dominance of F or Cl complexing of the REE, either in the magmatic or hydrothermal regimes.

The apparent partitioning of the REE in fluorite was estimated by normalizing the fluorite to a fluid composition calculated, using appropriate vapour/melt partition coefficients, from a late-stage St. Lawrence Granite phase (granitic porphyry dyke). The REE in fluorite suggest a strong influence of the size (ionic radius) of the substituting ion (i.e. crystal structure control) on trace element partitioning, with a preferred substitution site size at or near the ionic radius of Dy (0.103 nm [1.03Å]). Since REE substitution in the fluorite structure is believed to primarily involve 'free-ion' REE species, the relative stability of REE fluoro-complexes, in the aqueous fluid, dramatically affect the availability of REE for substitution. The stability of such aqueous REE-complexes, and consequently the concentration of REE in fluorite, is strongly dependant on the temperature, pH and F activity of the fluid.

This work is dedicated to my late father and mother, Gerald and Veronica Collins, whose inspiration, guidance and unending support allowed me to pursue my goals and persevere.

Acknowledgements

I would like to express my sincere thanks to my supervisor, Dr. D.F. Strong, and my co-advisor Dr. B.J. Fryer for their ongoing support of my thesis project.

Thanks are also due to the following at the Earth Science Department of Memorial University: Rick Soper, Lloyd Warford and Foster Thornhill for the preparation of fluid inclusion and thin sections; Pam King for ICP-MS and Sr-isotope analysis; Gert Andrews for AA analysis; Daryl Clarke for XRF analysis; Roger Mason for cathode luminescence scans; and Henry Longerich for ICP-MS analysis and many helpful discussions with regard to the statistical analysis of the geochemical data. I would also like to thank Carolyn Emerson, of the Biology Department, for help with the SEM work and photomicrographs.

Thanks are also extended to the following people at the Newfoundland Department of Mines and Energy: Ambrose Howse for support and advice with the field work and sample collection; Norm Mercer and Randy Meehan for providing literature; Wayne Ryder and Sid Parsons for logistical support; and Karl Freake, Peter Bull and Leonard White for summer field assistance. Andy Kerr is gratefully acknowledged for providing access to recent unpublished geochemical data on the St. Lawrence Granite.

I express my thanks to Dr. George Jenner for kindly volunteering to read the first draft of this manuscript.

I express my thanks to P. Möller for providing a wealth of literature on his research into REE behaviour in fluorite and calcite.

Finally, I express my never ending gratitude to my wife, Anne Collins, for tolerating me through this ordeal, and her capable assistance in preparing some of the illustrations.

Most of the analytical work and other expenses were funded through various NSERC grants to Dr. D.F. Strong. Dr. B.J. Fryer supported the Sr-isotope analyses and some ICP-MS analysis. Field work was supported by the Newfoundland Department of Mines and Energy.

Table of Contents Page

Table of Contents Page

Table of Contents Page

Table of Contents

List of Tables

Page

List of Figures

Page

List of Figures

Page

List of Figures

Page

List of Figures

Page

List of Figures

Page

List of Figures

Page

1 Introduction

1.1 Preface

Recent studies suggest that fluid directly evolved from magmas can be an important source of metals (Holland, 1972; Burnham, 1979; Urabe, 1985; Candela and Holland, 1986) and other constituents (Candela, 1989; 1990) in a wide variety of mineral deposits, such as volcanogenic massive-sulphide deposits (Ishihara and Sasaki, 1991; Urabe and Marumo, 1991; Large, 1992), mafic-ultramafic magmatic deposits (Whitney and Naldrett, 1989), and especially in the wide variety of granite/granitoid hosted mineral deposits. The origin, distribution and characteristics of granite-hosted and granite-related mineral deposits are reviewed in volumes by Evans (1982), Taylor and Strong (1988), Whitney and Naldrett (1989), and Stein and Hannah (1990). The origins of many "non-magmatic" mineral deposits have been attributed to convective circulation of meteoric or other waters driven by the heat from deeper plutonic bodies. Such an intimate association would imply that, at least in a shallow magmatic environment, both processes could be involved, to varying degrees, in the formation of ore deposits. The relative importance of the magmatic input compared with sea-water convection has been

suggested by Large (1992) to explain the diversity of deposit styles and spatial distribution of Australian volcanic-hosted massive sulphide deposits.

The composition of magmatic fluids, at least initially, should reflect the composition of the magma from which they were derived, taking into account factors such as pressure/temperature conditions at the time of formation and mineral/melt/fluid distribution coefficients. The compositions of these fluids are predicted to change systematically as the composition of the magma changes in response to crystallization and/or vapour ebullition. The composition of the evolved magmatic fluids can also be changed by interaction with wall rocks, precipitation of various mineral phases and/or mixing with non-magmatic fluids, between the site of fluid generation and the site of formation of resultant "ore deposits".

It is also well established that the mineralogy of ore deposits is highly dependent on the composition of the fluid(s) from which they formed as well as the physical and chemical conditions at the site of deposition. Most hydrothermal minerals, in some way reflect the chemical composition (ion activity of solutes) of the fluid from which they are formed in both their major and minor (trace) constituents. The uptake of trace constituents by minerals can occur through substitution in the host lattice, absorption along grain boundaries and/or micro-fractures and as fluid inclusions (± daughter minerals) in the host mineral. The first, and possibly the second, of these processes will be highly dependant upon the chemical and physical characteristics, as well as the 'aqueous' speciation, of the trace elements involved.

Mineral/melt partitioning of both major and trace elements (especially the REE) in magmatic systems is largely governed by the crystal structure of the host mineral and the size and charge of the substituting ion. Therefore, it can also be assumed that the partitioning of the chemical constituents between, at least some, minerals and aqueous fluids will be governed by crystal chemical controls related to the structure of the individual mineral. This fluid/mineral partitioning will not necessarily be based on bulk fluid composition but rather the 'effective composition' available for substitution that will be related to, and limited by, the speciation of the components of the fluid. The speciation of constituents is controlled by the activity of various anionic species, and the pressure, temperature, Eh and pH of the fluid.

If there are established constraints on physical and chemical conditions prevailing at the time of formation of some hydrothermal minerals, then the composition of these minerals will reflect the 'effective composition' of the fluid from which they formed. The composition of this fluid will, in turn, reflect the composition of the fluid source and/or the rocks with which the fluid interacted. Trace element, especially rare earth element (REE), concentrations in hydrothermal minerals "...can provide information regarding solution histories but only in a general way" (Cullers and Graf, 1984). The major obstacle to interpretation of REE patterns in hydrothermal minerals is the lack of a comprehensive experimental database on their partitioning behaviour and the properties of the aqueous solutions from which they form. To better understand the behaviour of trace elements in hydrothermal fluid/mineral interactions it is necessary to rely partly on theoretical, rather than empirical, modelling techniques.

The Ca-bearing minerals fluorite and calcite are found in many hydrothermal mineral deposits. Both of these minerals are efficient scavengers of REE from aqueous solutions with both LREE and HREE readily substituting for Ca in their crystal lattices (Möller and Morteani, 1983). Since fluorite is a highly ionic crystal, the partitioning of REE between fluid and mineral should be strongly dependant on crystallographic controls, and consequently the partitioning should show systematic or predictable variations. However, there is a high degree of variability in REE concentrations of fluorite which may reflect changing fluid composition and/or changing physical/chemical conditions at the site of deposition, along the fluid pathway and/or at the fluid source.

It is proposed that a detailed study of a fluorite-bearing hydrothermal deposit, for which there is reasonable geological, physical and chemical control on the source, pathways and site of deposition, combined with an adequate geochemical data base (including REE), could aid in assessing the viability of using REE geochemistry of Ca-bearing minerals to monitor changing fluid conditions during ore-forming processes. A comprehensive paragenetic sequence of Ca-bearing mineral(s) representing the entire ore-forming process would be a necessary prerequisite in such a study, as well as the capability to precisely analyze individual grains or zones.

1.2 Present Investigation

Strong et al. (1984) presented reconnaissance results of a study on fluorite samples from the fluorspar deposits at St. Lawrence, Newfoundland (figure 1.2.1). The study utilized fluid inclusion, rare earth element (REE) and oxygen isotope data to

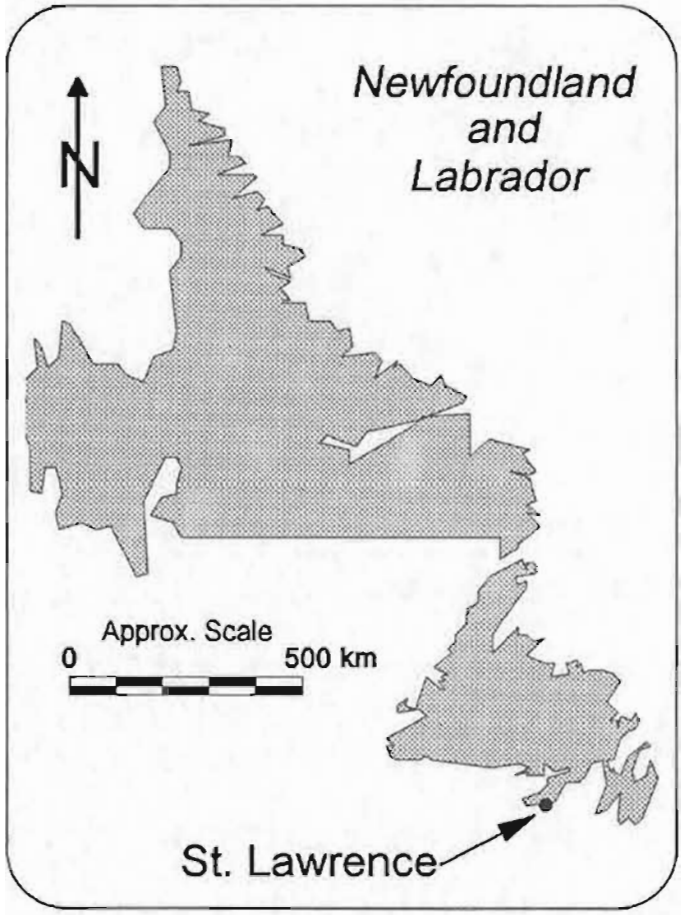

Figure 1.2.1 Sketch map showing the general location of the study area at St. Lawrence, Newfoundland.

examine variations both between fluorite samples and individual growth-zones within samples. The study revealed quite varied, albeit systematic, variations in REE concentrations between individual growth zones that were interpreted to be related to changing physical and chemical conditions of the mineralizing fluid in response to fluorite precipitation. The samples used in the study were somewhat limited, being primarily from only two deposits with the exact locations of most samples not adequately documented.

Considering the results of the previous study (Strong et al., 1984) and the suitability of fluorite for both REE geochemical and fluid inclusion studies, the St.

Lawrence fluorspar deposits were chosen by the author as an M.Sc. thesis study area under the supervision of Drs. D. F. Strong and B. J. Fryer. The purpose of this study was to better document and define the physical and chemical changes which occur across sequential growth zones in selected samples from the St. Lawrence fluorspar veins, utilizing fluid inclusion microthermometry and REE geochemistry as the primary tools of the investigation. The emphasis is to better understand the systematics of these variations in the context of a fluid evolution model and to attempt to document the same characteristics in a number of spatially separate veins. The ultimate goal was to generate data to develop a model that would explain the characteristics of the fluorite in terms of magmatic fluid ebullition, fluid transport and fluorite deposition. The systematics of modelling the fluid evolution of the hydrothermal system should be simplified by the fact that the fluorspar veins are primarily hosted by the St. Lawrence Granite and related rocks and field evidence indicates only minor localized wall-rock alteration associated with the veins. It is therefore assumed that fluid/wall-rock interaction may have been minimal, and thus have had little or no effect on fluid composition.

1.3 Scope and Methodology

The field work for this study, involving sampling all previously documented and exposed fluorite veins and related showings in the St. Lawrence area, was carried out during the summers of 1983-84. Wherever possible, continuous sections were sampled across the entire width of the veins or as far as exposure would allow. A suite of selected samples was chosen, on the basis of mineralogy and field relationships, and

subsequently cut with a diamond saw to examine internal zoning. Final samples were selected on the basis of well developed growth zones, distance from the centre of mineralization (the St. Lawrence mine area) and contrasting host rocks. Samples of individual growth zones were separated by hand for geochemical analysis, thin sections and fluid inclusion sections (doubly polished wafers).

In order to document the physical and chemical variations between samples and between individual growth zones within samples, a fluid inclusion and trace element geochemical study was initiated. The fluid inclusion study involved petrographic study of the vein mineralogy and determinations of temperature and salinity data from 12 different veins. Some preliminary results of this study formed part of an B.Sc. (honors) dissertation by the author (Collins, 1984a), and subsequent publications (Collins, 1984b; Collins and Strong, 1985; Collins, 1988a,b; Collins and Strong, 1988, 1992).

Samples of the host St. Lawrence granite and near-contact metasediments were analyzed for major and trace elements. This analysis was designed to provide the major and trace element (including REE) composition of potential "source rocks" for mineralizing fluids. The fluorite/vein samples were analyzed for major (some semi-quantitative) and selected trace elements by XRF, and for selected trace elements (including REE) by ICP-MS. Several fluorite zones were analyzed for $^{87}Sr/^{86}Sr$ isotopic ratios to determine if the genetic link between the granite and the fluorspar deposits could be confirmed, or discounted by isotopic evidence. A variety of fluorite zones were examined using the SEM to determine if the REE patterns observed in the fluorite could be attributed to separate REE-bearing mineral phases. Cathode-luminescence scans were

used to probe the oxidation state of europium (Eu^{3+}, Eu^{2+}) and samarium (Sm^{3+}, Sm^{2+}) as well, luminescence colour variation was used to determine the extent of subtle intra-zone growth zoning on a microscopic level.

2 The St. Lawrence Granite

2.1 Tectono-stratigraphic Setting

The Devonian St. Lawrence Granite intrudes significantly older Cambrian and Precambrian rocks which form part of the Avalon Terrane of the Appalachian Orogen as defined in Newfoundland (figure 2.1.1). The Avalon Terrane comprises an extensive but discontinuous tectono-stratigraphic unit within the Appalachian Orogenic Belt of eastern North America, from Newfoundland to Florida (Williams, 1964, 1978; 1979; Williams et al., 1972; 1974). It encompasses a variety of late Precambrian geologic elements which led Williams and Hatcher (1982) to suggest that the Avalon Terrane may itself be composed of Precambrian "suspect" terranes. If composite, it was assembled in the late Precambrian, since its younger Cambrian rocks have similar faunas and stratigraphic sequences (Williams and Hatcher, 1982). It is believed that the Avalon terrane was accreted to the North American continent during mid-Paleozoic time (Blackwood and O'Driscoll, 1976; Elias and Strong, 1982).

The Avalon Terrane is characterized by mainly upper Precambrian sedimentary and volcanic rocks that are relatively unmetamorphosed and undeformed compared to those of nearby terranes (Williams, 1979). The Avalon Terrane is separated from the Dunnage

Terrane by the Gander Terrane, indicating that the Avalon Terrane did not directly face or abut the Iapetus Ocean (Williams and Hatcher, 1982). The Avalon Terrane was a stable platform during the Cambrian period and locally during the Ordovician Period when the generation and destruction of Iapetus was most active (Williams, 1979).

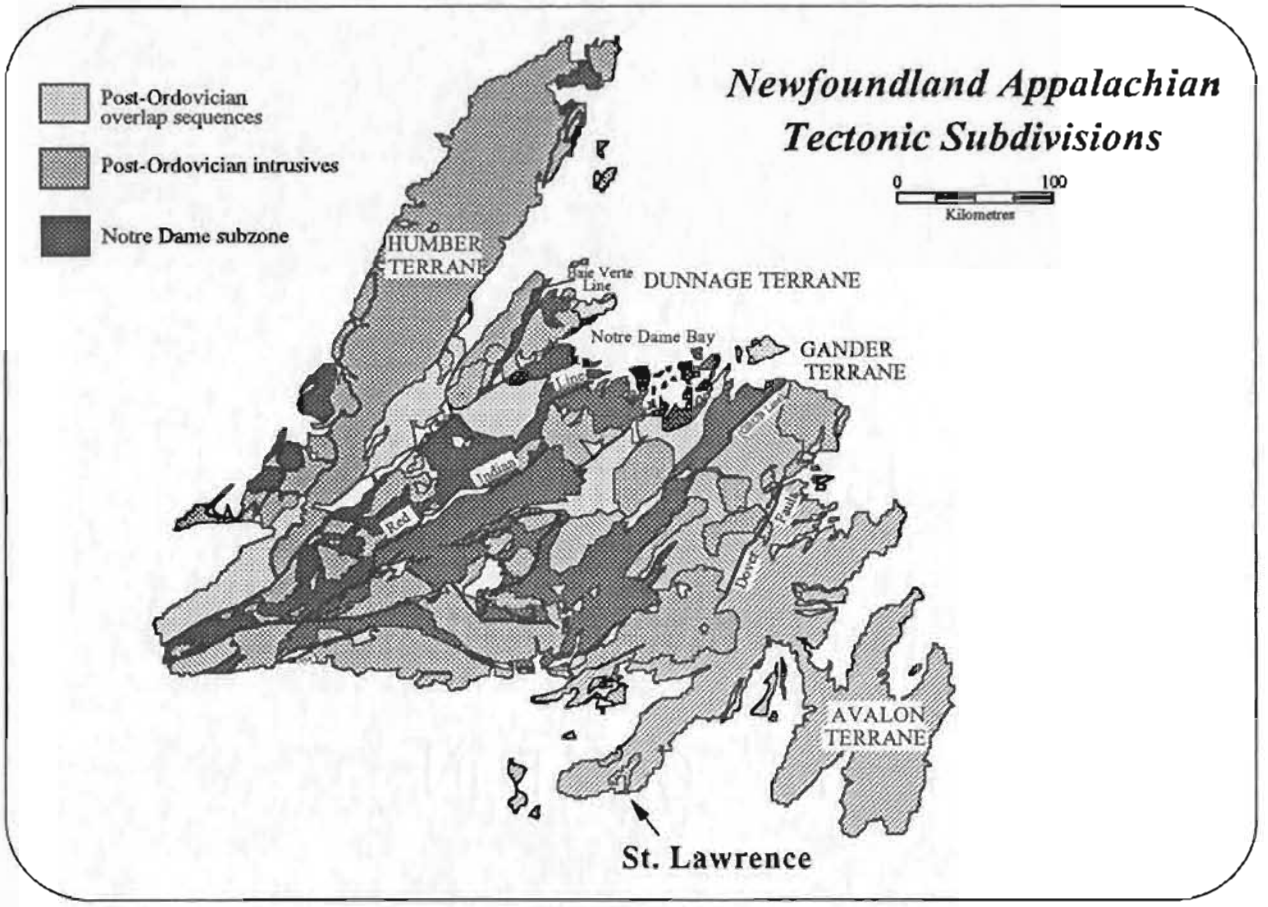

Figure 2.1.1 Map of the island of Newfoundland outlining the tectono-stratigraphic subdivisions and the location of the St. Lawrence Granite (modified after Williams [1978] and others).

Two distinct periods of Avalonian magmatic activity have been defined by U-Pb geochronology (Krogh et al., 1988). The oldest is defined by ophiolitic rocks of the Burin Group (760 Ma) and the youngest by the subaerial volcanic rocks of the Marystown and Harbour Main Groups which span a period from about 630 to 585 Ma. These plutonic-volcanic events are difficult to separate into distinct pulses related to specific orogenic events and are relatively continuous over a large time span. It has been suggested

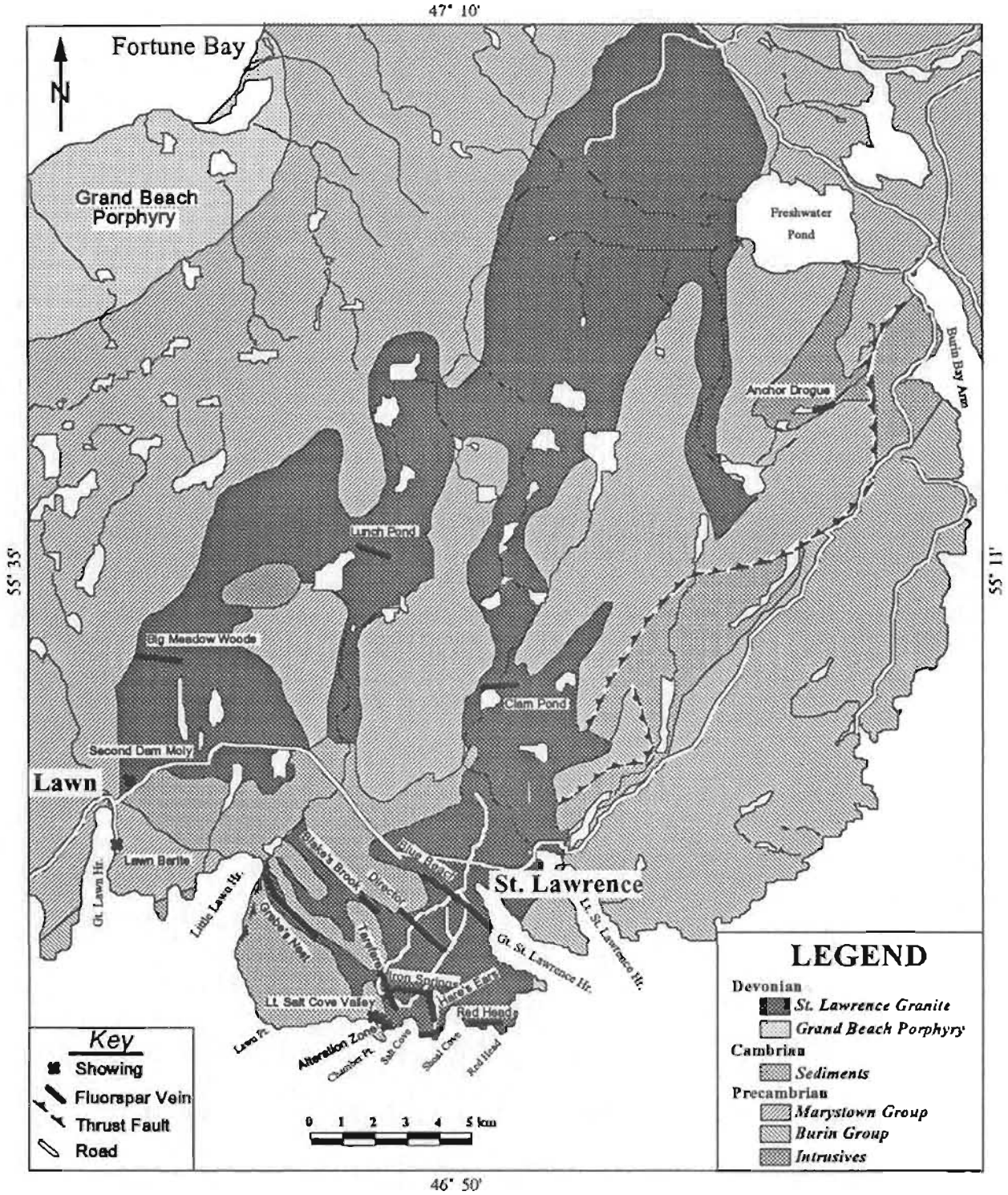

Figure 2.2.1 Generalized geologic map of the St. Lawrence Area showing the St. Lawrence Granite and the major lithologic units which it intrudes. The locations of the major fluorspar veins and mineral occurrences are also shown. See legend in text. The drawing was modified from Howse and Collins (1985) and based primarily on mapping by O'Brien et al. (1977) and Strong et al. (1978).

(Krogh et al., 1988) that they may be analogous to epicontinental volcanic fields such as in the Basin and Range area of the southwestern United States. This implies that subduction of oceanic lithosphere (of which the Burin ophiolitic rocks may be remnants) beneath a stable (Pan-African?) continent, could have produced the extensive and long-term subaerial volcanism characteristic of the Newfoundland Avalon Terrane. This suggests that the Avalonian Precambrian ophiolitic, volcanic and clastic sequences may all be related to a major orogenic event as Krogh et. al. (1988) concluded that "they (new U-Pb dates) do not support suggestions that the Avalon Terrane comprises a 'collage of suspect terranes'". However, Nd-isotopic data (Fryer et al., 1992) suggest the absence of significant amounts of very old crust beneath most of the Avalon Terrane. These Late Precambrian sequences may therefore be representative of the crustal rocks with which the St. Lawrence granitic magma interacted during accent.

2.2 Geologic Setting and Field Relations

The St. Lawrence Granite is located on the southern part of the Burin Peninsula near the community of St. Lawrence from which the name is derived. The St. Lawrence Granite batholith, shown in figure 2.2.1, defines a north-south trending, relatively continuously exposed body measuring approximately 30 km long by 10 km wide (O'Brien et al., 1977; Strong et al., 1978). It includes Precambrian volcanic rocks of the Burin and Marystown Groups as well as Cambrian sedimentary rocks of the Inlet Group (Teng, 1974; Strong et al., 1978). The granite is characterized by sharp contacts and an irregular top, marked by a preponderance of roof pendants and cupolas, indicating that the bulk of the exposures represent the extreme top of the batholithic body.

The granite contact is predominantly flat, with a gentle dip towards the northwest, although the southeast contact is much steeper, suggesting stronger structural control. Localized steep contacts observed along the coast west of St. Lawrence may be the result of stoping of the country rock. A reconnaissance gravity survey (Hodych, pers. comm.) indicates that the granite is characterized by a strong negative anomaly, sharply defined at the eastern granite contact and extending westward to the limit of the survey, across the western granite contact. This evidence supports a steeply dipping eastern contact and, when combined with exposures of the western granite contact (roof) in a deeply eroded stream bed near the mouth of the Northwest Brook at Lawn (figure 2.2.1), suggests that the gently dipping granite body may extend considerably further westward at shallow depths below the Precambrian cover. Paleomagnetic studies (Irving and Strong, 1985) suggest that the St. Lawrence Granite has not been tilted by more than 5° since the time of emplacement.

The St. Lawrence pluton consists of medium to coarse grained pink coloured, locally porphyritic, alkaline to peralkaline granite and associated granitic rocks (Teng, 1974; Teng and Strong, 1976). The granite shows a progressive decrease in grain size towards its contacts. Minor phases, with irregular conformation, occur having sharp intrusive contacts and varing from coarse to fine-grained grained, locally porphyritic. Tuffisites (gas breccias), consisting of discrete angular to rounded granite fragments in a fine comminuted matrix, and miarolitic cavities are common, with the latter observed within a few metres of the contacts (Teng, 1974).

In the area between St. Lawrence and Lawn (figure 2.2.1) there are many exposures of pink quartz-feldspar porphyry dykes which have been termed "rhyolite porphyry" by

Van Alstine (1948) and many mining company geologists. These dykes are known to cut the granite (Van Alstine, 1948) but similar mineralogical and chemical characteristics (Teng, 1974; Teng and Strong, 1976) suggest that they are cogenetic with the granite and are probably related to later-stages of magmatic activity. These dykes generally trend northwest and are exposed as far west as Great Lawn Harbour. At least one of these dykes, herein termed the "*Grebe's Nest Porphyry*" hosts fluorite mineralization. Narrow aplitic dykes are commonly observed near the contacts, especially in the vicinity of Chamber Point (figure 2.2.1).

In the northern part of the batholith, reibeckite-bearing ignimbritic volcanic rocks, termed the 'Rocky Ridge Complex", have been interpreted to be extrusive equivalents of the St. Lawrence Granite (Strong et al., 1978). The presence of volcanic equivalents, the low regional metamorphic grade of the country rocks, the presence of tuffisites (gas breccias), sharp chill margins and miarolitic cavities collectively suggest that the pluton was intruded at shallow crustal levels (Strong et. al., 1978).

2.3 Mineralogy and Petrology

A detailed petrographic study of the St. Lawrence Granite was conducted by Teng (1974), and the following discussion is drawn largely from his study. He described it as a pink to red alaskite granitic composed essentially of quartz, orthoclase and albite with minor amounts of riebeckite, aegirine, biotite, fluorite, magnetite and hematite. Its texture varies from medium grained hypidiomorphic to aphanitic and porphyritic depending upon proximity to the contacts (Teng and Strong, 1976).

The granite contains 20 to 40 percent quartz, 30 to 60 percent alkali feldspar and up to 20 percent plagioclase (albite). Quartz crystals are usually clustered between larger feldspars but locally form phenocrysts, up to 2 mm in length. In the marginal phases of the granite, quartz commonly occurs as deeply embayed phenocrysts and, as micrographic intergrowths with orthoclase, displaying a granophyric texture. Alkali feldspars are generally orthoclase and microcline perthites which are usually turbid and contain finely disseminated hematite. The perthitic plagioclase, primarily exsolved from the alkali feldspars, is generally albite with a composition between An_0 and An_{10}. The mafic minerals and plagioclase, when present, tend to be euhedral, while most of the alkali feldspar is subhedral, and quartz occupies irregular interstices.

Hematite and magnetite are common accessory minerals with the former commonly being an alteration product. Riebeckite is a common accessory mineral and is usually associated with, and crystallized after, aegirine or magnetite. Hornblende is only present in the marginal rocks from the west lobe of the pluton north of Lawn where the granite approaches granodiorite in composition. Biotite is rare, but where present it is usually chloritized. Fluorite occurs as an accessory mineral, often in association with the chloritized biotite. Zircon and apatite are rare, but when present, are commonly associated with biotite. Miarolitic cavities are commonly lined with quartz and, in some cases, fluorite.

The porphyry dykes consist of essentially the same mineralogy as the granite, differing only in texture. Feldspar phenocrysts are commonly perthitic alkali-feldspar, sporadically sanidine, and rarely albite. Quartz phenocrysts are typically euhedral but show embayed and corroded boundaries. Ferromagnesium minerals are sparse, never occur

as phenocrysts, and are only rarely evidenced in the groundmass. Magnetite and hematite occur disseminated in the groundmass with quartz and feldspar (Teng and Strong, 1976).

2.4 Age and Correlations

The St. Lawrence Granite has been dated by Rb-Sr radiometric methods at 315 ± 5 Ma (Bell et al., 1977), using a 4-point isochron, and 353 ± 30 Ma (Fryer and Strong, unpub. data, circa 1984), using an 11-point isochron, suggesting ages of crystallization from Lower Devonian to Middle Carboniferous and initial $^{87}Sr/^{86}Sr$ ratios of 0.722 ± 0.003 and 0.709 ± 0.006 respectively. Combining the two data sets, a Lower Devonian age of 353 ± 22 Ma and an initial $^{87}Sr/^{86}Sr$ ratio of 0.708 ± 0.005 is defined.

The Grand Beach Porphyry, a flat-lying sheet of subaerial ash flow tuff and volcanic porphyry, is interpreted to be volcanic and sub-volcanic equivilants of the St. Lawrence Granite (Strong et al, 1978), based on its similar enrichment in Nb and other elements. A sample from the Grand Beach Porphyry (Fryer and Kerr, unpubl. data, circa 1992) displays similar chondrite normalized REE patterns to those from the St. Lawrence Granite (figure 2.4.1), supporting the correlation. A more complete discussion of the geochemistry of the granite and related rocks is presented later in this chapter. A sample of ash-flow tuff from the Grand Beach Porphyry yielded a tentative U-Pb zircon age of 394 (+6/-4) Ma with data 5 and 9% discordant (Krogh et al., 1988).

The correlation between the St. Lawrence Granite and the Grand Beach Porphyry suggests that the earliest phase of magmatic/volcanic activity may be of similar age to the youngest phase of the North Bay Granite and the Chetwynd Granite which have yielded U-Pb zircon ages of 396 +6/-3 Ma and 390 ± 3 Ma respectively (Dunning et al., 1990).

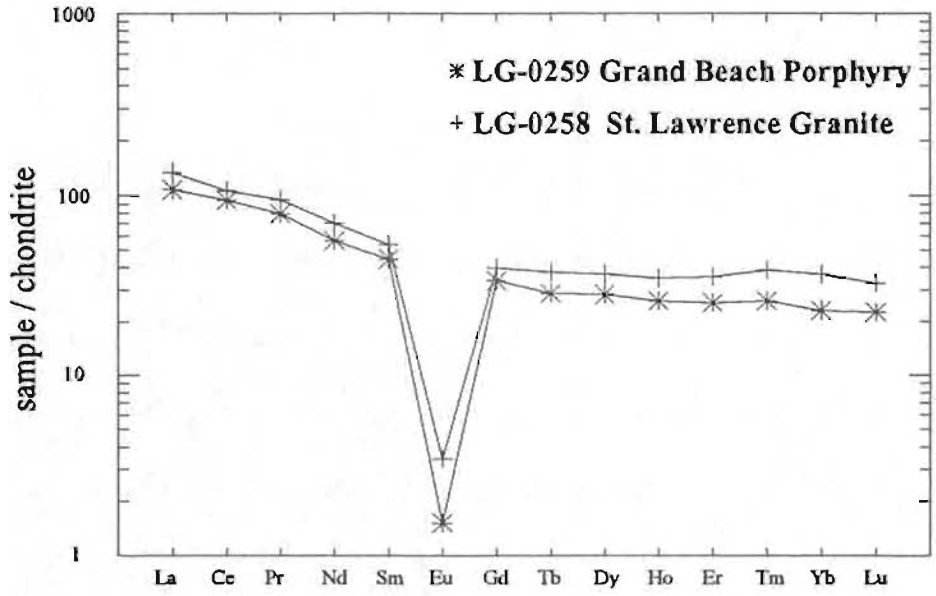

Figure 2.4.1 Chondrite normalized REE patterns for samples from the Grand Beach Porphyry and the St. Lawrence Granite (Fryer and Kerr, unpublished data, circa 1992).

These granites are interpreted to represent post-tectonic plutons emplaced near the end of the Silurian orogenic event. These ages overlap those of the *'Ackley association'* (400 to 380 Ma) of Williams et al. (1989), which consists of a major northeast-southwest trending belt of post-tectonic plutons. These granitoids are characterized by associated Mo-Sn-W mineralization and ring-complex to lobate geometry, suggesting a relatively high level of emplacement (Fryer et al., 1992).

2.5 Description of Granite and Related Samples

In order to obtain an extended database of REE and other trace elements in a representative suite of host rocks to the fluorspar veins, 9 samples were selected for analysis of major and trace elements. The discussion of the geochemistry of the St. Lawrence Granite and related rocks will utilize the analyses of these samples as well as available geochemical data from other sources (Teng, 1974: Strong et al., 1974: Kerr,

unpubl. data, circa 1990). The 'host rock' samples analyzed as part of this study are briefly described below.

Sample HCT-111 was a powder from Teng's (1974) study which he described as an unaltered, red, medium grained, equigranular granite from a coastal exposure at Shoal Cove (figure 2.2.1). This granite sample was selected as a typical 'mine area' granite, an assumption substantiated by subsequent comparison with other geochemical analysis.

Samples HCT-187 and HCT-188, from the Grebe's Nest Porphyry Dykes (figure 2.2.1) were also taken from Teng's (1974) samples. He describes these as unaltered, red quartz-feldspar porphyry with an aphanitic groundmass. Sample HCT-188 contains minor unspecified sulphides (probably pyrite). These samples were chosen to represent the host rock to the Grebe's Nest Vein.

Samples SDMS-2-B and SDMS-4 were collected from the 'Second Dam Moly Showing' north of Lawn (figure 2.2.1). The former is a relatively unaltered, pink, medium grained, equigranular granite adjacent to the molybdenite-bearing quartz vein and the latter is an unaltered, pink, coarse grained, equigranular granite approximately 50 metres away from the vein. These samples were chosen because of their proximity to the quartz vein and the lack of coverage of this part of the pluton ('Lawn Lobe') from previous surveys.

Sample BBS-84-64 is a tuffisite or 'gas-breccia' which occurs along the margin of the Blue Beach Vein (figure 2.2.1). This sample consists of sub-rounded fragments of pink granite (up to 3 cm) in a fine grained comminuted matrix of pink to purple granitic material. The tuffisite was chosen because of its unique mode of origin and close spatial relationship to some fluorspar veins.

Samples AZ-2 and AZ-4 are from a sericitic 'Alteration Zone' near the granite contact at Chamber Point (figure 2.2.1). This zone contains barite and fluorite veining as well as chalcopyrite and molybdenite as disseminations in the granite and associated with narrow fracture-filling quartz veins. Sample AZ-2 is a pink, fine grained, aplitic granite with disseminated molybdenite and chalcopyrite mineralization and is the least altered of the two. Sample AZ-4 is a pink-buff, fine grained granite with intense sericite alteration and minor disseminated chalcopyrite. These samples were chosen to characterize the varying degrees of sericitic alteration, a phenomenon rarely observed in this granite.

Sample CV-6 is a sample of relatively unaltered green to black fine grained Cambrian metasediment from the Inlet Group near the granite contact at Chamber Point (figure 2.2.1), adjacent to the 'Alteration Zone' described above. This sample was chosen to represent the hornfelsed Cambrian metasediments which typically overlie the granite and locally host minor fluorspar mineralization. These metasediments show the influence of thermal metamorphism but little metasomatic effects except near the margins of fluorite veins.

2.6 Geochemistry

The geochemistry of the St. Lawrence Granite was first documented as part of a government lithogeochemical study (Strong et al., 1974) combined with an M.Sc. thesis study by Teng (1974) and published in a subsequent paper (Teng and Strong, 1976). During the late 1980's, the Geological Survey Branch of the Newfoundland Department of Mines and Energy undertook a program of compilation and improvement of the existing geochemical database pertaining to Newfoundland plutonic suites, in order to supplement

the many new isotopic and related studies (Kerr et al., 1990). As part of this program, 99 sample powders were selected from Teng's (1974) original study of the St. Lawrence Granite and re-analyzed for major and trace elements at the Geological Survey Branch Laboratory.

A subset from the new geochemical data (Kerr, unpubl. data, circa 1990) was combined with data from the present study to produce the summary tables and diagrams presented in the following discussion. This subset was selected based on rejection of some samples after comparing their analyses to those of Teng (1974) and after comparing sample locations to geological information from subsequent (to Teng's study) mapping (O'Brien et al., 1977; Strong et al, 1978) and the author's field work in the area. On this basis 10 samples were rejected, seven of which were considered to have a high probability to be from units other than the St. Lawrence Granite (i.e. 5 from the Precambrian Marystown Group Volcanics and 2 from the Precambrian Loghlin's Hill Intrusive) and three were rejected due to potential mislabelling since they differed significantly from Teng's (1974) analyses.

In order to expand coverage, especially for the western part of the pluton, 12 granite related samples from the present study were added to the data set (101 total samples) to calculate the average geochemical composition of the St. Lawrence Granite (Table 2.6.1). A total of 12 samples were excluded from the table because they were either from dykes, altered zones or tuffisites and not truly representative of 'average' granite.

2.6.1 Major Elements

The major element data of Kerr (unpubl.) reaffirms Teng's (1974) conclusions that the St. Lawrence Granite is alkaline to peralkaline in composition and characterized by

Table 2.6.1 Average geochemical composition of the St. Lawrence Granite.

	Mean	RSD	SD	Max	Min	n =
SiO2	77	1%	1.1	79	74	89
TiO2	0.12	29%	0.03	0.29	0.02	89
Al2O3	11	4%	0.44	12	9	89
Fe2O3	1.3	51%	0.65	4	0.01	89
FeO	0.56	52%	0.29	1.7	0.25	89
MnO	0.02	81%	0.02	0.12	0.01	89
MgO	0.12	33%	0.04	0.28	0.01	86
CaO	0.39	98%	0.38	2.2	0.03	89
Na2O	3.5	12%	0.42	5.8	1.9	89
K2O	4.7	13%	0.6	6	1.2	89
P2O5	0.01	48%	0.01	0.03	0.01	89
LOI	0.85	34%	0.28	2.2	0.32	89
Total	99.5					
Li	22	90%	20	99	4	84
Be	8	38%	3	18	2	83
F	1,271	95%	1,211	6,760	38	80
V	2	50%	1	5	1	82
Cr	2	101%	2	12	1	86
Ni	2	42%	1	5	1	82
Cu	7	75%	5	26	2	89
Zn	57	94%	53	295	3	89
Ga	29	12%	4	40	18	89
Rb	288	21%	61	406	64	89
Sr	9	83%	8	58	2	89
Y	104	34%	35	207	29	89
Zr	618	52%	323	2,094	258	89
Nb	92	53%	49	434	30	89
Mo	5	34%	2	14	3	83
Ba	66	106%	70	506	15	89
La	60	34%	21	118	8	82
Ce	143	27%	38	278	50	83
Pb	33	108%	36	273	3	89
Th	33	55%	18	158	10	89
U	8	54%	4	39	3	89
Ga/Al*	4.9	12%	0.6	6.6	3	89
Rb/Sr	45.1	67%	30.1	196	0.3	89
Rb/Ba	6.5	62%	4	26.1	0.3	89
Al	0.98	5%	0.05	1.02	0.61	89

Average geochemical composition is based on compilation of 89 analysis of the granite: 82 samples from analysis by the Newfoundland Department of Mines and Energy (A. Kerr, unpubl. data) and 7 from the present study (HCT-111, HCT-87, SDMS-1-A, SDMS-2-B, SDMS-3-B, SDMS-3-D and SDMS-4). Elements with n < 89 have missing values in the data set, some of which may be below detection limits. The Ga/Al* is calculated as (10000*Ga)/Al.

high concentrations of SiO_2, Na_2O and K_2O (averaging 76, 3.5 and 4.7 wt. % respectively) and low Al_2O_3, MgO and CaO (averaging 11.2, 0.12 and 0.4 wt. % respectively). A statistical summary of the geochemical data for the St. Lawrence Granite is presented in Table 2.6.1. The relative standard deviation (RSD) of major elements in the granite clearly demonstrate that SiO_2 and Al_2O_3 show very little variability and that Na_2O and K_2O show only small variability, attesting to the geochemical homogeneity of the pluton. The higher variation in Fe can be attributed to the irregular distribution of magnetite as an accessory phase and hematite as inclusions in feldspars and as an alteration product. The high variation of other major elements, excluding CaO, can be attributed to their low average concentrations and their association with accessory and/or mafic mineral phases, both of which are rare in the granite. The high variability of CaO probably reflects the sequestering of Ca into accessory fluorite or other F-bearing phase due to increased F activity in the melt and/or the addition of fluorite (± calcite) during hydrothermal alteration. This relationship between F and Ca is evidenced by the strong positive correlation shown in figure 2.6.1.

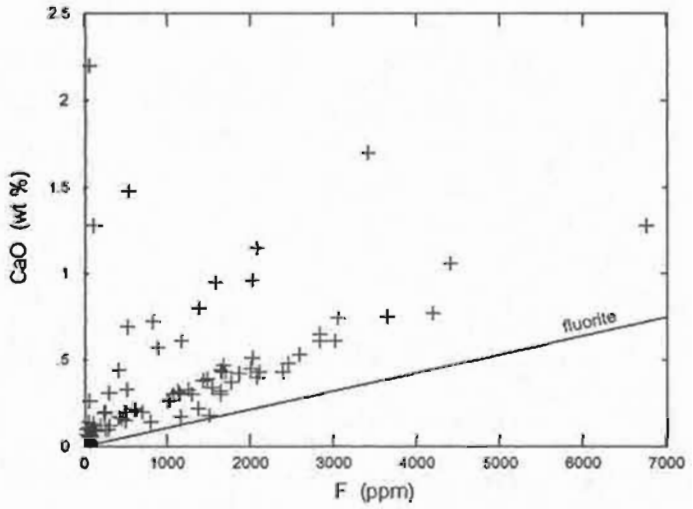

Figure 2.6.1. Rocks of the St. Lawrence Granite plotted on a CaO versus F variation diagram (solid line represents Ca/F ratio of fluorite composition).

2.6.2 Trace Elements

The trace element concentrations in the St. Lawrence Granite show a high degree of variation (Table 2.6.1), especially the elements Ba, Sr, Cu, Pb, Zn and F, the most extreme of which may be related to hydrothermal activity but some probably reflect changes in magma composition resulting from assimilation and fractional crystallization.

Compared to bulk continental crust (figure 2.6.2), the St. Lawrence Granite is enriched in Be, Rb, Th, U, Ce, Y, Zr, Nb and Pb but depleted in Ba, Sr, V, Cr, Ni and Cu. The granite has near average abundances of Li and Zn as well as Ga/Al ratios only slightly above crustal values. The granite has an average F value of close to 1300 ppm, attesting to its F-rich nature compared to average granite values of around 800 ppm (Bailey, 1977) but within the range of 1,000 to 3,000 ppm proposed for alkali granites of varying alkalinity.

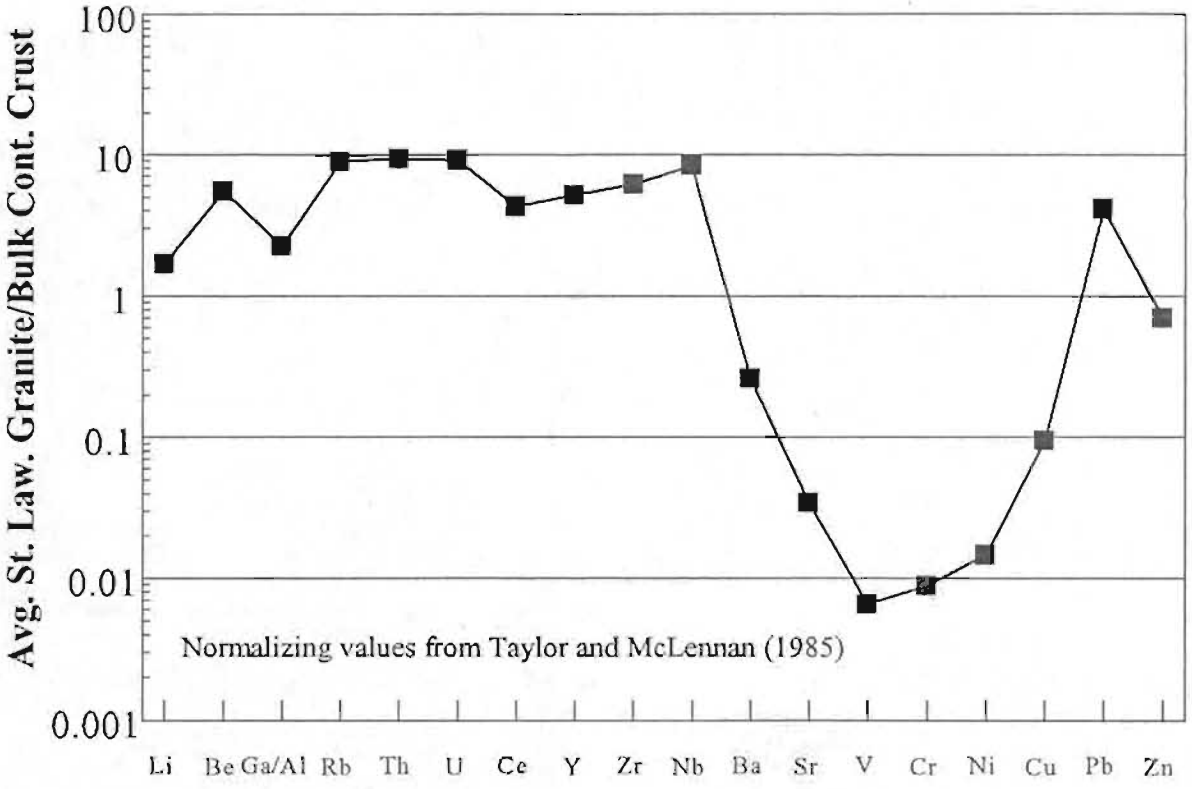

Figure 2.6.2. Bulk continental crust normalized plot of average selected trace elements in the St. Lawrence Granite.

2.6.3 Rare Earth Elements

As part of this study, the rare earth element (plus other trace and major elements) were determined in 9 samples of the St. Lawrence Granite and related rocks , including a sample of tuffisite (gas breccia) and near-contact metasediment. Analyses of these samples are presented as Table 2.6.2. Chondrite normalized REE plots (figure 2.6.3) show that the granitic samples generally have an enriched, relatively flat to V-shaped REE pattern with a slight light rare earth (LREE) enrichment (La_N/Yb_N = 3.5 to 1.5), and pronounced negative Eu anomalies (Eu/Eu^* = 0.074 to 0.001). The REE concentrations in the granitic rocks are approximately 100 times chondritic values.

Unaltered granite sample HCT-111, because of its similar trace element chemistry to the average St. Lawrence Granite (Table 2.6.1), is considered to represent a *'typical'* chondrite normalized REE pattern for the granite (figure 2.6.3a). This chondrite-normalized REE pattern is characterized by a relative enrichment in the LREE with respect to chondritic values, with $La_N > Sm_N$ and a relatively flat MREE- HREE pattern, with the exception of Eu which displays a strong negative anomaly. Of the unaltered granitic samples, HCT-111 has the highest concentration of all REE ($\sum$ REE = 374 ppm), except for Eu.

The tuffisite sample, BRS-84-64, displays a chondrite normalized REE pattern (figure 2.6.3a) that is virtually identical to that of the 'typical' granite (HCT-111), except for slightly lower concentrations of the HREE.

The REE patterns of samples HCT-187 and HCT-188 (figure 2.6.3a) , from the Grebe's Nest Porphyry Dykes, show similar HREE concentrations to the 'typical' granite (HCT-111) with a momotonic depletion from HREE to LREE compared to the 'typical'

Table 2.6.2 Geochemical analyses of St. Lawrence Granite and associated rocks.

Sample	HCT-111 Granite	SDMS-4 Granite	SDMS-2-8 Granite	HCT-187 Porp Dyke	HCT-188 Porp Dyke	BBS-84-84 Tuffisite	AZ-2 Alt Granite	AZ-4 Alt. Granite	CV-8 Metaseds
Method	AA/XT-IH	XM/XT-IH	AA/XT-IN	AA/XT-IH	AA/XT-IH	XM/XT-IH	AA/XT-IN	AA/XT-IN	XM/XT-IH
SiO2	77.3	77.8	77.7	77.4	78.7	82.1	71.4	87.5	58.9
TiO2	0.13	0.06	0.06	0.06	0.06	0.08	0.23	0.13	1.02
Al2O3	10.4	11.4	11.1	11.2	11.4	8.05	10.4	7.14	22.9
Fe2O3	1.88	1.51	0.97	0.4	0.25	1.78	1.34	0.9	8.13
FeO	0.3		0.38	0.75	0.51		0.38	0.24	
MnO	0.01	0.02	0.02	0.03	0.04	0.01	0.04	0.06	0.07
MgO	0.01	< 0.02	0.01	0.03	0.07	< 0.02	0.01	< 0.02	2.3
CaO	0.43	0.05	0.18	0.1	1.3	0.68	2.5	0.9	0.79
Na2O	3.28	3.73	3.78	3.58	5.01	2.38	2.52	0.12	0.69
K2O	4.8	4.53	4.5	4.71	2.22	3.54	5.81	6.19	5.39
P2O5	<0.004	< 0.003	0.01	<0.004	<0.004	< 0.003	0.02	0.02	0.12
LOI	0.89	0.53	0.42	0.65	1.5	0.61	2.1	5.2	4.7
Total	99.5	99.4	98.8	98.9	99.1	99.2	98.9	94.6	105
S	5	5	55	29	45	3	331	213	8
Cl	27	40	17	23	22	23	17	34	18
F	2 400			120	120				
Sc	< 7	< 7	< 7	< 7	< 7	< 7	< 7	7	23
V	< 7	< 7	< 7	< 7	< 7	< 7	< 7	< 7	145
Cr	< 6	11	7	< 6	< 6	13	8	< 6	138
Ni	< 4	< 4	< 4	< 4	< 4	< 4	< 4	< 4	61
Cu	< 3	8	< 3	48	164	4	442	1,508	10
Zn	< 3	45	36	72	23	70	427	193	227
Ga	30	28	28	29	31	18	50	< 4	33
Rb	302	323	379	408	142	200	285	283	313
Sr	8.8	4.7	5.6	11.7	19.6	11.3	28.5	28	47.3
Zr	544	270	318	280	264	342	291	247	147
Nb	111	71	104	110	101	51	42	28	17
Ba	41	46	596	55	92	84	1 231	821	989
Pb	19	52	48	64	143	16	5,065	866	39
Li	11	59		10.3	19	58			107
Y	121	484	754	117	95.6	122	62.7	91.8	36.6
Mo	<0.08	6.1		9.5	<0.08	1.6			1
Cs	4.39	6.27		5.41	1.7	2.28			19.6
La	61.8	253	417	46.2	28.3	63.2	84.9	113	46.9
Ce	131	547	755	99.5	59.4	136	129	227	93.7
Pr	17.5	6.39	8.73	11	7.16	16.1	15.5	27.1	10.6
Nd	66.3	22.6	29	39	26.5	62.7	57.9	101	40.3
Sm	16.6	5.63	7.56	10.5	7.91	15.6	10.5	19.3	7.46
Eu	0.41	0.08	0	0.23	0.65	0.38	0.43	0.73	1.42
Gd	16.3	5.18	7.34	11.7	8.18	16.6	7.73	14.5	6.87
Tb	3.33	1.05	1.73	2.42	2.12	2.76	1.35	2.28	0.98
Dy	22.4	8.27	12.7	18.2	15.4	17.8	7.61	11.8	6.03
Ho	4.72	1.93	2.83	4.11	3.42	3.84	1.58	2.29	1.24
Er	15.1	6.75	9.71	13.6	11.4	11.9	4.84	6.5	3.59
Tm	2.26	1.18	1.66	2.22	1.83	1.87	0.88	0.83	0.55
Yb	14.7	8.23	11.8	15.5	12.7	12.6	4.54	5.13	3.89
Lu	2.03	1.19	1.8	2.17	1.84	1.82	0.68	0.78	0.54
Hf	14.1	14.1	4.79	15.8	15	12.5	5.84	7.41	2.81
Ta	<0.006	1.57	0.77	1.45	<0.006	0.56	3.39	0.87	1.28
Tl	1.2	2.32		1.32	1.02	1.13			3.97
Bi	0.61	0.71		1.17	0.35	0.29			0.14
Th	31.7	23.7	44.3	41.6	39.1	19.2	12	10.8	12.5
U	8.36	6.03		16.4	15.3	4.74			2.72

Major elements are reported in weight percent and traces in ppm. Majors determined by AAS or XRF (fused bead), trace elements Sc - Pb (plus S & Cl) determined by XRF (pressed pellet) and trace elements Li - U determined by ICP-MS using conventional HF-HNO_3 or Na_2O_2 sinter dissolutions. F values from Teng (1974). Values less than limit of detection (LOD) reported as <LOD. Blanks indicate that the element was not analyzed by the analytical method used. Abbreviations: AA - AAS; XM - XRF (majors); XT - XRF (traces); IH - ICP-MS (HF/HNO_3); IN - ICP-MS (Na_2O_2).

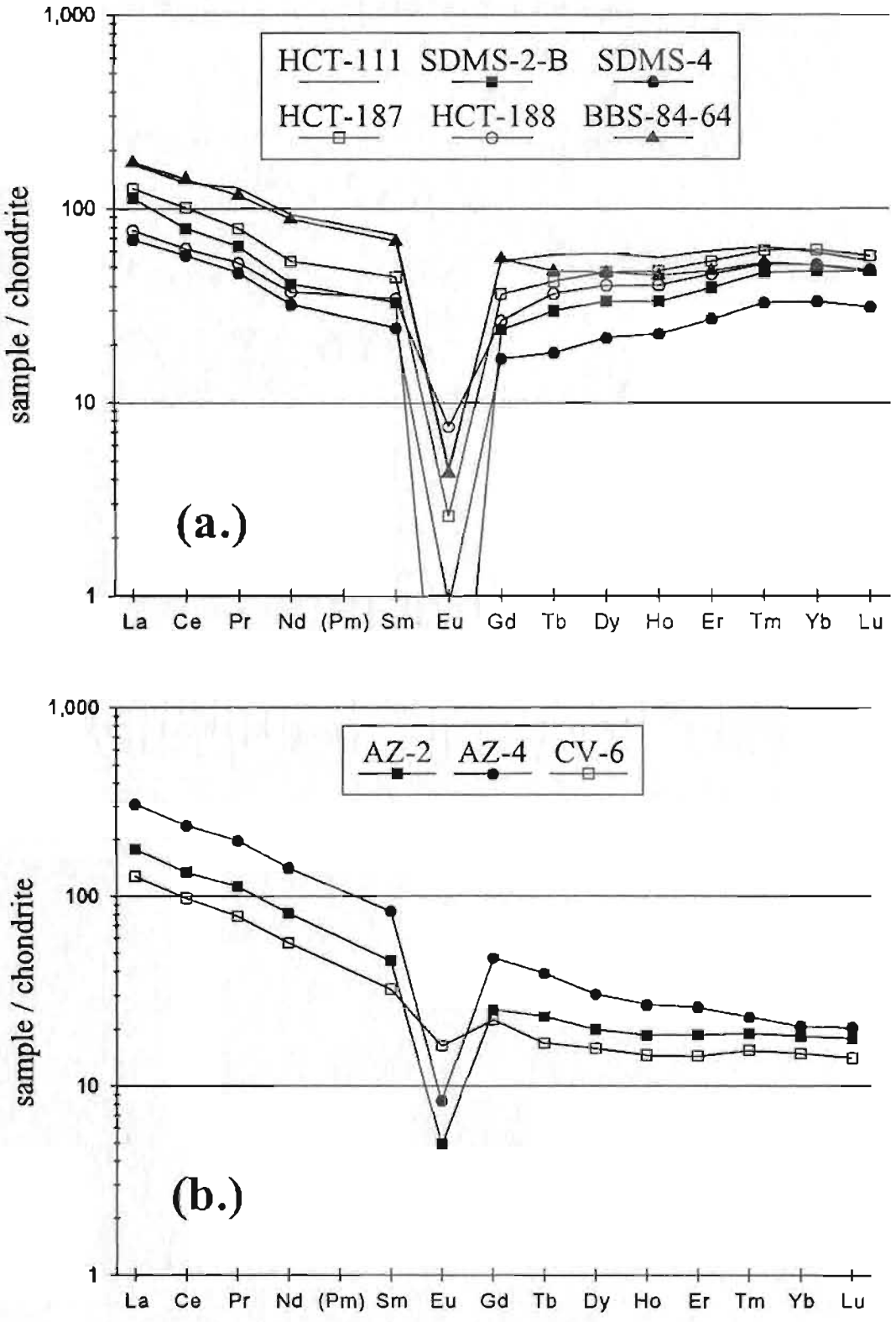

Figure 2.6.3. Chondrite normalized REE patterns for samples from (a) relatively unaltered St. Lawrence Granite and related rocks and (b) variably altered granite and contact metamorphosed sediment (CV-6). Chondrite normalizing values from Taylor and McLennan (1985).

granite. This effect is strongest in sample HCT-188 which is characterized by lower REE concentrations than HCT-187, especially in the LREE, as well sample HCT-187 displays a stronger negative Eu anomaly than sample HCT-188. The normalized REE patterns in these samples have a distinctive, moderately developed V-shape, characterized by lowest values in the MREE, near Gd (excluding Eu), and increasing towards La and Lu, with a stronger increase in the LREE.

Samples SDMS-2-B and SDMS-4, from the 'Lawn Lobe' of the St. Lawrence Granite, display REE patterns (figure 2.6.3a) more closely resembling those of the porphyry dykes than those of the 'typical' granite. These samples display the characteristic V-shape as seen in the porphyry dykes as well as similar minor inflections (or negative anomalies) at Nd and Ho. Sample SDMS-2-B, from near the margin of the mineralized vein, displays a similar shaped, but enriched, normalized REE pattern compared to the unaltered granite (SDMS-4), which has $\sum$ REE = 149 ppm, the lowest REE concentration (especially HREE) of the unaltered granites.

More intense fluid-rock interaction is represented by altered granite samples AZ-2 and AZ-4 from a zone of sericitic alteration with Mo-Cu mineralization. The chondrite normalized REE patterns (figure 2.6.3b) of the altered granite show a gradual decrease from La to Lu (La_N/Yb_N = 10 to 15) and the typical, but weaker negative Eu anomaly (Eu/Eu^* ~ 0.14). The most highly altered sample (AZ-4) shows a marked LREE enrichment and HREE depletion compared to the 'typical' granite sample, while the less altered sample from the same exposure (AZ-2) has La-Nd and Eu concentrations similar to the 'typical' granite but displays a steady decrease from Sm to Lu.

Sample CV-6, a fine grained metasediment from near the granite contact, displays a chondrite normalized pattern (figure 2.6.3b) with LREE concentrations similar to the granite, or granitic porphyry, but with significantly lower HREE concentrations (La_N/Yb_N = 8.6) and only a comparatively slight negative Eu-anomaly (Eu/Eu* = 0.6). When normalized to average upper continental crust (Taylor and McLennan, 1985), the metasediment displays a flat pattern (figure 2.6.4) less than twice the average upper crustal REE concentration. The granite and porphyry (HCT-111 and HCT-187) display enriched (especially HREE) patterns compared to upper crust. The 'Lawn Lobe' of the granite displays near upper crustal abundances of LREE but is progressively enriched in MREE-HREE. The altered granite (AZ-2) displays a relatively flat normalized REE

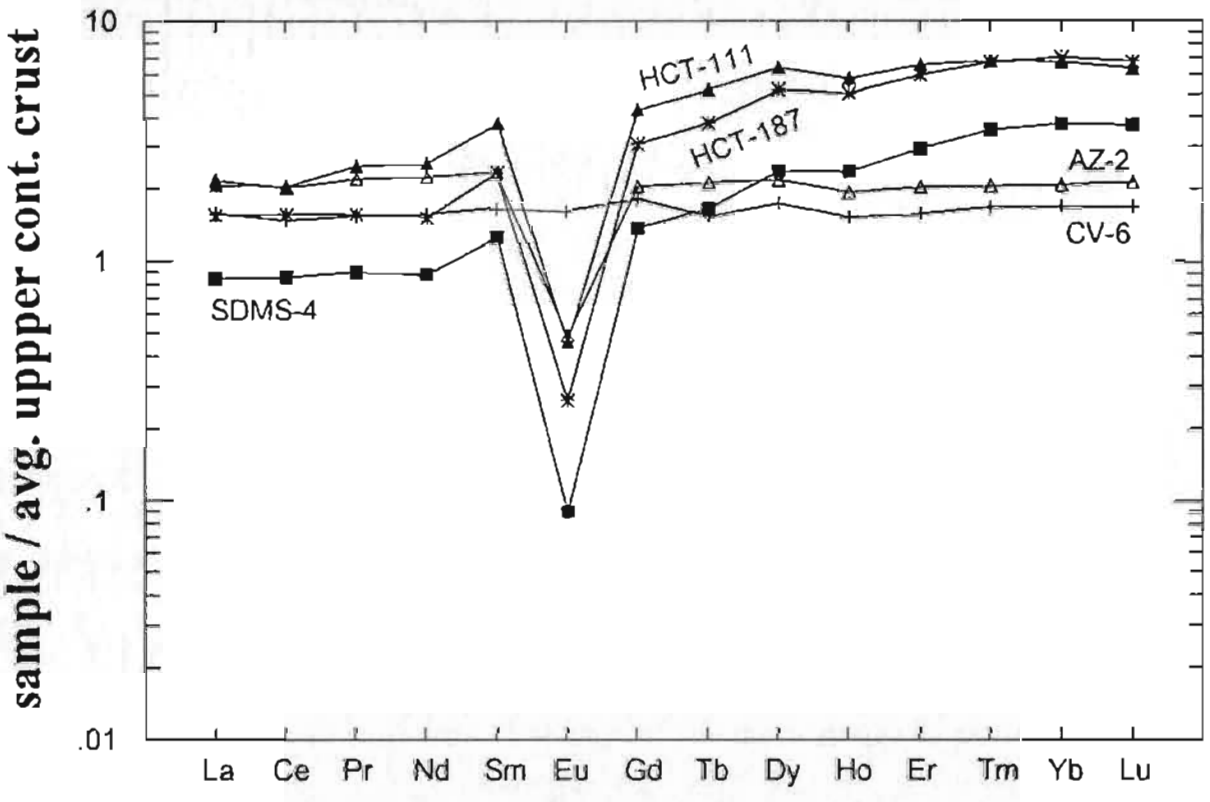

Figure 2.6.4 Rare earth elements in granites and metasediment from the St. Lawrence area normalized to average upper crust. Normalization values from Taylor and McLennan (1985).

pattern parallel that of the sediment. All the granitic samples display a negative Eu anomaly but this anomaly is absent in the metasediment. Both the metasediment and altered granite sample AZ-2 are from the same granite-sediment contact zone.

2.6.4 Local Geochemical Variation

Previous studies of the St. Lawrence Granite only involved reconnaissance mapping and sampling of the pluton as a whole and, consequently, no separate phases have been documented within the pluton. Although the marginal contacts of the pluton are well defined and separate intrusive phases have been noted (Teng, 1974), very little is known about the spatial relationships of these phases, except that they are more prevalent near the granite contact. The previous sampling program (Teng, 1974) was not conducted on a regular grid pattern, was restricted to a number of widely spaced traverses across the pluton, and was heavily biased toward coastal and road exposures.

To evaluate local geochemical variability within the pluton, the database was subdivided on the basis of 10 quasi-geological (primarily geographical), largely spatial subdivisions. These subdivisions are: the Little St. Lawrence area (LSL), near the southeast corner of the pluton; the St. Lawrence Harbour area (SLH), west of LSL in and around the town; the Red Head area (RH) in the southeast part of the mine area exposures; the Hare's Ears area (HE) in the central part of the mine area; the Chamber Point area (CP), the westernmost portion of the mine area near the granite contact; the Grebe's Nest Dykes (GND), quartz-feldspar porphyry granitic dykes west of the mine area; the Little Lawn Harbour (LLH) which probably represents the exposed top of the granite between St. Lawrence and Lawn; the Lawn Lobe (LL), the southwestern corner of the pluton; the

Mount Margaret area (MM), north of LSL; and the Burnt Woods Hill area (BWH), north of SLH.

Of these subdivisions, only the Grebe's Nest Dykes (GND) is geologically distinct, representing porphyritic granitic dykes which intrude both the main granite body and its country rocks. The Lawn Lobe (LL) is characterized by a coarse grained pink granite which appears to contain a higher concentration of mafic minerals than the average St. Lawrence Granite. The "mine area" subdivisions (RH, HE and CP) are characterized by containing the heaviest concentration of fluorite veins and showings in the area. The other subdivisions are based almost entirely on the geographic distribution of the granite exposures for which sample analyses were available.

The average values for each subdivision given in Table 2.6.3, indicates that there is very little spatial variability in major element (and most trace elements) chemical composition throughout the pluton. The plot of the subdivisions in figure 2.6.5 graphically displays the variation with regard to the 'Average St. Lawrence Granite' composition. Most of the granite samples from the vicinity of the fluorspar mining area (figure 2.6.5a) show little variation from the average composition, which is not unexpected since the majority of the samples were taken from this area. The most variable unit within this grouping is the Chamber Point (CP) area which displays moderate depletions in Be, Th, U and Nb compared to the average.

A normalized plot of the subdivisions from outlying parts of the pluton and the porphyry dykes and sills are shown in figure 2.6.5b. These units show much more variability, with the most notable being the lower Zr and Ce concentrations in the GND and the LL subdivisions (< 300 ppm Zr compared to > 500 ppm Zr in other subdivisions). As

well, the Lawn Lobe (LL) is characterized by an enrichment in Li, Ba and Cr relative to the average granite, while the Grebes Nest dykes (GND) show an enrichment in Sr and Cu.

Table 2.6.3 The St. Lawrence Granite Geochemistry subdivided into spatially distinct subdivisions (for explanation of subdivisions, see text).

n =	*89*	*13*	*5*	*14*	*15*	*9*	*12*	*12*	*3*	*6*	*9*
Group	Mean	RH	BWH	SLH	CP	HE	MM	LSL	LLH	LL	GND
SiO2	77	76	76	77	77	77	77	77	78	78	77
TiO2	0.12	0.12	0.14	0.12	0.14	0.13	0.14	0.12	0.06	0.06	0.09
Al2O3	11	13	11	11	11	11	11	11	12	11	12
Fe2O3	1.3	0.8	1.4	1.1	1.5	2	1.5	1.3	0.4	0.8	0.6
FeO	0.56	0.67	0.88	0.48	0.51	0.42	0.51	0.56	0.47	0.63	0.62
MnO	0.02	0.03	0.05	0.02	0.02	0.01	0.03	0.02	0.01	0.02	0.02
MgO	0.12	0.14	0.13	0.13	0.12	0.1	0.14	0.12	0.13	0.06	0.12
CaO	0.39	0.66	0.17	0.43	0.39	0.45	0.17	0.48	0.19	0.15	0.34
Na2O	3.5	3.6	3.6	3.4	3.3	3.7	3.6	3.3	3.9	3.8	4.5
K2O	4.7	4.7	4.7	5	5.1	4.4	4.8	4.7	4.6	4.2	3.4
P2O5	0.01	0.02	0.01	0.02	0.01	0.02	0.01	0.01	0.01	0.02	0.01
LOI	0.85	1.1	0.78	0.81	0.83	0.81	0.77	0.92	0.6	0.61	0.93
Total	99.5	99.4	99.4	99.3	99.6	99.8	99.9	99.5	99.6	99.4	99.7
Li	22	30	58	19	18	21	16	14	7	55	17
Be	8	9	10	9	5	10	8	8	10	12	11
F	1,271	1,735	1,041	1,704	1,382	2,100	354	627	710	2,120	301
V	2	1	1	2	1	1	2	2	1	2	2
Cr	2	1	1	1	1	1	2	2	1	7	1
Ni	2	2	1	1	2	1	2	2	1	2	2
Cu	7	5	4	6	9	7	7	7	13	10	28
Zn	57	72	137	39	38	29	70	56	16	83	42
Ga	29	31	29	30	25	30	30	29	30	26	27
Rb	288	301	305	314	252	271	263	279	261	375	216
Sr	9	11	5	8	8	13	7	11	10	7	18
Y	104	130	139	93	83	104	114	100	92	89	80
Zr	618	630	749	524	572	699	642	809	554	295	266
Nb	92	109	97	88	58	107	87	117	91	91	68
Mo	5	5	6	5	4	6	5	6	4	6	6
Ba	66	62	31	55	70	58	50	79	62	143	72
La	60	63	78	58	59	56	62	61	42	50	36
Ce	143	153	178	132	135	139	158	147	104	81	86
Pb	33	21	48	20	23	20	46	53	38	57	52
Th	33	35	34	37	20	32	30	41	26	44	11
U	8	10	9	8	6	7	8	10	10	11	10
Ga/Al	4.9	5.3	4.9	5	4.2	5.2	4.9	5	4.9	4.4	4.2
Rb/Sr	45	38	64	41	35	37	46	39	49	99	16
Rb/Ba	6	7	10	6	4	6	6	6	5	11	4
A1	0.98	0.98	0.99	0.98	0.98	0.99	0.97	0.98	0.99	0.96	0.93

Data is primarily from Nfld. Dept. of Mines and Energy (Kerr, unpubl data, 1992) with contributions of selected samples from the present study. This table is compiled from the same data set as Table 2.6.1 with the addition of 9 extra dyke samples (GND).

- higher concentrations of highly charged cations such as Nb, Ga, Zr, Y, REE (except Eu), Pb and Zn
- higher concentrations of Sn, W and Mo
- lower concentrations of the transition elements V, Ni, Co and Cr
- higher F and Cl abundances (usually F > 1000 ppm)

As established in the earlier discussion on geochemistry, the St. Lawrence Granite has most of the characteristics which have been used to distinguish A-type granites from other granite types. The granite is strongly alkaline to mildly peralkaline, as indicated by Shand's index (figure 2.7.1), is not deformed, and can be considered anorogenic since it has not been directly linked to any specific orogenic event.

Whalen et al., (1987) compared geochemical analyses of 148 samples from A-type granites with 1569 analysis from I- and S-type granites and developed effective

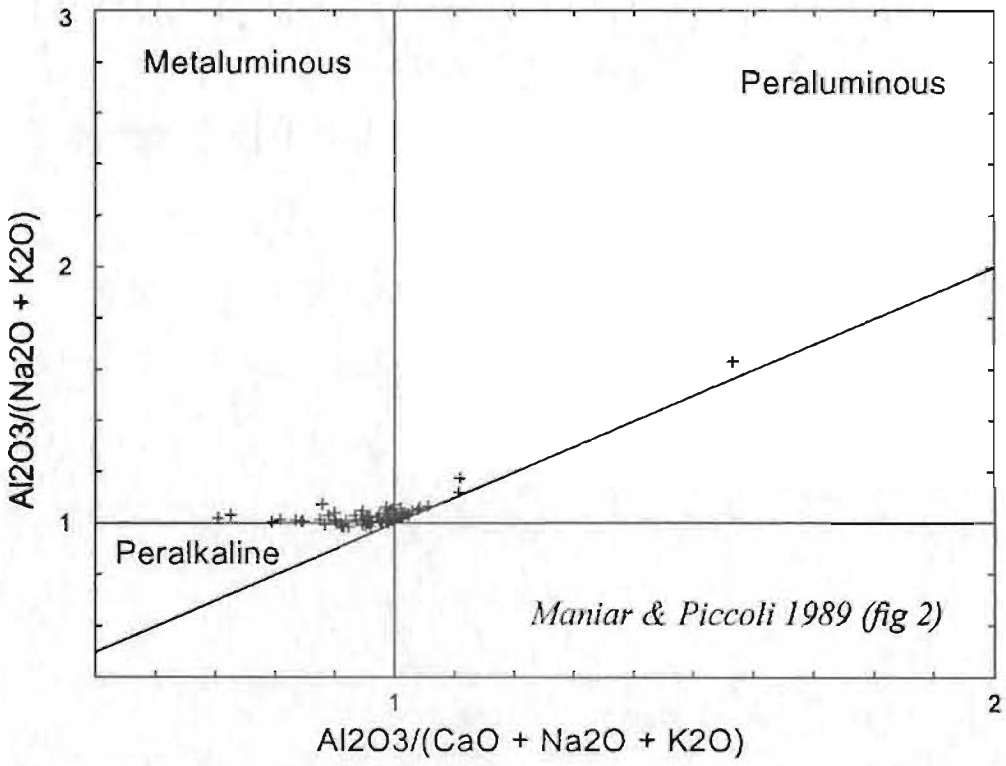

Figure 2.7.1 St. Lawrence Granite samples plotted on 'Shand's Index' showing the strongly alkaline to mildly peralkaline nature of the granite.

schemes. Presentation of all these various schemes is beyond the scope of the present study, therefore the basics of what are considered the most applicable classification schemes will be introduced and discussed in terms of the St. Lawrence Granite.

Chappell and White (1974) proposed a genetic classification scheme which subdivided granites into two basic types, those derived from a sedimentary protolith (S-type) and those derived from an igneous protolith (I-type). From the I-type granites, subgroups were defined based on specialized characteristics of some granites. Two such subgroups distinguished from other I-type granites are those, at least partially, derived from dehydrated continental crust (A-type: Loiselle and Wones, 1979; Collins et al., 1982) and those derived directly from melting of subducted oceanic crust or overlying mantle (M-type: White 1979; Pitcher 1983; Whalen 1985).

The A-type granites can be distinguished from other granite types by using the mineralogical/chemical classification presented by Collins et al. (1982). This was extended by Whalen et al. (1987) to include an expanded set of trace elements. In summary, the major mineralogical characteristics of A-type granites are:

- the feldspar is dominantly alkali feldspar often with albite-orthoclase solid solutions or intergrowths
- micrographic intergrowths of quartz and alkali feldspar are common
- annite-rich biotites and/or alkali amphiboles occur and are usually intimately associated with fluorite
- mafic minerals, when present, occur late in the crystallization history, often as interstitial grains or clots between alkali feldspar and quartz

The major chemical characteristics of A-type, compared to other granite types are:

- higher SiO_2 , Na_2O+K_2O content, and Fe/Mg ratio
- lower contents of CaO, Ba and Sr

- higher concentrations of highly charged cations such as Nb, Ga, Zr, Y, REE (except Eu), Pb and Zn
- higher concentrations of Sn, W and Mo
- lower concentrations of the transition elements V, Ni, Co and Cr
- higher F and Cl abundances (usually F > 1000 ppm)

As established in the earlier discussion on geochemistry, the St. Lawrence Granite has most of the characteristics which have been used to distinguish A-type granites from other granite types. The granite is strongly alkaline to mildly peralkaline, as indicated by Shand's index (figure 2.7.1), is not deformed, and can be considered anorogenic since it has not been directly linked to any specific orogenic event.

Whalen et al., (1987) compared geochemical analyses of 148 samples from A-type granites with 1569 analysis from I- and S-type granites and developed effective

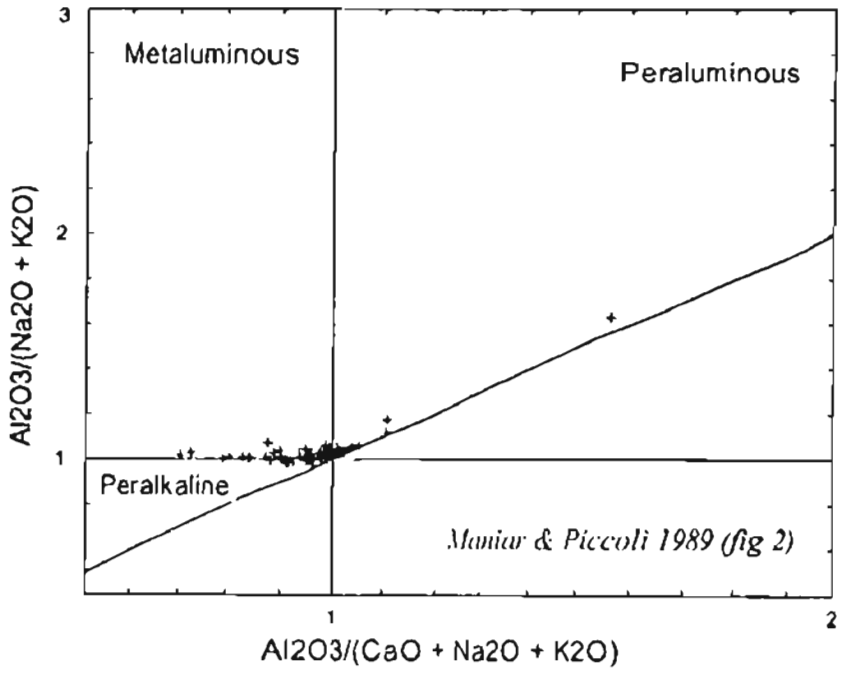

Figure 2.7.1 St. Lawrence Granite samples plotted on 'Shand's Index' showing the strongly alkaline to mildly peralkaline nature of the granite.

discrimination diagrams utilizing plots of Ga/Al (x 10,000) against certain major and trace elements to clearly define separate fields for A-type versus I-, S- and M-type granites. The major and trace element geochemical data for the St. Lawrence granite were used to produce a series of these discrimination diagrams (figure 2.7.2a-f). All of the diagrams show that the St. Lawrence Granite compositions plot well within the field of A-type granites and, in most instances, the analyses form tight clusters. The plots displaying the most scatter involve the elements Ca and Zn which may be artificially enriched in some samples due to widespread effects of hydrothermal activity. The discrepancy between the FeO*/MgO ratios in the M & E data (Kerr, unpubl. data, 1992) and the data from this study (figure 2.7.2b) may be due to inconsistency in MgO analysis between analytical laboratories and/or methods. Regardless, both data sets plot well within the field for A-type granites.

Pearce et al. (1984) proposed a tectonic classification of granites based on discrimination diagrams using Rb, Y, Nb, Yb and Ta data. Plots of the St. Lawrence data on their Rb vs. Y+Nb and Y vs. Nb diagrams show that most of the samples can be classified as within-plate (WPG) type granites (figure 2.7.3a,b). The St. Lawrence samples plot in a field similar to that of the Nigeria ring-complex granite suite for which Pearce et al. (1984) suggest a petrogenetic origin based on an enriched mantle source evolving with combined assimilation-fractionation at intermediate to acid compositions. Unlike the St. Lawrence Granite this complex contains a diverse array of granitoids from peralkaline granite and volcanics to syenites, gabbros and mafic volcanic equivalents (Bowden and Turner, 1974) suggesting a more direct involvement of mantle derived magma.

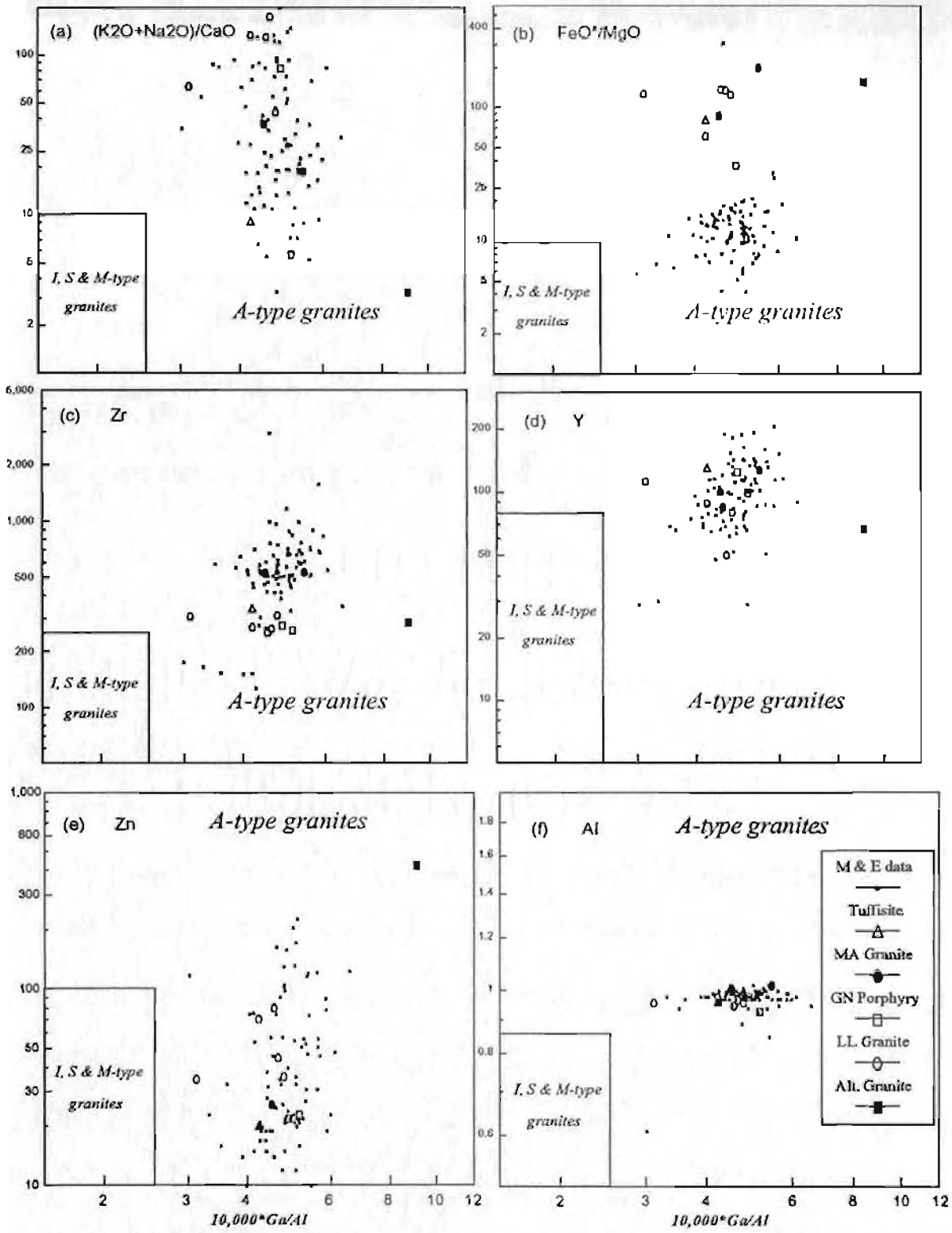

Figure 2.7.2 Plots of the St. Lawrence Granite samples on selected A-type granite discrimination diagrams from Whalen et al., 1987. Plots are of 10000*Ga/Al versus: (a) (K_2O+Na_2O)/CaO: (b) FeO*/MgO; (c) Zr; (d) Y, (e) Zn and (f) Al. Samples from this study designated by larger symbols. Abbrev.: Nfld. Dept. of Mines and Energy (M & E); St. Lawrence mine area (MA); Grebe's Nest (GN); Lawn Lobe (LL); (Al) agpaitic index (Na+K/Al).

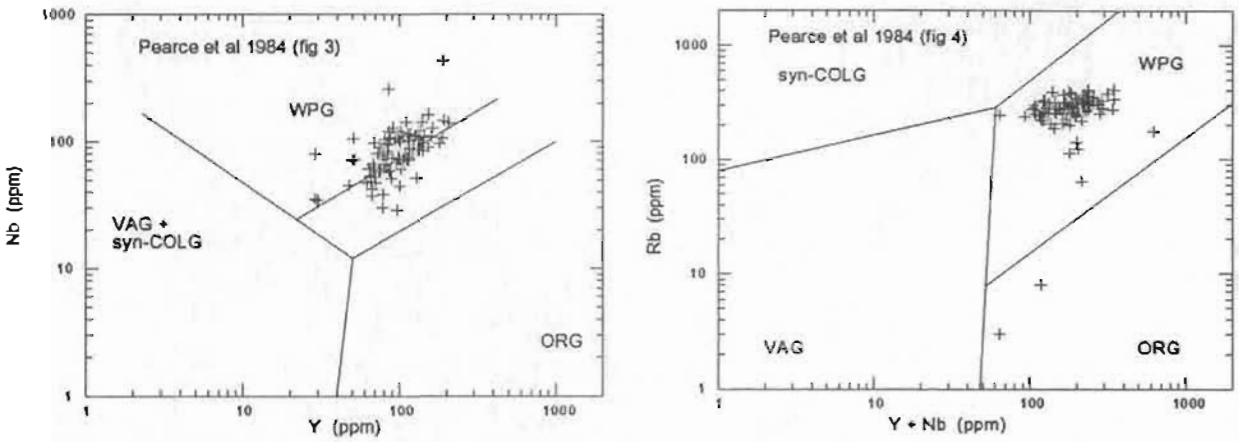

Figure 2.7.3 Plots of St. Lawrence Granite samples on the Nb-Y and Rb-(Y+Nb) tectonic environment discrimination diagrams of Pearce et al., 1984. The fields are for syn-collision granites (syn-COLG), volcanic arc granites (VAG), within plate granites (WPG) and ocean ridge granites (ORG). Post-collision granites can plot in all but the ORG field.

Considering their contrasting tectonic settings, Batchelor and Bowden (1985) suggested that A-type granites should be further subdivided on the basis of either late-orogenic association of short duration or alkaline-peralkaline anorogenic suites of episodically emplaced plutons over a long time interval, such as those of Niger-Nigeria (Bowden and Turner, 1874). They do not consider post-orogenic alkaline magmatism as a continuation of the compressional (orogenic) cycle, but rather the result of a relaxation after plate collision which would generate tensional rifts and give rise to alkaline magmas. Batchelor and Bowden (1985) suggested using the multicationic plot of de la Roch et al. (1980) to discriminate between tectono-magmatic associations and to show that there is a systematic change through an orogenic cycle which ultimately leads to the development of alkaline magmas. The St. Lawrence Granite samples, plotted on the multicationic diagram (figure 2.7.4), form an enlongate narrow cluster in the field of post-orogenic granites (7). Most of the R2 scatter observed in some of these samples can be attributed to Ca enrichment in response to hydrothermal alteration. This is demonstrated in figure 2.7.4 by

the variably altered granite samples (solid squares), from the Alteration Zone at Chamber's Point, which have significantly higher R2 values.

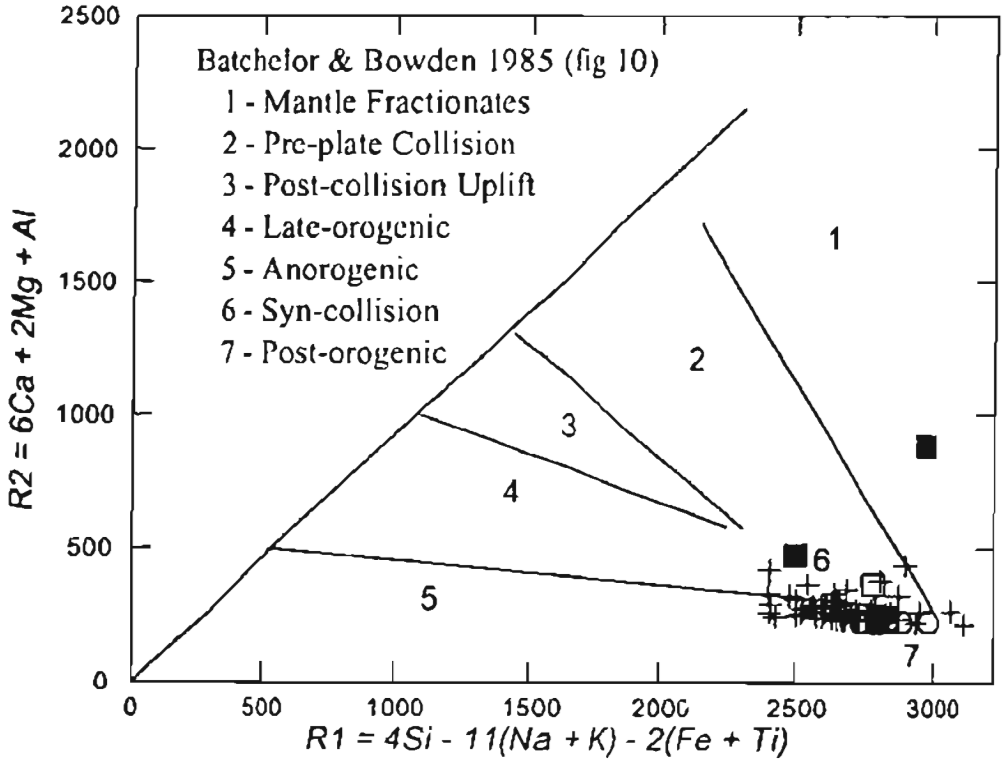

Figure 2.7.4 Plot of St. Lawrence Granite compositions on the de la Roche R1-R2 multicationic diagram showing Batchelor and Bowden's granitoid associations (1-7). Symbols as in figure 2.7.2.

Maniar and Piccoli (1989) also developed a systematic approach, using major element analyses to discriminate between granites from different tectonic environments. When plotted on the various discrimination plots proposed by Maniar and Piccoli (1989), the St. Lawrence samples clearly point to the classification of the granite as 'continental epeirogenic uplift granite' (CEUG). CEUG are defined as granitoid rock associated with continental areas that have experienced epeirogenic crustal uplift with no subsequent

development into a rift; the Younger Granites of Niger-Nigeria are an example. Maniar and Piccoli (1989) attribute such uplift to hot-spot activity or an aborted rifting event.

The homogeneity of the St. Lawrence Granite, combined with the lack evidence for extensive related episodic plutonism and the narrow range displayed in figure 2.7.4, all suggest that the granite can be considered to be of late-orogenic origin. This supports emplacement in a tensional regime that was developed in response to crustal relaxation after the compressional Silurian orogenic event defined by Dunning et al. (1990).

2.8 Petrogenesis

The St. Lawrence Granite and associated volcanic rocks are composed essentially of quartz, orthoclase and albite with very minor amounts of mafic minerals or calcic plagioclase. They are characterized by modal aegirine and riebeckite, alkaline to peralkaline compositions and high concentrations of trace elements such as Rb, F, Nb and Zr and low K/Rb ratios, which result from advanced differentiation and volatile enrichment (Teng, 1974; Strong et al., 1974; Teng and Strong, 1976). The elevated $^{87}Sr/^{86}Sr$ initial ratio of either 0.722 (Bell and Blenkinsop, 1977) or 0.709 (Fryer and Strong, pers. comm., circa 1984) suggests at least some degree of continental crustal involvement in their origin. Teng and Strong (1976) suggested an origin by melting of continental crust and subsequent plagioclase fractionation from the parental melt.

The St. Lawrence Granite magma is considered by Teng and Strong (1974) to have been a relatively low-P_{water}, high-T hypersolvus granite magma. They cite the presence of perthite as evidence that the granite cooled both too rapidly for complete unmixing, and too slowly for homogeneous quenching in the absence of water vapour. The occurrence of

tuffisites (gas breccias) provide additional evidence of a shallow depth of emplacement. The rarity of hydrous minerals such as biotite and amphibole, and the absence of significant amounts of pegmatite or aplite (except for minor veins and dykes), also led them to suggest that the melt was relatively anhydrous. They cited field evidence that the granite produced abundant thermal, but minimal metasomatic effects, on the country rocks as indicating a relatively hot but anhydrous melt.

Deeply embayed quartz phenocrysts and micrographic intergrowths of quartz and orthoclase with granophyric textures, noted in the marginal phases of the granite, have been attributed to quenching due to a sudden release of pressure (Teng, 1974). The abundance of tuffisites and breccia textures observed in the fluorspar veins lend support to such an explosive release of volatiles during crystallization of the granite. The bulk compositions of the St. Lawrence Granite plot near the ternary minimum at 50 MPa in the Q-Or-Ab-H2O system, suggesting crystallization under very shallow conditions, in agreement with field evidence (Strong, et. al., 1978).

From the St Lawrence Granite geochemical data, a ternary plot of normative Q:Ab:Or values (figure 2.8.1) was constructed. The diagram also includes the 2 to 0.5 kbar cotectic lines and 10 to 0.5 kbar ternary minima for a fluorine-free system (Luth et al., 1964: Tuttle and Bowen, 1958), and the trend of 1 kbar minima for fluorine-rich melts for varying F concentrations (Manning, 1982). The majority of the St. Lawrence Granite samples plot in a well defined field centred near the ternary minimum between the 0.5 to 1 kbar cotectic lines. This is in agreement with the findings of Teng and Strong (1976) who placed the centre of the field at the ternary cotectic at 0.5 kb for 80% of the samples studied. This would indicate that the P_{water} was no more than 2 kb allowing for maximum

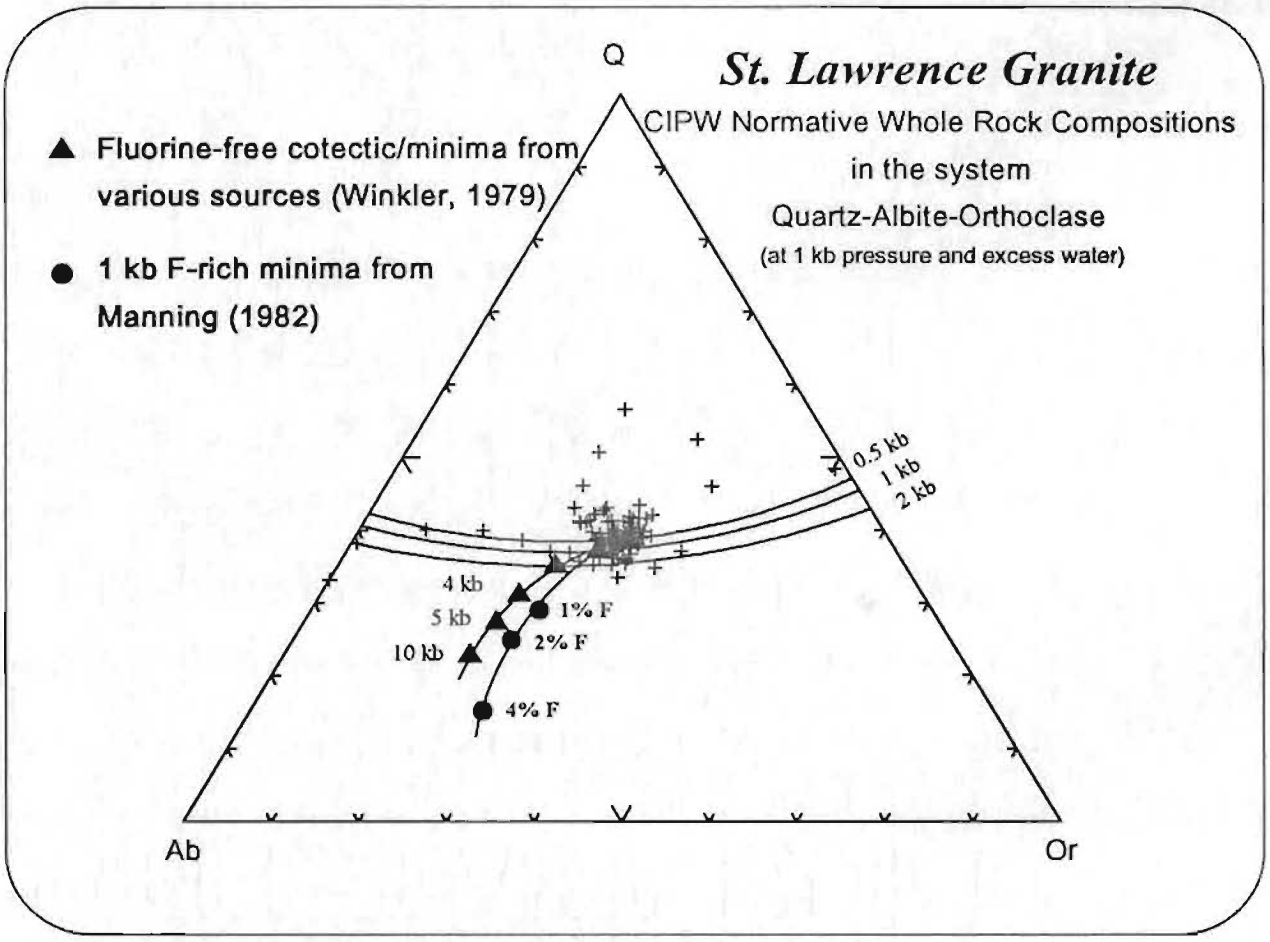

Figure 2.8.1 Normative Q-Ab-Or (wt%) in samples from whole rock analysis of the St. Lawrence Granite. Cotectic curves and minima (symbols) show the experimental data for the effects of differing water pressure (from Winkler, 1979) and F content (Manning, 1982) in the melt.

scatter. The P_{water} was probably much less (1 to 0.5 kbar) since, as shown by Manning (1982), the addition of only a minor amount of F to the melt would tend to expand the quartz field and drive the ternary minima along the F-rich trend. Ebadi and Johannes (1991) have also shown that if the melt is under-saturated with respect to water the Or/Ab-ratio would increase with decreasing water activity . Since the granite melt is expected to initially be relatively dry, but becoming closer to water saturation and more F enriched with progressive crystallization, both of these factors would contribute to the increased scatter of the data.

Since most of the St. Lawrence Granite data plot in a field centred near the 0.5 kbar ternary minimum, the temperature of crystallization of the granitic magma would be at approximately 770°C assuming water saturation (Winkler, 1979). Experimental studies on peralkaline melts (Bailey, et al., 1974), showing pantellerite minima at 850-830°C at 0.2-0.1 kbar for anhydrous melts, led Teng and Strong (1976) to suggest that the crystallization temperature of the relatively anhydrous St. Lawrence Granite may have been that high.

The lack of normative compositions along the trace of F-rich minima (figure 2.8.1) suggests that the actual F content of the melt, from which the batholith formed, may have been as low as, or considerably lower than, the average F content (0.13%) of the St. Lawrence Granite as indicated from samples of surface exposures. These elevated F values (up to 0.67%) may actually represent the addition of secondary fluorine through hydrothermal alteration of the early granite, by late-stage F-rich fluid evolving from the solidifying core of the pluton, rather than elevated F concentrations in the initial granitic melt. Such a process has been proposed (Manning, 1982) to account for some of the fluorite-bearing granites of Cornwall. Another possible explanation is that the fluorine content of the melt may have been buffered to lower concentrations by the crystallization of fluorine-bearing phases from the melt. Both processes may have been involved since fluorite is known to be associated with "chloritized" biotite, and occurs as a discrete accessory phase within the granite as well as lining miarolitic cavities in the granite.

Whitney (1988) states that the presence of rounded or embayed quartz phenocrysts or crystals in granitic rocks or volcanic equivalents suggests isothermal decompression in the water-vapour-undersaturated region, a phenomenon which should not occur for most

granitic compositions under vapour-saturated conditions. The presence of deeply embayed quartz phenocrysts, quartz-orthoclase granophyric intergrowths and tuffisites in the St. Lawrence Granite suggest such vapour-absent conditions.

In contrasting the crystallization history of vapour-absent and vapour-saturated granites, Whitney (1988) discussed the crystallization of the Cape Anne Granite, an alkaline granite very similar in composition to the St. Lawrence Granite. Whitney (1988) states that "if only 2% water is present, however, crystallization starts well above 800°C (probably above 900°C by comparison with other data) and continues to 680°C. At 2 kb this process is nearly constant until the composition is about 75% crystalline at 685°C, at which point the composition becomes vapor saturated and finishes crystallization within 10°C". In the case of the St. Lawrence Granite, it is probably this final 25% of vapour-saturated crystallizing magma that evolved the F-rich mineralizing fluids responsible for the fluorite mineralization. Therefore, the bulk of the exposed pluton represents the coarse-grained, slowly crystallized, high temperature and vapour-undersaturated phase of the pluton. The late-stage magma may be more closely represented by aplitic and porphyritic dykes which locally cuthe main granite body.

2.9 Granite-related Mineralization

The most economically significant form of granite-related mineralization known to occur in the area are the fluorspar veins. These veins occur almost entirely in the granite and are considered genetically related to it (Kauffman, 1936; Van Alstine, 1944, 1948; Williamson, 1956; Teng, 1974; Teng and Strong, 1976; Strong et al., 1984; Collins, 1984).

Other minerals such as galena, sphalerite, chalcopyrite and barite occur in the fluorspar veins but none reach economically exploitable concentrations or size.

Various lake and stream sediment surveys conducted over the St. Lawrence Granite as part of various government and industry programmes have recorded widespread highly anomalous uranium values. In spite of intensive exploration programmes, including diamond drilling, the only reported uranium (pitchblende) mineralization occurs in a road-cut at the north end of Little Lawn Harbour, at the contact between a porphyritic offshoot of the St. Lawrence Granite and black shales of the Inlet Group (Strong et al., 1978).

Widely distributed anomalous Mo and Sn values have been reported in various industry soil surveys over the granite, especially north of the community of Lawn. Molybdenite mineralization occurs in a micro-pegmatitic quartz vein and as disseminations in the granite near the 'Second Dam' north of Lawn and in an sericitized granite (with chalcopyrite) near Chamber Point.

Numerous minor sulphide bnearing veins occurrences have been reported in both the granite and its country rock, usually associated with fluorite or calcite. The most significant are at Mine Cove and Little Salt Cove where high silver values have been reported associated with galena-bearing fluorite veins. Numerous pyrite-bearing gossen zones occur in the metasediments adjacent to the granite contact, but no significant base or precious metal values have been reported from them.

3 The St. Lawrence Fluorspar Deposit

3.1 Introduction

The first official documentation of fluorspar in the St. Lawrence area was made by Jukes, who wrote in his general report for the Geological Survey of Newfoundland for the years 1839 to 1840:

> *"On the western side of the Harbour of Great St. Lawrence, a small vein or string was seen in the sienite, containing crystals of galena or lead ore, and fluate of lime; they were trifling and did not promise to lead to anything more abundant." Jukes (1843, p. 154).*

In the late 1800's, Murray and Howley (1881) visited a fluorite-galena prospect in Little Lawn (probably the Mine Cove Vein), and in his report on the mineral statistics and mines of Newfoundland for the year 1900, Howley (1917) noted the presence of fluorite at Lawn.

More than 40 individual fluorite veins or vein systems are known to occur in the St. Lawrence area, but less than half of these have proven to be of economic proportions. Mining began on the St. Lawrence fluorspar veins in 1933 and was more or less continuous since then, until, with a total of 3.43 million tonnes of 70-95% CaF_2 concentrates shipped, the mines closed on February 1, 1978. The St. Lawrence deposits constitute a major high-grade source by world standards, and were the only major

Canadian producer until their closure (Tilsley, 1984). The largest three of the known veins (Blue Beach, Director, and Tarefare) still contain close to 8 million tonnes of 'possible' reserves with a cut-off grade of 35% CaF_2 down to a maximum depth of 300 metres and an average grade of 45-48% CaF_2 (Hodge et al., 1977).

In 1983, five years after the mines closed, the mineral rights reverted to the crown and, in 1984, the Newfoundland provincial and Canadian federal governments heavily subsidized the re-activation of the St. Lawrence mine. The parent company Minworth Limited of the U.K., incorporated a subsidiary, St. Lawrence Fluorspar Limited, which started surface and underground development of the Blue Beach North Mine in 1985. Market conditions and problems with underground development forced this company to close the mines again by 1990, after having produced approximately 500,000 tonnes of ore from the Blue Beach North Deposit and a number of small surface operations.

3.2 Geologic Setting of the Fluorspar Veins

3.2.1 Review of Previous Geological Studies

During 1935, Kauffman carried out reconnaissance mapping in an area north and east of St. Lawrence as part of a B.A. thesis at Princeton University (Kauffman, 1936). He recognized the intrusive nature of the St. Lawrence Granite and concluded that it was intruded at a relatively shallow depth (less than two miles) and enriched in volatiles. He also recognized that the granite exposed at St. Lawrence, and Lawn, to the west, were part of the same fluorite-bearing batholithic mass.

During the summers of 1939 and 1940, Van Alstine mapped an approximately 300 square mile map area around St. Lawrence for the Geological Survey of

Newfoundland (Van Alstine, 1939; 1944; 1948). Petrographic studies of the St. Lawrence Granite, found it to be an alaskite or alkali granite composed essentially of quartz, orthoclase and albite. Van Alstine (1948) considered the granite and the "*rhyolite*" porphyry to be almost contemporaneous and to have formed from a highly differentiated magma reservoir. He also stressed the epithermal nature of the fluorite veins and their close genetic link to the granitic magma.

During 1956, Williamson carried out detailed mapping of some forty distinct fluorspar veins and produced a comprehensive summary of the regional geology of the St. Lawrence Area which also supported a magmatic origin for the fluorite veins (Williamson, 1956). His work involved a detailed analysis of the structure of the area and the relationships between the regional structural patterns and the fluorspar veins.

In 1974, Teng completed a study of the geochemistry and petrology of the St. Lawrence granite, describing it as alkaline to peralkaline in composition and intruded and crystallized at shallow levels. He concluded that it was the hypersolvus relatively anhydrous high-temperature granitic magma that, during the final stages of cooling and crystallization, provided the source of the mineralizing fluids from which the fluorspar veins formed (Teng, 1974; Teng and Strong, 1976).

A mapping program was carried out on the southern Burin Peninsula, between 1974 and 1976, by Memorial University for the Newfoundland Department of Mines and Energy under the direction of Dr. D. F. Strong. This programme better defined the contacts and contact relationships of the granite, especially in the northeast portion. The mapping covered the Grand Bank (1M/4) and Lamaline (1L/13) NTS map sheets

(O'Brien, et al., 1977), as well as the Marystown (1M/3) and St. Lawrence (1L/14) sheets (Strong et al., 1978) at a scale of 1:50,000.

3.2.2 Distribution of the Fluorite Veins

Almost all the fluorite veins are found within the St. Lawrence granite or its related porphyry dikes, and all occur as open-space filling in tension fractures. These probably developed as a result of regional stress and contraction during cooling of the granite. Indications of fluorite veining are present throughout most of the granite batholith and, to a limited extent, in country rocks near the granite contact. Most of the larger, more continuous veins occur immediately west and north of the community of St. Lawrence. Two major groups of fluorite veins are recognized:

- The ***Northwest-Southeast Veins*** are generally lower grade and wider. They average about 7 metres in width (but locally attain widths up to 30 m) and grade approximately 70-65% CaF_2 content. The average strike varies from 160-135° azimuth. Examples are the Director, Tarefare and Blue Beach veins.

- The ***East-West Veins*** are generally higher grade and narrower. They average one metre or less in width and are characterized by 'acid grade' ore averaging 95% CaF_2. The average strike varies from 115-60° azimuth. Examples are the Lord and Lady Gulch, Iron Springs, and Canal veins.

No major veins are known to mutually intersect but subsidiary (or offshoot) veins are common, usually oriented sub-parallel the major veins. The veins range from a few hundred metres to more than 2 km long but, in many cases, their irregular form and dilution by wall rock prevent commercial grade ore from being available throughout their entire lengths.

3.2.3 Structural Relationships

The major structural trend preserved in the Cambrian-Precambrian rocks is at approximately 050° and is marked by repeated folding and low-angle thrust faults,

produced in response to regional northwest-southeast compression (Williamson, 1956). This compressional regime would have pre-dated the emplacement of the St. Lawrence Granite (circa. 394 Ma) and is Silurian in age (Dunning et al., 1990).

These earlier structures were later transected by normal (gravity) faulting, some of which were of major proportions (Williamson, 1956). These faults, trending between 020° to 010°, were produced in response to uplift and release of pressure following the earlier period of compression (Williamson, 1956). This period of uplift was followed, probably very closely, by the intrusion of the St. Lawrence Granite along predetermined zones of weakness provided by the large tensional fault structures. This is evidenced by the elongate nature of the granite, in a somewhat east of north direction, and the strong evidence for a sharp, steep, structurally controlled eastern contact. This structural regime is similar to that proposed by Batchelor and Bowden (1985) for post orogenic alkaline magmatism (group 7 in figure 2.13) like the St. Lawrence Granite. They state:

> *"Thus the place of post-orogenic alkaline magmatism within the orogenic cycle cannot be considered as a continuation of the compressional cycle, but may be viewed as the result of a relaxation effect after plate collision which would generate tensional rifts and give rise to alkaline magmas." (Batchelor and Bowden, 1985, p. 53).*

Such crustal scale faulting could provide the pressure release (and to a lesser extent, frictional heat) to trigger partial melting in the region of the lower crust or upper mantle. This distensional environment would favour the channelling of volatiles (Black et al., 1985; Bailey, 1978) and/or basaltic magmas (Clemens et al., 1986) from the upper mantle, generating A-type magmas by partial melting of depleted I-type source rocks (Clemens et al., 1986) or directly from mantle derived magmas by fractional

crystallization and varying degrees of assimilation of crustal rocks (Pearce et al., 1984; Irby, 1990, 1992).

Once in place, the granite body cooled, crystallized and contracted causing the development of tension and shear fractures. Williamson (1956) concludes that the prominent orientations of the fluorspar veins can be predicted or explained by structural interpretation. Since the granite is enlongate in a direction 010°, tension fractures would be developed perpendicular to this direction (at 100°), coincident with the 'east-west' trend of fluorspar veining (Williamson, 1956). Symmetrically disposed on either side of the direction (tension fractures), at angles related to the confining pressure, there would be developed two directions of minimum stress and maximum shear along which predominantly horizontal movement could take place (Williamson, 1956). One of these predicted directions (140°) is coincident with a relict tensional fracture direction from the earlier compressional regime, as well as the 'northwest-southeast' trend of the larger fluorspar veins (and the Grebe's Nest porphyry dykes). He also pointed out that at least two of the veins which do not conform to one of the two prominent trends, are coincident with the other predicted direction of maximum shear.

Regardless of whether the mode of origin of the structures responsible for the fluorspar veins was partially controlled by pre-existing tectonic regimes or is simply related to the cooling and contraction of the pluton, it is apparent that the fluorspar veins are indeed fissure-filling veins which were deposited largely in open fracture and/or fault structures and show evidence of continuous syn-depositional movement with episodic gas and tectonic brecciation. Slickensides, common on the vein and joint surfaces, generally

have a sub-horizontal plunge (Van Alstine, 1948) reflecting minor late horizontal adjustment in the waning stress regime.

3.3 Mineralogy and Texture of the Vein Mineralization

The fluorite, especially in the 'east-west' veins, is mostly massive and coarse grained, filling veins from wall to wall. The fluorite occurs in many colours such as green, white, yellow, blue, red, purple, colourless and rare black or very dark blue varieties. The colouration in fluorite is highly variable but several general trends related to colour have been noted by previous workers (Van Alstine, 1948; Williamson, 1956). These are:

- green fluorite is common in near-contact veins (e.g. Tarefare, Grebe's Nest, etc.)
- purple fluorite is 'early-stage' (i.e. associated with granite and early 'breccia-ore')
- red colouration is usually due to the presence of hematite inclusions

A prominent feature of the veins is the occurrence of large vugs which are commonly extensive either along the vein or vertically, some measuring up to 30 metres, and often lined with euhedral fluorite crystals, some up to 35 cm, along the edge. Cubic forms are more common than octahedra which are more abundant in veins occurring in the porphyry dykes and country rocks, (e.g. the Grebes Nest and Mine Cove veins). Octahedral, growth-zoned, coarse grained, green fluorite from the Grebe's Nest and Anchor Drogue Veins display a platy or fibrous texture perpendicular to the growth-zoning. This texture was also noted by Van Alstine (1948) and Williamson (1956).

Quartz forms the most abundant gangue mineral, occurring in material locally known as "blastonite", consisting essentially of brecciated fluorite cemented by a mixture of microcrystalline quartz and fluorite, that probably formed as a result of both gas- and

fault-brecciation. Fluorite-free quartz veins are rare, but in some veins blastonite is reported to grade into zones of white, coarse grained, conchoidally fracturing quartz, running down the centre of the vein (Williamson, 1956).

Calcite is found in nearly all of the fluorite veins, both as bands alternating with fluorite, and as coatings on exposed fluorite crystal surfaces. Calcite coating fluorite crystals in vugs commonly display 'nail-head' and 'dog-tooth' forms as well as doubly terminated scalenohedral crystals (Williamson, 1956). Calcite also forms an important constituent of the fluorite/granite gas-breccias, mainly in the matrix cement.

Barite is a relatively common gangue mineral in most of the veins studied. At the Iron Springs and Canal veins it occurs as clear honey-yellow tabular crystals intimately intergrown with the fluorite. White and pink platy aggregates of barite are found in a number of other veins such as the Big Meadow Woods, Tarefare, Blue Beach, and others. A small vein at Lawn, hosted by Cambrian sediments, has barite as its primary mineral phase and displays rhythmically banded white and red barite growth-zones.

Sulphides are commonly associated with the veins, especially near the granite contact or in 'country-rock' veins such as the Grebes Nest, Big Meadow Woods, Mine Cove, Lead, and Chambers Cove veins. Galena and sphalerite are the most abundant sulphides, especially in the near-contact veins, with chalcopyrite being more abundant in the veins hosted entirely within the granite. Pyrite is rare but is known to occur in the Director and Blue Beach North veins. Van Alstine (1948) also reported covellite, bornite, and chalcocite in several veins.

Apart from the veins, fluorite is also seen as both fragments and matrix cement to gas breccias (tuffisites), the repeated generation of which gave rise to a great variety of

complex textures. As well, the margins of some veins contain 'breccia-ore', which consists of fragments of granite cemented by coarse grained purple fluorite. This 'breccia-ore' is interpreted to represent brecciation, associated with initial fault movements, and coincident fluorite precipitation, from early mineralizing fluids, preceding the development of significant 'open-space' regimes within the system. Such regimes, resulting from subsequent fault movement and or dilation, provided an ample locus for fluorspar mineralization. The repeated generation of tectonic/gas breccias and 'sand seams' (consisting of primarily pulverized and granulated fluorite) attest to both syn- and post-depositional tectonism.

The fluorite is often strikingly growth-zoned parallel to the vein walls, with concentric bands that reflect unidirectional growth and crustification in open spaces. The growth bands are quite variable in colour and thickness but locally consistent colour-banding sequences can be determined. Often these sequences rapidly change, even between individual lenses within the same vein. Therefore, interpretations determined from growth-zoning should only be applied on a local scale, as it is not necessarily representative of the entire vein.

Close to the vein walls the mineralization tends to be fine grained and banded, often containing variable percentages of quartz and calcite accompanied by rhythmic variations in colour. This banding may be composed of barite, quartz, fluorite or calcite or any combination of these. In some complex sequences, the banding may reflect reopening and refilling of the vein structures, in response to structural movements, rather than simple concentric growth banding from continuous 'open-space' precipitation.

In addition to the 'breccia-type' and blastonite textures, nodular banding is commonly observed in the Director and Blue Beach veins. This texture is produced by fluorite bands, of different colours and/or textures, surrounding a nuclei of breccia fragments. These fragments can be granite, porphyry, hornfels or previously deposited ore in a variety of textures and types. Nodules near the walls of the veins commonly have centres composed of wall rock fragments while those from the central part of veins commonly have centres composed of ore fragments (Van Alstine, 1948). Some nodules show concentric banding all the way around the centres suggesting that the fragments were periodically rotated and/or suspended due to intense fluid movement.

3.4 Fluid-rock Interaction - Alteration

Most of the fluorite veins in the area show sharp, relatively unaltered contacts with the granite, except for local fluorite supported marginal 'breccia-ore'. Sericitization and silicification have locally affected the wall rock of some veins, in particular, where the host rock to a vein is hornfels, it is usually bleached from dark green (or black) to light green, and where it is 'rhyolite porphyry', it is locally bleached from pink to tan or gray (Van Alstine, 1948).

Contact metamorphism around the St. Lawrence Granite was the subject of a B.Sc. (Honours) thesis by Evans (1977). His study of mineral assemblages in hornsfelsed calc-silicate and pelitic rocks in contact zones indicated temperatures of formation of 525-500°C with pressures of 1.0-0.5 kb. He also examined the alteration associated with the fluorspar veins and concluded that alteration effects were more widespread than previous work had indicated. In underground workings (Tarefare mine) he noted

progressively decreasing degrees of alteration, from kaolinization to sericitization, away from the vein contacts. The effects of the alteration on the granite did not extend much more than several metres beyond the contact.

A similar type of alteration was noted at the margin of the Little Salt Cove Vein where the granite, within 1 metre of the contact, is variably sericitized. The pink granite is sericite altered to a light beige colour and contains numerous tiny veinlets of silica and fluorite, as well as up to 1% disseminated and stringer pyrite. Between this location and the granite contact at Chamber Point (figure 2.2.1) there is a zone of highly altered granite, herein referred to as the ***"Alteration Zone"***, in which the normally red granite is altered to beige or orange in colour and locally sericitized. The zone is mineralized with small cross-cutting fluorite and barite veins and with disseminations of molybdenite and chalcopyrite, locally weathered to malachite.

The chondrite normalized REE patterns (figure 2.6.3) from the most highly altered sample (AZ-4) show marked LREE enrichment and HREE depletion compared to the 'typical' granite sample while the less altered sample from the same exposure (AZ-2) has La, Ce and Eu concentrations similar to the 'typical' granite but displays a steady decrease from Pr to Lu. The sericitic granite displays similar Lu values as the moderately altered granite but shows a progressive enrichment towards the LREE. Compared to totally unaltered St. Lawrence Granite porphyry dykes (samples HCT-187 & HCT-188, figure 2.6.3) both of these altered granite samples are LREE enriched and HREE depleted. This suggests equilibration with a mineralizing fluid which was highly enriched in LREE and depleted in HREE compared to the granite, or a reactive fluid which preferentially leached and transported HREE and other elements (Na, Al, Ga) out

of the system. An alternative hypothesis involves a fluid reacting with the granite to produce a LREE enriched minor phase(s) which effectively enriched the LREE and diluted the HREE in the altered granite resulting in the observed chondrite normalized REE patterns (figure 2.6.3).

This REE enrichment is similar to characteristic trends attributed to potassic alteration in granodiorite porphyry from Bakircay, Turkey by Taylor and Fryer (1983). They concluded that such early potassic alteration is produced by high salinity hydrothermal fluids expelled from a magma during intermittent boiling at near magmatic temperatures. The altered granite samples have higher Eu than the unaltered granite. Such Eu behaviour in hydrothermal fluids of this type can be attributed to divalent behaviour in low fO_2 environments (Flynn and Burnham, 1978, Kerrich and Fryer, 1979). The changes in REE abundances observed in the Alteration Zone granite samples are similar to those accompanying potassic alteration which Taylor and Fryer (1983) consider "...consistent with the separation of a chloride rich aqueous brine...".

A detailed study of one well-exposed contact metasomatic zone of "carbothermal" alteration was carried out by Strong (1982). REE concentrations, determined for fresh and altered St. Lawrence Granite, show chondrite normalized REE patterns similar to the relatively flat to slightly LREE enriched REE patterns obtained from the 'Lawn Lobe' of the granite (figure 2.6.3). The altered granite displays a REE enrichment (especially LREE) which suggests high Cl and/or CO_2 activity in the fluids (Strong, 1982). A study of oxygen isotopes in the rocks from this locality (Coleman et al., 1984), indicated that large volumes of carbon dioxide interacted with the rock, being introduced to the margin

and released from it episodically. This suggests enhanced volatile activity (especially CO_2) in the St. Lawrence alkaline-peralkaline magma system.

3.5 Genesis of the Fluorspar Deposits - A Review

Kauffman (1936) was the first to formally describe the St. Lawrence fluorspar deposits and noted the division of the veins into two genetically related groups: a north-south system characterized by larger lower-grade veins and an east-west system characterized by more narrow higher-grade veins. He concluded that the fluorite was of a "primary" nature and deposited from successive "surges" of mineralizing solutions emanating from the late-stage granitic magma. He noted the wide variety of textures from coarse grained (cubic and octahedral) to fine grained fluorite in the veins and the presence of silica-rich breccia ores in the north-south veins. Kauffman (1936) acknowledges the contributions of Dr. W. S. Smith (St. Lawrence Corporation geologist), C. K. Howse (Newfoundland government geologist) and Dr. A. K. Snelgrove (Princeton University) to his interpretation of the geology and mineralization of the St. Lawrence area.

Van Alstine (1948) recognized a paragenetic sequence for the fluorspar veins (figure 3.2.1) such that fluorite, hematite, calcite, pyrite, chalcopyrite, sphalerite, galena, barite and quartz were all classified as primary `hypogene' minerals while chalcocite, covellite, malachite, azurite, chrysocolla, limonite and psilomelane were all classified as secondary `supergene' minerals. Hematite, calcite and quartz are found as both primary and secondary minerals.

Van Alstine (1948) classified the St. Lawrence fluorspar veins as epithermal, based on the low-temperature and low-pressure mineral assemblages, the vuggy nature of the veins and the abundance of breccia, colloform and crustification structures. He also emphasised the genetic relationship between the fluorite veins and the St. Lawrence Granite, based on:

- the close spatial relationship between the fluorite veins and the granitic rocks
- the abundance of fluorite as an accessory mineral in the granite
- the high concentration of F in the granite
- the presence of euhedral, colourless or purple fluorite cubes in the small vugs or miarolitic cavities within the granite

These factors led him to conclude that the source of the fluorite was in the same magma chamber that supplied the granitic magma. These ore fluids, released as a result of late-stage differentiation, formed fluorite veins along pre-existing faults and shears formed as the granite cooled and contracted.

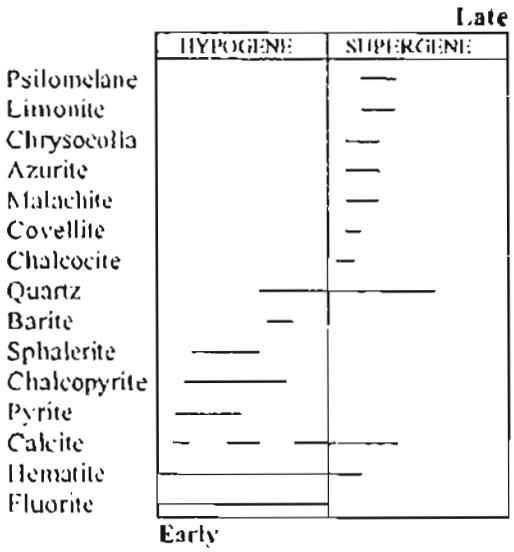

Figure 3.2.1 Paragenetic sequence of mineralization in the St. Lawrence Fluorspar Veins as determined by Van Alstine (1948)

Williamson (1956) studied the structural patterns of the fluorite veins and the granite, concluding that they reflect the earlier tectonic history of the underlying rock units, and that the primary control on fluorite mineralization was the development of a fracture pattern in response to a stress system produced by the cooling of the granite, but whose orientation was dictated by the fact that the granite was emplaced along structures developed by earlier tectonic activity. He recognized the cyclic nature of the mineralization and related it to repeated movement along the vein structures, creating new open spaces for ore deposition and causing brecciation of pre-existing vein material and country rock. He pointed out that the lack of fluorite mineralization in the overlying sediments was due to the fact that open fissures rapidly narrowed and closed on passing from the granite into the country rock.

Teng (1974) added that continued movement along the fractures produced varying degrees of brecciation of the wall rocks. Later volatile materials were separated and escaped along innumerable channel-ways to be deposited as veins in the structure already developed in the upper part of the granite. The escape of volatiles beyond the boundaries of the granite was largely prevented by the impermeability of the overlying hornfels which effectively impounded them. Such a 'ponding' of fluids, at the granite contact, can result in alteration of the granite such as that described by Strong (1982).

Based on their own results and the experimental results of others (over a wide range of salinities), Richardson and Holland (1979b) suggested that fluorite is deposited as either:

1 a result of decreasing temperature and pressure along the fluid flow path
2 a result of fluid mixing to cause dilution or compositional change
3 a result of fluid interaction with wall rocks to cause an increase in pH

Strong et al. (1984) concluded that all but one of the specific mechanisms of fluorite precipitation proposed by Richardson and Holland (1979 a; b) can be eliminated for the St. Lawrence veins. They state that the results of fluid inclusion, oxygen-isotopic and REE geochemical investigations all appeared to rule out precipitation of fluorite as a result of a decrease in temperature or fluid mixing. They emphasize an increase in pH as an important potential cause of fluorite deposition. Since there is little evidence of extensive wall-rock alteration at or near the vein margins, they suggest that the boiling of fluids, and in particular the ebullition of carbon dioxide, possibly along with a loss in fluorine as SiF_4 or HF, would provide a ready means of increasing the pH, and thus exercise the main control on fluorite deposition.

The results of the study of fluorite from growth-zoned samples (Strong et al., 1984) indicated that there were quite variable yet systematic changes in the physical and chemical character of the mineralizing fluid during fluorite precipitation. It is the purpose of the current study to expand on the earlier study in an attempt to better define this physical and chemical variability in terms of the genesis of the fluorspar deposits.

4 Veins and Samples - Present Investigation

4.1 Veins Sampled

The selected hand samples used in this study were taken from a number of different localities and represent a variety of environments and styles of vein mineralization. The following section includes a brief description of each vein or showing and a detailed description of each hand sample used in the study. In the case of samples displaying multiple growth zones, each zone is described in detail. For a more detailed description of the geology and development history of any of the fluorspar veins, the reader is referred to Williamson (1956), Smith (1957) and Farrell (1967).

Growth zoned samples from eight different veins were studied and the samples are listed below, along with the sample number of each and the number of individual growth zones separated from each sample:

1	Grebe's Nest Vein	GNV-8	16 zones
2	Iron Springs Vein	ISV-1	7 zones
3	Lawn Barite Vein	LBV-7	8 zones
4	Hare's Ears Vein	HEV-1	5 zones
5	Blake's Brook Vein	BBV-2	9 zones
6	Lunch Pond Vein	LP-2	10 zones
7	Clam Pond Vein	CPV-4	7 zones
8	Salt Cove Valley Vein	SCVV-A	3 zones

In addition eight individual samples were analyzed from various veins or zones to encompass varying locations and/or types of mineralization. Geochemical analysis of 4 of 11 zones from 'sample 2', originally prepared for the study of Strong et al. (1984), were completed primarily to confirm the existence of rare 'early REE patterns' (see later section), similar to those identified in sample GNV-8. Sample GNV-7, a coarse grained green fluorite from the Grebe's Nest Vein was used as an internal standard in the geochemical studies.

4.1.1 Grebe's Nest Vein

The Grebes Nest Vein differs from most other fluorite veins in the area because it occurs within the quartz-feldspar porphyry phase of the St. Lawrence Granite and the Inlet Group metasediments (figure 4.1.1). The vein is located approximately 6.5 km west of St. Lawrence and is exposed on the eastern shore of Little Lawn Harbour. A 15 metre development shaft was sunk on the vein 500 metres east of the shore-line. The Grebes Nest Vein has a strike length of more than 3 km, but it may not be continuous over this entire length. At the shore the vein strikes 120 degrees and dips 70 degrees to the north, but strike and dip vary locally along the strike-length of the vein. The width of the vein is reported (Smith, 1957) to vary between 1.8 and 0.3 metres. Like other veins in the area, it pinches and swells along both its strike and dip directions.

Fluorspar in the Grebes Nest Vein is coarse grained, high grade and generally green in colour. Octahedral crystals were observed in the fluorite along with banded and colloform structures. Sphalerite and galena are the most abundant minor phases, but lesser pyrite and chalcopyrite has been noted.

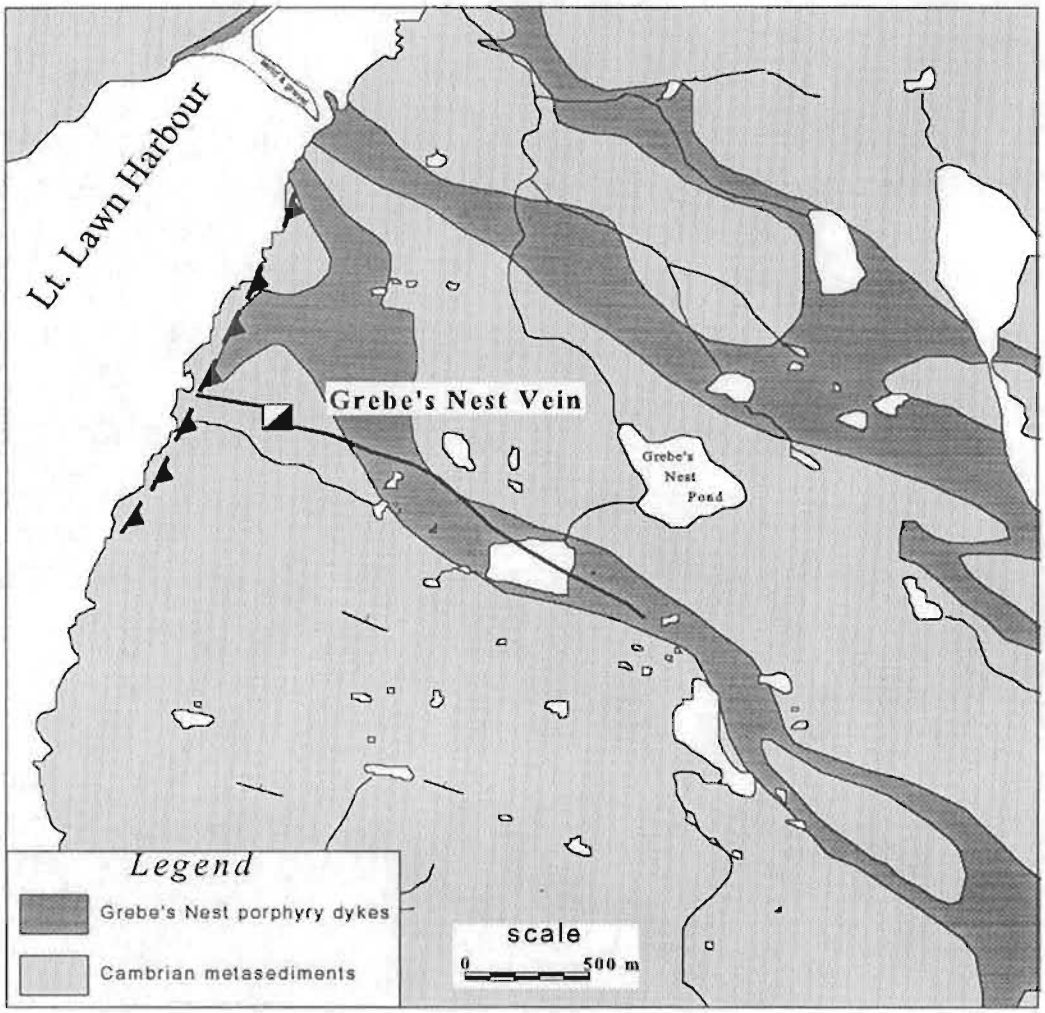

Figure 4.1.1 Sketch map showing the location of the Grebe's Nest Vein and granitic porphyry dykes. Geology revised from Strong et al., 1978.

Sample GNV-8 (figure 4.1.2) was collected from the dump pile near the abandoned shaft on the Grebes Nest Vein. This sample can be considered in terms of three major subdivisions based on the colour of the fluorite. The subdivisions are as follows:

1 an early sequence of green fluorite (zones A to I)
2 a later sequence of blue fluorite (zones I to N)

3 a late sequence of white fluorite (zone O), capped by a late layer of goethite or limonite (zone P).

The earliest zone of green fluorite (zone A) is characterized by coarse-medium grained green fluorite with micro-veinlets and lenses of quartz. Zones B to D consist primarily of fine to medium grained green fluorite, commonly displaying radial (dendriform) micro-textures. Depressions, created by crystal forms at the contact between two sub-zones within zone D, are filled by a `detritus' composed of a fine grained aggregate of fluorite and quartz with minor opaques (limonite and chalcopyrite). This suggests that the fluid had a high 'suspended solid' load in the period between the precipitation of the two zones, possibly reflecting relatively contemporaneous tectonic or

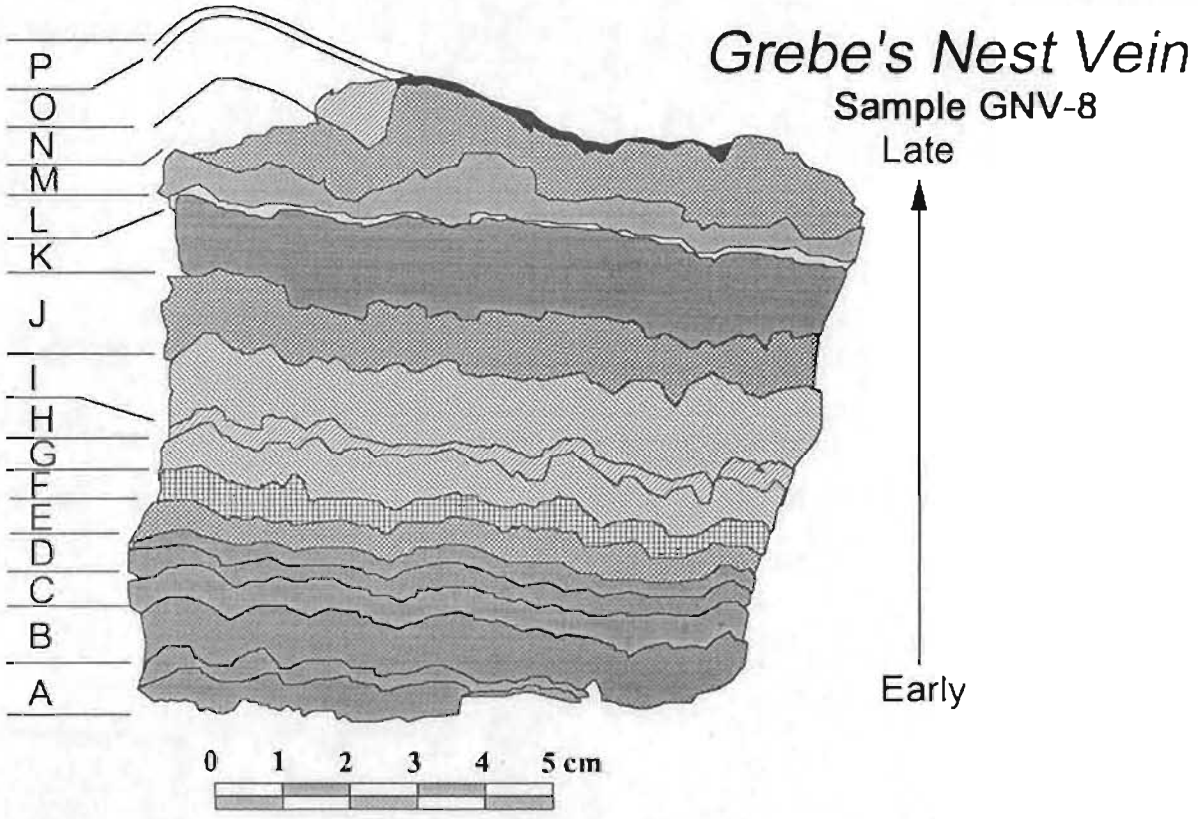

Figure 4.1.2 Sketch of sample GNV-8, from the Grebe's Nest Vein, outlining the sequence of growth zoning from the earliest zone (A) to the latest zone (P).

gas brecciation elsewhere in the conduit system. As well, it suggests that there may be a significant 'time-lag' between individual growth zones, and that the zones represent 'episodic' rather than continuous precipitation.

Zones E to G are characterized by coarse grained green fluorite which becomes increasingly coarse as precipitation continues. Sedimentary-like 'detritus', similar to that in zone D, occurs at the contact between zones E and F. Chalcopyrite and galena occur in zone E while only minor chalcopyrite was noted in zone G.

Zones H and I mark the transition between green and blue fluorite. Zone H and the base of zone I are composed of medium to coarse grained blue fluorite while the upper portion of zone I grades into essentially coarse grained green fluorite. Chalcopyrite is intergrown with fluorite in both zones especially at the base of zone I. Hematite and limonite were noted in both zones. The colour change and the appearance of Fe-oxides suggest the waning of a major cycle in fluid evolution.

Zones J to L are composed essentially of coarse grained blue fluorite. Small intergrown crystals of chalcopyrite are common. Hematite and limonite occur in the upper portion of zone K and in zone L where they form zoned intergrowths which appear to fill pre-existing cavities in the fluorite, suggesting a secondary or late-stage origin for the Fe-oxides.

Zones M and N are composed of blue fluorite which contains many cavities of irregular shape suggesting possible leaching. Some cavities have been filled with zoned Fe-oxides similar to that described in zone L. Hematite is common as small inclusions in fluorite crystals, often defining microscopic growth zones. Fe-oxides, noted on surfaces of macroscopic growth zones, appear to have a secondary origin similar to

Fe-oxides seen lining cavities. Therefore, it seems that Fe-oxide precipitation in these zones is related to both primary and secondary processes, the former being co-precipitated with the fluorite and the latter being introduced later by infiltrating fluids.

Zones O and P mark a late-stage highly oxidized zone. Zone O is characterized by coarse grained white fluorite intimately intergrown with Fe-oxide. Much of the Fe-oxide is deposited on growing crystal faces giving the zone a blocky appearance. Zone P forms a Fe-rich, locally botryoidal oxide/hydroxide cap which appears to represent secondary deposition of goethite/limonite on crystal faces exposed in vugs. Since goethite is known to result from the weathering of iron minerals (abundant in the granite) and precipitate directly from meteoric water (Deere et al., 1977), the late-stage fluids responsible for the Fe-oxide/hydroxide deposition probably contained a significant meteoric component.

4.1.2 Iron Springs Vein

The Iron Springs vein was discovered in 1931 by Dr. W.S. Smith and Michael Clark, a local prospector (Martin, 1983). It was first mined as an open cut in 1934, with underground mining commencing in 1938. The mine operated until June 1957 and has been mined to the 270 metre level (Williamson, 1956). During it's lifetime, the Iron Springs Mine produced over 400,000 tonnes of fluorspar (Howse, et al., 1983).

The Iron Springs vein (figure 4.1.3) occurs entirely within the St. Lawrence granite near the western granite-sediment contact. The vein strikes 110 degrees and dips 70 degrees to the south, although locally strike and dip are variable. It attains a strike-length of more than 1100 metres with an average width of 0.76 metres, locally

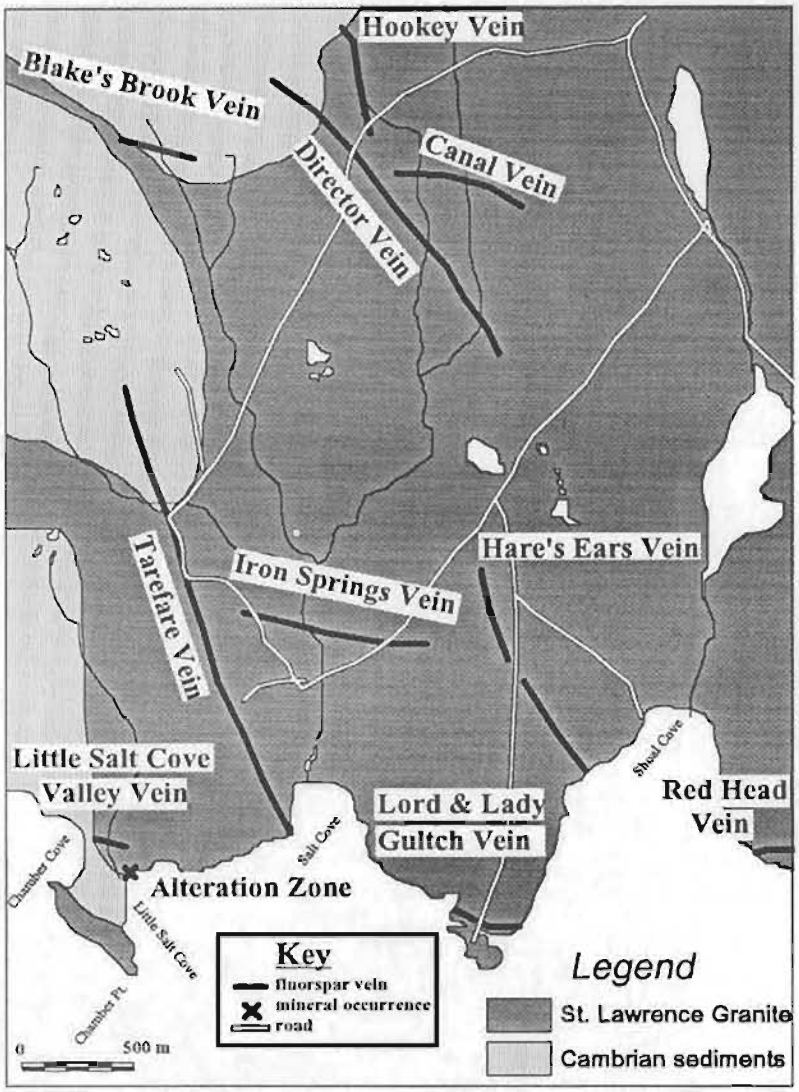

Figure 4.1.3 Sketch map showing the location of the major fluorspar veins in the south-western part of the St. Lawrence mining area. Geology revised from Strong et al. (1978).

reaching up to 2.5 metres in width, pinching and swelling both laterally and vertically (Williamson, 1956).

In the Iron Springs Vein the fluorspar ore is characteristically colour-banded parallel to the vein walls (Williamson, 1956). The fluorite is generally coarse grained but parallel bands of fine grained fluorite-quartz-calcite are also common, usually close to the

vein walls. The Iron Springs Vein has an abundance of vugs which contained some of the largest perfectly formed cubic crystals (up to 0.35 metres on a side) found in the St. Lawrence deposits. Red Fe-oxide staining is common on the surfaces of most of the cubic crystals. Williamson (1956) interpreted this Fe-oxide as a late stage feature, which suggests that this vein may have been formed during a predominantly 'later' phase of mineralization. The most common gangue mineral is calcite, with quartz and yellow, tabular barite occurring less abundantly. Quartz and calcite occur with fluorite in the finely banded zones while all three are found in vugs, usually as well formed crystals coating fluorite crystals. The major sulphide mineral is chalcopyrite, occurring throughout the vein, with galena and sphalerite occurring in the upper levels of the vein (Williamson, 1956).

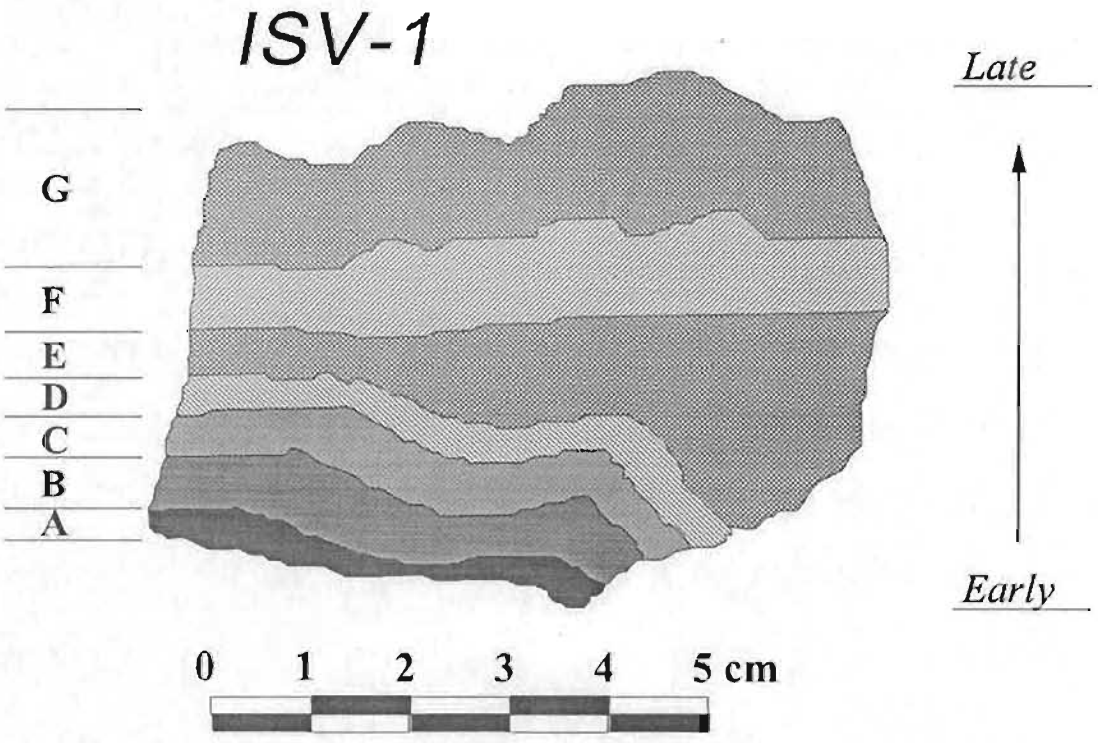

Figure 4.1.4 Sketch of sample ISV-1, from the Iron Springs Vein, showing consecutive growth zoning from the earliest zone (A) to the latest zone (G). See text for complete descriptions of the zones.

Sample ISV-1 (figure 4.1.4) was collected from the mine dump at the site of the abandoned Iron Springs Mine. The sample contains 7 individual zones but can be considered in terms of three genetic subdivisions:

1 early fine grained quartz, carbonate and fluorite (zones A to C)
2 middle coarse grained yellow and red fluorite (zones D and E)
3 coarse grained clear fluorite (zones F and G)

The earliest mineralization precipitated was the fine grained quartz, carbonate and fluorite of zones A to C. These zones are characterized by very fine grained crystals or grains of quartz, fluorite and carbonate in a fine grained fluorite groundmass. Zone B is the most quartz-rich while carbonate concentrations remain fairly constant throughout the three zones. These zones are colour banded (red-white) reflecting the concentration of interstitial hematite.

Zones D and E reflect the next episode of fluorite precipitation. These zones are dominated by coarse grained yellow fluorite. Zone D displays a reddish colour due to fine inclusions of hematite aligned along microscopic growth zones. Chalcopyrite and sphalerite are intergrown with fluorite in zone D.

The latest stage of mineralization noted in the sample is clear coarse grained fluorite (zones F and G). Zone F has a reddish colour due to fine bands of hematite rimming microscopic growth zones in otherwise clear fluorite. Zone G has large cubic crystal faces on the outer surface, suggesting growth into an open vug (i.e. the last stage of vein mineralization). Chalcopyrite and sphalerite are intergrown with fluorite especially in zone F, where the chalcopyrite displays well developed crystal forms indicative of contemporaneous precipitation with fluorite. Sphalerite contains rare

inclusions of chalcopyrite, suggesting that the chalcopyrite may have been precipitated earlier than the sphalerite or alternatively exsolved from it.

4.1.3 The Hare's Ears Vein

The Hare's Ears Vein is located approximately 500 metres west of the Iron Springs mine site (figure 4.1.3). It was discovered in 1936, while building an access road to the Iron Springs Mine, and mined intermittently until 1962 (Farrell, 1967). This vein is hosted entirely by the St. Lawrence Granite and is described by Van Alstine (1948) as striking 155° with a near vertical dip, with widths ranging from 4.5 to 0.6 metres over a strike-length of approximately 150 metres. This vein was exceptionally high grade for a 'north-south' vein, but quite irregular on the surface with pinching and swelling defining intermittent lenses of ore grade material. Underground, at a depth of 84 metres, the vein is reported to carry ore grade over an average width of 3.7 metres over a strike length of approximately 150 metres (Farrell, 1967). The vein structure is reported to continue north (~170m) and south (~60m) of a 1943 shaft for a total strike-length of 230 metres. The vein is quite irregular both along strike and down dip. The reported sudden termination of ore and bad ground conditions suggest that the vein may be structurally offset.

The fluorite in this vein is primarily coarse grained fluorite with gray, white, yellow, green and purple colours reported (Williamson, 1956). Common gangue minerals are quartz and calcite as well as 'blastonite'. Galena and sphalerite are common with lesser chalcopyrite, rare pyrite and minor amounts of barite and Fe-oxides.

Sample HEV-1 (figure 4.1.5) consists of primarily white to green coarse grained fluorite containing varying amounts of galena. Since this vein is no longer exposed at

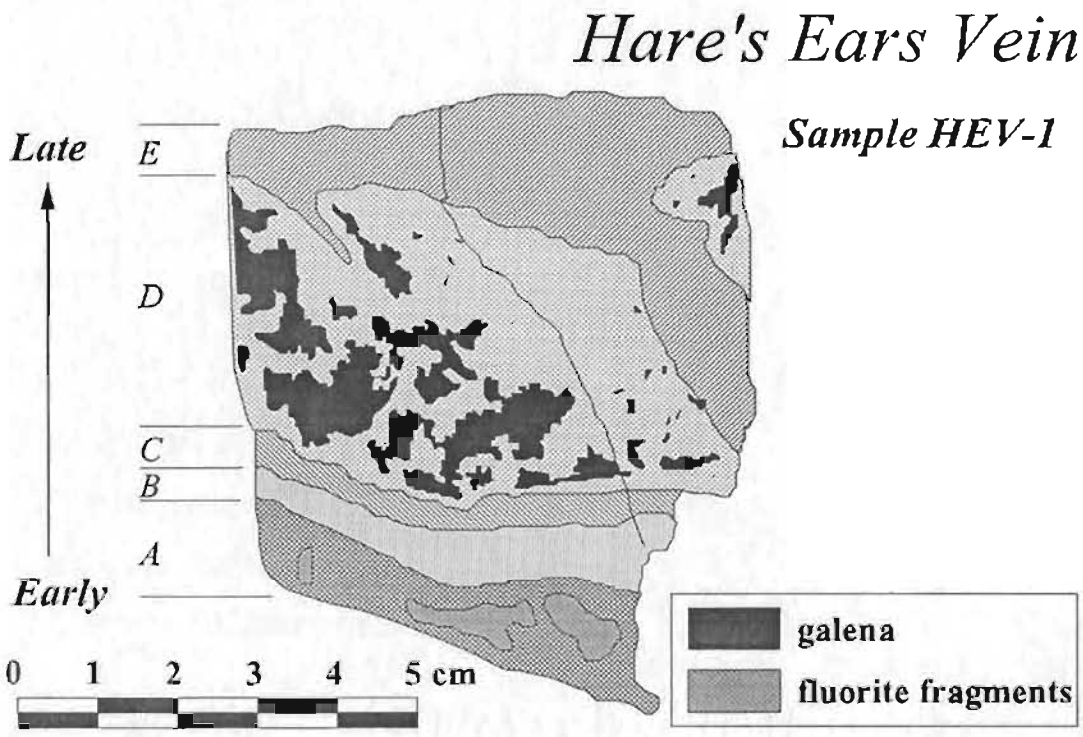

Figure 4.1.5 Sketch of sample HEV-1, from the Hare's Ears Vein, showing progressive growth zones from A to E.

surface, the sample is a 'grab sample' and its position with respect to the vein wall is uncertain. Based on macro and microscopic growth textures, this sample is considered in terms of five distinct growth zones with increasing chronology from A to E. The zones are as follows:

A coarse grained white fluorite with sub-angular fragments of previously deposited 'blastonite'. The fragments, themselves, contain small sub-rounded fragments of quartz and fluorite in a matrix of crystalline fluorite with minor disseminated galena.

B coarse grained white to green fluorite locally containing orange halos which appear to surround oxidized pyrite grains. Minor stringer veinlets of fine grained galena are emplaced along fractures.

C similar to zone B except that this zone contains only white fluorite and a slightly higher content of sulphides.

D coarse grained gray to green fluorite with ~50% intergrown galena with minor intergrown sphalerite and chalcopyrite. Zone also contains minor fragments of previously deposited fluorite.

E coarse grained green fluorite which locally has an orange colour, possibly due to Fe-oxides as in zone B. This zone locally cuts and fragments zone D mineralization. The zone contains minor galena, sphalerite and chalcopyrite and rare pyrite.

4.1.4 Blake's Brook Vein

The Blake's Brook Vein, discovered in 1937 (Smith, 1957), is located approximately 3 kilometres west of the community of St. Lawrence. The vein occurs near the contact of the St. Lawrence granite and granitic porphyry dyke with Inlet Group metasediments (figure 4.1.3). There are actually two veins separated by approximately 30 metres. The larger northern vein, which strikes 105° with a near vertical dip, has widths between 1.8 and 0.2 metres and has been traced on surface for approximately 400 metres (Smith, 1957). The smaller southern vein strikes 110° and dips 45°N with widths ranging from 0.5 to 0.2 metres (Van Alstine, 1948). The vein quickly pinches upon entering the metasediments but a 6 metre shaft indicated that the fluorspar vein persists in the granite beneath the metasediment contact which dips 15° N in this location (Smith, 1957).

The Blake's Brook Vein is a high-grade 'east-west' vein containing primarily coarse grained fluorite from wall to wall. The fluorite is massive to rhythmically zoned and occurs as colourless, green, yellow and gray varieties. This vein contains abundant red sphalerite and lesser galena with minor chalcopyrite, quartz and calcite.

Sample BBV-2 (figure 4.1.6), from the Blake's Brook Vein, consists of colourless to white, coarse grained fluorite with varying amounts of sulphides, primarily galena and

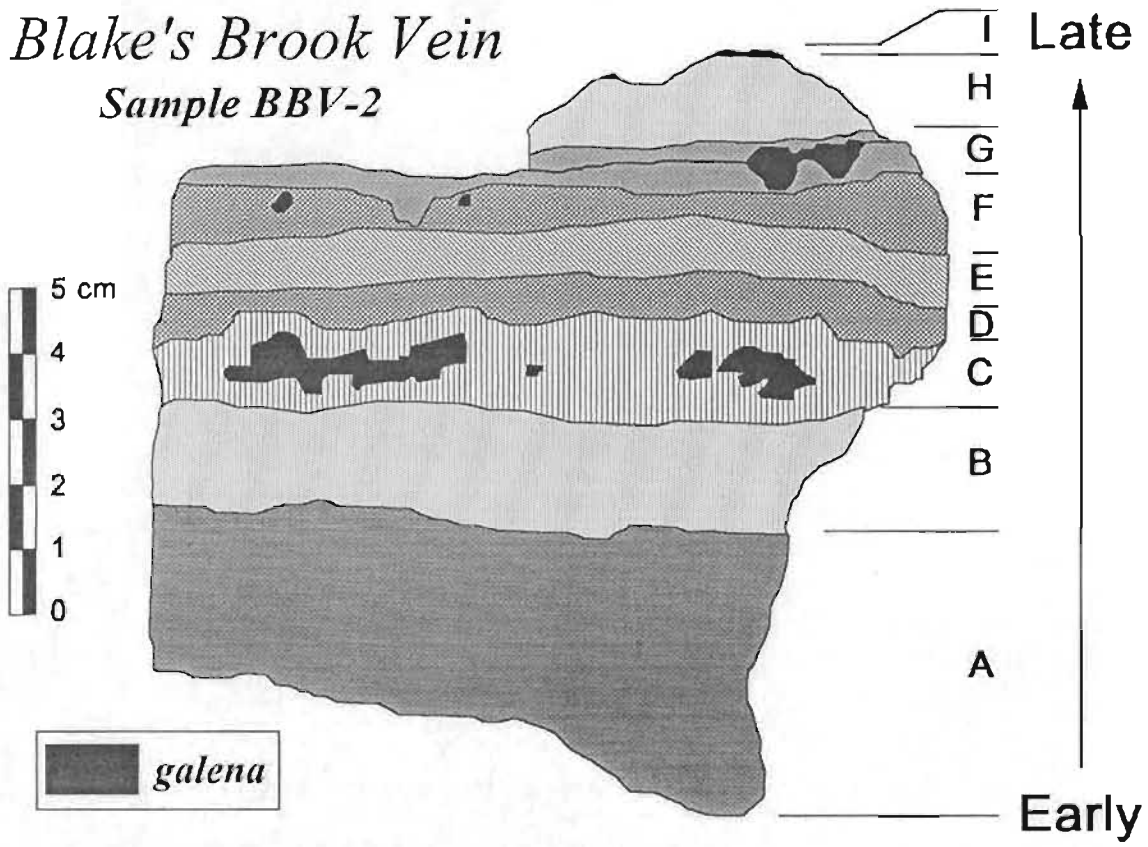

Figure 4.1.6 Sketch of sample BBV-2, from the Blake's Brook Vein, showing consecutive growth zones from the earliest (A) to the latest (I).

sphalerite. This sample was also a grab sample, chosen because it displayed the most comprehensive set of continuous growth zones of any sample from this vein. Based on growth textures, this sample can be considered in terms of 9 distinct growth zones with increasing chronology from A to I. The zones are as follows:

A coarse grained colourless fluorite with minor intergrown red sphalerite and galena (trace chalcopyrite)

B coarse grained colourless fluorite with traces of sphalerite, galena and chalcopyrite

C coarse grained colourless fluorite with approximately 50% sulphides (primarily coarse grained galena with minor chalcopyrite and lesser sphalerite)

D coarse grained colourless fluorite with traces galena and chalcopyrite

E coarse grained colourless fluorite with traces of galena and rare pyrite

F coarse grained colourless fluorite with minor coarse grained galena and rare pyrite

G fine grained white fluorite which appears to be later mineralization filling a fracture. The zone has a series of quartz-lined vugs at its centre. The quartz is colourless. The central vuggy part of the zone locally filled with galena and sphalerite with minor chalcopyrite and pyrite. Locally, where the zone narrows, it is 'styolitic-looking' suggesting a possible origin related to dissolution, either chemical or pressure-related

H coarse grained colourless fluorite with traces of galena and sphalerite

I late-stage cap of gray, fibrous mineral(s) originally interpreted to be sphalerite with intergrown galena. Subsequent analysis indicates low Zn concentrations but the small amount of sample available did not allow for more extensive analysis. This mineral may be some type of hydrous oxide.

4.1.5 Clam Pond Vein

The Clam Pond Vein is located approximately 5 kilometres north of St. Lawrence, immediately north of Clam Pond (figure 2.2.1). It is hosted entirely by the St. Lawrence Granite, probably close to the 'roof-zone' as suggested by its proximity to contacts of the granite with Precambrian Marystown Group volcanic rocks. The vein was discovered in 1938 (Farrell, 1967) and has been intermittently exposed by trenching. The vein strikes 081° and dips 80° N, with a strike-length of approximately 300 metres Narrow widths, from 1.0 to 0.1 metres were reported by Van Alstine (1948), although Farrell (1967) reports an average width of 1.2 metres over a 30 metre strike-length. Since many of the veins in the area display a high degree of pinching close to the 'roof-zone' contact, this vein may be wider at depth.

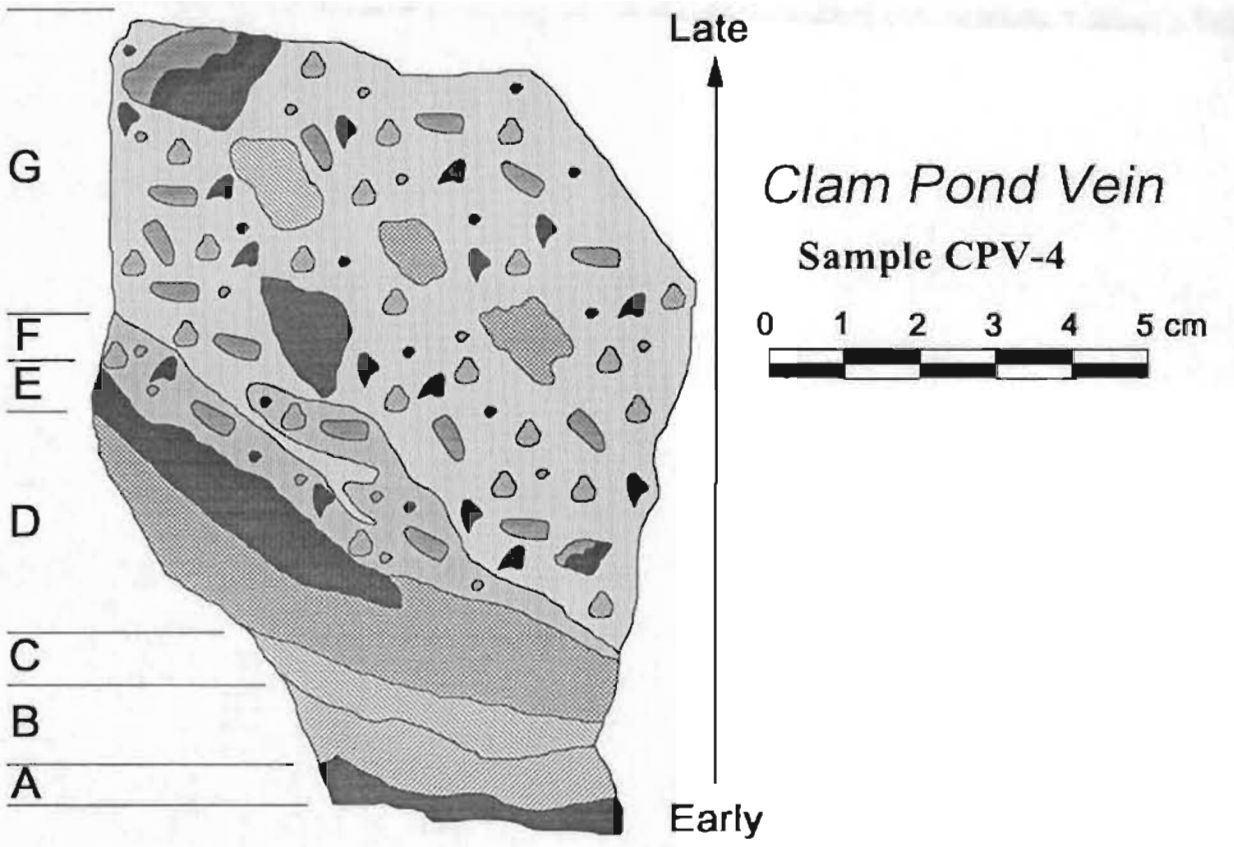

Figure 4.1.7 Sketch of sample CPV-4, from the Clam Pond Vein, showing interpreted growth zoning from the earliest (A) to the latest (G) mineralization.

The vein mineralogy at Clam Pond is dominantly fluorite but locally it contains high percentages of quartz and barite as well as minor galena and sphalerite. A large number of granite inclusions dilute the fluorite grade in most of the exposed intersections. The fluorite is coarse grained, occurring in white, green, blue and red varieties. Barite occurs as coarse, pink-orange platy aggregates, locally forming bands in the central part of the vein.

Sample CPV-4 (figure 4.1.7) is a grab sample collected from a trench beside Clam Brook. Based on growth textures and breccia zones, the sample is interpreted to contain four early zones of primarily coarse grained fluorite (A-D) and three later zones of quartz-fluorite breccia ore (E-G). The breccia zones contain fragments of previously

precipitated coarse grained fluorite, some displaying concentric growth bands. The descriptions of the zones are as follows:

- **A** coarse grained red fluorite with intergrown white quartz and minor red to orange barite. Locally the zone appears brecciated and may contain some material of secondary origin. The red colouration in fluorite reflects its hematite content.
- **B** coarse grained white to purple fluorite
- **C** coarse grained white to purple fluorite
- **D** coarse grained white to purple fluorite with minor orange quartz. This zone appears to have been disturbed by the subsequent emplacement of the 'breccia-type' mineralization of zone E
- **E** reddish-brown 'breccia-type' mineralization containing fragments of quartz and minor pyrite in a fine matrix of fluorite, quartz and minor carbonate
- **F** yellow-beige 'breccia-type' mineralization containing fragments of 'zone E' material, pyrite and quartz in a fine matrix of yellowish fluorite, quartz and minor carbonate
- **G** orange-purple 'breccia-type' mineralization containing large fragments (up to 2 cm) of predominantly coarse grained fluorite (some banded) in a fine orange matrix of fluorite, quartz and minor carbonate

4.1.6 Lawn Barite Vein

In early November, 1982, during construction of a road through the community of Lawn, a local resident reported the discovery of fluorite and galena mineralization (for more details on this showing, the reader is referred to Collins, 1984a). The occurrence is located within the town of Lawn, only 15 kilometres west of the once productive fluorspar mines at St. Lawrence. The occurrence itself is on the eastern side of Lawn Harbour and is accessible by road (figure 4.1.8). It is hosted by the Webbers Cove

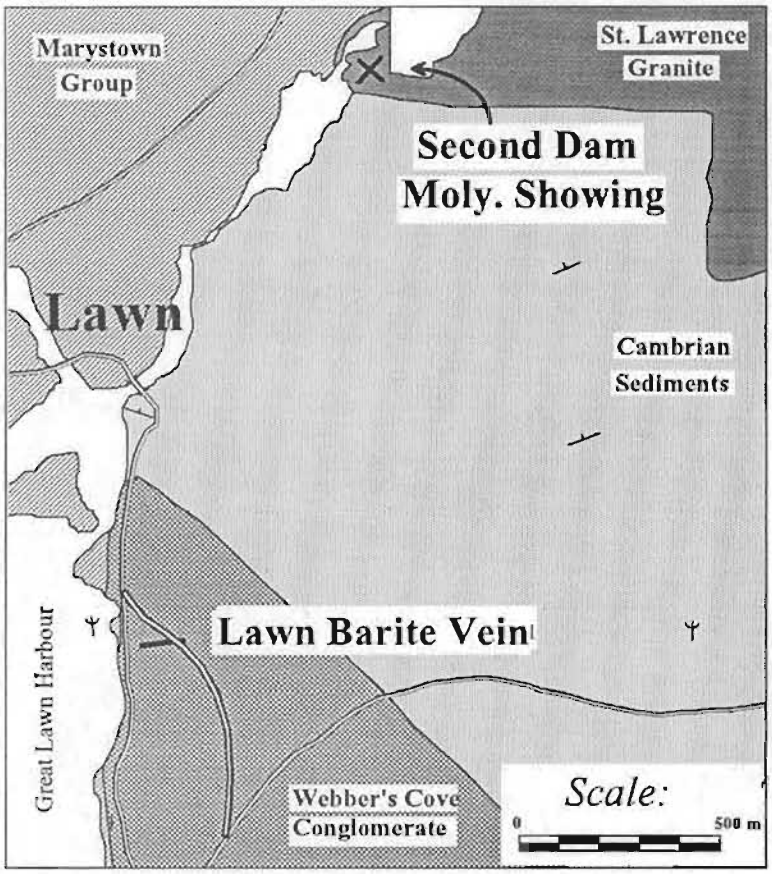

Figure 4.1.8 Sketch map of the Lawn area showing the location of the Lawn Barite Vein and the Second Dam Moly Showing. Geology revised from Strong (1976) and O'Brien et al. (1977).

Conglomerate (Strong, 1976) which is part of the larger Marystown Group volcanic sequence (O'Brien et al., 1977). The St. Lawrence Granite outcrops only 1 km northeast of the occurrence, and several granitic porphyry dykes occur nearby.

The Webbers Cove Conglomerate consists of a coarse-grained conglomerate with a sandy matrix. Most fragments are well rounded but range from rounded to sub-angular. The fragments are derived from a variety of lithologies being primarily from sedimentary and volcanic regimes, but fragments of pink equigranular (and porphyritic) granite are common. Except in the vicinity of the veining, the conglomerate is relatively fresh and

unaltered. Near the vein, the conglomerate is altered over a 20 metre width with alteration consisting of primarily white to yellow clay mineral (kaolinite and/or sericite) and carbonate alteration, presumably the result of hydrothermal activity. Several felsic (porphyritic) and mafic dykes, which occur within the altered zone, are generally narrow and apparently of limited strike-length. The mafic dykes show a high degree of epidote alteration, suggesting that they pre-date the alteration.

The main vein strikes 105° with a near vertical dip and extends approximately 25 metres along the exposure. The vein appears to widen with depth, having a width of only 0.15 metres at sub-outcrop level (1 metre below surface), and a width of 0.60 metres at the road level (approximately 4 metres deeper). Two smaller veins (10 cm wide) were noted near the main vein, one parallelling the main vein and the other striking 125° and dipping 50° south. These smaller veins are probably offshoots from the main vein.

The mineralization noted in the main vein is primarily pink to white barite with intergrown fluorite and minor zones of galena and sphalerite. Narrow zones of massive galena and sphalerite were also noted. Although no significant amount of massive fluorite was noted in the main vein, the presence of fluorite-rich boulders in nearby rubble suggests that some parts of the vein system may contain high grade fluorite. Microscopic examination revealed a high percentage of fluorite intimately intergrown with both pink and white barite in samples from the main vein.

Breccias are common in these veins, consisting of conglomerate fragments within zones of crystalline barite and fluorite. Conglomerate with a matrix composed entirely or partially of barite, fluorite and calcite with or without veins or veinlets suggests some degree of preferential replacement of the matrix.

Sample LBV-7 (figure 4.1.9) is from the road-cut exposure at Lawn. The sample contains 8 consecutive growth zones which are considered in terms of four major

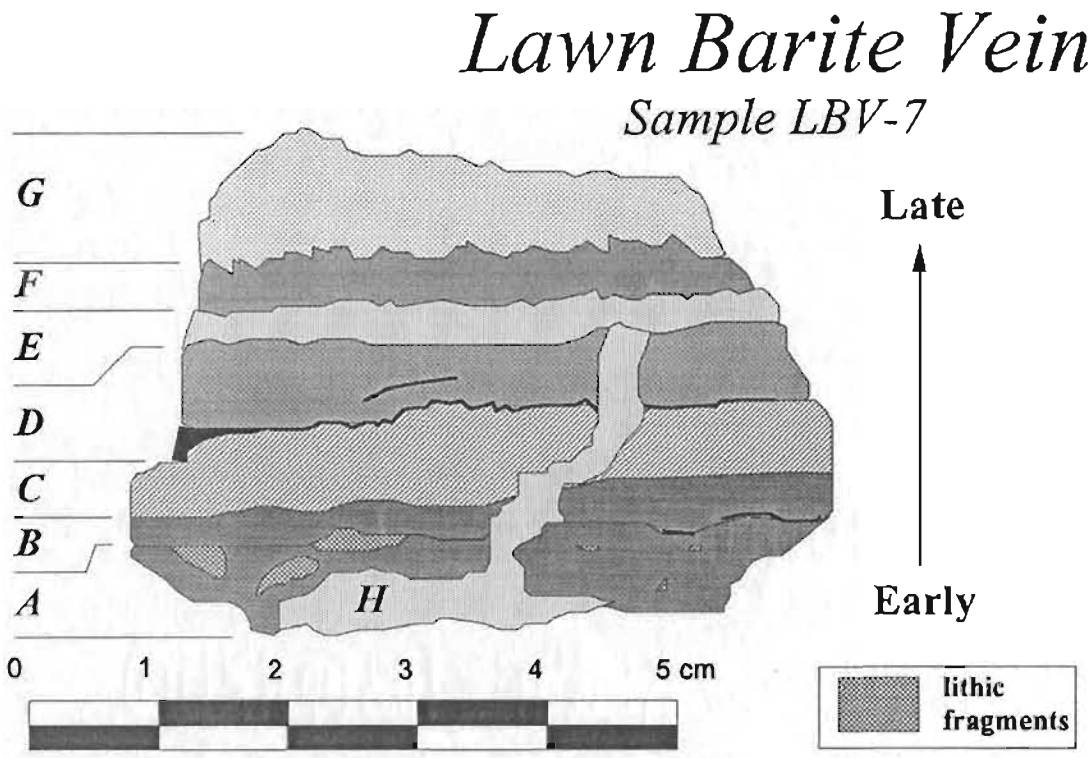

Figure 4.1.9 Sketch of sample LBV-7, from the Lawn Barite Vein, showing consecutive growth zoning from the earliest (A) to latest (G) mineralization. Zone H is a small veinlet cross-cutting zones A to D.

subdivisions based on chronology, colour and mineralogy:

1 brecciated country rock with barite-fluorite-calcite in matrix (zone A)
2 red barite with minor fluorite (zone B to D)
3 white barite and fluorite (zone E & F), minor galena & sphalerite (F)
4 late-stage pure white barite (zone G)

The earliest stage of development of the vein is a breccia zone (A). This zone, occurring at the vein wall, is characterized by fragments of country rock, quartz and calcite in a groundmass of fluorite and barite. This type of mineralization probably resulted from infiltration of hydrothermal fluids into the porous sandy matrix of the conglomerate wall rock causing varying degrees of precipitation and/or replacement.

Zones B to D are composed primarily of red to orange barite with lesser colourless to white fluorite as intergrown crystals or small veinlets. Minor fragments of country rock occur in some of these zones, as well as coarse grained quartz and calcite, intergrown with barite.

Zones E, F and H (a cross-cutting veinlet) are composed of intergrown, coarse grained white barite and white to colourless fluorite. The top of zone F and the base of zone G are marked by internal bands of virtually pure coarse grained fluorite. There is a narrow internal band of galena and sphalerite, near the top of zone F, which appears to be intimately associated with the fluorite. The sphalerite appears to be earlier than galena but intergrowths of one within the other suggest a close co-genetic relationship.

The latest stage of mineralization, zone G, consists of pure, coarse grained, white barite. The well developed crystal faces and geometric relations observed in the vein indicate that this was the final phase of mineralization in this part of the vein and suggests that some of the barite in this zone grew freely in open vugs.

4.1.7 Lunch Pond Vein

The Lunch Pond vein was discovered in 1950 and is located 10 kilometres northwest of St. Lawrence. This is the most northerly granite-hosted vein used in this study. The vein is hosted entirely within the St. Lawrence Granite (figure 2.2.1) but again close to the 'roof-zone' as indicated by nearby contacts with the Precambrian Marystown Group volcanics (Strong et al., 1978). This showing is rather discontinuous at surface but diamond drilling intersected 43.3% CaF_2 over 11.5 metres at a depth of approximately 30 metres below surface (Smith, 1957).

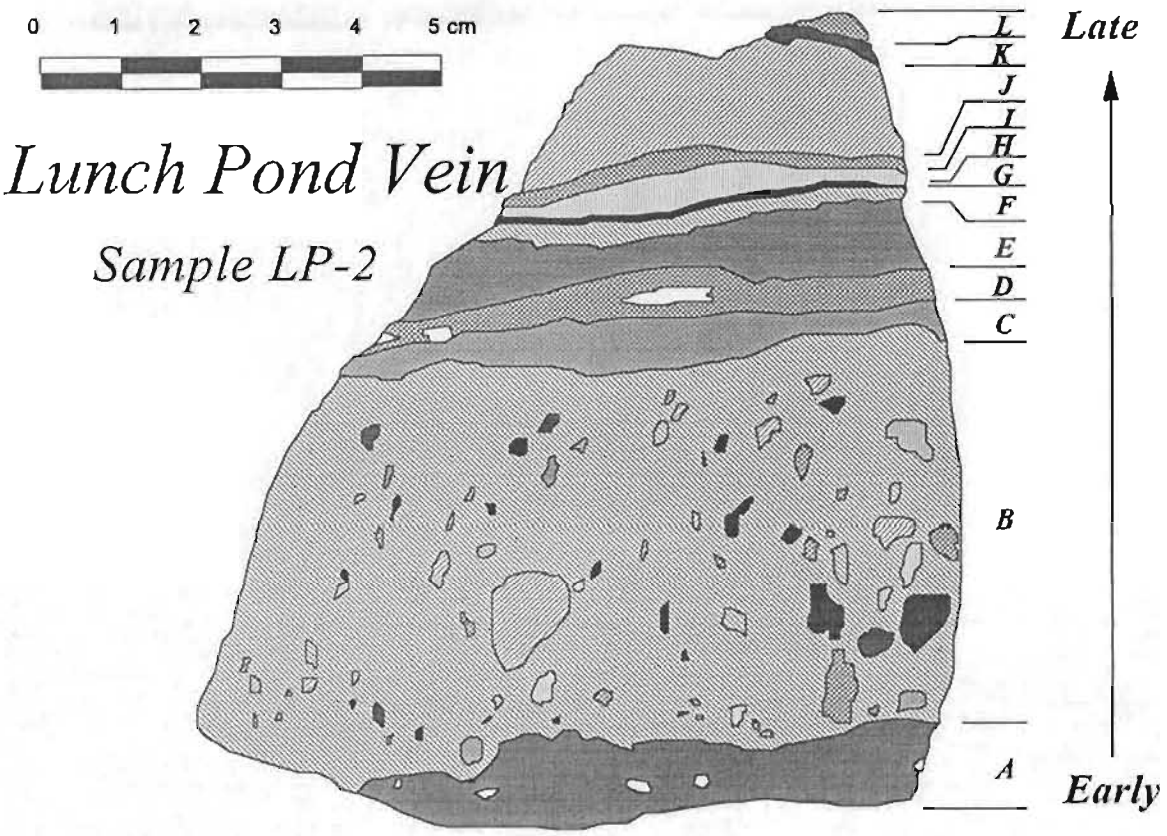

Figure 4.1.10 Sketch of sample LP-2, from the Lunch Pond Vein, showing consecutive growth zones from A to L.

The vein is not exposed but, from a study of local float, the vein appears to contain variable mineralogy including fluorite, barite and calcite with some samples containing up to several percent galena. This vein is reported to strike 065° and dip 80° N (Smith, 1957).

Sample LP-2 (figure 4.1.10) was collected from rubble near a trench. The sample contains 12 continuous growth zones, but the fine nature of the banding in some zones and the brecciated nature of others make the chronological sequence of mineralization difficult to determine. The texture and distribution of extremely fine grained fluorite near the boundaries of some zones was the criteria used to determine the 'best estimate' of the chronological order, increasing from zone A to zone L.

The sample contains 12 individual zones but, due to difficulty in separating some extremely fine zones, the zones F to H were combined for sampling purposes. The 12 zones are:

A red to brown, fine grained 'breccia-type' mineralization consisting of quartz-rich fragments in a purple to gray fine grained matrix of carbonate with minor barite and fluorite

B red to brown, coarse grained 'breccia-type' mineralization consisting of quartz and carbonate fragments in a fine grained matrix of carbonate with minor fluorite and traces of galena and sphalerite

C coarse grained green fluorite with minor galena and sphalerite

D coarse grained quartz and barite containing fragments of zone C and E material suggesting a late origin along fractures. Minor galena and sphalerite

E coarse grained green to white fluorite with micro-crystalline white fluorite at the top of the zone. Minor quartz and barite (trace galena)

F fine grained pink barite at the base of the zone grading into pink-orange barite with minor quartz. ***Note: Zones F-H combined into one sample***

G fine grained pink to orange quartz grading laterally into fine grained gray to pink quartz suggesting flow-related facies change (minor chalcopyrite)

H fine grained pink to orange barite with minor quartz.

I fine grained gray to green fluorite with minor intergrown quartz and barite

J coarse grained white to gray quartz with minor intergrown fluorite and traces of barite (rare pyrite)

K fine grained orange to white quartz with minor intergrown fluorite and traces of barite and galena

L coarse grained white to gray fluorite and intergrown quartz with minor barite and traces of pyrite

4.1.8 Little Salt Cove Valley Vein

The Little Salt Cove Valley Vein, discovered in 1932 (Farrell, 1967), is located on the coast approximately 5 kilometres southwest of St. Lawrence (figure 4.1.3) near the western contact between the St. Lawrence Granite and Cambrian metasediments of the Inlet Group. The mineralization in this vein consists of fluorite, calcite, and quartz with minor barite and galena. The fluorite is coarse grained, displaying white, red and gray-blue colours. Calcite is massive to coarse grained and white to yellow in colour. Barite usually occurs as coarse grained white to pink platy aggregates.

Since this vein is not exposed, sample SCVV(A) (figure 4.1.11) is a 'grab sample' from the old workings. This sample contains coarse grained white calcite cut by later gray to blue coarse grained fluorite. The fluorite-bearing fluids appear to have invaded the calcite causing dissolution and limited recrystallization of calcite near the contact with

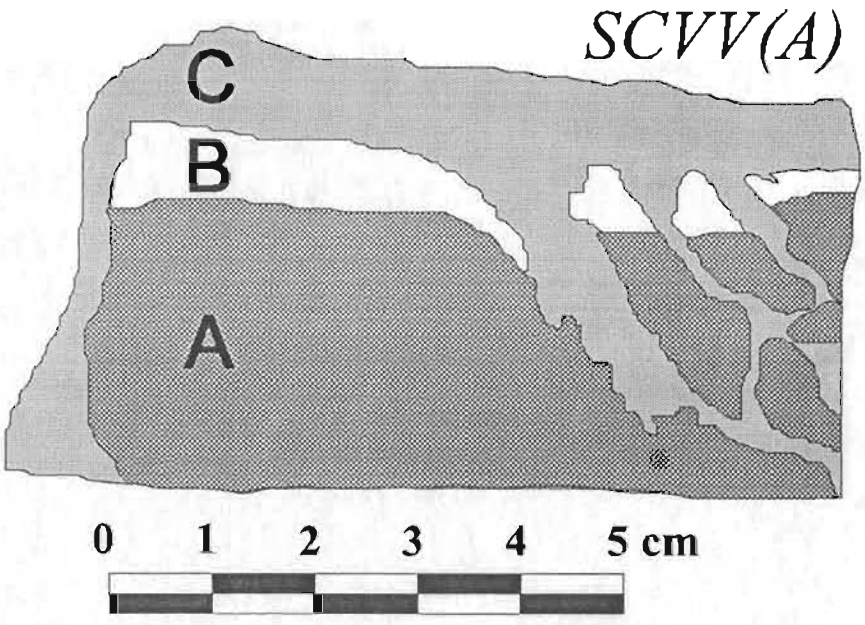

Figure 4.1.11 Sketch of sample SCVV(A), from the Little Salt Cove Valley Vein, showing later fluorite cutting earlier calcite.

the fluorite. On this basis the sample is subdivided into three distinct zones representing the interpreted cycle of mineralization. The zones are as follows:

A coarse grained white calcite which displays a 'ghosted' fragmental or vuggy texture

B coarse grained white to colourless calcite which appears to form a rim of recrystallized material surrounding the earlier calcite of zone A. The outer edge of this zone (calcite-fluorite contact) displays textures suggesting some dissolution. Geochemical analysis indicates that some of the colourless mineral may be quartz

C coarse grained gray to blue fluorite which locally displays an orange to red colouration possibly reflecting the presence of oxidized pyrite (?)

4.1.9 Miscellaneous Veins

In addition to the growth zoned samples described above, individual samples from 10 additional veins were analyzed to expand the spatial extent of the survey and to study some unique mineralizing environments or crystal forms not represented in the growth zoned samples. The samples and their locations are briefly described below:

- **Sample 2.** This sample was part of the original study by Strong et al. (1984) on the St. Lawrence fluorite deposits. This sample was re-analyzed by ICP-MS to examine REE patterns since preliminary analysis (Fryer and Strong, unpublished data) indicated similar patterns to 'early-stage' patterns observed in sample GNV-8 (see following section on REE geochemistry). Since GNV-8 was the only sample from the previous group which displayed such a signature, it was imperative to confirm that similar patterns exist in early mineralization from other veins. The exact location of sample 2 is uncertain, but it is reported (Strong et al., 1984) to be from the Tarefare or Director veins (figure 4.1.3). From the colour and nature of the sample, the former is more likely. The sample (figure 4.1.12) contains 11 alternating zones of coarse grained green fluorite and fine crystalline to micro-crystalline white fluorite. Samples 2-2 and 2-4 are from zones of earlier

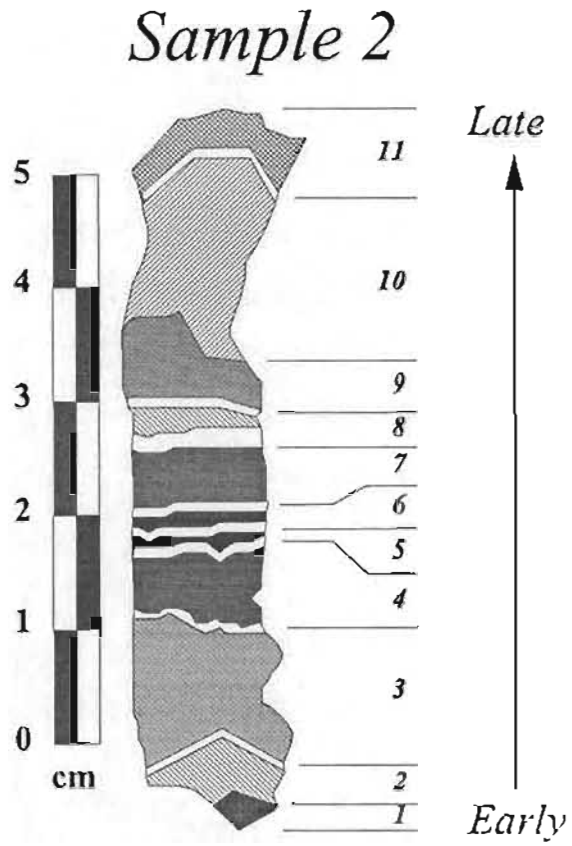

Figure 4.1.12 Sketch of sample 2, from an original sketch (Strong and Fryer, unpublished data), showing consecutive growth zones from the earliest (1) to the latest (11) periods of fluorite precipitation.

coarse grained green fluorite, while 2-8 is from a later zone of coarse grained green fluorite and 2-10 is from a wide zone of coarse grained white fluorite, the second-latest zone represented in the sample.

- **AD-1-A.** This sample is from the Anchor Drogue Vein, located approximately 18 kilometres northeast of St. Lawrence (figure 2.2.1). This vein is unique since it is the only vein hosted by the Precambrian Anchor Drogue Granodiorite (Strong, et al., 1978), approximately 3 kilometres from the nearest exposure of St. Lawrence Granite. The sample is from an early (near-wall) zone in a rhythmically zoned sample of coarse grained green fluorite. The sample has a strong radial texture suggesting octahedral habit. The zone (A) sampled contains minor intergrown coarse grained tabular pink to white barite and disseminated small crystals of galena.

- **AZ-1.** This sample is taken a small fluorite vein which cuts through the sericitic *'Alteration Zone'* at Little Salt Cove (figure 4.1.3). The sample consists of coarse grained white to green fluorite with minor galena. The host rock is a zone of variably sericitic altered, fine grained, aplitic granite with minor disseminated molybdenite and chalcopyrite mineralization. Two samples of the altered granite were also analysed. Sample AZ-4 is the most highly altered granite characterized by intense sericite alteration with minor disseminated chalcopyrite. Sample AZ-4 is a less altered pink aplitic granite with disseminated molybdenite and chalcopyrite. The zone is characterized by intense fracture-filling veins of quartz, fluorite and barite, with minor larger veins containing variable proportions of fluorite and quartz.
- **BB-84-11.** This sample is from the Blue Beach North Vein, located immediately west of St. Lawrence (figure 4.1.3). This vein is one of the large 'northwest-southeast' trending veins which is, where sampled, hosted entirely by granite. The sample is coarse grained fluorite from the central part of the vein.
- **BBS-84-D3C (79').** This sample is from a narrow 'offshoot' vein, of coarse grained yellow to purple fluorite, near the Blue Beach North Vein (see above). The vein, occurring entirely within the granite, was intersected in a diamond drill hole at a vertical depth of 17 metres.
- **BMWV-10-1.** This sample is from the Big Meadow Woods Vein, located 5 kilometres north of Lawn (figure 2.2.1). The vein is hosted by the 'Lawn Lobe' of the St. Lawrence Granite. The sample is a 'breccia-type' ore characterized by fragments of coarse grained quartz and fluorite in a blue-gray matrix of coarse grained fluorite with large, well developed, intergrown crystals of pink to white barite and galena.
- **GNV-7.** This sample was collected from the shaft dump at the Grebe's Nest Vein (figure 4.1.1). It consists of coarse grained green to colourless fluorite with minor intergrown colourless quartz and disseminated galena. The sample displays some zoning but it was crushed in bulk to use as an internal control standard for geochemical analysis.

- **GNV-ST.** This sample is also a grab sample from the Grebe's Nest Vein. It is composed of coarse grained blue fluorite with minor reddish brown, radial, spheroidal inclusions or intergrowths of hematite. The sample displays well developed, delicately growth-stepped crystals of presumably octahedral-form (i.e. do not in any way resemble cubic or modified cubic forms). This sample is interpreted to represent a late-stage period of fluorite growth into open vugs in the central part of the Grebe's Nest Vein. It is inferred that this sample correlates with a period of fluorite precipitation which followed the precipitation in zone O of sample GNV-8 but preceded, or was contemporaneous with, the deposition of the Fe-oxide/hydroxides of zone P. It is conceivable that the area of the vein in which GNV-8 was formed was somehow isolated from the fluid from which GNV-ST was formed, possibly by local blockages in the conduit system near the stage of final sealing by precipitating minerals.
- **LC-1.** The location from which this sample was taken is not known since it was given to me by a miner who worked in the St. Lawrence mines. Considering which mines were operating at the time he worked there, it is probably from either the Director or Canal vein (figure 4.1.3). The sample is a single cubic crystal of coarse grained colourless fluorite which measures approximately 10 cm across. Due to its size and perfect crystal form it is interpreted to have formed, from late stage fluids, in an open space (vug) in the central part of the vein. The only associated impurity in the sample is hematite, as small inclusions and as thin films on crystal faces, locally producing a reddish tinge of colour in the fluorite.
- **RHV-1.** This sample is from the Red Head Vein located on the coast 4 kilometres south of St. Lawrence (figure 4.1.3). This vein is one of the high-grade 'east-west' trending veins but has a lower grade 'gas breccia' zone developed on its western extension. This breccia zone consists of rounded fragments (up to 0.5 metres but averaging cobble size) of relatively unaltered pink, coarse grained granite in a matrix of coarse grained blue-green to white fluorite. The fluorite locally displays subtle 'nodular-type' textures around a core of granite fragments but this texture is not extensively developed. The sample RHV-1 is of coarse grained blue-green fluorite from the matrix of the 'breccia-type' mineralization.

- **SDMS-2-A.** This sample is from a molybdenite-bearing quartz (or micro-pegmatite) vein located approximately 1 kilometre northeast of Lawn, near the old second power dam (figure 4.1.8). For the purpose of this report, this occurrence will be referred to as the '*Second Dam Moly Showing*'. The vein is hosted by the coarse grained to quartz-feldspar porphyritic, red granite which forms the 'Lawn Lobe' of the St. Lawrence Granite, near the contact with Cambrian Inlet Group metasediments. The vein consists primarily of coarse grained white to gray quartz with minor intergrown coarse grained pink K-feldspar crystals and sporadic large (up to 5 cm) radial, platy crystals, and more frequent smaller aggregates, of molybdenite. The sample represents a composite section across the entire width of the vein (~10 cm).

5 Fluid Inclusion Study

5.1 General Statement

The present fluid inclusion study involved more than 500 microthermometric determinations of homogenization and melting temperatures from 12 different veins. Fluid inclusion data, calibration results and methodology are given in Appendix 2. The fluorite samples were found to contain numerous, often large fluid inclusions, measuring up to 100 μm in diameter but averaging 30 to 40 μm. Most of the fluid inclusions in the fluorite can be considered primary since they usually occur within crystals (occupying negative crystal forms) or along microscopic crystal growth zones. Some rounded and lenticular inclusions, defining a somewhat linear trend, and some irregular inclusions, occurring along cleavage planes, appear to be secondary.

Since most of the fluorite zones contain an abundance of relatively large inclusions, only inclusions (normally from the central parts of crystals) which fit Roedder's (1979) criteria for 'primary' inclusions were used in this study. The fluid inclusions shown in figure 5.1.1 are typical of the primary inclusions used. Occasionally, in zones where definitely 'primary' inclusions were not available, inclusions along crystal boundaries or cleavage planes were used. Since no significant systematic temperature or

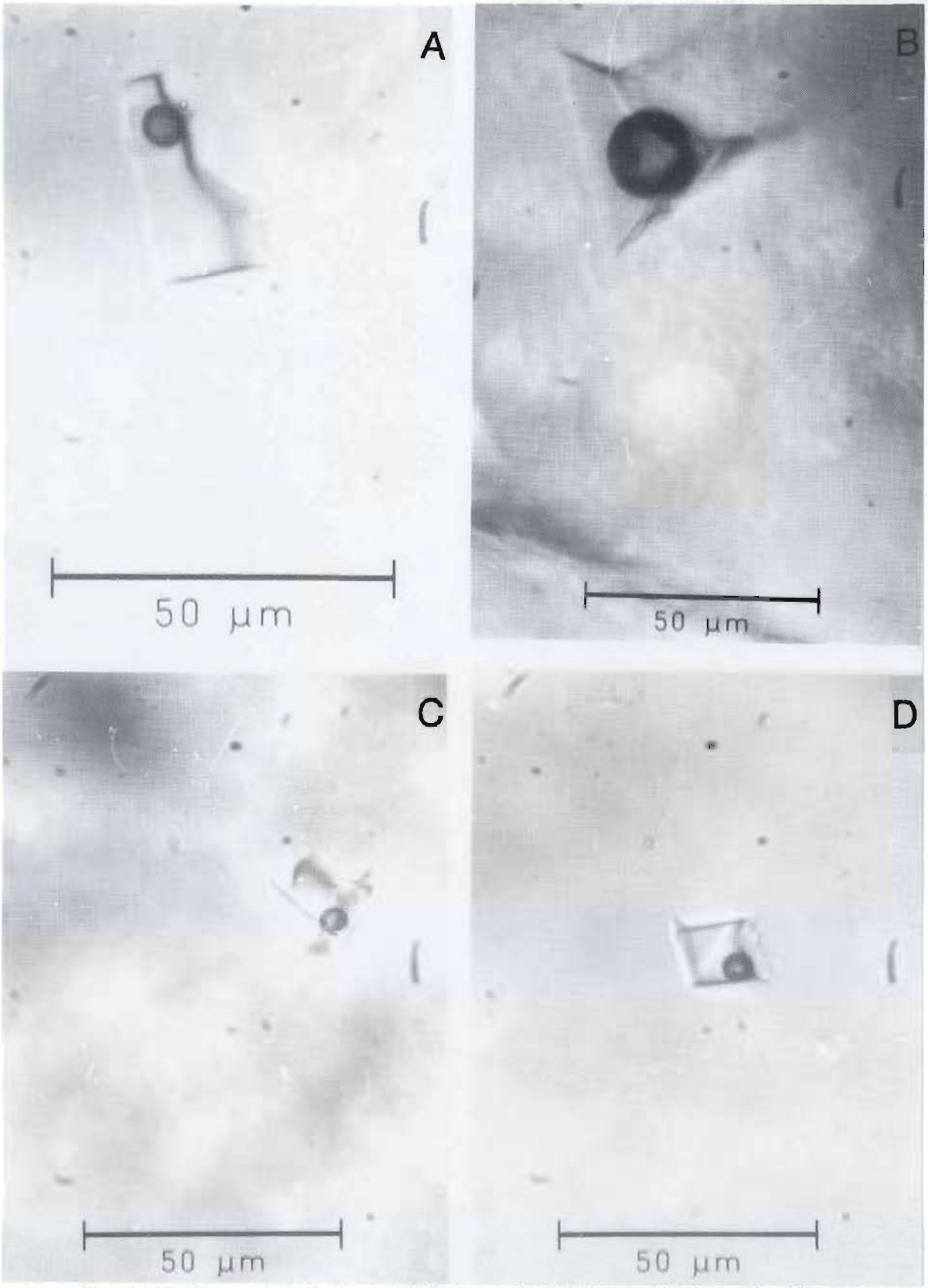

Figure 5.1.1 Photomicrographs of 'typical' fluid inclusions in the St. Lawrence fluorite samples. These are: (a) large two-phase inclusion from zone GNV-8-J; (b) large two-phase inclusion from zone GNV-8-A, occupying a well developed negative crystal form; (c) irregular-shaped primary two-phase inclusion from zone GNV-8-G; and (d) small rhombohedral-shaped primary two-phase inclusion from zone GNV-8-J.

salinity differences were detected between these and 'primary' inclusions they can be considered pseudo-secondary.

For the most part, the inclusions studied, especially those in fluorite were simple two-phase vapour-liquid inclusions with no daughter minerals or CO_2, despite evidence for CO_2 effervescence indicated by the abundance of calcite in gas breccias (Strong et al., 1984), alteration zones (Strong, 1982) and many fluorspar veins. Some fluid inclusions contain solid inclusions, most of which are opaque and appear to be hematite. Rather than 'daughter minerals', these were trapped as particles, similar in origin to solid inclusions (commonly hematite) observed within fluorite crystals. For most of the fluid inclusions in fluorite, the fluids were relatively dense (1.17 - 0.96 g/cm^3) and vapour bubbles occupy less than 10 volume percent of the inclusion.

The fluid inclusion results from the present study indicate that homogenization temperatures have a positively skewed uni-modal distribution with a broad, but well defined, maximum at about 100°C (figure 5.1.2) over a broad range between 380°C and 50°C, but with more than 90% of the data being between 140°C and 70°C. No direct evidence for boiling was observed in fluorite samples from the present study but most of the samples measured were below the temperature range (450°C to 220°C) in which Strong et al. (1984) found evidence for boiling.

Freezing temperatures from this study indicate a relatively bi-modal distribution (figure 5.1.3) with the largest population defining a maximum around 12 eq. wt. % NaCl and a smaller population with a maximum around 25 eq. wt. % NaCl, throughout a broad range between 28 and 0 eq. wt. % NaCl. All samples with estimated salinities greater than 23.3 eq. wt. % NaCl were defined based on the identification of the clathrate

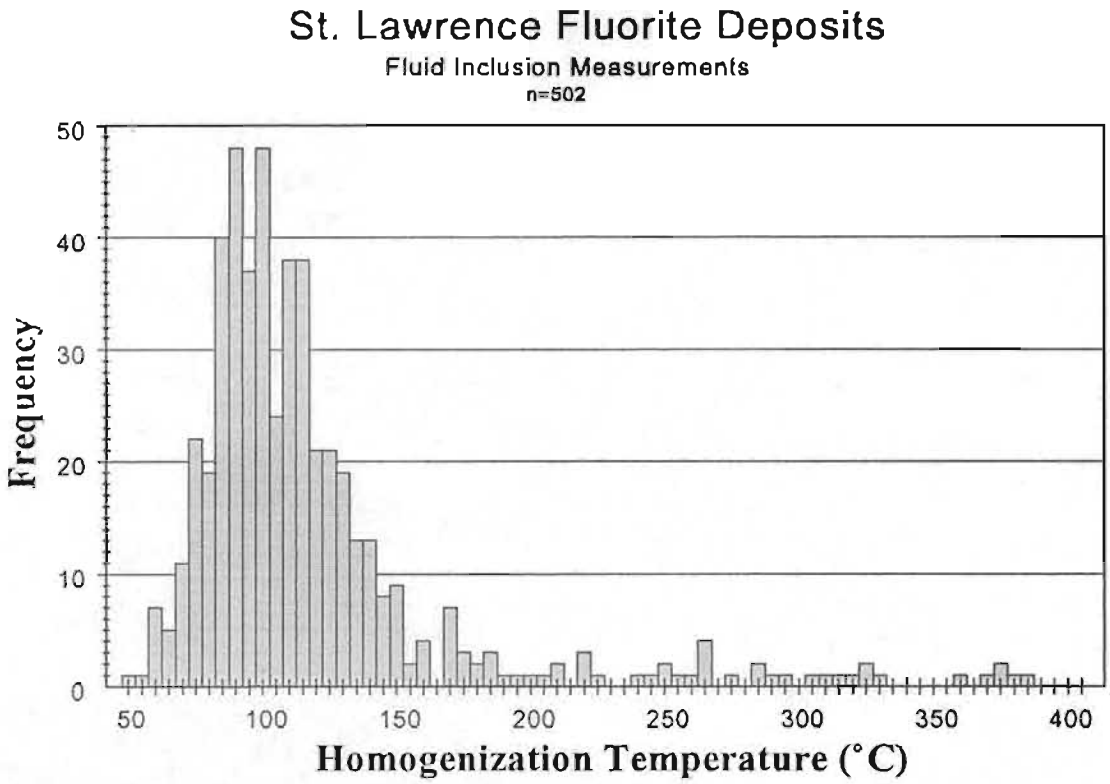

Figure 5.1.2 Histogram plot of the distribution of homogenization temperatures from all the samples used in this study.

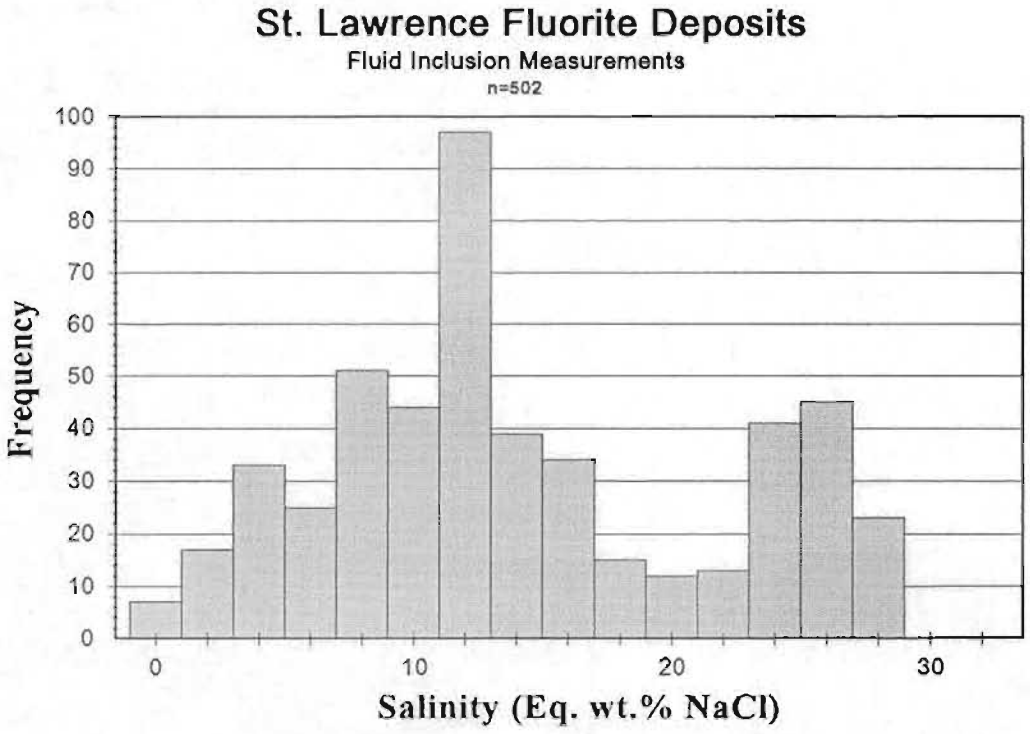

Figure 5.1.3 Histogram plot of calculated salinity data for all fluid inclusions from this study. Salinity is in equivalent weight percent NaCl.

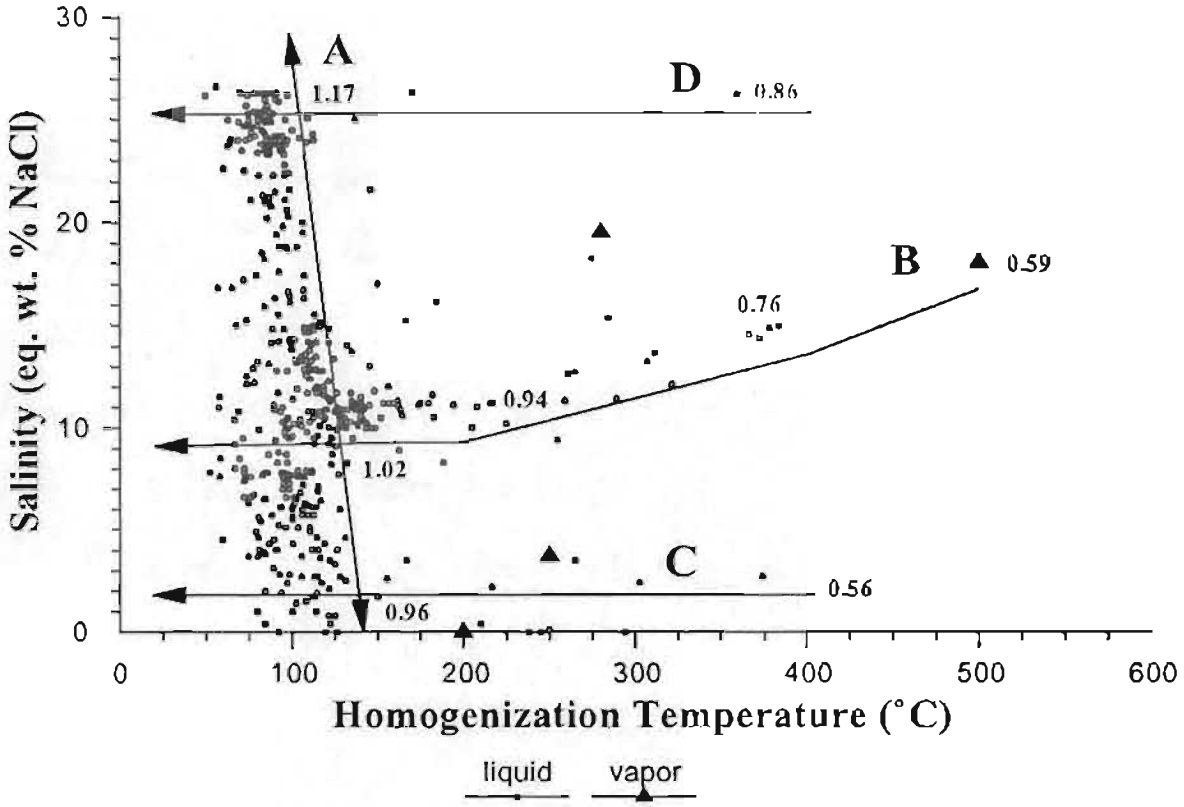

Figure 5.1.4 Plot of salinity versus homogenization temperature for fluid inclusions from all samples in this study. The numbers represent estimated fluid densities calculated from homogenization temperature and salinity relationships using the equation given by Bondar (1983).

hydrohalite. In these inclusions, ice would melt near the eutectic, or more often the metastable eutectic temperature, but hydrohalite would persist to higher temperatures. Failure to distinguish hydrohalite ($NaCl \cdot 2H_2O$) from ice may have led to underestimating of salinity in a few of the smaller inclusions. Estimates of temperature of first melting range from -20.8°C ($NaCl-H_2O$ eutectic) to less than -50°C suggesting a significant amount of CaCl in the system. This data might best be interpreted in terms of the ternary $NaCl-H_2O-CaCl$ system, but all interpretations are based on equivalent relationships in the $NaCl-H_2O$ binary system, which is adequate for the discussions presented.

For most fluid inclusions, homogenization temperature and freezing temperature 'pairs' were measured. In a plot of homogenization temperature versus salinity, shown in

figure 5.1.4, several trends are evident. The bulk of the measurements fit the well defined trend 'A', which displays either increasing salinity with decreasing temperature or decreasing salinity with increasing temperature. The higher temperature inclusions mainly define trend 'B', which displays slightly decreasing salinity with decreasing temperature. The lower salinity, high-temperature inclusions define trend 'C', a trend of constant salinity with decreasing temperature. A parallel, but less well defined trend (D) is interpreted to persist for the high salinity inclusions.

The density of the St. Lawrence fluids was estimated from the homogenization temperature and salinity data using the equation (A1) given by Bodnar (1983, p.542) for calculating the density of vapour-saturated NaCl solutions. Bodnar's (1983) equation was calculated using a FORTRAN IV stepwise multiple-regression program utilizing experimental data from a number of sources for input. The density of inclusion fluids s from this study range from 1.17 to 0.56 g/cm^3 but most (trend 'A') are relatively high density inclusion fluids in the range of 1.17 to 0.96 g/cm^3. The density of inclusion fluids

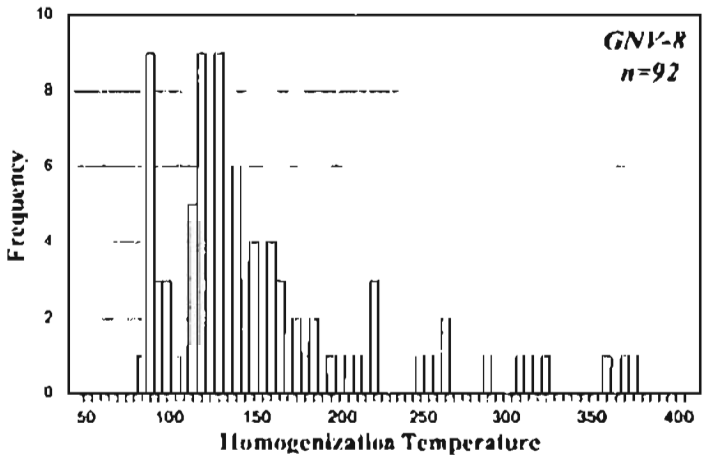

Figure 5.2.1 Histogram plot of homogenization temperatures in all samples from the Grebe's Nest Vein. All measurements are from fluorite.

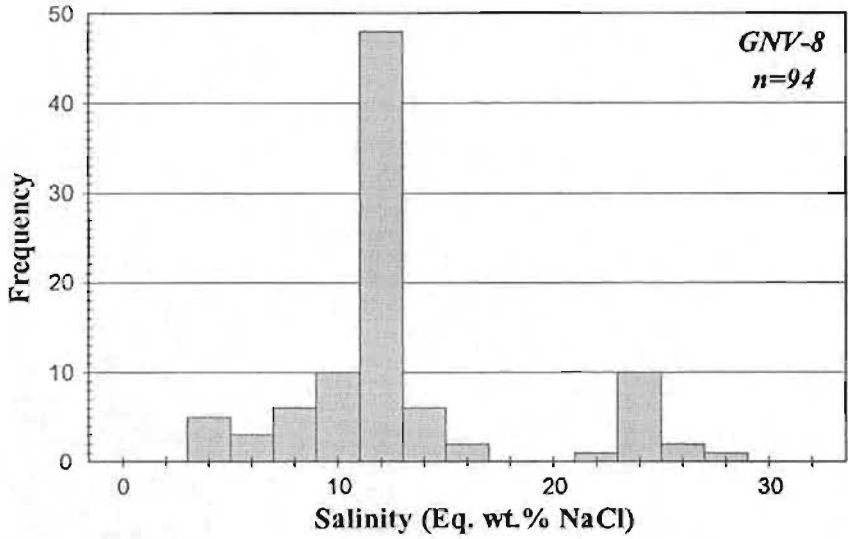

Figure 5.2.2 Histogram plot of calculated salinity from all samples from the Grebe's Nest Vein. All measurements are from fluorite. Salinity was calculated using phase relationships in the NaCl-H_2O binary system and is expressed in equivalent weight percent NaCl.

fromtrend 'B' range from 1.02 to 0.59 g/cm³, while those from trend 'C' range from 0.96 to 0.56 g/cm³, and those from trend 'D' range from 1.17 to 0.86 g/cm³.

5.2 Fluid Inclusion Results from Selected Veins

The following section will briefly discuss temperature and salinity relationships within individual veins or samples. The main discussions will focus on the growth zoned samples and the systematics of temperature and salinity variations.

5.2.1 Grebe's Nest Vein

The overall distributions of homogenization temperature and salinity in this vein are presented as histograms in figure 5.2.1 and 5.2.2 respectively. The homogenization temperatures define a somewhat disjointed, positively skewed, distribution similar to the overall distribution shown in figure 5.1.1, with a maximum at around 125°C and a range of between 110°C and 375°C. A separate lower temperature population can be distinguished which has a maximum at 90°C and a range between 110°C and 80°C. The

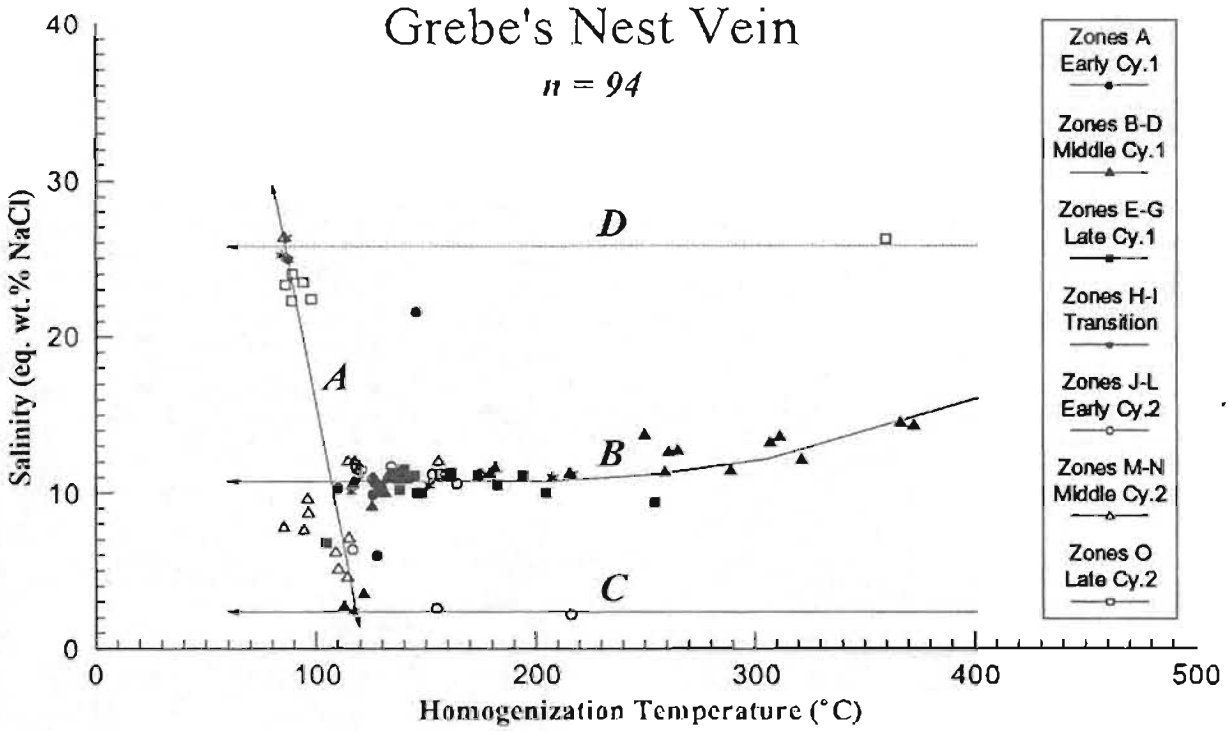

Figure 5.2.3 Plot of homogenization temperature versus salinity for the Grebe's Nest Vein. Symbols represent the sequence of growth zones from which the measurements were taken. Cycle 1 (Cy1) is earlier coarse grained green fluorite while cycle 2 is later blue - white fluorite.

salinity data, shown in figure 4.22, shows a definite bi-modal distribution. The higher salinity group has a maximum at around 24 eq. wt. % NaCl and a range between 28 and 22 eq. wt. % NaCl, while the lower salinity group is slightly negatively skewed with a maximum at around 12 and a range between 16 and 4 eq. wt. % NaCl.

A plot of salinity versus homogenization temperature (figure 5.2.3) displays a strong 'trend B' (figure 5.1.3), which has been identified and defined from this sample. This trend shows an increase in temperature and a corresponding slight increase in salinity from zone A to B-C, peaking at a temperature near 400°C, and following a reverse path to merge with low temperature 'trend A'. The variation in homogenization temperature, through growth zones in sample GNV-8, is presented as histograms in figure 5.2.4. The homogenization temperature in zone A is around 125°C with a rapid rise to

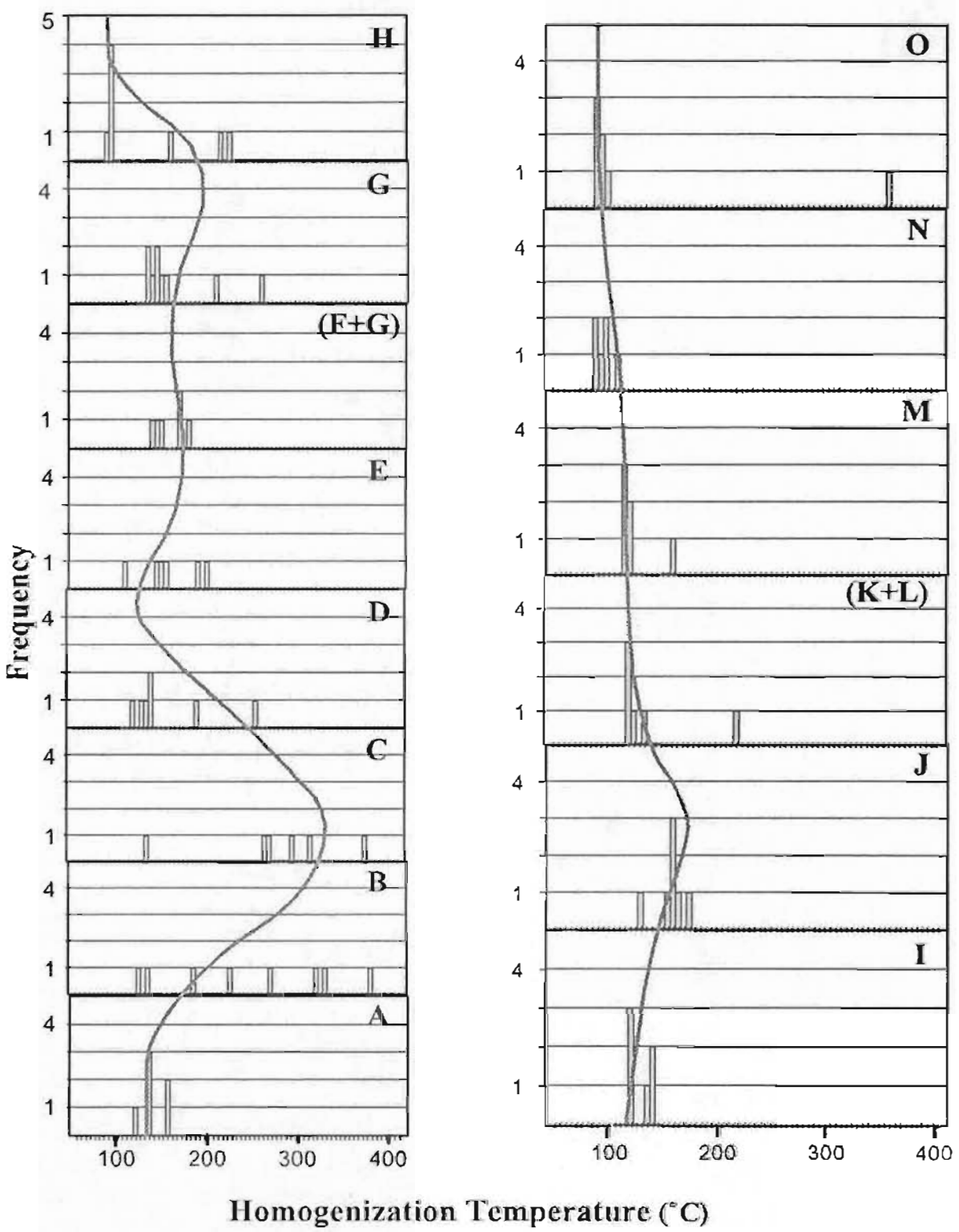

Figure 5.2.4 Histogram plots showing the distribution of homogenization temperatures in consecutive growth zones within sample GNV-8 from the Grebe's Nest Vein. Zone A is the earliest fluorite zone while zone O is the latest. The gray lines on the plots represent interpreted temperature variation through successive periods of fluorite precipitation.

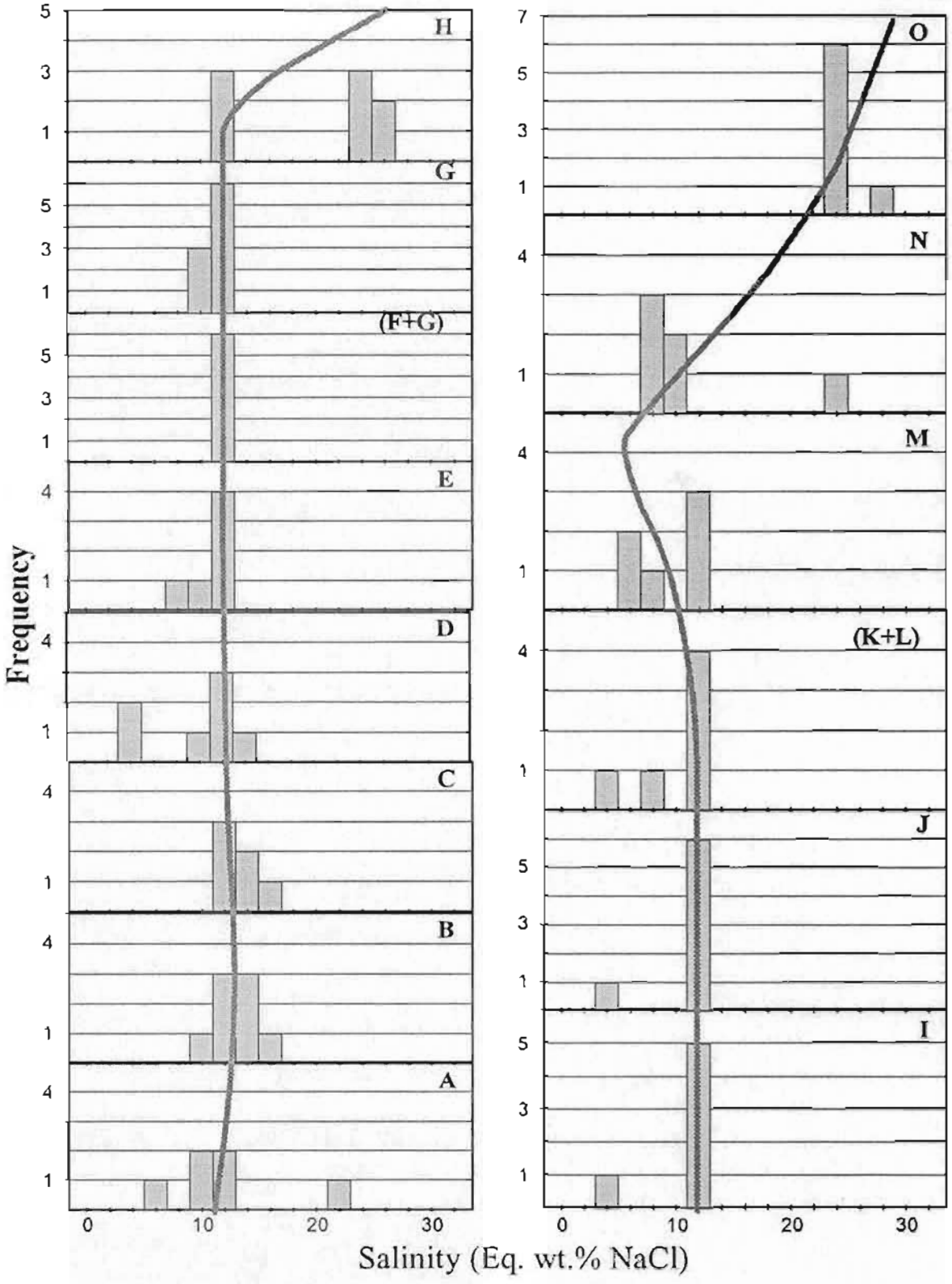

Figure 5.2.5 Histogram plots showing the distribution of calculated salinity ($NaCl-H_2O$ binary system) in consecutive growth zones within sample GNV-8 from the Grebe's Nest Vein. Zone A is the earliest fluorite zone while zone O is the latest. The gray lines on the plots represent interpreted salinity variation through successive periods of fluorite precipitation.

near 400°C, through zones B and C, and subsequently decreasing to around 125°C by zone D and E. Due to the large variations in homogenization temperature within zones B and C, it appears that most of the temperature increase occurred during the deposition of 'zone B' fluorite while most of the temperature decrease occurred during the deposition of 'zone C' fluorite. From zone D to E there is a rise in homogenization temperature from 125°C to around 150°C which continues through to zone G. Zone H appears to be characterized by two groups of inclusions, a higher temperature (250-200°C) group which, through an apparent rapid temperature drop, evolves into a lower temperature (90-85°C) group. The homogenization temperature for zone I is approximately 125°C and increases to around 160°C in zone J. From zones J to O there is a steady decrease in homogenization temperature from 160°C to around 90°C.

The salinity data for growth zones in sample GNV-8, presented as histograms in figure 5.2.5, do not show quite as much variation as the homogenization temperature data, but some significant variations are apparent. The salinity data from zones A through L are remarkably consistent at around 12 eq. wt. % NaCl except for several notable exceptions. The salinity values in zone A range from 12 to 6 eq. wt. % NaCl while zones B and C range up to 16 eq. wt. % NaCl, suggesting an increase and decrease in salinity accompanying the increase and decrease in temperature noted above. Zone H can again be considered in terms of two distinct groups, an early 'normal' salinity group and a later high salinity group ranging from 26 to 24 eq. wt. % NaCl. This high salinity group is also characterized by lower homogenization temperatures (90-85°C) as noted above. Zones M to O show a trend of decreasing salinity followed by rapidly increasing salinity, deviating from the 'normal' value of around 12 eq. wt. % NaCl. Salinity data in

zone M has a range from 12 to 6 eq. wt. % NaCl, indicating decreasing salinity across the zone with a local minimum possibly late in the zone, while salinity data from zone N ranges from 24 to 10 eq. wt. % NaCl, indicating increasing salinity across the zone which culminates in zone O which shows a rather consistent salinity of 24 eq. wt. % NaCl. These salinity variations occur during steadily decreasing temperatures from 120°C in zone M to 90° in zone O (figure 5.2.4).

5.2.2 Iron Springs Vein

The homogenization temperature data from growth zoned sample ISV-1 show a bi-modal distribution (figure 5.2.6a) with well defined maxima at 115°C and 90°C over a range between 140°C and 85°C (with a high temperature outlier at 285°C). The salinity data define a tri-modal distribution (figure 5.2.6b) over a wide range of salinities from 30 to 6 eq. wt. % NaCl, with maxima at 24, 14 and 9 eq. wt. % NaCl. A plot of salinity versus homogenization (figure 5.2.7) clearly indicates that fluid inclusions from this sample fall on 'trend A' (defined above) and show a progressive evolution from early high salinity to later low salinity fluids with a corresponding increase in temperature over a narrow range. The three early, fine grained, zones of fluorite, quartz and calcite (A to

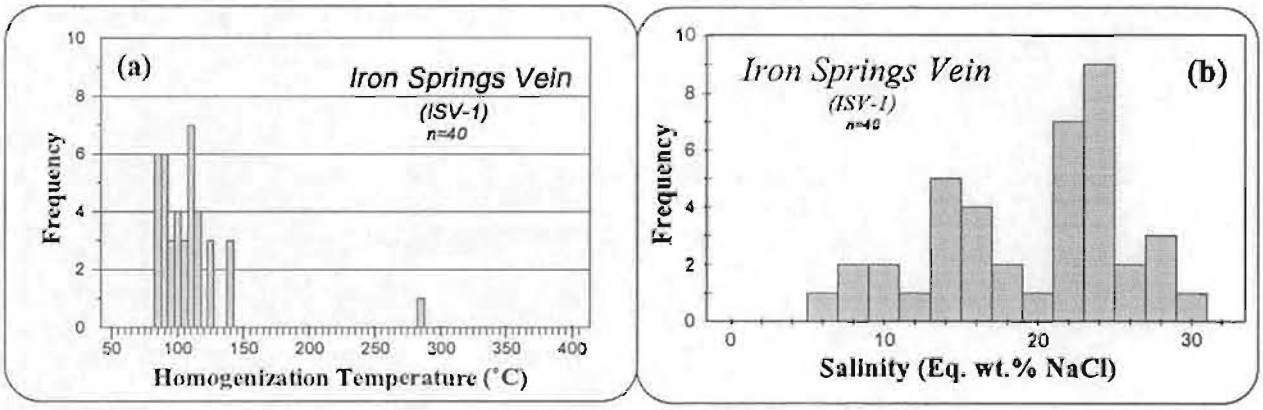

Figure 5.2.6 Histogram plots of (a) homogenization temperatures and (b) calculated salinity ($NaCl$-H_2O binary system) for fluid inclusions in fluorite from the Iron Springs Vein.

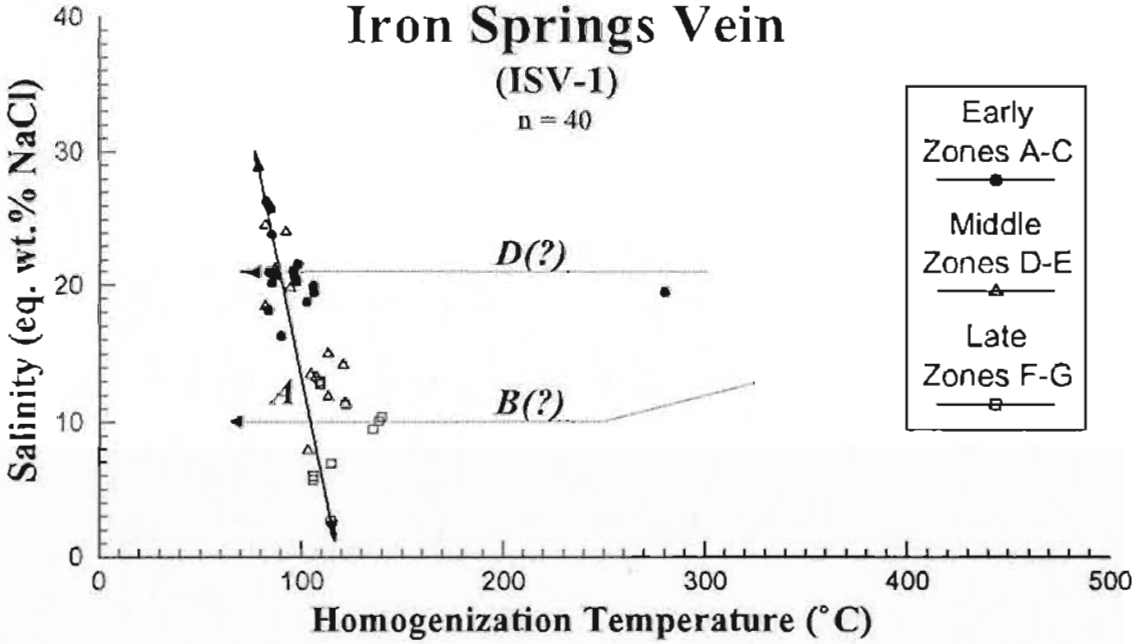

Figure 5.2.7 Plot of calculated salinity ($NaCl-H_2O$ binary system) versus homogenization temperature for samples from the Iron Springs Vein. The symbols represent the sequence of fluorite precipitation for consecutive growth zones.

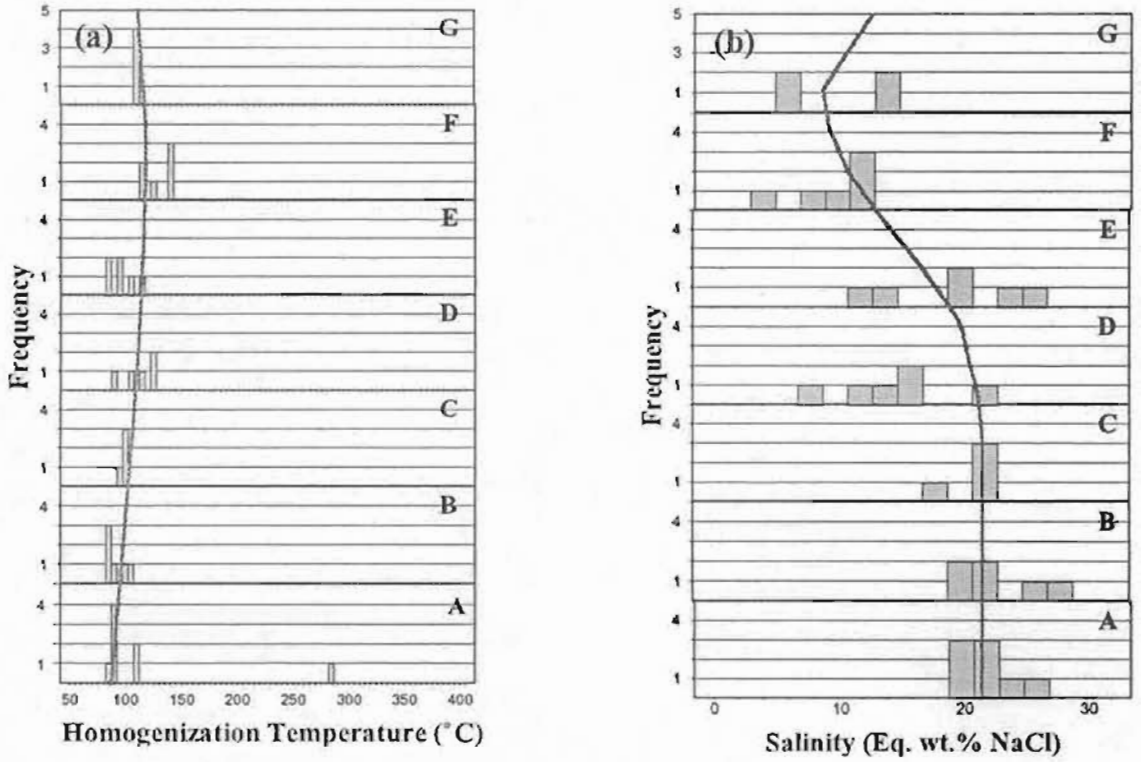

Figure 5.2.8 Histogram plots of the distribution of (a) homogenization temperatures and (b) calculated salinity in fluorite from the Iron Springs Vein. Sample labels refer to consecutive growth zones from the earliest (A) to the latest (G) periods of fluorite precipitation.

C), show consistent homogenization temperatures and salinities (figure 5.2.8a,b) near 90°C and 22 eq. wt. % NaCl respectively. The coarse grained fluorite zones (D to G) display quite variable but slightly increasing temperatures, ranging from approximately 150°C to 90°C, culminating in zone G with a temperature of approximately 110°C. Throughout the same interval the salinity data shows an irregular but persistent trend of decreasing salinity from approximately 22 to 8 eq. wt. % NaCl.

5.2.3 Other Veins

Fluid inclusion measurements on fluorite from most of the other veins show considerable variability but consistently fall on 'trend A', forming a continuum between higher temperature (125 - 100°C) lower salinity (near zero) and lower temperature (100 - 80°C) higher salinity (26-24 eq. wt. % NaCl) measurements. As can be seen in comparing 'trend A' fluid inclusions from successive growth zones in the Grebe's Nest Vein to those in the Iron Springs Vein, it is apparent that fluid evolution proceeds in either direction along the trend suggesting somewhat irregular and intermittent mixing of fluids.

The results from other samples will not be discussed individually because of the high degree of similarity in terms of the overall distribution. A listing of the data is appended (Appendix 2) and relevant fluid inclusion results will be incorporated into discussions of other aspects of the study.

5.3 Discussion of Fluid Inclusion Results

The results of this study, as well as those of Strong et al. (1984), demonstrate that fluid inclusions in fluorite from the St. Lawrence deposits are consistently simple

two-phase liquid-vapour inclusions, with no daughter minerals or separate CO_2 phase. Although some groups of inclusions show alignment and could be considered secondary, the systematic variations between growth zones and fragment-matrix relationships in brecciated fluorite, lead to the conclusion that most of the inclusions were trapped during fluorite deposition.

The tri-modal distribution of homogenization temperatures recognized by Strong et al. (1984), with maxima around 350°C, 230°C and 120°C, within a range from 490°C to 90°C, was recognized (i.e. early zones of GNV-8) but not widely represented in the suite of samples studied. The discrepancies between the two studies may be due to several reasons:

- the samples used by Strong et. al. (1984) were reported to be primarily from two veins, the Director and Tarefare which were mined underground. Some of these samples may represent deeper (hotter) levels in the conduit system. No samples from these two veins were included in the present survey

- the samples used by Strong et al. (1984) contained a higher percentage of nodular and/or gas breccia samples which themselves may reflect a higher temperature regime. Breccia or nodular ores were more common in the Director and Blue Beach mines (Williamson, 1956).

- the growth zoned samples reported by Strong et al. (1984; figure 6, p. 1150) show that the temperature is usually systematically higher in the earlier zones.

It appears that the higher temperature inclusions are usually associated with the early phases of recognized mineralizing cycles or zones of explosive (gas) brecciation. Most of the samples in this study have relatively low homogenization temperatures (ca. 100°C) attesting to the dominance of relative late-stage, passive mineralizing processes in

the formation of many of the veins. Combining the results of this fluid inclusion study with that of Strong et al. (1984), it is concluded that fluorite deposition took place continuously throughout an extremely wide temperature range (500°C to 50°C) and that the detection of systematic rising and falling temperatures, with successive fluorite precipitation, suggests periodic recharge (sometimes explosive) of hot fluids. This is consistent with the conclusions of Strong et al. (1984), who interpreted their results in terms of repeated pulses of hot fluid emanating from deeper within the magma chamber, possibly with admixtures of meteoric water. Using this evidence, they concluded that the cooling of fluids was not the main control on fluorite deposition.

From their fluid inclusion data, Strong et al. (1984) suggested that the fluids were boiling through the temperature range 450°C to 223°C. They cite the case of adjacent fluid inclusions (with contrasting liquid/vapour ratios) which homogenize to a liquid and a vapour respectively at similar temperatures, as evidence that the fluids were boiling (Roedder, 1984). This supports their conclusions that homogenization temperatures in the St. Lawrence fluorite samples closely approximate temperatures of formation, something that is not totally unexpected since the deposits probably formed in a very low-pressure regime.

The freezing temperature data indicate quite variable fluid salinity during the deposition of the fluorite veins, ranging from 30 to 0 equivalent weight percent NaCl, consistent with the range from 25 to 6 (eq. wt. %NaCl) reported by Strong et al. (1984), a range which they conclude could either be primary (i.e. magmatic) or alternatively generated as a result of boiling and condensation of fluids. The fluids are relatively

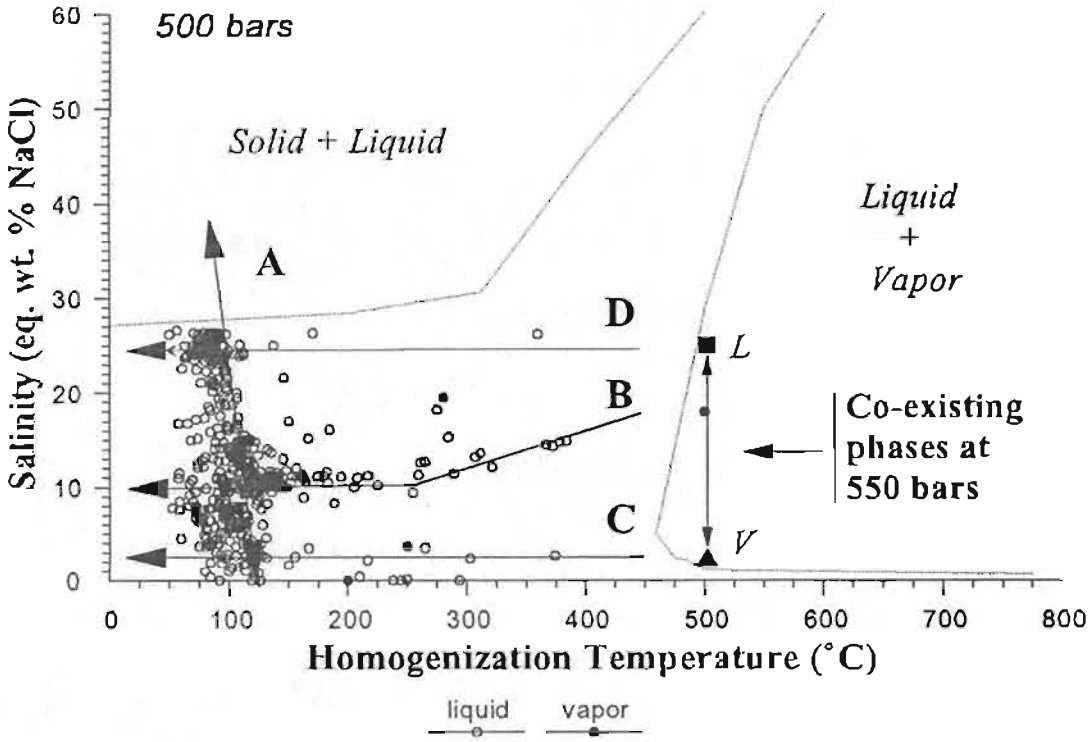

Figure 5.3.1 Plot of homogenization temperature versus salinity for all fluid inclusions from this study showing fluid evolution trends (A - D). The solid+liquid and liquid+vapour fields (H_2O-NaCl binary system) are from Shibue (1991) and the co-existing liquid (*L*) and vapour (*V*) compositions at 550 bars are from Sourirajan and Kennedy (1962).

dense, with vapour bubbles generally occupying less than 10 volume percent, although vapour occupies up to 25 volume percent in some samples, particularly in gas breccias.

Based on fluid salinity and temperature, Strong et al. (1984) concluded that the boiling curves for the binary H_2O-NaCl system indicated pressures between 650 and 65 bars persisted during fluorite precipitation, in accord with other geologic evidence. The extended liquid+vapor and solid+liquid two-phase regions in the binary H_2O-NaCl system, at 500 bars (Shibue, 1991 - compiled from various sources), has been added to a plot of temperature versus salinity for fluid inclusions from the present study as shown in figure 5.3.1. The trends previously discussed and shown in figure 5.1.4 are similarly

indicated by the labels A, B, C, and D. Trend 'A', displaying either increasing salinity with decreasing temperature and/or decreasing salinity with increasing temperature, is interpreted to represent the mixing of a low salinity, possibly condensed vapour (from low-pressure boiling) or meteoric fluid, and a higher salinity, probably magmatic, fluid in a low temperature regime. The higher temperature inclusions generally define trend 'B', displaying slightly decreasing salinity with decreasing temperature, suggesting variable mixing of a hotter, more saline fluid with cooler, low salinity fluid (i.e. the low salinity end of trend 'A'). This trend may be better defined by a curved, rather then a linear trend, with the sloping part (figure 5.3.1) being dominated by mixing and the flat part by simple conductive cooling. Trend 'C', in which the high temperature end is defined primarily (but not exclusively) by inclusions in quartz is interpreted in terms of the simple cooling of a low salinity fluid.

These salinity and temperature variations can be considered in terms of the simple boiling and condensation of fluids as suggested by Strong et al. (1984). Since the low salinity fluid reaches temperatures near 400°C, it could represent simple cooling of low salinity vapour originating from low pressure boiling of high salinity magmatic fluid (liquid) deeper in the conduit system. The parallel, but less well defined trend (D), could be explained by simple cooling of the high salinity magmatic fluid. Trends A and B may represent variable mixing of the liquid and condensed vapour, combined with the possible influx of meteoric water, in the upper levels of the conduit system.

Figure 5.2.1 shows the liquid+vapor phase boundary for the binary H_2O-NaCl system (Shibue, 1991) and the equilibrium composition of co-existing liquid and vapour separating from a fluid of critical composition at approximately 500°C and 550 bars

(Souririajan and Kennedy, 1962). At 500 bars, the liquid+vapour phase boundary is near the higher limit of temperature for fluid inclusions found in the fluorite, but lower pressure would move the boundary towards lower temperatures overlapping the high temperature end of trend 'B'.

The fluid inclusion trends observed in the St. Lawrence samples may be best explained (figure 5.3.1) in terms of a supercritical magmatic fluid unmixing at shallow depths and evolving both seperate low salinity vapour and high salinity liquid phases. The vapour phase would rapidly rise through the conduit system, often producing explosive products (gas-breccias), to eventually cool and condense as a low-salinity liquid (trend 'C') in the upper levels of the system. As the system is recharged, the high salinity fluids would tend to infiltrate into higher levels of the conduit system, being variably mixed with the low salinity fluids already filling much of the conduit system (trend 'B'). These cycles (or pulses) of fluid infiltration would be accompanied by initial increases in temperature followed by decreases in temperature as the thermal effects of the cycle diminished (conductive cooling). Invariably in the late stages of such cycles the fluid in the conduit system would be dominated by cool, saline, residual magmatic fluids (trend 'D'). It is conceivable that such fluids would be significantly cooled prior to infiltrating the upper regions of the conduit system, possibly explaining the lack of higher temperature inclusions along trend 'D'.

The fluid inclusion data shows that most of the fluid mixing (trend 'A'), and fluorite precipitation, took place in a relatively low temperature regime. This would suggest that, if the 'magmatic pulse' model is valid, then these cycles would have to be primarily of long duration, allowing time for substantial conductive cooling and complete

infiltration of the conduit system by cool residual magmatic fluid. In such a long time span of relatively passive fluid movement, it is quite probable that meteoric waters would enter the conduit system and mix with the magmatic fluids. Oxygen isotopic studies (Strong et al., 1984) on hydrothermal quartz and inclusion fluids in fluorite from the St. Lawrence veins have yielded $\delta^{18}O$ values which range from primary magmatic to meteoric signatures. Although mixing of a meteoric component could explain most of the trend 'A' results, it would be difficult to rationalize the low-temperature high-salinity inclusions, or indeed the overall distribution, in terms of a simple two end-member mixing model. The low-temperature deviation from trends 'A' and 'B' may be the effects of simple conductive cooling.

6 Geochemistry of the Vein Samples

6.1 General Statement

The samples of various growth zones and individual vein samples were analysed using X-ray fluorescence (XRF) and inductively coupled plasma (ICP-MS) techniques. The XRF (conventional pressed pellet) analyses are representative of the whole sample or zone while the ICP-MS (boric/nitric acid dissolution) represents analysis of primarily the fluorite and/or calcite (acid soluble) components of the zone. The common gangue minerals barite and quartz are relatively (< 5%) insoluble in the boric/nitric dissolution procedure. The common accessory sulphides show limited solubility in the boric/nitric dissolution with approximately 10% of the chalcopyrite and galena dissolving but sphalerite is relatively insoluble. The limited solubility of the sulphides should not seriously affect the REE analysis since sulphides (particularly galena) do not favour incorporation of the REE (Morgan and Wandless, 1980).

A complete listing of all the analytical data is presented in Appendix 1 as well as in variable file formats on the accompanying IBM-compatible floppy disk. The table format used for the geochemical data presentation is broken down into the following categories:

1 **Boric Acid Dissolution** gives a measure of the degree of dissolution of samples based on residue weight (i.e. [total - residue] ~ fluorite and/or calcite content)
2 **Calculated from XRF** is an estimate of the sample zone mineralogy based on the XRF analysis (for reference only, semi-quantitative)
3 **XRF Majors** presents major element data which again should be regarded as semi-quantitative
4 **XRF Traces**
5 **ICP-MS Traces**
6 **ICP-MS REE**
7 **ICP-MS Ratios**

To assess the various major and trace element components in the vein zones, the analytical data was subdivided into four groups based on the major mineralogy of the zones. The groups were analyzed statistically to determine mean, standard deviation, maximum and minimum values for each element and the results are tabulated (by analytical method) in tables in the following section. These statistics are given to facilitate presentation of the magnitude and range of the 'raw' analytical data and are not meant to infer 'true mean', or average values, characteristic of the various groupings. For the purpose of statistical analysis elements with values less than detection limits were interpolated to a value equal to ½ the limit of detection, in accord with standard methods of dealing with missing values in statistics (Rock, 1988: *p. 207*).

If the group average value for any element is below the limit of detection (LOD), it is reported as ' < LOD', and if the average value is less than the limit of quantitation (LOQ) or the effective limit of quantitation (ELOQ), it is presented as the 'average value' enclosed in parenthesis. The derivation of the ELOQ for the ICP-MS from calibration and reagent blanks, outlined in Appendix 1, followed the guidelines proposed by Keith et al. (1983) for data quality evaluation in environmental chemistry. For comparison to

ICP-MS confidence limits, LOQ for the XRF data was assumed to be 3.33 times the LOD.

6.2 Major and Trace Elements in Fluorite

Analyses of coarse grained fluorites containing no minor phases are presented in Table 6.2.1 and the calculated mineralogy verifies that only very minor amounts of quartz or silicate minerals coexist with the fluorites in this group. Therefore, it is assumed that the trace element analyses from this group of samples reflect the chemical character of the fluorite, and assuming nearly complete dissolution, the ICP-MS and XRF trace element analyses should be equivalent. The correlation between ICP-MS and XRF is good for most of the elements with the exception of Nb and Sc. The Nb values are considerably higher (10 times) by XRF, while the Sc values average 41 ppm by XRF and less than the detection limit (4 ppm) by ICP-MS. The discrepancy in the Nb values may be due to its concentration level in the fluorite being close to the XRF limit of detection. The discrepancy in the Sc values may be due to inadequate correction for Ca interference on the XRF data due to the high Ca levels in these fluorite/calcite bearing samples.

The majors are dominated by CaO since Ca is a major component in fluorite (CaF_2). The CaF_2(c) was calculated based on the XRF CaO analysis corrected to a factor determined from multiple XRF analysis (Appendix 1B) of a fluorite standard (NBS-79a). As well, SiO_2 values below 20% were corrected to reported values for NBS-79a. The detectable levels of SiO_2 (0.2%) and Fe_2O_3 (0.05%) in the fluorite samples probably reflect minor accessory quartz and hematite which commonly occur with the fluorite. Trace amounts of Al, Na and K may be due to contributions from fluid inclusions which

Table 6.2.1 Summary of the geochemical analyses of coarse grained fluorites from the St. Lawrence fluorspar veins. These samples are from zones which contain no apparent minor phases.

Coarse Grained Fluorite (no visible minor phases)

(n = 12)

	Mean	SD	Max.	Min.
Calculated from XRF (wt.%)				
CaF2(c)*	104	1.75	106	98.7
BaSO4(c)	0.007	0.006	0.018	0.002
SiO2(c)	0.105	0.059	0.192	0.036
PbS(c)	0.003	0.001	0.006	0.001
ZnS(c)	0.000	0.000	0.002	0.000
CuFeS2(c)	0.001	0.001	0.002	0.000
Total	104			
XRF Majors (wt.%)				
SiO2	0.203	0.114	0.371	0.070
TiO2	< 0.003	NA	(0.005)	< 0.003
Al2O3	0.031	0.034	0.088	< 0.006
Fe2O3	0.046	0.022	0.103	0.020
MnO	< 0.002	NA	(0.004)	< 0.002
MgO*	< 0.02	NA	< 0.020	< 0.020
CaO*	74.8	1.26	76.2	71.3
Na2O	(0.039)	0.070	0.244	< 0.014
K2O	(0.006)	0.008	0.026	< 0.002
P2O5	(0.004)	0.002	(0.009)	< 0.003
LOI*	0.595	0.096	0.730	0.410
XRF Traces (ppm)				
S	179	109	427	74
Cl	134	190	658	(21)
Sc*	41	5	54	31
V	< 7	NA	< 7	< 7
Cr	(10)	4	(18)	< 6
Ni	< 4	NA	< 4	< 4
Cu	24	17	58	(8)
Zn	< 3	NA	12	< 3
Ga	< 4	NA	< 4	< 4
Rb*	< 0.7	NA	< 0.7	< 0.7
Sr	65	24	134	45
Y	688	268	1266	331
Zr	< 1.0	NA	(1.7)	< 1.0
Nb	(1.7)	0.7	3	< 0.6
Ba	(39)	34	104	< 23
Ce	109	56	205	(39)
Pb	28	10	49	(9)
Th	< 3	NA	(3)	< 3
U	< 4	NA	< 4	< 4

	Mean	SD	Max.	Min.
ICP-MS Traces (ppm)				
Li	< 0.3	NA	(0.4)	< 0.3
Be	(7.9)	4.3	22	(5.0)
Sc	< 4	NA	(8)	< 4
V	< 2	NA	(4)	< 2
Cr	< 8	NA	(15)	< 8
Cu	26.6	13.7	53.5	12.2
Zn	(9)	5	25	(3)
Rb	(0.13)	0.16	0.58	< 0.08
Sr	67.1	21.8	130	47.1
Y	662	244	1183	317
Zr	1.8	3.1	12	< 0.4
Nb	0.209	0.109	0.426	0.097
Mo	1.01	1.93	7.40	0.246
Cs	(0.028)	0.026	0.105	< 0.010
Ba	2.7	3.5	13	(0.4)
Hf	(0.08)	0.08	0.28	< 0.07
Ta	0.203	0.133	0.464	0.078
Tl	< 0.06	NA	(0.08)	< 0.06
Pb	21.1	9.05	36.9	3.93
Bi	0.31	0.24	0.90	< 0.05
Th	(0.13)	0.09	0.31	< 0.04
U	0.60	0.20	0.96	0.31
ICP-MS REE (ppm)				
La	20.9	9.39	37.1	9.47
Ce	54.9	33.1	118	20.2
Pr	8.51	6.02	20.2	2.72
Nd	42.5	31.2	102	12.4
Sm	12.4	8.21	25.8	3.71
Eu	1.71	1.06	3.59	0.726
Gd	21.4	11.9	44.0	7.91
Tb	4.13	2.04	7.79	1.69
Dy	29.9	14.0	61.9	13.2
Ho	6.82	3.01	14.3	3.36
Er	19.1	8.21	40.8	10.1
Tm	2.20	0.970	4.80	1.22
Yb	12.0	5.43	24.6	5.71
Lu	1.53	0.686	2.87	0.649
Total REE	238	109	414	96.3
ICP-MS Ratios				
[illegible]	1.175	0.027	1.223	1.128
[illegible]	2.450	0.046	2.517	2.382
[illegible]	0.186	0.046	0.333	0.153
[illegible]	0.003	0.008	0.021	-0.004

All elements with RSD < or = 20% are denoted by (*). Values less than the limit of detection (LOD) are given as < (LOD). Values less than the limit of quantitation (LOQ) but greater than the LOD are given in parenthesis.
Abbreviations: NA - not applicable; SD - standard deviation; Max. - maximum; Min. - minimum

are abundant and often large in coarse grained fluorites. The bulk of the Cl and S, not directly related to sulphide or sulphate phases, may also be related to fluid inclusion contributions.

It is evident that the most abundant trace elements in the fluorite are the dominantly trivalent Yttrium and the rare earth elements (REE), with Y and REE_{total} averaging 662 and 238 ppm respectively. The REE and Y exhibit extreme variability between fluorite samples within the group. Most other elements that would be expected to substitute into the fluorite structure (appropriate ionic radius and charge) are present in detectable concentrations. The elements Cu, Sr, Ba and Pb, which occur in the divalent state, attain average concentrations of 27, 67, 3 and 21 ppm respectively. The presence or absence of minor accessory sulphate and/or sulphide phases must be carefully examined when considering the significance of these elements with regard to true fluorite composition. Minor concentrations (≤ 1 ppm) of Cs, Bi, Mo, Zr, Nb, Ta, Th and U were detected, while concentrations of Li, Be, Ti, V, Cr, Ni, Zn, Ga, Rb, Hf and Tl in fluorite are near or below the detection limits.

Table 6.2.2 presents the average analytical data for samples from zones containing variable mineralogy but in which fluorite is the major mineral phase (i.e. >50% CaF_2). These zones average approximately: 96% fluorite; 2% quartz; 1% barite; 1% sulphides (primarily galena and sphalerite); and 0.4% hematite. Most of the major elements (except Ti, Mg and P) are slightly elevated above trace levels, suggesting the incorporation of minor silicate phases as inclusions in crystals and/or as fragments in some brecciated zones. In these fluorite-bearing zones with variable mineralogy, the trace elements Ba, Pb and Zn are notably enriched, compared to the fluorite zones containing no visible minor phases (Table 6.2.1). This can be accounted for by the inclusion of barite and/or sulphide-bearing samples within this group. A slight enrichment in Ni, Cr, Tl and Ga is probably related to the increased sulphide influence,

Table 6.2.2 Summary of the geochemical analyses of coarse grained fluorites from the St. Lawrence fluorspar veins. These samples are from zones which contain minor phases but are composed of at least 50% fluorite.

Fluorite-rich Zones (greater than 50% fluorite)

(n = 47)

	Mean	SD	Max.	Min.
Boric Acid Dissolution (wt.%)				
% undissol.	17.2	12.2	47.0	3.18
% dissol.*	82.8	12.2	96.8	53.0
Calculated from XRF (wt.%)				
CaF2(c)*	97.5	9.79	106	59.9
BaSO4(c)	0.794	3.02	20.1	0.002
SiO2(c)	2.13	3.71	14.3	0.036
PbS(c)	0.672	3.06	21.1	0.001
ZnS(c)	0.548	3.45	23.9	0.000
CuFeS2(c)	0.005	0.010	0.050	0.000
Total	102			
XRF Majors (wt.%)				
SiO2	4.12	7.15	27.6	0.070
TiO2	(0.004)	0.006	0.022	< 0.003
Al2O3	0.157	0.272	1.41	< 0.006
Fe2O3	0.392	1.11	6.46	< 0.002
MnO	0.027	0.066	0.312	< 0.002
MgO*	< 0.02	NA	< 0.020	< 0.020
CaO*	70.4	7.06	76.2	43.2
Na2O	0.064	0.206	1.393	< 0.014
K2O	0.058	0.149	0.840	< 0.002
P2O5	(0.008)	0.007	0.031	< 0.003
LOI	1.64	1.88	7.72	0.410
XRF Traces				
S	2501	6644	38720	74
Cl	183	200	974	(21)
Sc	43	10	73	(19)
V	< 7	NA	< 7	< 7
Cr	32	59	323	< 6
Ni	(10)	27	172	< 4
Cu	151	276	1435	< 3
Zn	3676	23139	160481	< 3
Ga	40	214	1480	< 4
Rb	4.2	10.3	60.1	< 0.7
Sr	146	366	2534	24
Y	721	348	1556	214
Zr	3.6	7.5	41.2	< 1.0
Nb	2.1	1.6	9	< 0.6
Ba	4672	17795	118161	< 23
Ce	(61)	56	257	< 32
Pb	5816	26491	182558	(9)
Th	(4)	11	71	< 3
U	< 4	NA	23	< 4

	Mean	SD	Max.	Min.
ICP-MS Traces (ppm)				
Li	2.4	6.4	34.1	< 0.3
Be	(8.2)	6.4	26	< 0.4
Sc	< 4	NA	(11)	< 4
V	(2)	2	8	< 2
Cr	(14)	36	228	< 8
Cu	127	429	2963	< 0.3
Zn	126	291	1466	< 3
Rb	3.56	8.96	48.6	< 0.08
Sr	96.4	109	744	28.7
Y	722	365	2051	240
Zr	2.6	3.5	17	< 0.4
Nb	0.521	0.690	3.07	< 0.009
Mo	1.91	2.26	9.69	< 0.05
Cs	0.222	0.505	2.76	< 0.010
Ba	976	2319	10922	(0.4)
Hf	(0.15)	0.17	0.90	< 0.07
Ta	0.304	0.304	1.309	< 0.007
Tl	0.54	1.63	10.03	< 0.06
Pb	4107	16088	109779	3.64
Bi	1.31	4.83	33.3	< 0.05
Th	0.32	0.55	3.19	< 0.04
U	1.05	1.84	11.56	< 0.02
ICP-MS REE (ppm)				
La	16.0	11.3	48.9	0.42
Ce	41.2	33.9	173	1.3
Pr	6.02	5.63	30.9	0.23
Nd	28.5	27.3	147	1.3
Sm	10.5	6.47	28.6	1.71
Eu	1.05	0.92	3.68	0.118
Gd	20.2	9.7	44.0	6.88
Tb	4.51	2.24	10.3	1.41
Dy	34.5	18.7	85.0	9.8
Ho	8.05	4.59	21.1	2.07
Er	24.2	15.1	67.3	5.2
Tm	3.16	2.11	8.71	0.49
Yb	19.7	14.6	55.7	2.19
Lu	2.56	1.89	7.10	0.265
Total REE	220	115	494	64.8
ICP-MS Ratios				
[illegible]	1.159	0.172	1.223	0.000
[illegible]	2.385	0.355	2.517	0.000
[illegible]	0.263	0.112	0.778	0.000
[illegible]	0.108	0.270	1.609	-0.004

All elements with RSD < or = 20% are denoted by [*]. Values less than the limit of detection (LOD) are given as <(LOD). Values less than the limit of quantitation (LOQ) but greater than the LOD are given in parenthesis.
Abbreviations: NA - not applicable; SD - standard deviation; Max. - maximum; Min. - minimum

while increases of Rb and Sr may be attributed to the increased silicate and barite content respectively.

The REE and Y are the dominant trace elements not related to sulphate or sulphide phases, with total REE averaging slightly lower (220 ppm) and Y slightly higher (722 ppm) than in the pure fluorite zones. There also appears to be an overall trend of depletion of LREE and enrichment of HREE.

Table 6.2.3 summaries the analytical data for galena-rich zones (> 2% galena) with either fluorite and/or barite as the other major mineral phase. These zones average approximately: 70% fluorite; 25% galena and sphalerite; and 5% barite and quartz. The only anomalous behaviour noted in the major element data is a significant increase of Na_2O in at least one zone. Besides the normal sulphide related elements, Cu, Pb and Zn, increases were also noted in Cr, Ni, Ga, Tl, Bi and U + Th. The higher U + Th values are only apparent in the XRF analysis, and are probably be related to uncorrected Pb interferences. Enrichments in Sr and Ba, and possibly Cr and Cs, can be related to preferential incorporation of these elements in sulphates such as barite. The REE and Y concentrations (235, 819 ppm) are similar to those of the previous group reflecting the overwhelming influence of the fluorite.

Table 6.2.4 summarizes the analytical data for barite-rich zones which contain less than 50% fluorite. These zones average approximately 27% fluorite ($\pm$ calcite) and 70% barite as well as several percent quartz and varying amounts of sulphides. The higher variation in major element values probably reflect barite/quartz/carbonate associations in some zones and the incorporation of lithic fragments in some marginal zones. The high barite content of these zones accounts for the anomalously high concentrations of Ba, Sr, Rb and Cs, while sulphides account for the high Cu, Pb and Zn. The barite-rich zones show abnormally low Sc values from the XRF analysis, with the

Table 6.2.3 Summary of geochemical analyses of galena-bearing fluorite zones from the St. Lawrence fluorspar veins. These samples are from zones which contain greater than 1% galena.

Galena-rich Zones (greater than 1% galena)

(n = 8)

	Mean	SD	Max.	Min.
Boric Acid Dissolution (wt.%)				
% undissol.	29.2	26.1	55.3	3.18
% dissol.	70.8	26.1	96.8	44.7
Calculated from XRF (wt.%)				
CaF2(c)	72.4	26.8	100	34.6
BaSO4(c)	8.85	23.4	70.8	0.002
SiO2(c)	1.09	2.02	6.41	0.109
PbS(c)	27.1	39.3	105	1.00
ZnS(c)	3.60	7.78	23.9	0.000
CuFeS2(c)	0.057	0.110	0.339	0.001
Total	113			
XRF Majors (wt.%)				
SiO2	2.11	3.91	12.4	0.211
TiO2	< 0.003	NA	< 0.003	< 0.003
Al2O3	0.040	0.037	0.126	(0.011)
Fe2O3	0.095	0.094	0.290	< 0.002
MnO	< 0.002	NA	(0.002)	< 0.002
MgO*	< 0.02	NA	< 0.020	< 0.020
CaO	52.3	19.4	72.3	25.0
Na2O	0.213	0.450	1.39	< 0.014
K2O	0.008	0.011	0.030	< 0.002
P2O5	(0.010)	0.003	0.017	(0.005)
LOI	2.46	NA	2.46	2.46
XRF Traces				
S	25629	26885	80280	1115
Cl	157	142	424	38
Sc	34	17	59	< 7
V	< 7	NA	< 7	< 7
Cr	67	92	228	< 6
Ni	24	56	172	< 4
Cu	1655	3166	9795	38
Zn	24177	52197	160481	< 3
Ga	1836	2710	6669	< 4
Rb	(1.4)	1.6	5.4	< 0.7
Sr	606	1401	4312	33
Y	768	435	1492	276
Zr	3.9	8.9	27.3	< 1.0
Nb	8.0	11.2	37	(1.7)
Ba	52100	137725	416486	< 23
Ce	< 32	NA	< 32	< 32
Pb	234291	339918	908657	8672
Th	14	23	71	< 3
U	45	76	231	< 4

	Mean	SD	Max.	Min.
ICP-MS Traces (ppm)				
La	(0.6)	0.2	(1.0)	< 0.3
Be	(7.6)	4.9	(15.0)	< 0.4
Sc*	< 4	NA	< 4	< 4
V	< 2	NA	(5)	< 2
Cr	(16)	30	94	< 8
Cu	196	179	607	< 0.3
Zn	4513	10506	32275	< 3
Rb	0.66	1.12	3.58	< 0.08
Sr	156	229	755	24.9
Y	819	299	1327	444
Zr	(0.7)	0.7	2	< 0.4
Nb	0.263	0.184	0.569	< 0.009
Mo	1.82	1.15	4.09	0.452
Cs	0.262	0.566	1.76	(0.013)
Ba	1051	2742	8307	(1.3)
Hf	< 0.07	NA	0.22	< 0.07
Ta	0.384	0.299	0.888	0.024
Tl	4.56	4.13	11.1	0.35
Pb	29594	31650	109779	6821
Bi	17.0	27.5	84.2	(0.12)
Th	(0.08)	0.05	0.14	< 0.04
U	0.59	0.67	1.66	(0.03)
ICP-MS REE (ppm)				
La	12.2	4.34	20.0	6.41
Ce	31.4	10.8	49.7	17.0
Pr	4.53	1.44	6.51	2.58
Nd	22.1	6.74	32.4	13.0
Sm	11.1	3.17	16.9	6.65
Eu	0.725	0.362	1.59	0.369
Gd	23.3	6.04	32.1	14.3
Tb	5.64	1.74	8.20	3.12
Dy	44.2	15.8	68.2	23.7
Ho	10.6	4.14	17.5	5.48
Er	32.6	14.1	57.1	15.3
Tm	4.30	1.88	7.14	1.67
Yb	29.0	13.4	47.9	8.45
Lu	3.69	1.69	5.99	0.913
Total REE	235	71	354	134
ICP-MS Ratios				
[illegible]	1.086	0.220	1.204	0.514
[illegible]	NA	NA	NA	NA
[illegible]	0.311	0.034	0.360	0.267
[illegible]	0.014	0.012	0.033	0.002

All elements with RSD < or = 20% are denoted by ( ). Values less than the limit of detection (LOD) are given as <(LOD). Values less than the limit of quantitation (LOQ) but greater than the LOD are given in parenthesis.
Abbreviations: NA - not applicable; SD - standard deviation; Max. - maximum; Min. - minimum

maximum being close to the limit of detection, contrasting with averages of 30-40 for other groups. This is probably related to the lower CaO content of these samples (2 versus 36%) which allows for more adequate correction of Ca interferences on Sc. If this

Table 6.2.4 Summary of geochemical analyses of barite-rich zones from the St. Lawrence fluorspar veins. These samples are from zones which contain greater than 50% barite.

Barite-rich Zones (greater than 50% barite)

(n = 8)

	Mean	SD	Max.	Min.
Boric Acid Dissolution (wt.%)				
% undissol.	74.0	16.1	96.1	54.7
% dissol.	25.3	16.2	45.3	3.92
Calculated from XRF (wt.%)				
CaF2(c)	30.1	17.0	49.6	2.60
BaSO4(c)	77.0	19.0	113	49.7
SiO2(c)	3.18	2.27	6.00	0.191
PbS(c)	0.178	0.437	1.33	0.000
ZnS(c)	0.624	1.27	3.96	0.000
CuFeS2(c)	0.004	0.001	0.006	0.002
Total	111			
XRF Majors (wt.%)				
SiO2	6.14	4.38	11.57	0.369
TiO2	0.022	0.017	0.055	< 0.003
Al2O3	0.290	0.356	1.21	0.055
Fe2O3	0.095	0.178	0.524	< 0.002
MnO	(0.004)	0.008	0.024	< 0.002
MgO*	< 0.02	NA	< 0.020	< 0.020
CaO	21.7	12.3	35.8	1.87
Na2O	(0.029)	0.057	0.180	< 0.014
K2O	0.099	0.151	0.489	0.007
P2O5	(0.005)	0.003	(0.010)	< 0.003
LOI	2.93	1.60	5.48	0.300
XRF Traces				
S*	72555	9869	87063	54060
Cl	77	32	125	(28)
Sc	< 7	NA	(8)	< 7
V	< 7	NA	< 7	< 7
Cr	339	161	668	208
Ni	28	15	52	(9)
Cu	127	35	176	72
Zn	4189	8491	26560	< 3
Ga	< 4	NA	< 4	< 4
Rb	9.4	13.0	42.9	(1.9)
Sr	5858	1891	8376	3076
Y	254	135	424	20
Zr	37.5	17.8	58.8	< 1.0
Nb	2.2	0.7	3	(1.2)
Ba	452819	111732	666963	292478
Ce	< 32	NA	< 32	< 32
Pb	1540	3783	11537	< 4
Th	< 3	NA	< 3	< 3
U	(4)	3	(11)	< 4

	Mean	SD	Max.	Min.
ICP-MS Traces (ppm)				
Li	6.1	9.4	30.7	(0.3)
Be	(17.7)	11.6	31	< 0.4
Sc	(5)	4	(14)	< 4
V	(4)	3	10	< 2
Cr	(56)	36	96	< 8
Cu	376	275	934	87.4
Zn	8512	11424	32275	23
Rb	16.5	17.6	59.4	2.62
Sr	2337	1189	4581	755
Y	782	231	1056	337
Zr	4.4	3.5	10	(0.4)
Nb	1.40	1.40	4.84	0.265
Mo	2.41	1.53	5.39	0.480
Cs	6.64	6.94	23.7	0.587
Ba	36354	69875	220927	3059
Hf	0.38	0.39	1.19	< 0.07
Ta	1.59	1.57	5.29	0.090
Tl	1.81	2.17	6.79	< 0.06
Pb	5045	8444	22705	111
Bi	0.35	0.33	1.05	(0.05)
Th	0.34	0.29	1.00	(0.04)
U	0.63	0.89	2.86	(0.07)
ICP-MS REE (ppm)				
La	24.3	6.71	36.4	14.87
Ce	56.7	18.9	85.2	25.2
Pr	8.30	2.76	12.7	3.68
Nd	38.9	12.5	58.6	17.5
Sm	16.7	4.73	21.7	7.69
Eu	2.31	1.22	4.25	0.048
Gd	35.3	11.2	46.8	13.5
Tb	6.44	2.08	9.60	2.74
Dy	45.6	17.1	76.0	18.5
Ho	9.84	4.14	18.2	3.86
Er	27.5	14.4	60.5	10.6
Tm	3.40	2.26	8.97	1.36
Yb	18.3	17.0	62.1	6.86
Lu	2.22	2.23	7.99	0.798
Total REE	296	102	454	132
ICP-MS Ratios				
208Pb/207Pb*	1.178	0.014	1.201	1.153
208Pb/206Pb*	2.433	0.017	2.463	2.408
147Sm/144Nd	0.262	0.022	0.305	0.222
87Rb/86Sr	0.033	0.056	0.180	0.003

All elements with RSD < or = 20% are denoted by [*]. Values less than the limit of detection (LOD) are given as < (LOD). Values less than the limit of quantitation (LOQ) but greater than the LOD are given in parenthesis.
Abbreviations: NA - not applicable; SD - standard deviation; Max. - maximum; Min. - minimum

is the case, higher values for Sc (XRF) in the other groups are inaccurate and should not be considered representative of the samples.

The REE and Y concentrations in fluorite from the barite-rich zones average 296 and 782 ppm respectively, and are comparable, or slightly higher, than other zones for both the LREE and HREE. The XRF vs ICP-MS average values for Y (254 vs 782 ppm) suggests that most of the Y, and consequently the REE, is concentrated in the acid soluble material, namely fluorite and/or calcite.

The breakdown into groups of samples based on mineralogy presented in tables 6.2.1 to 6.2.4 indicates no systematic change in fluorite chemistry from group to group. Most of the variation between groups can be directly accounted for by the dissolution of minor amounts of mineral phases (other than fluorite) in the ICP-MS analysis, or the direct contribution of such phases in XRF analysis. This is particularly true of the REE which seem to display as much variation within mineralogically distinct groups as between these groups.

These results also indicate that the dissolution of small amounts of barite, quartz or sulphide does not systematically alter the REE balance, especially in zones with only a low percentage of non-fluorite phases. This can be further demonstrated using a plot of Y_{XRF} versus Y_{ICP-MS} for the samples in the data set (figure 6.2.1). The XRF analysis is representative of the whole zone, while the ICP-MS analysis represents only the elemental concentration in the fluorite (± calcite) component of the zone. All ICP-MS sample weights submitted as dissolved component weights, calculated prior to analysis from the weight of the undissolved fraction (i.e. $weight_{sample} = weight_{original} - weight_{residue}$). Most of the scatter in the uncorrected raw data ($R^2 = 0.57$) plotted in figure 6.2.1a can be attributed to samples from zones containing non-fluorite (or non-calcite) phases. Based on the assumption that most of the Y in the zone would be incorporated in fluorite but not

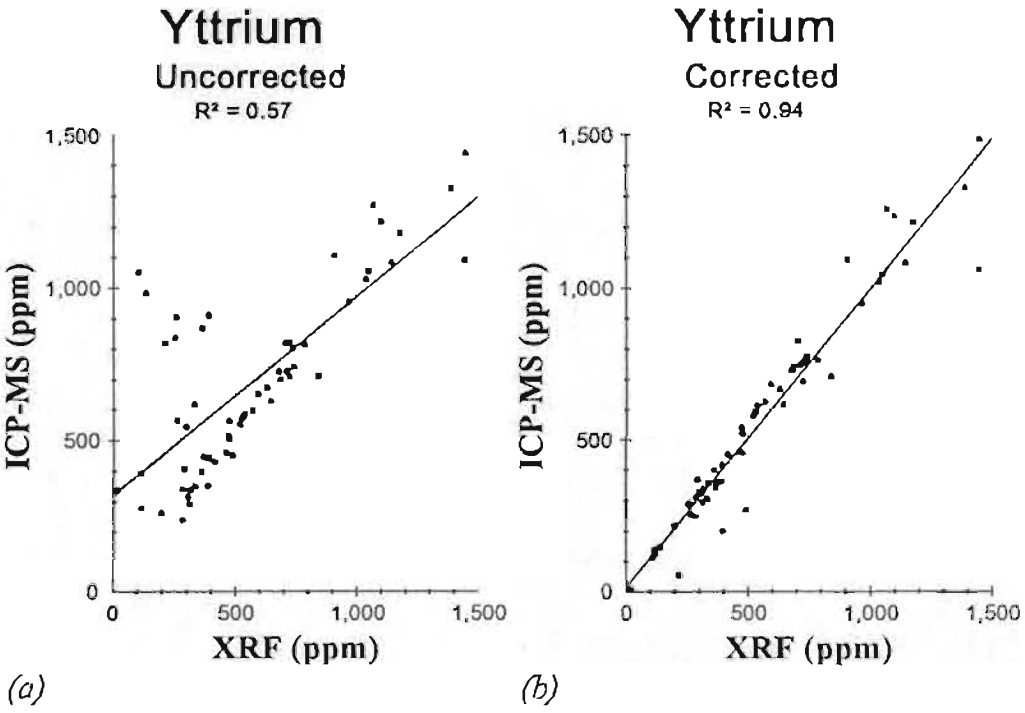

Figure 6.2.1 Plot of (a) uncorrected and (b) corrected ICP-MS Yttrium data versus XRF Yttrium data. The ICP-MS data are from boric acid dissolution of fluorite from various zones. Corrected data are adjusted based on the estimated fluorite content of the zones (see text), assuming all Y is contained in the fluorite fraction.

in the other mineral phases, the data was modified by multiplying the $Y_{ICP\text{-}MS}$ value by weight fraction of fluorite [CaF_2(c)] in the zone (i.e. zones with 25% fluorite would be reduced to 25% of the original ICP-MS value, assuming that the XRF analysis of the whole zone represents a 3:1 dilution by Y-free components). The modified data, shown in figure 6.2.1b, display a well defined linear trend with considerably less scatter (R^2 = 0.94) than the uncorrected data.

This supports the assumption, used throughout the remainder of this discussion, that in the zones analyzed by ICP-MS (boric/nitric) the analytical data very closely approximates Y and REE concentrations in the fluorite (± calcite) component of the zone. As well, taking into account the effects of other mineral phases which may be

present, it can provide reasonable estimates of the concentrations of other trace elements in the fluorite component of the zones.

6.3 REE systematics in fluorite and related minerals

The discussion of the REE geochemistry of selected samples from the fluorspar veins is presented on a sample by sample basis, starting with sample GNV-8, from the Grebe's Nest Vein, which displays the most continuous series of growth zones of any of the samples used in this study. The discussion of REE in fluorite (or calcite) will rely primarily on the ICP-MS data but will utilize XRF data to determine the more complete chemical character of the zones. A previous study of REE in growth zoned fluorite from St. Lawrence (Strong et al., 1984) indicated moderate to high REE concentrations which are highly but systematically variable. The discussion which follows will demonstrate that, despite the high degree of variability in the chemistry of these samples, the REE and other trace elements define a systematic pattern, reflecting the precipitation of fluorite from a dynamic fluid system.

The REE geochemistry is presented as chondrite normalized plots to facilitate comparison with other published studies. Normalizing values are those of CI carbonaceous chondrites compiled by and listed in Taylor and McLennan (1985). Since this section is aimed primarily at presenting the data, interpretation will be limited to correlation of the REE patterns with mineralogical and fluid inclusion data already presented.

6.3.1 Grebe's Nest Vein

Sample GNV-8, from the Grebe's Nest Vein, contains 16 continuous growth zones of which 15 are coarse grained fluorite (figure 4.1.2). Sample GNV-ST is not from the same sample but is a sample of late-stage blue coarse grained fluorite from this vein. The chondrite normalized distribution of REE in sample GNV-8 (figure 6.3.1) displays a systematic variation with progressive periods of precipitation. The earliest precipitated fluorite (GNV-8-A) displays a sub-parabolic pattern with a pronounced enrichment of light-REE (LREE) over heavy-REE (HREE) and a maximum at Pr decreasing towards both La and Lu. The zone has a well defined negative Eu anomaly combined with a less well defined positive Gd anomaly. With progressive precipitation, zones B and C show very similar patterns to A but with a pronounced 'flattening' resulting from depletion of the LREE and enrichment of the HREE compared to A, while Sm, Eu and Gd remain virtually unchanged. Zone D displays continued 'flattening' of the REE pattern through HREE enrichment and lesser LREE depletion, despite the flattening the Eu and Gd anomalies remain and the HREE from Ho to Lu retain their negative slope, hereafter informally termed the 'tail'. The pattern in the next zone (E) is virtually identical in shape but has a somewhat lower concentration of all REE. Fluid inclusion data indicate a corresponding homogenization temperature increase from A, with a peak between B and C (up to 380°C), and decreasing to E, with a slight increase in salinity parallelling the temperature trend. The fluid inclusion data from these zones follow 'trend B' as opposed to the majority of samples which follow 'trend A' (see figure 5.1.4 and figure 5.3.1). The LREE (La - Nd) have evolved, with progressive precipitation, from strongly concave upward in A to relatively flat in E.

Grebe's Nest Vein (sample GNV-8)

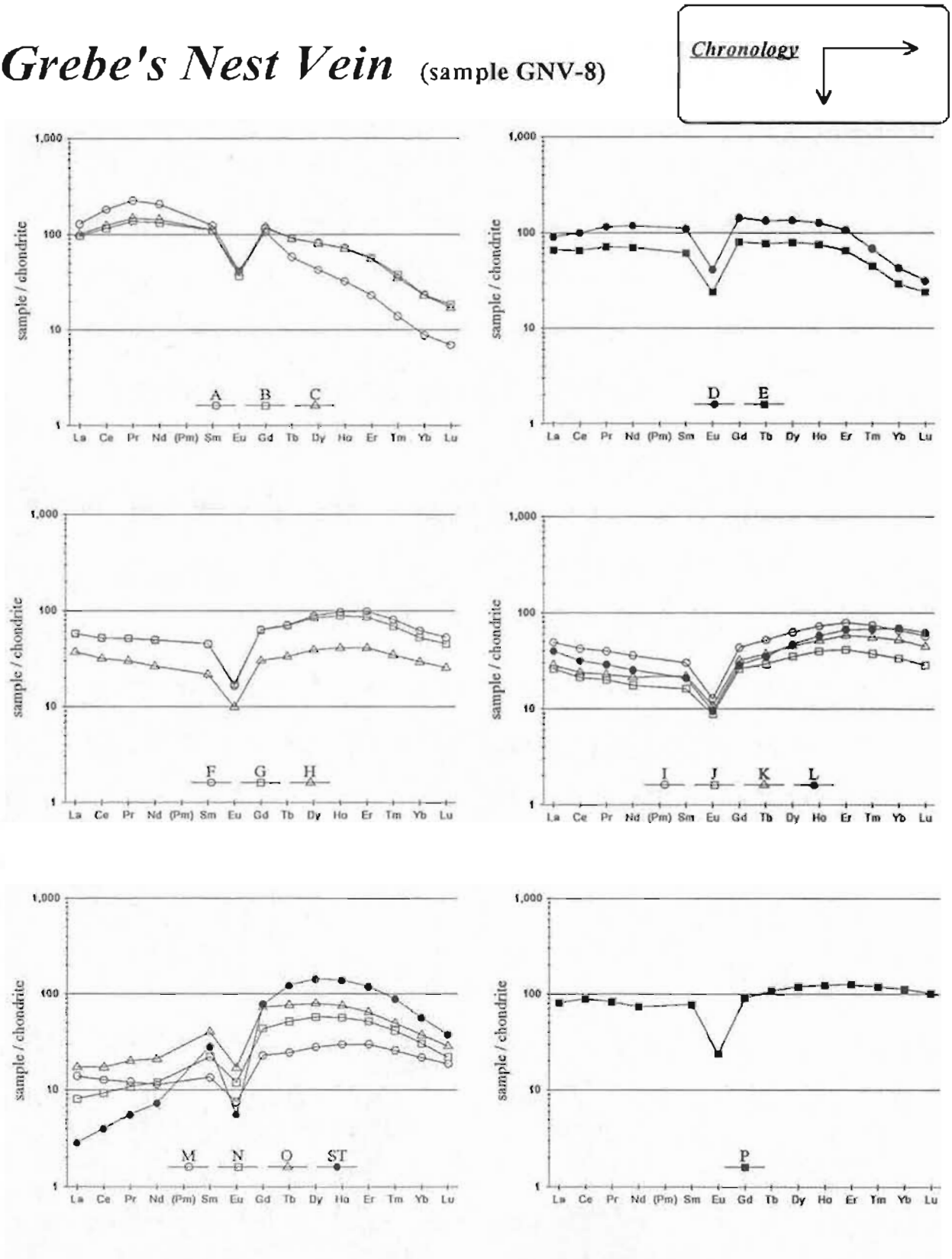

Figure 6.3.1 Chondrite normalized REE patterns for sample GNV-8 from the Grebe's Nest Vein displaying evolving patterns with successive growth zones. Symbols refer to specific zones. Zone P is a late-stage incrustation of "iron oxides" and zone ST refers to sample GNV-ST, a sample of late-stage, growth-stepped fluorite from the Grebe's Nest Vein.

The crystallization of the last two zones of coarse grained green fluorite (F and G), shows the development of what I informally term the 'V and tail' pattern, characterized by a slight negative slope from La to Nd (the apex of the V), a moderate positive slope from Nd to Er and a moderate negative slope from Er to Lu. This pattern retains the negative Eu anomaly but loses the positive Gd anomaly. This 'V and tail' pattern persists through to zone L, with progressive precipitation of coarse grained fluorite. The later zones of blue fluorite (J to L) have lower total REE contents than the earlier zones of green fluorite (F and G) displaying similar patterns. The zones H and I which show an apparent reversal of sequence with regard to total REE concentrations (i.e. H < I) also show colour reversals (i.e. H is blue; I is green) as these zones mark the transition from green to blue fluorite in the sample GNV-8 (figure 4.2.1). Fluid inclusion data show relatively stable temperature and salinity conditions throughout these zones with the exception of the 'late' part of zone H which has a high salinity/low temperature signature. Another diagnostic feature of the 'early' chondrite normalized (N) patterns which occur in zones A to L is moderately negative to flat slope from Nd to Sm (i.e. $Nd_N/Sm_N \geq 1$).

The chondrite-normalized pattern of zone M displays the transition from the 'V and tail' pattern to the 'late-stage' patterns observed in zones N, O and ST. The pattern in zone M could be considered a 'V and tail' pattern except for the development of a slightly positive slope from Nd to Sm (i.e. $Nd_{cn}/Sm_{cn} < 1$). Zones N and O display patterns that characterize the latest zones of fluorite precipitation in sample GNV-8. These 'late-stage' patterns are characterized by a flat to positive slope from La to Nd (i.e. extreme LREE depletion), a concave upward trend from Nd to Lu with a maximum around Dy or Ho,

and $Nd_{cn}/Sm_{cn} < 1$. The type of REE pattern observed in sample GNV-ST is considered to be an example of 'extremely late-stage' fluorite similar to that in samples ISV-1-G and LC-1 in the following sections.

Fluid inclusion data show a steady decrease in temperature from zone M through O with zone O being characterized by low temperature and high salinity. The fluid inclusion homogenization temperature versus salinity plot (figure 5.2.3) indicates that zones M to O fall on 'trend A' as opposed to zones A to L which fall predominantly on 'trend B'. The last recorded stage of mineralization is the deposition of a hydrous Fe-oxide (limonite, goethite) cap (zone P) which displays a flat REE pattern with the characteristic negative Eu anomaly. This zone contains minor amounts of fluorite and/or calcite accounting for 10-6% of the zone.

The LREE enriched chondrite normalized patterns observed in fluorites in zones A to E are not typical of the majority of St. Lawrence fluorite samples analyzed in this study or those of the earlier study by Strong et. al. (1984). The typical REE patterns documented in St. Lawrence fluorites are the HREE enriched patterns. This type of HREE enriched fluorite is characteristic of fractionated, late-stage fluids (Möller, 1983; Möller and Morteani, 1983). These 'late-stage, HREE enriched patterns are developed in sample GNV-8 during the later stages of fluorite precipitation as shown by zones M to O, and especially in GNV-ST, in figure 6.3.1.

6.3.2 Sample 2

The significance of the identification of the 'early' LREE enriched patterns in sample GNV-8 was uncertain since they were only identified in one sample from one vein. All the other St. Lawrence fluorite samples analyzed in the current study, plus the

previous published analysis (Strong et al., 1984), had failed to identify similar patterns. An examination of some unpublished data (Strong, D.F. and Fryer, B.J.), from the original study by Strong et al. (1984), resulted in the identification of some anomalous REE values in several growth zones in sample #2 (figure 4.1.12). Subsequently, ICP-MS analysis was completed on four of the 10 growth zones in Sample 2.

The chondrite-normalized REE patterns for Sample 2 are presented in figure 6.3.2. The earliest zone (2-2) displays a remarkable resemblance to zone GNV-8-A with the exception of a slightly higher La and Lu content. The relationship between zones 2-2 and 2-4 is identical to that between zones A and B-C in sample GNV-8, suggesting that they may have been formed during the same period of fluid evolution and/or as a result of similar processes. Fluid inclusion data (Strong et al., 1984) indicate that these zones

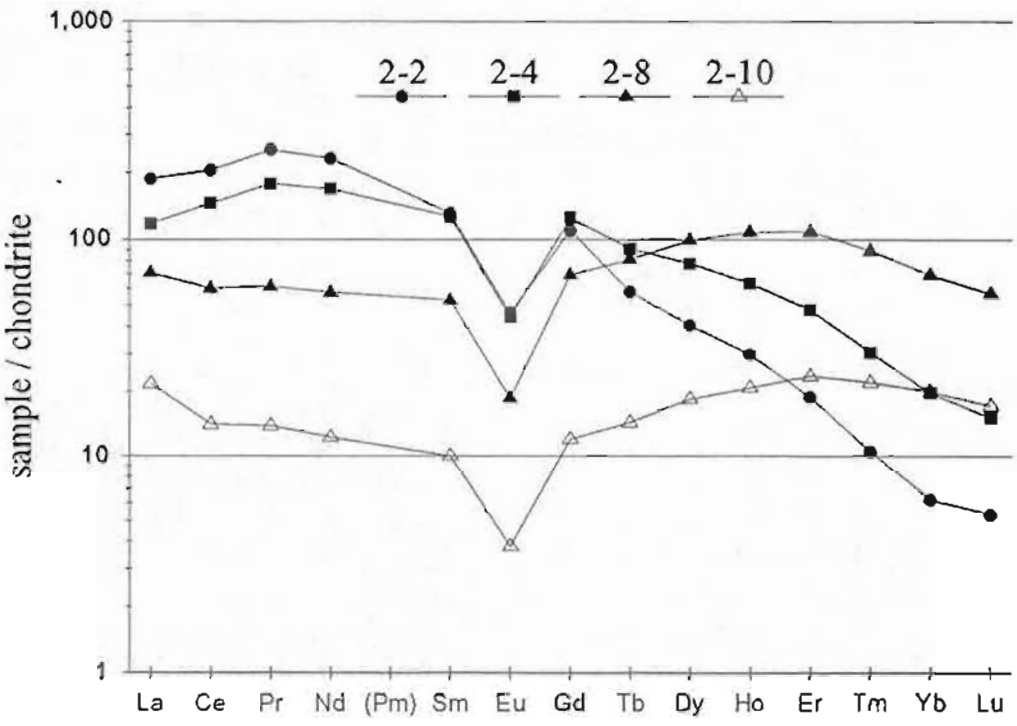

Figure 6.3.2 Chondrite normalized plot of REE patterns from Sample 2 of Strong et al. (1984), analyzed as part of this study. Note the similarity between these patterns and those in sample GNV-8.

formed at temperatures around 400°C to 300°C similar to results for zones A to C in sample GNV-8.

The chondrite-normalized REE patterns in zones 2-8 and 2-10 display patterns that are very similar to the 'V and tail' patterns in zones F to L from sample GNV-8. These zones also show the characteristic decrease in total REE content in the later zone (2-10) as well as the disappearance of the positive Gd anomaly that is evident in zones 2-2 and 2-4. Fluid inclusion data (Strong et al., 1984) show that these zones formed at temperatures less than 200°C to 150°C, again similar to temperatures in zones F to L in sample GNV-8. This indicates that either these two samples were formed from the same fluid source or from separate fluid sources which had parallel fluid evolution.

One notable difference between Sample 2 and GNV-8 (as well as GNV-7 from the Grebe's Nest Vein) is that Sample 2 contains anomalously high (more than an order of magnitude) concentrations of Nb and Ta (20-80 ppm and 20-35 ppm respectively) compared to that in samples from the Grebe's Nest Vein (1.2-0.1 ppm and 0.5-0.1ppm respectively). Since the location of Sample 2 was not documented there was always the remote possibility that it came from the Grebe's Nest Vein as well, in spite of the fact that all the samples used in the Strong et al. (1984) study were from the Director and Tarefare mines, except for the LBV and BMW samples donated by the author. The extreme difference in Nb and Ta concentrations preclude any possibility that Sample 2 and GNV-8 were sub-samples of the same larger sample, and it also appears highly unlikely that they were taken from the same vein.

6.3.3 Iron Springs Vein

The earliest three zones (A to C) are composed of a fine grained aggregate of particles of quartz, calcite and fluorite in a matrix of fluorite, with the fluorite content increasing from A to C. Similar fine grained fluorite was interpreted, by Strong et al. (1984), to represent rapidly precipitated (quenched) fluorite but micro-structures indicate a particulate rather than crystalline nature. The chondrite-normalized REE patterns developed in zones A to C (figure 6.3.3) resemble 'late' patterns observed in sample GNV-8 (M) which occur near the transition from the 'V and tail' patterns to the characteristic 'late-stage' patterns. The Nd_N/Sm_N ratios in fluorite from this vein ($Nd_N/Sm_N < 1$) is characteristic of 'late-stage' fluorite REE patterns.

The chondrite-normalized REE patterns in zones D and E display characteristic 'late-stage' patterns, except for the uncharacteristic 'flattening' between Gd and Lu in zone F . This may possibly be due to temporary 'closing' of the system causing fractionation

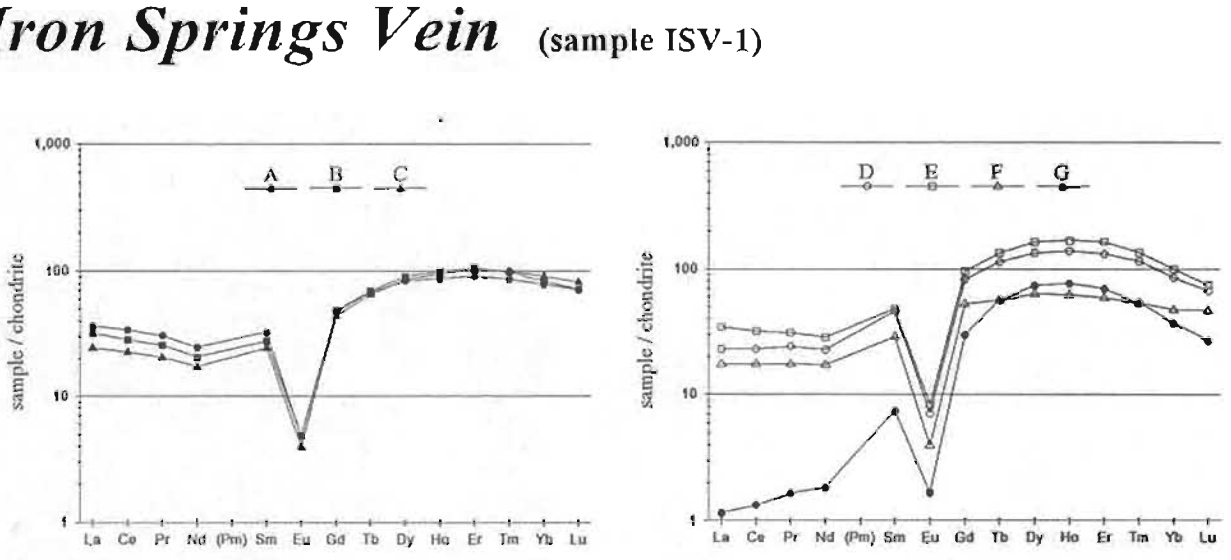

Figure 6.3.3 Chondrite normalized REE patterns for fluorite in sample ISV-1 from the Iron Springs Vein. The symbols represent successive growth zones from the earliest precipitated mineralization (zone A) to the latest (zone G). Zones A to C are characterized by fine grained fluorite, quartz and carbonate while zones D to G consist of coarsely crystalline fluorite.

due to preferential incorporation, by fluorite, of the REE with ionic radius close to Ho. Such preferential incorporation may account for the concavity of the HREE in the 'late-stage' fluorites.

The REE pattern of zone G is characteristic of the 'extremely late-stage' pattern, such as that developed in sample GNV-ST (figure 6.3.1). Fluid inclusions indicate that fluorite precipitation took place during a period of increasing temperature (90°C to 140°C) and decreasing salinity (24 to 8 eq. wt. % NaCl), except for a rapid decrease in temperature (140°C to 110°C) subsequent to the precipitation of zone G

6.3.4 Hare's Ears Vein

In sample HEV-1, from the Hare's Ears Vein, the chondrite-normalized patterns (figure 6.3.4) for all zones except E , are typical 'late-stage' patterns as recognized in the

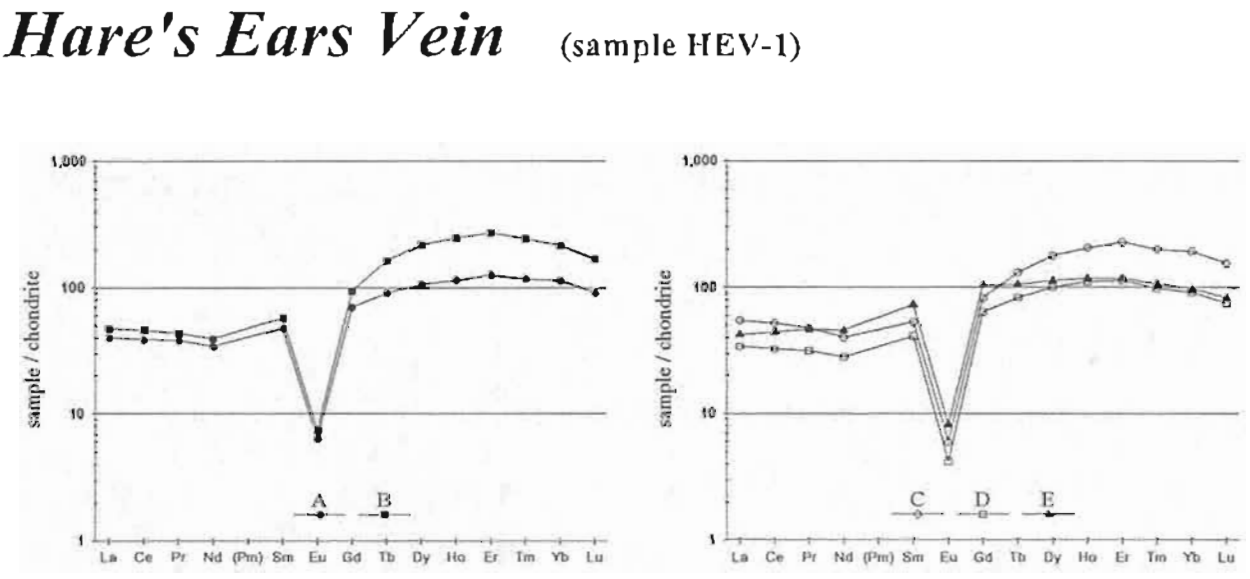

Figure 6.3.4 Chondrite normalized REE patterns for fluorite in sample HEV-2 from the Hare's Ears Vein. The symbols represent successive growth zones from the earliest precipitated mineralization (zone A) to the latest (zone E). Zone A contains fragments of earlier deposited "breccia-type" mineralization in a matrix of coarsely crystalline white fluorite. Zone D contains up to 40% coarsely crystalline galena intergrown with coarsely crystalline gray-green fluorite. The latest fluorite in zone E appears to cut and fragment the mineralization of zone D.

previous veins. Zones B to D display virtually identical shaped patterns with a systematic decrease in total REE with precipitation. The relationship of zone E to the other zones is uncertain as it appears to cut and fragment zone E mineralization. Apart from the higher concentration of REE relative to the preceding zone, E resembles the 'flattened' pattern of zone F in sample ISV-1 (figure 6.3.3) and may have a similar origin. The parallel relationships between the Hare's Ears and Iron Springs veins may be due to their close proximity, within 500 metres of each other.

Fluid inclusion data is variable but generally inclusions from all zones fall on 'trend A' of the temperature versus salinity diagram. Lack of well defined directional crystallization textures in this sample makes the exact sequencing of zones and other relationships uncertain, therefore conclusions drawn from this sample regarding REE variations with precipitation should be regarded as tenuous.

6.3.5 Blake's Brook Vein

Sample BBV-2, from the Blake's Brook Vein, contains 9 growth zones (A to I) of very similar white to clear coarse grained fluorite with minor sphalerite and galena. The only variable zones are zones G and I which appear to be of a later (secondary) origin with respect to the other zones. The chondrite-normalized pattern (figure 6.3.5) reflect the homogeneity of the fluorite as zones C to H have almost identical 'late-stage' fluorite patterns, with poorly developed concavity in the HREE. The abnormal HREE behaviour is most apparent in zones A and B which display a quite uncharacteristic REE pattern compared to the other fluorite samples. Zone A shows a positive Gd anomaly which is observed in 'early' zones in a number of samples. The patterns in zones A and B could be considered 'late-stage' except for the uncharacteristic relative 'flattening' of the HREE

Blake's Brook Vein (sample BBV-2)

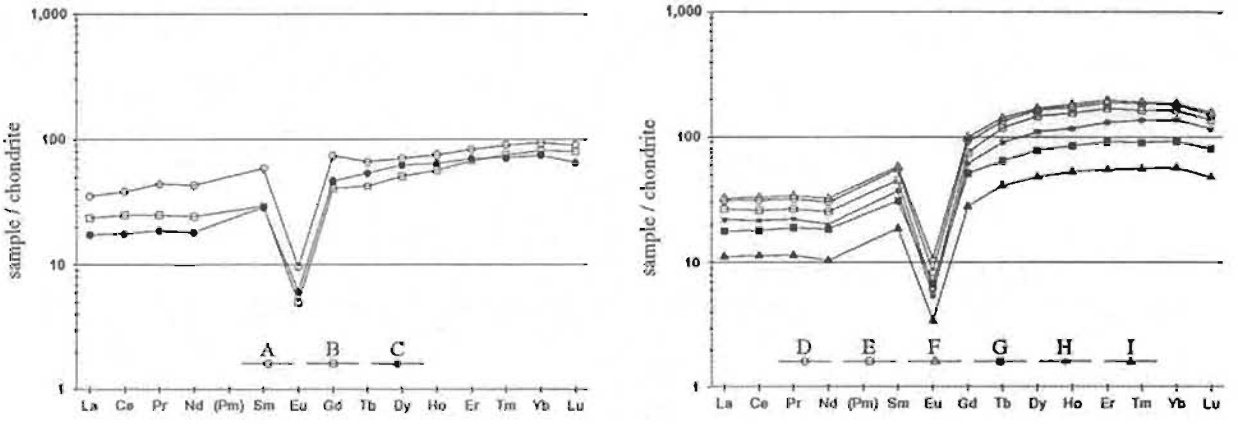

Figure 6.3.5 Chondrite normalized REE patterns for fluorite in sample BBV-2 from the Blake's Brook Vein. The symbols represent successive growth zones from the earliest precipitated mineralization (zone A) to the latest (zone I). Zones A to H are characterized by coarsely crystalline white-colourless fluorite, with variable amounts of galena and sphalerite (± chalcopyrite). Zones C and F contain a higher proportion of coarsely crystalline intergrown galena while zones G and I appear to be later mineralization consisting of fluorite, sphalerite and galena.

which, excluding the Eu and Gd anomalies, shows a rather monotonous increase from La to Lu. The REE pattern in zone C appears to be transitional between the early (A - B) and later zones (D - I).

The zones G and I, which appear to be 'later' than the zones D to H, have identical REE patterns to the latter except for a decrease in total REE suggesting the possibility of dilution by a REE-poor fluid. Fluid inclusions in zones A to C show decreasing salinity with precipitation during isothermal conditions (130°C), a significant drop in temperature to 100°C at zone D, followed by a slight rise in temperature and salinity with precipitation of the remaining zones. Two high temperature (380°C) inclusions in zone A indicate that this zone, being fairly wide (2 cm), may be a composite zone containing an unrecognized early zone of LREE enriched and HREE depleted fluorite, similar to the

early zones in GNV-8, resulting in a 'hybrid' REE pattern. The high temperature inclusions plot on 'trend B' of the temperature versus salinity diagram, while the remainder of the data plot on 'trend A'.

6.3.6 Clam Pond Vein

Chondrite-normalized REE patterns for sample CPV-4, from the Clam Pond Vein, are shown in figure 6.3.6. Early fluorite (zone A), with up to 10% intergrown white quartz and barite with a 'breccia-like' texture, displays a 'late-stage' REE pattern. This zone displays a prominent positive Gd anomaly, characteristic of the early zones of many samples, as well as a larger negative Eu anomaly compared to succeeding zones. This zone is followed by three zones (B - D) of coarse grained white to purple fluorite, all of which display typical 'late-stage' REE patterns. Zone E is a quartz-rich (approx. 60%) breccia, resembling the 'tuffisites' found in the granite, containing up to 3% Al and K, indicating a minor granitic component. The REE pattern of this zone appears to be

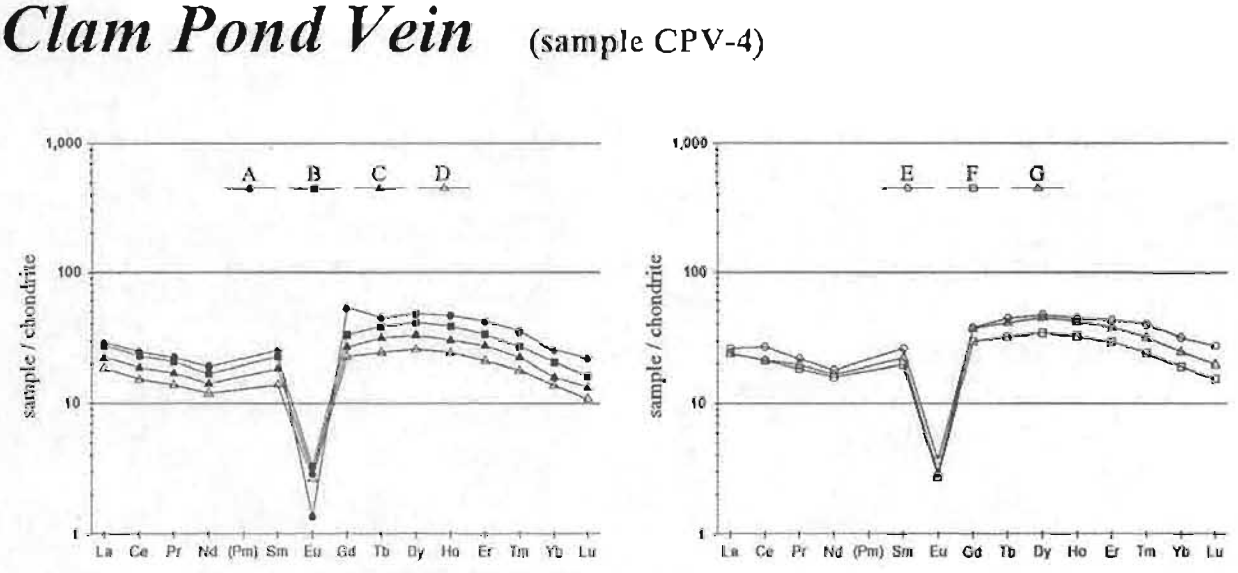

Figure 6.3.6 Chondrite normalized REE patterns for fluorite in sample CPV-4 from the Clam Pond Vein. The symbols represent successive growth zones from the earliest precipitated mineralization (zone A) to the latest (zone L).

dominated by the fluorite component (40%) as it is similar to the preceding fluorite zones, except for a minor positive Ce anomaly. Zones F and G are 'breccia-type' mineralization consisting of large sub-rounded fragments of coarse grained fluorite (locally banded) in a fine matrix of quartz, carbonate and fluorite. The REE patterns in these zones appear to be dominated by the fluorite component (85 - 75 %), since they are identical to the fluorite patterns in the earlier zones.

Fluid inclusion data from zones A, B, C, D and G indicate that fluorite in the Clam Pond Vein was deposited at very low temperatures, defining a bi-modal distribution with maxima around 75°C and 110°C with the fluorite fragments in zone G falling consistently in the higher temperature group and temperatures in zones A to D showing a trend of increasing temperature with precipitation. Salinity data shows a wide variability within zones but overall defines a tri-modal distribution with well defined maxima at 26, 12 and 8 eq. wt. % NaCl. All samples plot on 'trend A' on the temperature versus salinity diagram.

6.3.7 The Lunch Pond Vein

Sample LP-2, from the Lunch Pond Vein, contains two early zones of quartz-carbonate breccia followed by 10 narrow zones of fluorite, quartz and barite. The samples have been sub-divided into three groups, based on mineralogy, for the purpose of plotting their chondrite-normalized REE patterns (figure 6.3.7). The REE patterns of the early quartz-carbonate breccia zones can be interpreted in terms of a hybrid pattern resulting from REE incorporation into two phases, fluorite and calcite (see later section on the Salt Cove Valley Vein for discussion of 'typical' calcite patterns). The fluorite dominated zones show 'late-stage' REE patterns similar to those in other fluorite zones.

Lunch Pond Vein (sample LP-2)

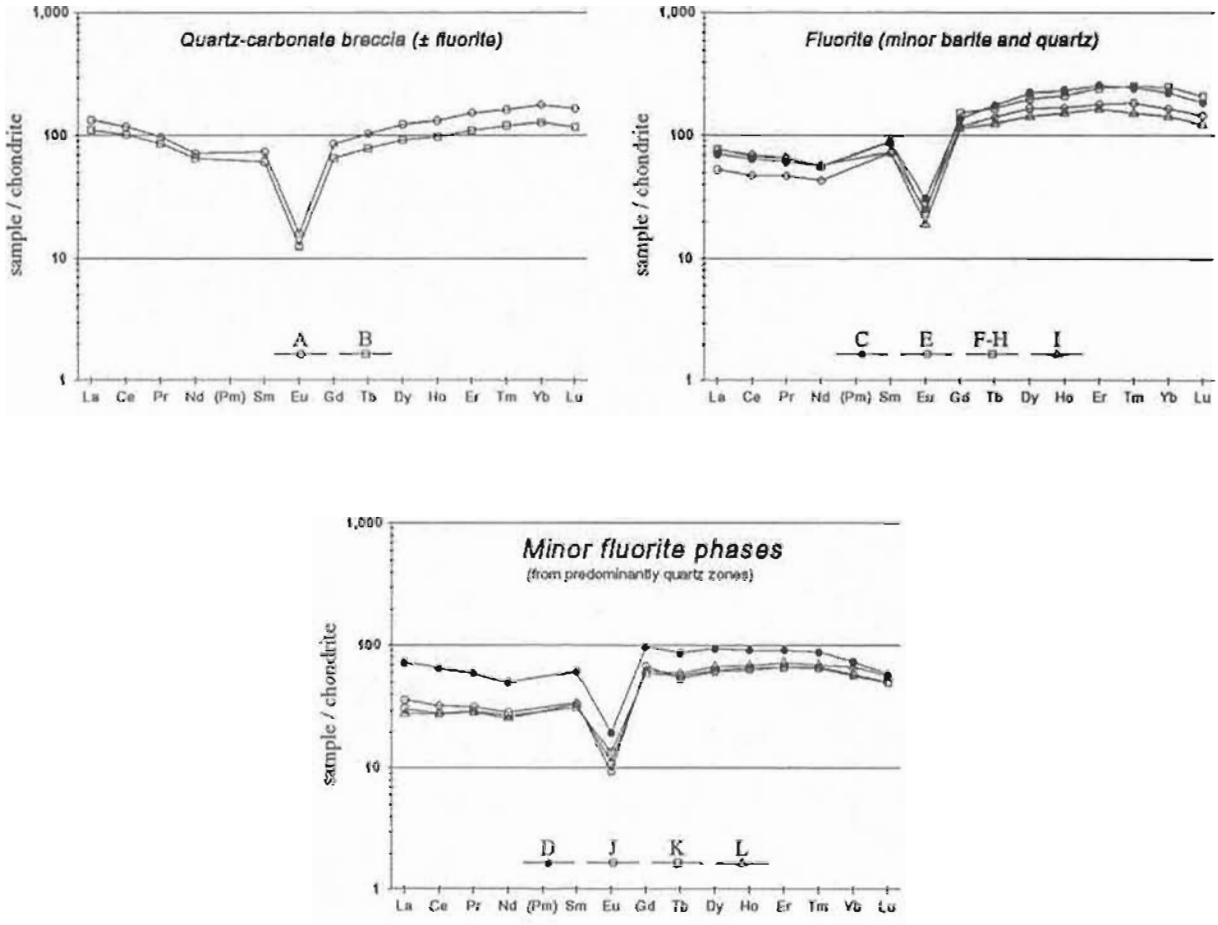

Figure 6.3.7 Chondrite normalized REE patterns for fluorite in sample LP-2 from the Lunch Pond Vein. The symbols represent successive growth zones from the earliest precipitated mineralization (zone A) to the latest (zone L).

The fluorite from the quartz-rich zones display abnormally flat patterns with consistent positive Gd anomalies. Both zones D and L contain 50 to 60% fluorite respectively, they have identical shaped REE patterns to zones J and L which contain only 30% fluorite. The higher total REE content in zone D may be attributed to its occurring earlier in the precipitation process from a possibly more REE-enriched fluid.

6.3.8 Lawn Barite Vein

Sample LBV-7, from the Lawn Barite Vein, consists of 8 zones of intergrown fluorite and barite (A - H), with minor amounts of quartz and calcite, except for zone G which consists of primarily coarse grained white barite. Zone H consists of white barite and fluorite which cuts across zones A to D. The barite and fluorite zones contain from 50 to 10% fluorite except for zone H which has only 3% fluorite.

The chondrite-normalized REE patterns for zones A to D (figure 6.3.8) are very similar showing a fluorite pattern resembling a 'flattened' version of the 'late-stage' type containing a positive Gd anomaly and a negative Eu anomaly. This pattern is similar to the transitional patterns between the 'V and tail' and 'late-stage' patterns of other veins. Fluorite in zone E displays a similar shaped pattern to the earlier zones but with a significantly lower total REE concentration and an insignificant Gd anomaly. Fluorite

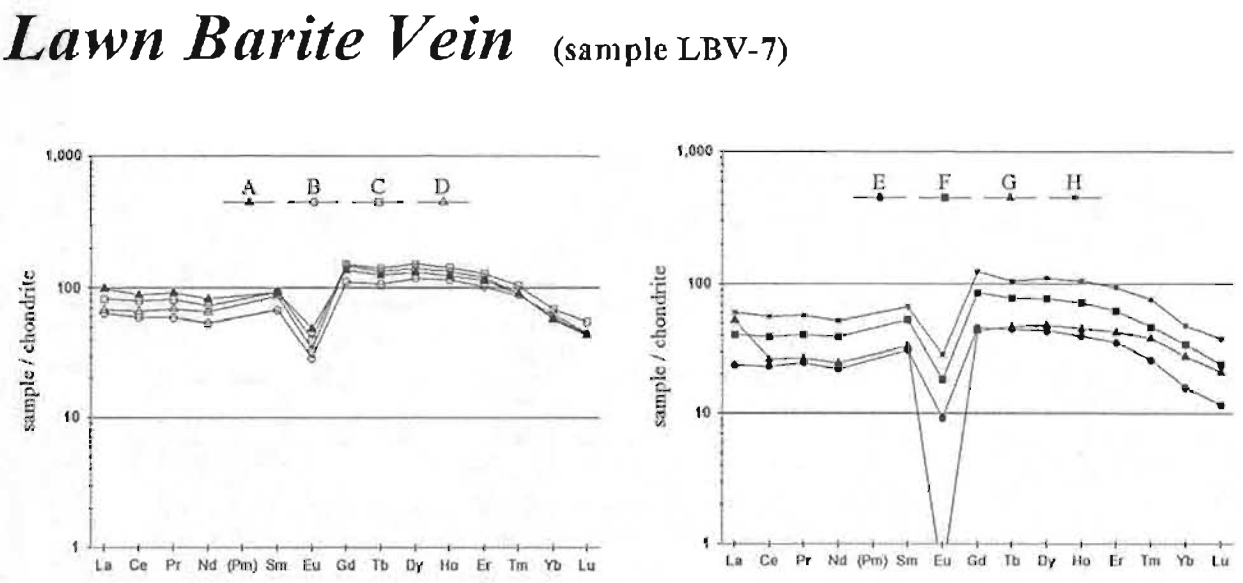

Figure 6.3.8 Chondrite normalized REE patterns for fluorite in sample LBV-7 from the Lawn Barite Vein. The symbols represent successive growth zones with zone 'A' representing the earliest mineralization and zone 'G' representing the latest. Zone 'H' is a later veinlet which cuts zones A to D and resembles zones E to F in colour and texture. Zone 'G consists primarily of white barite, the partial dissolution of which probably contributes to the anomalous La concentration in this zone.

from zones F and H show identical REE patterns to the first four zones and total REE concentrations approaching those of these zones. The fluorite from the late barite-rich zone (G) displays a pattern similar to that in zone E with the exception of a somewhat flatter HREE portion, an exceptionally high negative Eu anomaly and anomalously high La.

The ICP-MS analysis indicates that approximately 35% of the material analyzed in the zone G sample was barite which may account for some of the irregularity in the REE pattern. The relatively small negative Eu anomaly in the fluorites suggest that Eu is present as Eu^{3+} and as such will not be preferentially incorporated into barite as would Eu^{2+} (Morgan and Wandless, 1980). Instead Eu^{3+} would be preferentially incorporated into the fluorite structure because of the relative difference in ionic radius between the two oxidation states. The large negative Eu anomaly in zone G may reflect more reducing conditions causing most the Eu to be incorporated into barite as Eu^{2+}. The positive La 'spike' could also be explained by a contribution from dissolved barite. Morgan and Wandless (1980) found that in barite from Creede, Colorado, only La and Eu (Eu^{2+}) was present in detectable quantities and in referring to the REE, excepting Eu, "...abundances fall off steeply as atomic number increases (and ionic radius decreases)...". If barite is responsible for the elevated La in zone G, this would suggest that the REE content of barite in the St. Lawrence veins appears to be considerably higher that those of Creede, since La in the Creede sample was only slightly above chondritic values (Morgan and Wandless, 1980). The conclusions pertaining to Eu in these barite-rich samples should be treated with caution since the extremely high Ba levels may cause an interference of Ba on Eu making the ICP-MS results less than quantitative.

Fluid inclusion data for samples from the Lawn Barite Vein indicate homogenization temperatures in the range 330°C to 230°C and salinities in the range 22 to 15 eq. wt. % NaCl (Strong et al., 1984).

6.3.9 Salt Cove Valley Vein

Sample SCVV(A), from the Little Salt Cove Valley Vein, consists of two early zones (A and B) of white coarse grained calcite which is followed by a later zone of coarse grained fluorite. The chondrite-normalized REE patterns from the calcite zones (figure 6.3.9) display a convex downward pattern which is depleted in the middle REE (MREE) compared to the LREE and HREE which are present in equal normalized proportions. Calcite displays a strong negative Eu anomaly. The calcite from zone B is slightly more depleted in REE, especially the LREE than that from zone A. The fluorite

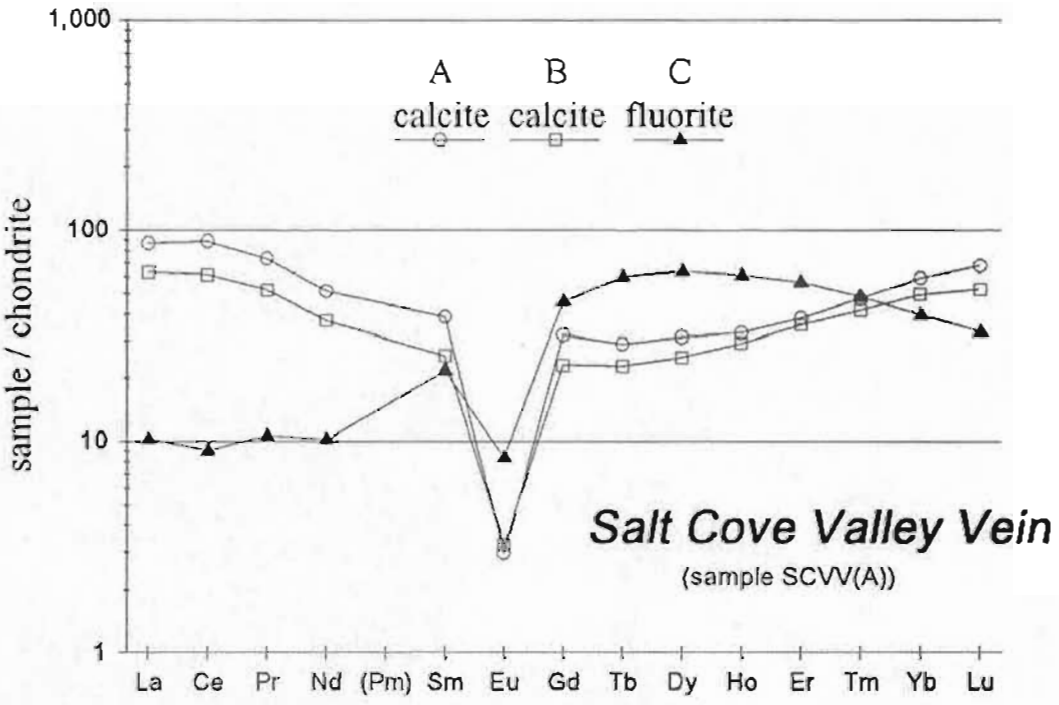

Figure 6.3.9 Chondrite normalized REE patterns for sample SCVV(A) from the Little Salt Cove Valley Vein. Zones A and B are earlier precipitated calcite while zone C is later fluorite.

from zone C displays a 'late-stage' type of REE pattern typical of most of the fluorites in the mine area. Fluid inclusion data show that the calcite was precipitated at temperatures between 150°C and 100°C from fluids with salinities around 12 eq. wt. % NaCl and the fluorite was precipitated at temperatures between 125°C and 80°C from fluids with salinities between 24 and 12 eq. wt. % NaCl.

6.3.10 Individual Mine Area Samples

Sample **BB-84-11** is a sample of coarse grained fluorite from the central part of the main Blue Beach North Vein. The chondrite-normalized REE distribution (figure 6.3.10) is a 'late-stage' type pattern which would be considered typical except for the negative slope from La to Nd suggesting a pattern transitional from the 'V and tail' type

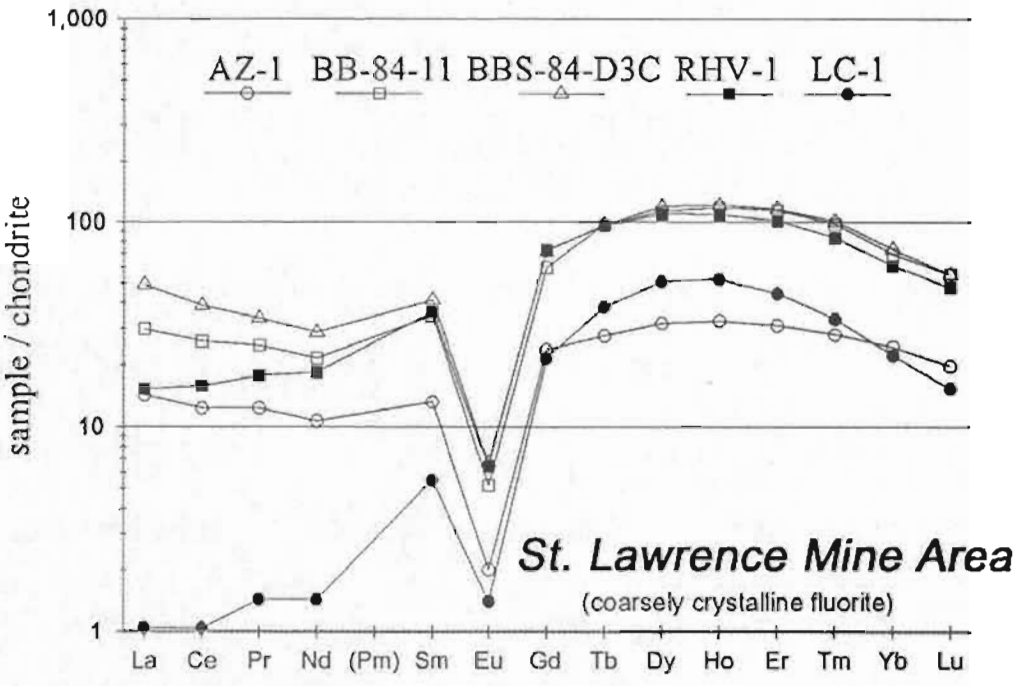

Figure 6.3.10 Chondrite normalized REE patterns for individual samples from the St. Lawrence mine area. Sample AZ-1 is from a narrow fluorite vein in an altered granite exposure at Chamber Point. Samples BB-84-11 and BBS-84-D3C are from the Blue Beach Vein, the latter being from a small offshoot vein. Sample RHV-1 is from fluorite, forming the matrix to a gas breccia in the Red Head Vein. Sample LC-1 is from a large cubic crystal of fluorite representing extremely 'late-stage' fluorite which probably formed in an open cavity (vug).

pattern. Sample BBS-84-D3C (79') is from a small 'offshoot' vein immediately east of the Blue Beach North Vein. It has a REE pattern virtually identical to that of BB-84-11 except for a slight enrichment in the LREE. Fluid inclusion data from BBS-84-D3C (79') indicate that the fluorite was deposited at temperatures around 100°C over a salinity range from 26 to 8 eq. wt.% NaCl.

Sample RHV-1, from the Red Head Vein, is a sample of blue to green coarse grained fluorite which forms the matrix to a fluorite 'tuffisite' or gas breccia on the western extremity of the vein structure. This breccia zone is characterized by rounded, cobble to gravel sized fragments of granite cemented by a matrix of coarse grained fluorite. The plot of the chondrite normalized REE pattern (figure 6.3.10) for RHV-1 shows that it has a typical 'late-stage' fluorite pattern like so many of the samples from the St. Lawrence mine area. Fluid inclusion data from this sample indicates that the fluorite formed from a moderately saline (8 to 6 eq. wt.% NaCl) fluid at a temperature between 95°C and 85°C.

Sample LC-1 is a sample from a large cubic fluorite crystal with faces 12 to 10 cm across probably representing late-stage fluorite growth into an open cavity. The chondrite normalized REE pattern (figure 6.3.10) of this sample is a classic example of the 'extremely late-stage' REE pattern in St. Lawrence fluorites. This pattern is very similar to that seen in samples GNV-ST and ISV-1-G the two other late-stage fluorites. This REE pattern shows an extreme LREE depletion, strong negative Eu anomaly, concave upward HREE pattern and $Nd_N/Sm_N << 1$, all characteristic of 'extremely late-stage' type REE patterns.

6.3.11 Outlying Veins

The following section will discuss analysis from veins that are remote from the main St. Lawrence Mine area. These are sample **BMWV-10-1**, from the Big Meadow Woods Vein and sample **AD-1-A**, from the Anchor Drogue Vein. The plot of the REE pattern from sample BMWV-10-1 (figure 6.4.11) shows a non-typical trend which is most comparable to the hybrid 'late-stage' type pattern but with a pronounced flattening of the HREE part of the pattern. The plot also shows a weak positive Gd anomaly and a strong negative Eu anomaly. Fluid inclusion data for this breccia sample indicates fluorite precipitation at a temperature of 125°C to 100°C from a variable salinity fluid ranging from 26 to 2 eq. wt.% NaCl.

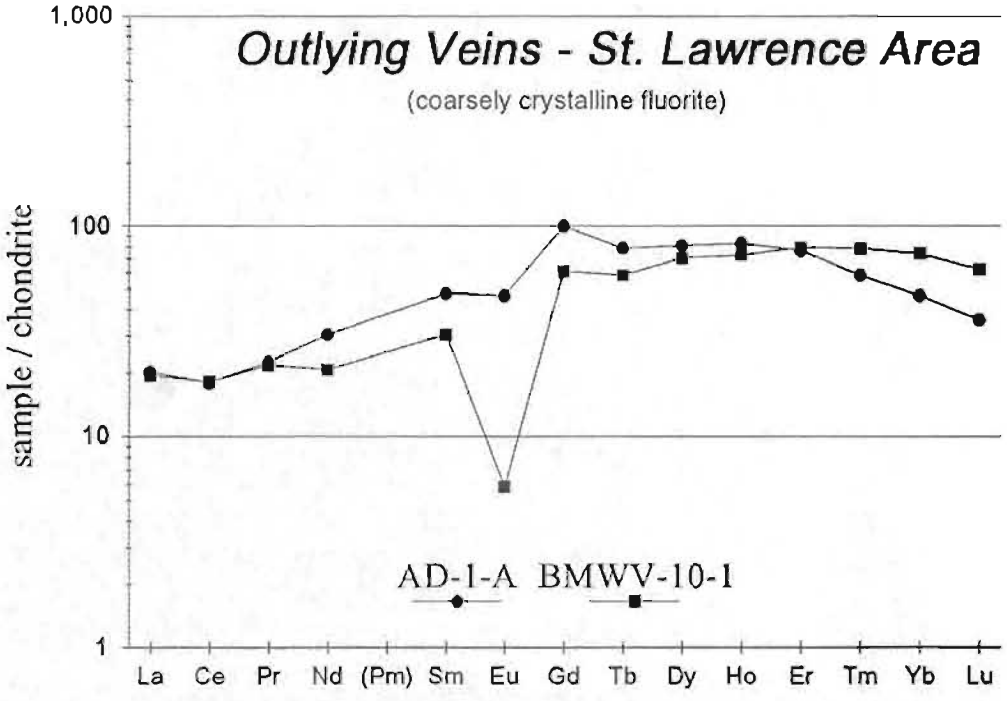

Figure 6.3.11 Chondrite normalized REE patterns for two outlying veins in the St. Lawrence Area. Sample AD-1-A is coarse grained green fluorite from the Anchor Drogue Vein. Sample BMWV-10-1 is fluorite in 'breccia-type' ore from the Big Meadow Woods Vein.

The chondrite-normalized REE plot for sample AD-1-A (figure 6.3.11) displays a remarkable similarity to that of BMWV-10-1 except for a stronger positive Gd anomaly and a much smaller negative Eu anomaly. As well this sample shows a depletion in the HREE, especially Lu, compared to BMWV-10-1. Preliminary fluid inclusion data from the Anchor Drogue Vein indicates fluorite precipitation over the temperature range 175°C to 80°C from a generally high salinity fluid (approx. 26 eq. wt.% NaCl).

6.3.12 Alteration Zone

Several samples of variably altered granite (**AZ-2** and **AZ-4**) and a sample of a fluorite vein (**AZ-1**) were analyzed from a molybdenite-bearing alteration zone near the granite contact at Chamber Point. Sample AZ-2 and AZ-4 are altered fine grained red aplitic granite with disseminated molybdenite and minor chalcopyrite. The chondrite normalized REE patterns (figure 6.3.12) which show a LREE enriched pattern with a negative Eu anomaly have been presented Chapter 2.

The chondrite-normalized REE pattern of fluorite sample AZ-1 (figure 6.3.12), from a vein within the alteration zone, is similar to 'late-stage' patterns as documented in other fluorite veins in the St. Lawrence area. Fluid inclusion data from this vein indicates fluorite deposition from a cool (120°C to 80°C) variably saline (dominantly 14 to 8 but up to 24 eq. wt.% NaCl) fluid.

6.3.13 Second Dam Showing

Two samples of host granite (**SDMS-2-B** and **SDMS-4**) and a sample of quartz vein or micro-pegmatite (**SDMS-2-A**), from the Second Dam Molybdenite Showing, were analyzed for REE by ICP-MS. The vein mineralization consists of large platy aggregates of molybdenite crystals in a narrow vein of quartz and K-feldspar which could

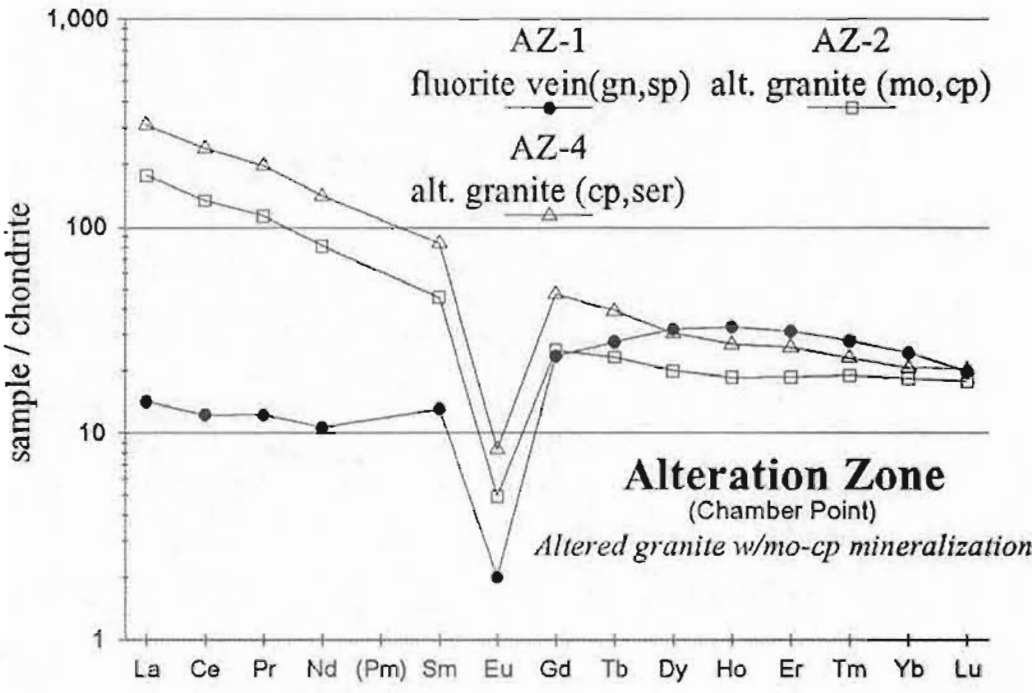

Figure 6.3.12 Chondrite normalized REE patterns for samples from the 'Alteration Zone' at Chamber Point. Sample AZ-1 is a fluorite vein cutting across altered granite represented by samples AZ-2 and AZ-4.

be termed a 'micro-pegmatite' since the 'quartz vein' locally has diffuse boundaries with the host granite. The K-feldspar content of the quartz 'vein' is estimated to be approximately 20% based on XRF analysis of Al, K and Na (i.e assuming all these elements are present in K-feldspar). The granite sample proximal to the mineralized vein shows a higher abundance of all REE (except Eu) in the chondrite-normalized plot (figure 6.3.13). The Eu concentration in sample SDMS-2-B is below the detection limit (<0.003 ppm) of the analytical procedure (Na_2O_2 sinter) making it less than 0.03 times chondritic values.

The chondrite-normalized REE patterns (figure 6.3.13) show a higher concentration of the REE, especially the LREE, in the quartz 'vein' than in either of the granite samples. The composition of quartz is normally very close to 100% SiO_2 and the

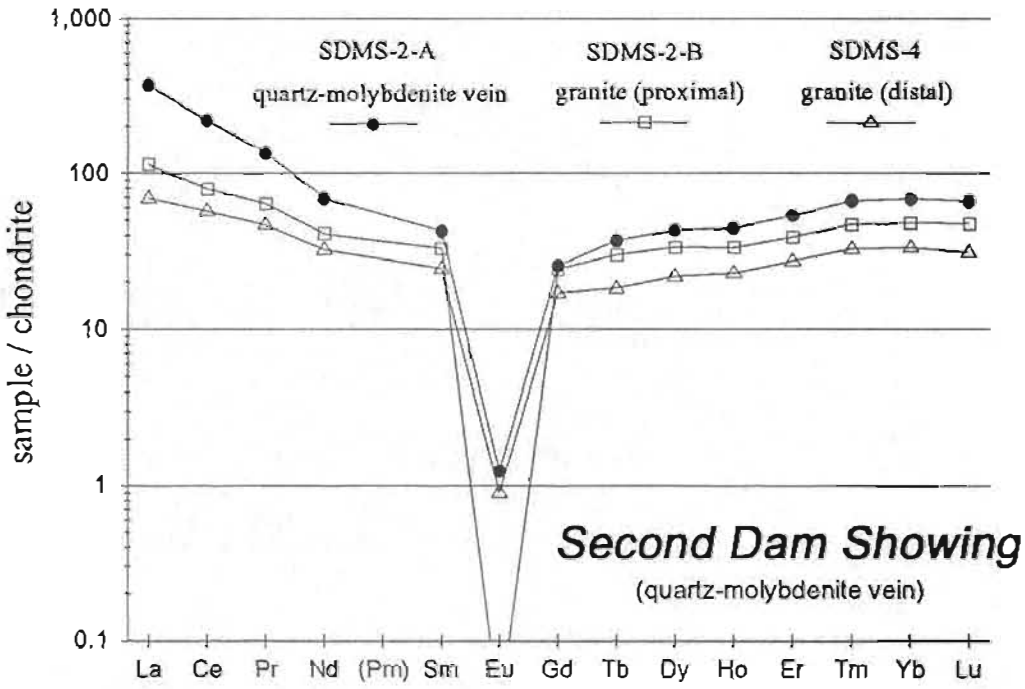

Figure 6.3.13 Chondrite normalized REE patterns for a quartz-molybdenite vein and host granite from the Second Dam Moly Showing. The proximal granite sample is adjacent to the vein while the distal sample is at least 50 metres from any observed mineralization.

small amount of impurities sometimes detected, can usually be attributed to small inclusions of other minerals or fluid inclusions (Deer, Howie and Zussman, 1977). Consequently, elements such as the REE which are not readily incorporated into the quartz structure and the observed REE pattern in the quartz vein is more likely due to the REE content of the K-feldspar and/or fluid inclusions and/or some unidentified minor phase. It is assumed that the molybdenite, like galena (Morgan and Wandless, 1980), would not incorporate significant amounts of REE into its structure because of the lack of chalcophile character of the REE.

6.4 Strontium Isotope Geochemistry

The measured $^{87}Sr/^{86}Sr$ ratio of hydrothermal fluorite is interpreted to represent the ratio in the fluid at the time of formation since ^{87}Rb, which decays to ^{87}Sr, does not fit into the fluorite structure (Ruiz et al., 1980, 1985). The small difference in mass between ^{87}Sr and ^{86}Sr indicates that these two isotopes should not be significantly fractionated during deposition of a strontium-bearing mineral from a hydrothermal fluid (Ruiz et al., 1985). The chemical and physical properties of Sr and Ca are very similar, therefore the evolution of Sr should parallel that of Ca and, by inference, the $^{87}Sr/^{86}Sr$ ratios of the St. Lawrence fluorite samples should provide clues as to the behaviour and source of the Ca in the mineralizing fluids.

The $^{87}Sr/^{86}Sr$ ratios of 5 fluorite samples from growth zones within sample GNV-8 and internal control sample GNV-7, both from the Grebe's Nest Vein, were determined by Thermal-ionization Mass Spectrometry (TI-MS) after separation of Sr by ion-exchange chromatography. The $^{87}Rb/^{86}Sr$ ratios and Rb and Sr concentrations in these samples were determined by ICP-MS. The results of the $^{87}Sr/^{86}Sr$ analysis of the St. Lawrence fluorites are tabulated below (Table 6.4.1) and presented graphically in figure 6.4.1. The samples show a consistent $^{87}Sr/^{86}Sr$ ratio averaging 0.70950 and, within 2-sigma errors, all samples overlap within ± 0.00013. Strontium concentrations range from 80 to 60 ppm while Rb concentrations, and consequently the $^{87}Rb/^{86}Sr$ ratios, are very low (< 0.5 and < 0.02 ppm respectively).

6.4.1 Discussion

There is little dispute over the concept that, in the absence of isotopic resetting, the $^{87}Sr/^{86}Sr$ ratio of hydrothermal fluorite (and other 'Rb-free' minerals) effectively

Table 6.4.1 Summary table of $^{87}Sr/^{86}Sr$ ratios of fluorite samples from the Grebe's Nest Vein, St. Lawrence area. The $^{87}Sr/^{86}Sr$ were determined by TI-MS and the $^{87}Rb/^{86}Sr$ ratios, plus Rb and Sr concentrations, were determined by ICP-MS. The number of analytical cycles is given as n. Standard NBS987(88) was run as a control sample.

St. Lawrence Fluorite Samples **1988-89**

Sample	Rb(ppm)	Sr(ppm)	87Rb/86Sr	87Sr/86Sr	1 sigma	n =
GNV-8-B(88	0.5	78.6	0.0214	0.70979	± 0.00040	40
GNV-8-C(88	0.3	80.0	0.0110	0.71083	± 0.00023	50
GNV-8-D	< 0.3	80.4	0.0082	0.70781	± 0.00085	16
GNV-8-E	< 0.3	60.3	< 0.0004	0.70950	± 0.00007	800
GNV-8-L	< 0.3	58.7	0.0004	0.70964	± 0.00004	250
GNV-7	< 0.3	62.3	0.0025	0.70952	± 0.00004	222
NBS Standard						
NBS987(88)				0.71030	± 0.00003	100
NBS987	(recommended value ± 2-sigma)			0.71025	± 0.00003	

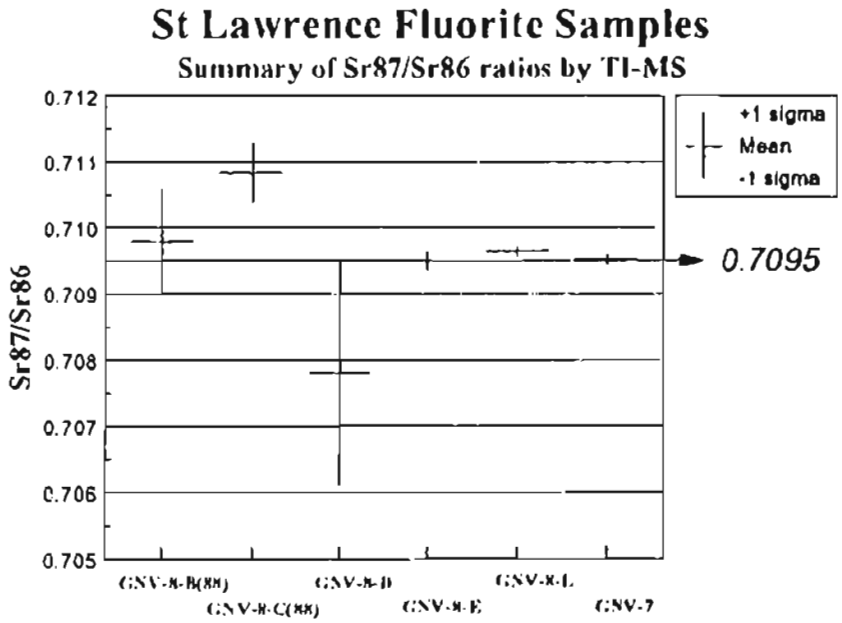

Figure 6.4.1 Plot of $^{87}Sr/^{86}Sr$ ratios in fluorite from the Grebe's Nest Vein, St. Lawrence. Diagram shows mean values plus range of 1-sigma errors.

preserves the initial isotopic ratio of the fluid from which they formed, but there is some dispute as to what the isotopic ratios of the fluid actually represent (see Norman and Landis (1983) for a discussion). If the fluid had a source rock different from the rock which now host the mineralization, the $^{87}Sr/^{86}Sr$ preserved in the hydrothermal minerals would depend on the amount of fluid interaction with wall-rock between the source and site of deposition. Any exchange of Sr between fluid and wall-rock should also involve exchange of Ca. For the case above, Ruiz et al. (1985) conclude that "If the strontium isotope composition of the fluorite differs significantly from that of the host rock, it could mean that the ore-bearing solutions carried important concentrations of strontium (and calcium) and thus less fluoride." Since, in the case of the St. Lawrence fluorite, both the host rocks and the source of the F are most likely the St. Lawrence Granite, the Sr-isotopes should confirm if the granite was also the source of the Ca in the fluorite.

An initial $^{87}Sr/^{86}Sr$ ratio of 0.722 ± 0.003 (315 ± 5 Ma) for the St. Lawrence Granite was determined by Bell et al. (1977) using a four-point isochron from a limited sample suite. As part of their 1984 study of the St. Lawrence Fluorspar Deposits, Strong and Fryer calculated an initial $^{87}Sr/^{86}Sr$ ratio of 0.709 ± 0.006 (353 ± 30 Ma) using an 11-point isochron from an expanded sample suite, and they analyzed $^{87}Sr/^{86}Sr$ ratios of calcite and fluorite from the fluorspar veins which measured 0.70945 ± 0.00009 (2-sigma) and 0.70801 ± 0.00017 respectively (unpub. data, B.J. Fryer). Combining the Rb-Sr data of Bell et al. (1977) with the unpublished data of Fryer (excluding the fluorite and calcite), a 15-point isochron was calculated (Yorkfit, 2-sigma errors) which yielded an initial $^{87}Sr/^{86}Sr$ of 0.708 ± 0.005 and an age of 353 ± 22 Ma for the St. Lawrence Granite. The $^{87}Sr/^{86}Sr$ ratio of 0.7095 determined for fluorite from the Grebe's Nest Vein

is identical, within errors, to the initial ratio of the granite. It is therefore conceivable that the fluids from which the fluorite formed were derived from or equilibrated with the granite. In either case it appears that the most likely source of the Sr, and by inference Ca, was the St. Lawrence Granite or its granitic magma.

The Rb-Sr age for the St. Lawrence Granite (353 Ma) is considerably younger than the U-Pb (zircon) age of 394 Ma (+6/-4 Ma) determined by Krogh et al. (1988) for the coeval Grand Beach Porphyry (ignimbrite), suggesting that the Rb-Sr systematics in the granite may have been modified by some later thermal event. Based on K-Ar studies, Kontak et al. (1988) concluded that Rb-Sr systematics in the Ackley Granite were modified by widespread, relatively low temperature (<200-250°C) fluid circulation resulting in low temperature alteration of feldspars, the primary host of Rb and Sr in the biotite-poor granite. Since the St. Lawrence Granite is also biotite-poor, similar widespread modification of the Rb-Sr systematics may have accompanied the mineralizing event during which the fluorspar deposits were formed.

6.5 SEM Analysis of Fluorite Samples

A scanning electron microscope (SEM) study was completed on a number of polished thin sections, concentrating on samples GNV-8 and ISV-1, in an attempt to determine if some of the REE patterns observed in the fluorite could be attributed to minor REE-bearing accessory phases or solid inclusions. A sample of altered granite from the 'Alteration Zone' was also examined to determine if its unusual LREE enrichment could be related to exotic REE-bearing accessories. Several sulphide bearing zones were also examined to determine if sphalerite displayed significant Fe content or

any other compositional zoning. The Fe-oxide/hydroxide minerals in late-stage zones of sample GNV-8 were also examined for compositional zoning.

The results in most cases were negative. No REE-bearing mineral phases or REE-rich zoning were detected in the fluorite, despite extensive examination. It appears that nearly all of the REE detected in the fluorite is the result of substitution for Ca in crystal lattice sites. The only exotic phase encountered was in zone ISV-1-A (fine grained zone of mixed fluorite, quartz and calcite) where a Ca-Y mineral (either fluoride, oxide or carbonate) with a platy habit appeared to be filling a void between fluorite crystals (figure 4.46), and hence is considered secondary. Several other zones show rare anomalous Y in fluorite suggesting the existence of minor YF_3, but this is only speculative as no separate phase was identified and it probably only reflects enhanced substitution of Y in CaF_2.

Several crystals of calcite and barite were examined but no unusual element concentrations were noted. The sphalerite examined appear to be relatively pure Zn sulphide and no significant zoning was noted in any of the sulphide minerals. The secondary zoned oxides appear to be primarily Fe-rich with quite variable amounts of other metals such as Cu and Pb. Examination of altered granite sample AZ-2 from the "Alteration Zone' at Chamber Point identified minor phases of zircon and rutile, but no REE-minerals.

6.6 Cathode Luminescence in Fluorites and Calcite

Selected fluorites and calcites were examined by cathode luminescence (CL) to examine internal zoning within growth zones in crystals and to examine the oxidation

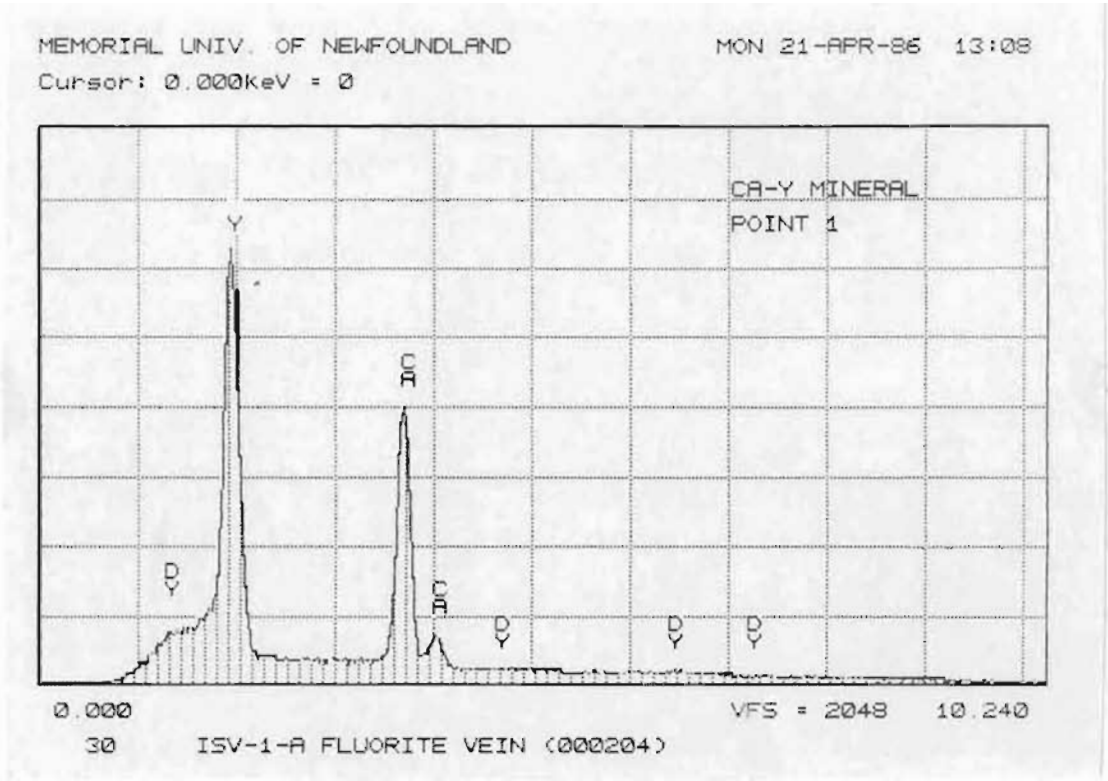

Figure 6.5.1 SEM scan and photomicrograph of minor Y-bearing phase occurring in a void between coarse fluorite crystals in sample ISV-1-A from the Iron Springs Vein. Note the fibrous platy habit. The numbers (1 - 5) represent points at which SEM scans were taken. The above scan was taken at point 1. FL = fluorite.

state of some rare earth elements. The REE are well documented CL activators in fluorite and Eu^{2+} has a distinctive signature on fluorite CL scans, giving a strong peak between wavelengths 430 - 410 nm (Marshall, 1988). The discussion presented here briefly summarize some preliminary observations.

Samples from the Grebe's Nest Vein (GNV-8), the Iron Springs Vein (ISV-1) and the Lawn Barite Vein (LBV-7) were examined visually as well as by spectral analysis. The fluorite displays luminescence which varies from deep violet, through various shades of blue to white-green. Internal microscopic crystal growth bands, as well as somewhat diffuse patches within crystals, in samples ISV-1 and GNV-8, display varying shades of blue possibly reflecting chemical and/or structural variations in the fluorite lattice. Calcite crystals in sample LBV-7 display alternating light and dark yellow bands reflecting compositional zoning which transects obvious optical crystal features such as twin lamellae. Fluorite in this sample often displays colour banding which is disrupted and transected by intergrown barite crystals. Barite and quartz in this sample are non-luminescent but sphalerite is seen to luminesce bright yellow.

Following the preliminary visual evaluation, CL spectroscopic scans were conducted on several samples by Dr. Roger Mason and the author. This work is of a preliminary nature, therefore only two brief points are to be made. First, a strong spectral response near a wavelength of 410 nm in sample GNV-8-A suggests an activation caused by Eu^{2+}, although such responses have also been attributed to defect structures in impurity-free synthetic fluorite (Marshall, 1988). Second, the fluorites do give strong and variable responses which, combined with further petrographic and analytical work

(i.e. laser ICP-MS) could give some insight into the distribution of REE in the fluorite crystals.

7 REE Systematics - Genetic Perspective

It has been shown that REE distributions in fluorite samples from the St. Lawrence veins display radical, but systematic changes through successive periods of fluorite precipitation. These systematic changes appear to be relatively independent of local temperature and salinity variations within the veins, implying that they may be more intimately related to bulk changes in the chemical composition of the source fluid throughout the broad evolutionary cycle. In the following section, a genetic classification scheme will be proposed, based on the observed REE distributions in fluorite. Fluorite samples from this study have been categorized and sub-divided, based on the proposed scheme. The validity of the classification scheme is evaluated in terms of correlation with geochemical and fluid inclusion data.

In terms of the following discussion, the REE variations are considered to be the result of bulk changes in chemical/physical conditions at the site of deposition. A more detailed discussion of the processes involved are presented in later sections. It must be stated that this classification scheme is based on fluid compositions and processes inherent in the St. Lawrence mineralizing system. Therefore, its application to other fluorite-bearing systems would have to be considered in terms of their individual source fluids and specific mineralizing processes.

7.1 Defining a Genetic Classification Scheme

The purpose of the classification scheme is to link the systematic variations in REE distributions to the chronological sequence, based on the growth zones, displayed in the fluorite samples. The systematics are presented graphically in terms of chondrite-normalized REE plots. This type of plot was chosen for simplicity and comparison with other published data and does not imply that the source fluid resembles chondritic proportions nor that the patterns reflect true fluid-mineral partitioning behaviour, although the effects of REE partitioning between the fluorite and the fluid influence the shape of the patterns.

Despite quite variable REE concentrations, most of the fluorite zones display very similar chondrite-normalized REE patterns, consistent with those reported by Strong et al. (1984). These zones represent a wide range of physical and chemical processes as evidenced by breccia (gas, tectonic and hydraulic) textures, crystal habit, grain size and associated mineral phases as well as fluid inclusion temperature and salinity data. This suggests that, despite varying conditions at the site of deposition, the overall REE balance in the fluid and the REE partitioning behaviour (fluorite/fluid) display remarkable consistency. In spite of this overall coherence, some notable exceptions occur (i.e. in sample GNV-8) which appear to be systematically related to the 'typical' fluorite REE patterns. It is possible that the REE variations reflect a broader cycle of fluid evolution in the hydrothermal system, as opposed to the more restricted intra-vein cycles evidenced by fluid inclusion data and mineralogy (Collins, 1984; Collins and Strong, 1988). If this assumption is valid, the REE systematics should, with a few local variations, define an

evolutionary trend that is reflected in the chronological order of fluorite precipitation within individual samples.

The genetic classification scheme relies heavily on REE systematics in sample GNV-8, from the Grebe's Nest Vein, and in well developed crystal forms indicative of late-stage fluorite precipitation. These were chosen for the following reasons:

- sample GNV-8 contains the most (16) consecutive growth zones of any of the samples in the study
- sample GNV-8 appears to represent a complete cycle of mineralization from fine grained early fluorite at, or near, the vein wall, to late oxide-coated, well developed fluorite crystals which appear to represent late-stage growth
- fluid inclusions in sample GNV-8 display a wide, systematic, range of temperatures from near 300°C in early zones to less than 100°C in later zones
- the REE distributions in sample GNV-8 show gradual systematic, rather than abrupt, changes with successive periods of fluorite precipitation
- the well developed crystal forms are interpreted to represent slow crystal growth in vugs during the final stages of fluorite precipitation

The proposed schematic evolution of REE distribution in St. Lawrence fluorite samples is considered in terms of six distinct classes as shown in figure 7.1.1. These are represented by the chondrite normalized REE patterns from the earliest to latest stages of fluorite precipitation, based on growth zone relationships in samples. The characteristics of each class, as shown in figure 7.1.1, are as follows:

1 **EARLY**: well defined LREE enriched pattern with generally a negative slope from La to Lu and a prominent maximum at Pr. Concentrations of LREE are usually greater than 100 times chondrite steadily decreasing to approximately 10 times chondrite at Lu. Moderate negative Eu anomaly.

2 **EARLY-MIDDLE**: relatively flat pattern with a characteristic 'tail' defined by a negative slope between Er and Lu. Concentrations of most REE are close to 100 times chondrite, decreasing, from Er to Lu, to near 30 times chondrite.. Moderate negative Eu anomaly.

3 **MIDDLE:** characteristic V-shaped pattern defined by a negative slope between La and Sm and a positive slope between Gd and Ho, with a variably developed 'tail' defined by a negative slope between Er and Lu. This pattern is informally referred to as a 'V and tail' pattern. Concentrations of LREE generally range between 20 and 60 times chondrite while concentrations of HREE range between 20 and 100 times chondrite.. Moderate negative Eu anomaly. **The early to middle fluorites are characterized by a $Nd_N/Sm_N \geq 1$, a characteristic which changes and becomes more diagnostic in later fluorites.**

4 **MIDDLE-LATE:** this class is transitional between the 'V and tail' patterns and the characteristic late-stage patterns, displaying a higher degree of variation than the other classes. The LREE generally display a negative slope from La to Nd with a Nd_N/Sm_N ratio slightly less than 1. The HREE generally display a relatively flat pattern which may, or may not, display a weak maximum at Er (a relict 'tail'). Concentrations of LREE are generally around 10 times chondrite while HREE vary between 20 to 50 times chondrite. Moderate negative Eu anomaly.

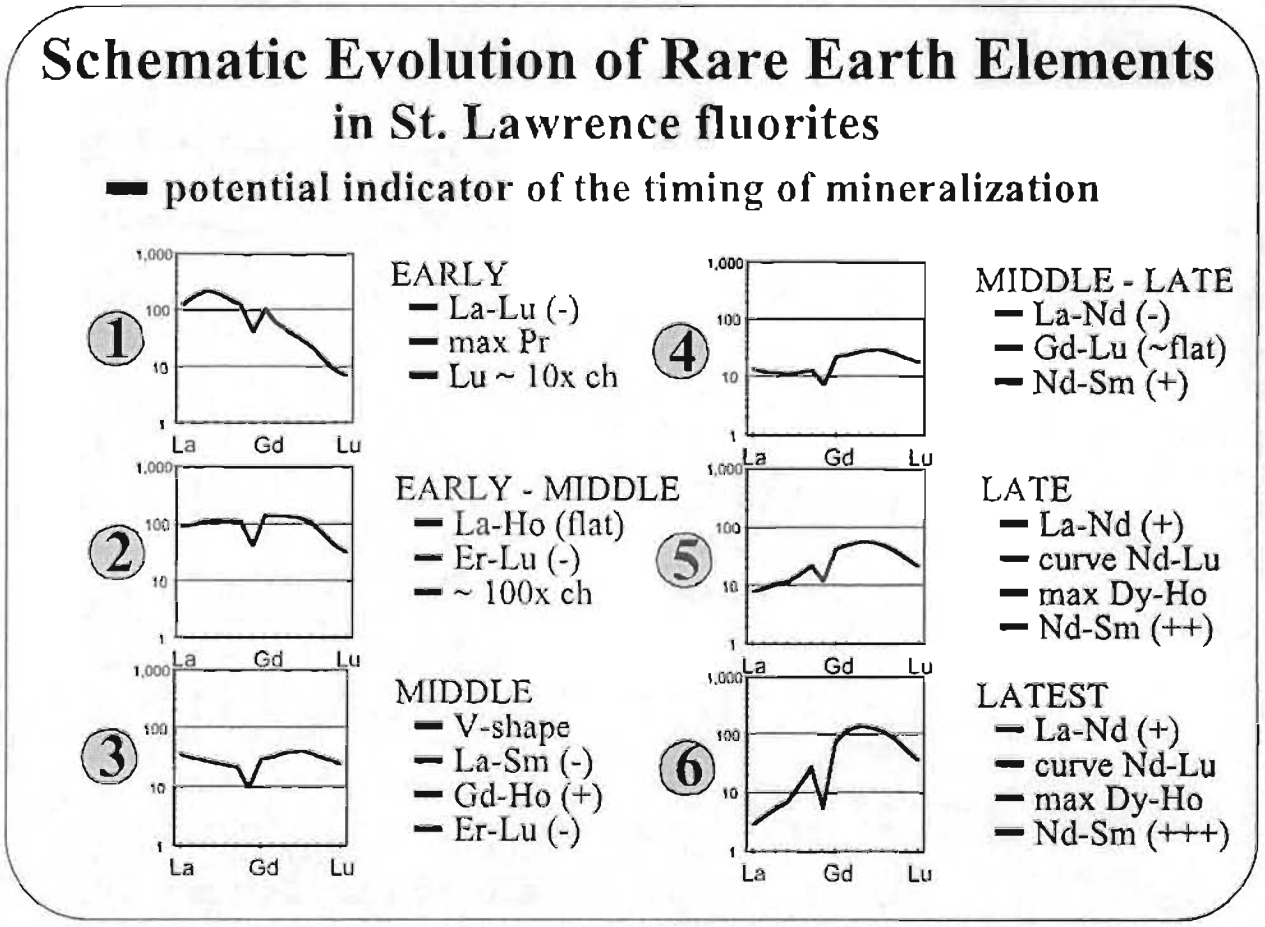

Figure 7.1.1 Schematic evolution of REE in St. Lawrence fluorite samples portrayed by chondrite normalized plots. The general characteristics of each of the six classes (1 to 6) are listed ("+" and "-" denote positive and negative slopes respectively; ch = chondrite).

5 **LATE:** characterized by LREE depletion with a positive slope from La to Nd and a Nd_N/Sm_N ratio less than 1. The HREE show the development of a concave upward shape with a well defined maximum near Dy-Ho, characteristic of 'late-stage' fluorite. Concentrations of LREE are approximately 10 times chondrite while HREE are variably enriched with maxima around 100 times chondrite. Moderate negative Eu anomaly.

6 **LATEST:** extremely 'late-stage' patterns are similar to those of the late fluorite except that the features are more strongly developed. They show extreme depletion of the LREE, especially La, a positive slope from La-Nd and a Nd_N/Sm_N ratio very much less than 1.The HREE show a parabolic, concave upward curve from Nd to Lu with a well defined maximum near Dy-Ho. Maximum normalized concentrations of HREE are generally an order of magnitude higher than the LREE. Strongest negative Eu anomaly of all the classes.

The samples from zones in which fluorite is the dominant mineralogy were categorized according to the criteria outlined above. Samples which have significant amounts of calcite were not included since the partitioning of REE into calcite would alter the REE pattern of the sample. Samples containing significant amounts of quartz or barite were included since neither are considered to host significant amounts of REE and both have very limited solubility in the acid dissolution procedure (ICP-MS). For similar

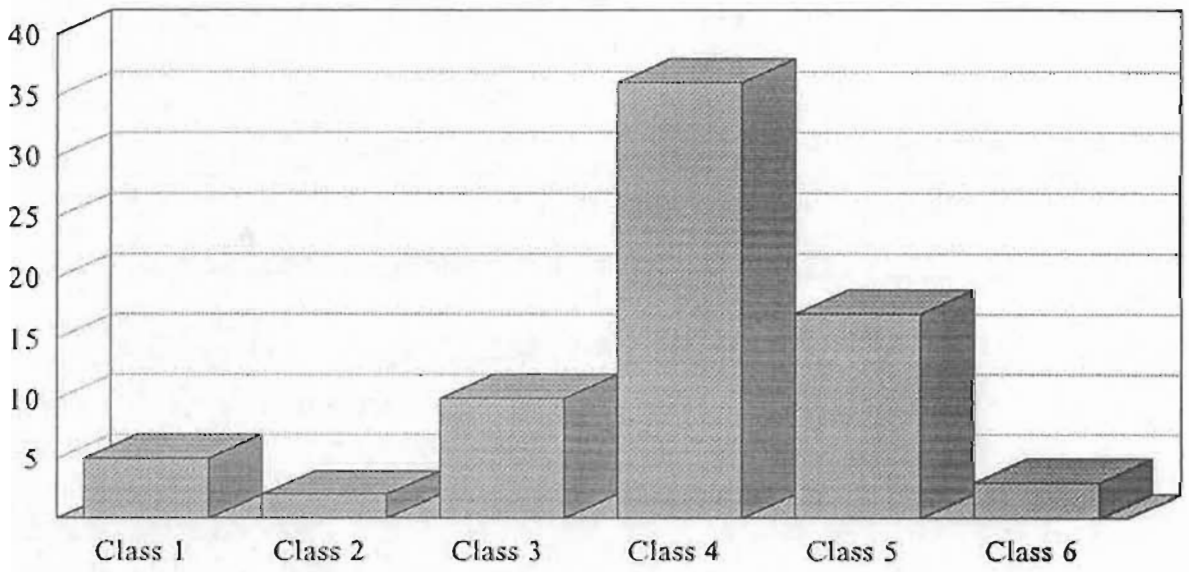

Figure 7.1.2 Histogram showing the distribution of St. Lawrence fluorite samples based on the genetic REE classification as outlined in the text.

reasons, samples containing significant amounts of galena (± sphalerite) were also included. In all, 73 fluorite-bearing samples were classified. The relative distribution is shown in figure 7.1.2 and the samples are individually listed in Table 7.1.1.

Table 7.1.1 Listing of fluorite-bearing samples, from the St. Lawrence area, subdivided according to the proposed REE genetic classification scheme as outlined in the text.

Class1	Class2	Class3	Class4		Class5	Class6
Sample	Sample	Sample	Sample		Sample	Sample
2-2	GNV-8-D	2-10	AZ-1	LBV-7-A	AD-1-A	GNV-ST
2-4	GNV-8-E	2-8	BB-84-11	LBV-7-B	BBV-2-A	ISV-1-G
GNV-8-A		GNV-7	BBS-84-D3C	LBV-7-C	BBV-2-B	LC-1
GNV-8-B		GNV-8-F	BMWV-10-1	LBV-7-D	BBV-2-C	
GNV-8-C		GNV-8-G	CPV-4-A	LBV-7-F	BBV-2-D	
		GNV-8-H	CPV-4-B	LBV-7-F	BBV-2-E	
		GNV-8-I	CPV-4-C	LBV-7-G	BBV-2-F	
		GNV-8-J	CPV-4-D	LBV-7-H	BBV-2-G	
		GNV-8-K	CPV-4-E	LP-2-C	BBV-2-H	
		GNV-8-L	CPV-4-F	LP-2-D	BBV-2-I	
			CPV-4-G	LP-2-E	GNV-8-N	
			GNV-8-M	LP-2-F-H	GNV-8-O	
			HEV-1-A	LP-2-I	HEV-1-E	
			HEV-1-B	LP-2-J	ISV-1-D	
			HEV-1-C	LP-2-K	ISV-1-F	
			HEV-1-D	LP-2-L	RHV-1	
			ISV-1-A		SCVV(A)-C	
			ISV-1-B			
			ISV-1-C			
			ISV-1-E			

7.2 Comparison of Classification to Fluid Inclusion Data

Comparison of the samples that have been classified on the basis of their chondrite-normalized REE patterns to fluid inclusion data for growth zoned vein samples show some obvious relationships. A strong correlation is apparent between the classes and the temperature data but no correlation can be made with the salinity data. Fluorite in the characteristic 'early' class (1) shows consistent evidence of being formed at higher

temperatures. The large spectrum of growth zoning in GNV-8 displays a general trend of decreasing temperature through classes 1 to 6. The relationships between growth zoning, temperature and REE distributions in fluorite samples suggests a paragenetic relationship between these samples. This apparent paragenetic sequence is shown in figure 7.2.1 for samples from eight different veins .

It is evident from figure 7.2.1 that, in the samples studied, the higher temperature fluorite displays distinctive REE distributions in comparison to the lower temperature fluorite which is the most abundant type in the St. Lawrence fluorspar veins. This relationship is especially apparent in the main mining area (including the Grebe's Nest Vein). Some of the outlying veins, such as the Lawn Barite, Anchor Drogue and Big Meadow Woods Veins, are more difficult to classify based on their REE patterns, but in matching with more typical fluorite patterns (figure 7.1.1) by visual 'best-fit', combined with fluid inclusion temperature data, they roughly correlate with mid-late stage criteria in the overall genetic classification schemes.

One exception is the Lawn Barite Vein. Fluid inclusion data (Strong et al., 1984) from this vein indicate temperatures from 300 to 250°C, a range normally associated with 'earlier' REE patterns. This deviation from normal REE behaviour may be related to its being hosted by a mixed lithology conglomerate unit, with which the fluids may have interacted, and to its distance from the main granite body (~ 1.5 km).

7.3 Comparison of Classification to Geochemical Data

Geochemical data from the fluorite samples were subdivided based on the classification scheme developed from the chondrite-normalized REE plots. The

Fluorite Paragenetic Sequence

as indicated by REE patterns

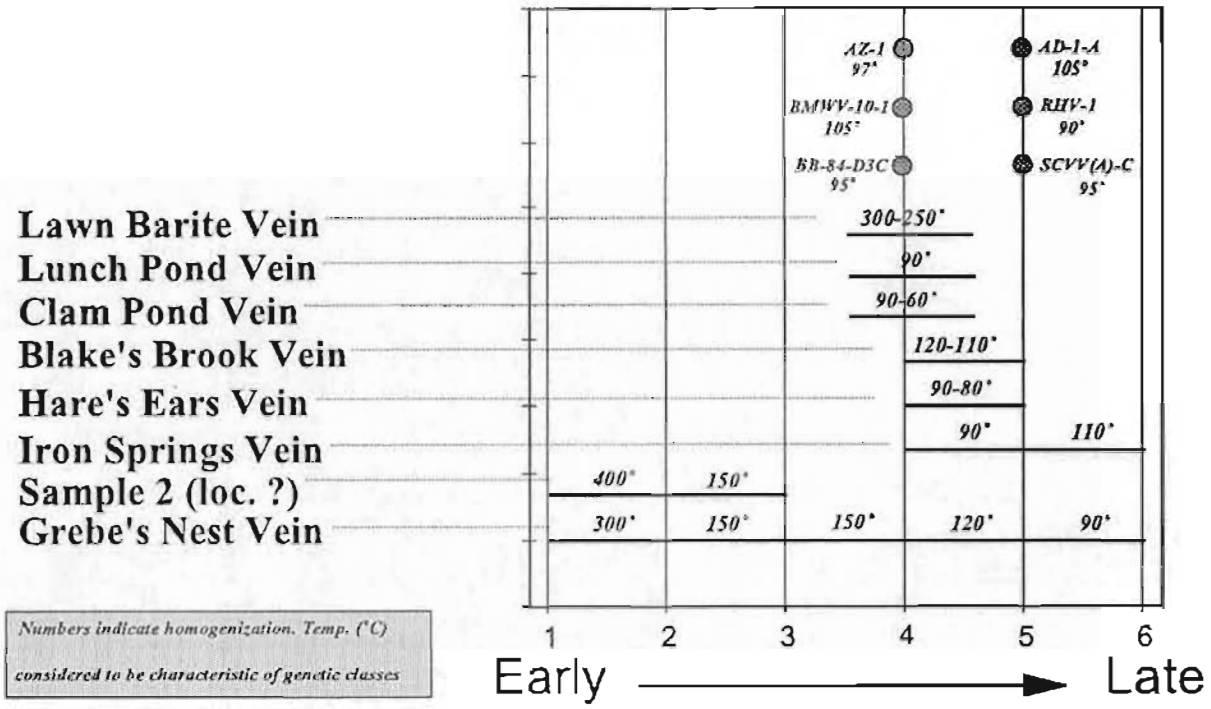

Figure 7.2.1 Paragenetic sequence suggested for various fluorite-bearing zones in samples from this study. The numbers 1-6 refer to genetic classes based on chondrite-normalized REE patterns. Temperatures refer to estimated temperatures of formation from fluid inclusion data.

statistical analyses of the geochemical data from the genetic classes are presented in detail in Appendix 3 and here summarized as tables of mean values. Table 7.3.1 gives a summary of all samples classified, while Table 7.3.2 gives a summary of all samples in which the major mineral phase is fluorite (i.e. > 75% CaF_2). From Table 7.3.,1 several conclusions can be made with regard to the proposed paragenetic sequence labelled 1 to 6. First, it is obvious that most of the co-genetic barite and quartz were deposited under fluid conditions characterized by mid-late stage fluorite (class 4). Secondly, although a significant amount of galena occurs with the barite, the bulk of the sphalerite and galena was deposited after the barite, under fluid conditions characterized by late-stage fluorite

(class 5). Chalcopyrite was also deposited under these conditions and is also found associated with very late-stage fluorite (i.e. ISV-1-G).

This is roughly consistent with the paragenetic sequence proposed by Van Alstine (1948), except that he concluded that most of the sulphides were deposited prior to the deposition of the barite. The co-genetic relationship between barite and galena is

Table 7.3.1 Average geochemical values for subdivisons of the data based on a genetic classification (classes 1 to 6) utilizing chondrite normalized REE patterns of the fluorite. This table includes all of the fluorite bearing-samples which characterize individual growth zones.

All St. Lawrence fluorite-bearing samples - genetic classes 1 to 6

	n = 5	n = 2	n = 10	n = 36	n = 17	n = 3
Genetic Class	1	2	3	4	5	6
Boric Acid Dissolution						
% undissolved	0.1363	NA	0.0931	46.2	1.11	0.835
% dissolved	99.9	NA	100.0	53.5	98.9	99.2
Calculated from XRF (wt.%)						
CaF_2(c)	104	103	103	21.5	93.1	100
$BaSO_4$(c)	0.021	0.001	0.010	22.4	0.165	0.086
SiO_2(c)	0.521	0.128	0.126	7.93	0.278	0.042
PbS(c)	0.011	0.001	0.076	3.73	7.91	0.007
ZnS(c)	0.011	0.001	0.003	0.188	1.85	0.001
$CaCl_2$(c)	0.001	0.001	0.001	0.005	0.037	0.028
Total	104	103	103	106	101	101
XRF Majors (wt.%)						
SiO_2	1.00	0.248	0.243	10.9	1.50	0.084
TiO_2	0.008	0.002	0.002	0.010	0.038	0.002
Al_2O_3	0.233	0.038	0.037	0.243	0.060	0.003
Fe_2O_3	0.118	0.031	0.046	0.220	0.902	0.248
MnO	0.003	0.001	0.001	0.020	0.008	0.003
MgO	0.01	0.01	0.01	0.01	0.01	0.01
CaO	74.6	35.0	71.5	51.6	67.2	72.5
Na_2O	0.032	0.003	0.005	0.035	0.112	0.007
K_2O	0.038	0.001	0.002	0.103	0.003	0.001
P_2O_5	0.003	0.001	0.003	0.008	0.031	0.002
LOI	1.00	0.638	0.623	5.26	0.15	0.560
XRF Traces (ppm)						
S	298	167	328	23196	6832	1156
Cl	122	33	185	142	123	51
Sc	39	42	12	83	42	30
V	4	3	4	4	4	4
Cr	13	7	10	150	31	3
Ni	2	2	2	21	16	2
Cu	19	14	41	152	1096	797
Zn	74	2	2	1262	12387	6
Ga	2	2	4	233	523	2
Rb	2.3	0.4	0.4	8.2	1.0	0.4
Sr	81	70	52	1277	74	24
Y	651	401	519	546	819	760
Zr	2.6	1.1	0.5	12	0.2	0.5
Nb	1.9	2.3	1.3	4.0	2.3	2.2
Ba	118	20	59	1315.76	937.1	906
Ce	210	103	68	34	26	16
Pb	113	93	672	32241	68813	57
Th	2	2	2	2	9	2
U	2	2	2	11	11	2

	n = 5	n = 2	n = 10	n = 36	n = 17	n = 3
	1	2	3	4	5	6
ICP-MS Traces (ppm)						
Li	1	0.2	0.3	4	0.8	0.3
Be	8	6	9	11	8	12
Sc	5	3	3	4	3	4
V	1	1	1	2	3	2
Cr	8	4	5	97	18	3
Cu	26	20	32	173	316	3.4
Zn	47	8	9	1945	608	5
Rb	1	0.1	0.1	11	0.4	0.1
Sr	89	70	53	720	73	39
Y	574	891	545	713	742	630
Zr	2	0.6	2	6	1	2
Nb	20	0.17	6.4	1.2	0.22	0.18
Mo	2.5	0.33	1.8	2.9	2.4	4.5
Cs	0.22	0.03	0.02	1.8	0.07	0.02
Ba	5	4	2	10788	423	43
Hf	0.2	0.1	0.3	0.3	0.1	0.2
Ta	8.6	0.14	5.8	0.73	0.29	0.08
Tl	0.07	0.03	0.27	0.86	2.3	0.05
Pb	60	23	665	4500	12009	28
Bi	0.76	0.76	0.35	3.1	3.3	0.45
Th	0.29	0.11	0.12	0.50	0.15	0.13
U	0.52	0.71	0.62	0.82	1.54	1.2
ICP-MS REE (ppm)						
La	46.5	28.9	16.5	13.9	8.03	0.630
Ce	148	79.1	36.6	37.5	21.2	2.04
Pr	25.9	12.8	5.06	5.22	3.25	0.308
Nd	126	67.2	24.1	24.0	16.8	2.50
Sm	27.9	19.9	6.96	10.6	9.23	3.15
Eu	7.64	2.84	1.04	1.12	0.876	0.253
Gd	35.2	34.3	12.8	23.2	20.6	13.1
Tb	4.51	6.13	2.79	4.92	4.75	4.21
Dy	24.7	40.9	22.6	37.5	35.9	34.1
Ho	4.57	8.66	5.64	8.59	8.33	7.59
Er	10.1	21.5	17.4	25.5	25.0	19.4
Tm	0.809	2.03	2.21	3.28	3.17	2.08
Yb	4.02	8.97	13.2	19.3	22.1	9.58
Lu	0.479	1.06	1.74	2.43	2.88	1.02
Total REE	472	334	169	219	182	100
ICP-MS Ratios						
Sm/Nd	1.172	1.156	0.192	1.146	1.152	1.284
Sm/Eu	2.412	2.450	2.450	NA	2.500	2.507
Th/La	0.139	0.179	0.174	0.257	0.341	0.356
Eu/Eu*	0.046	0.012	0.007	0.322	0.019	0.005

Values less than the limit of detection (LOD) are given as < (LOD).
Values < less than the limit of quantitation (LOQ) but greater than the LOD are given as the value in parenthesis.
Abbreviations: NA - not applicable, SD - standard deviation, Max. - maximum; Min. - minimum

Table 7.3.2 Average geochemical values for subdivisions of the data based on a genetic classification (classes 1 to 6) utilizing chondrite normalized REE patterns of the fluorite. This table includes only zones in which the fluorite component is greater than 75%.

St. Lawrence fluorite samples - genetic classes 1 to 6

	n = 5	n = 2	n = 10	n = 15	n = 14	n = 5
Genetic Class	1	2	3	4	5	6
Bor. Acid Dissolution						
% undissol.	0.100	NA	0.0[illegible]	[illegible]	1.11	0.855
% dissolved	99.9	NA	100.0	90.5	98.4	99.2
Calculated from XRF (wt.%)						
CaF2(c)	104	104	103	98.9	99.8	100
BaSO4(c)	0.025	0.003	0.010	0.980	0.193	0.060
SiO2(c)	0.321	0.128	0.126	1.71	0.350	0.042
PbS(c)	0.013	0.007	0.078	0.126	0.651	0.003
ZnS(c)	0.011	0.000	0.000	0.002	0.139	0.001
CuFeS2(c)	0.001	0.000	0.001	0.001	0.013	0.028
Total	104	104	103	102	101	101
XRF Majors (wt.%)						
SiO2	1.00	0.248	0.243	3.40	0.676	0.080
TiO2	0.008	0.002	0.002	0.004	0.004	0.002
Al2O3	0.233	0.018	0.037	0.123	0.066	0.004
Fe2O3	0.115	0.011	0.946	0.303	1.02	0.248
MnO	0.005	0.003	0.003	0.008	0.010	0.003
MgO	0.01	0.01	0.01	0.01	0.01	0.01
CaO	74.8	75.0	74.5	71.4	72.0	72.5
Na2O	0.052	0.003	0.055	0.035	0.014	0.007
K2O	0.045	0.001	0.008	0.046	0.009	0.001
P2O5	0.005	0.004	0.005	0.036	0.011	0.002
LOI	1.07	0.645	0.625	1.03	1.15	0.540
XRF Traces (ppm)						
S	298	107	320	1707	1660	1156
Cl	164	33	185	262	105	31
Sc	29	42	42	37	30	30
V	4	4	4	4	4	4
Cr	14	6	10	32	20	5
Ni	2	2	2	6	4	2
Cu	19	14	31	98	325	797
Zn	24	2	2	12	951	6
Ga	2	2	4	4	25	2
Rb	2.3	0.4	0.4	3.8	1.1	0.4
Sr	81	80	52	154	72	24
Y	643	911	549	812	876	201
Zr	2.8	1.1	0.6	6	0.7	0.5
Nb	1.9	2.3	1.3	2.6	1.6	2.2
Ba	135	20	59	5180	1134	506
Ce	210	163	68	46	30	16
Pb	115	30	672	1069	5608	57
Th	2	2	2	2	4	2
U	2	2	2	2	3	2

	n = 5	n = 2	n = 10	n = 15	n = 14	n = 5
	1	2	3	4	5	6
ICP-MS Traces (ppm)						
Li	1	0.2	0.3	2	0.8	0.3
Be	8	6	9	7	9	12
Sc	5	1	1	3	3	4
V	1	1	1	2	3	2
Cr	8	4	5	10	3	3
Cu	26	20	32	79	123	3.4
Zn	41	8	9	19	222	5
Rb	1	0.3	0.1	3	0.5	0.1
Sr	89	85	33	116	81	90
Y	574	891	545	824	810	230
Zr	2	0.6	2	2	1	2
Nb	20	0.17	6.4	0.40	0.20	0.18
Mo	2.3	0.17	1.8	3.4	2.2	4.5
Cs	0.22	0.03	0.02	0.18	0.08	0.02
Ba	5	4	2	1928	314	41
Hf	0.2	0.1	0.1	0.2	0.1	0.2
Ta	8.6	0.13	5.8	0.30	0.27	0.08
Tl	0.07	0.03	0.27	0.24	1.1	0.05
Pb	60	23	665	6170	4166	28
Bi	0.76	0.76	0.35	1.0	2.9	0.45
Th	0.29	0.31	0.12	0.29	0.10	0.13
U	0.52	0.71	0.62	0.78	1.8	1.2
ICP-MS REE (ppm)						
La	36.5	28.9	16.5	12.8	8.53	0.630
Ce	138	79.1	34.6	40.0	22.5	2.04
Pr	25.9	12.8	5.06	4.04	3.47	0.388
Nd	136	67.2	24.1	18.7	18.0	2.40
Sm	27.9	19.9	6.46	8.96	9.91	3.13
Eu	3.63	2.84	1.04	0.706	0.962	0.253
Gd	35.2	41.3	12.8	19.8	22.2	15.1
Tb	4.51	6.13	2.79	4.93	5.10	4.21
Dy	24.7	40.9	22.6	39.8	38.4	34.1
Ho	4.57	8.76	5.64	9.37	8.88	7.39
Er	10.1	21.5	17.4	28.6	26.5	19.4
Tm	0.940	2.03	2.21	3.70	3.54	2.08
Yb	4.07	8.97	14.2	22.3	27.9	9.58
Lu	0.479	1.46	1.74	2.79	2.98	1.02
Σ(REE)	462	334	169	207	194	100
ICP-MS Ratios						
Sm(N)/Sm(N)	1.172	1.156	1.182	1.095	1.192	1.284
Sm(N)/Sm(N)	2.412	2.450	2.459	2.256	2.436	2.503
La(N)/Sm(N)/Nd	0.153	0.179	0.174	0.256	0.343	0.756
(Tb/Ho)(N)	0.046	0.042	0.037	0.113	0.030	0.005

Values less than the limit of detection (LOD) are given as < (LOD).
Values less than the limit of quantitation (LOQ) but greater than the LOD are given as the value in parenthesis.
Abbreviations: NA - not applicable; SD - standard deviation; Max. - maximum, Min. - minimum

evidenced in the Lawn Barite Vein, Big Meadow Woods Vein , Anchor Drogue Vein and others. It is suggested that Van Alstine's (1948) sequence may have been highly influenced by the high grade veins within the St. Lawrence mine area which were actively mined during the period of his study. The present study suggests that these veins

were formed late in the overall mineralizing event, as defined by the fluid inclusion and REE data, therefore seemingly early-stage mineralization noted in these veins are not necessarily 'early-stage' in terms of the overall system.

Comparing classes 4 and 5 in Tables 7.3.1 and 7.3.2, it is apparent that most of the anomalous trace element variations can be accounted for by the presence of associated sulphate or sulphide phases. This is particularly true of such elements as Ba and Sr which are common in barite and Pb, Zn, Cu and Ga which are intimately associated with the sulphide phases. The anomalously high average Nb and Ta, in classes 1 and 3, result from the contribution of one sample (Sample 2), which contains anomalously higher concentrations of these elements than any of the other samples in the study.

Since the classification scheme is based on REE distributions, the REE show much more consistency than shown by the subdivision based on mineralogy presented in Chapter 6. Other elements (such as Sr) in fluorite show a much more systematic behaviour based in terms of this subdivision. The REE themselves reflect the systematic change from LREE domination to HREE domination on which the classification is based. Other, non-induced but significant characteristics of the REE distributions are: 1) the steady decrease in Nd_N/Sm_N ratio from class 1 to 6 (figure 7.3.1); and 2) the 2-fold nature of total-REE decrease, from classes 1 to 3 and from 4 to 6 (figure 7.3.2). Table 7.3.2 shows that these trends are preserved, even when a significant number of the samples from zones containing accessory phases are discarded. The 2-fold cyclic nature of fluid behaviour in the system has been noted in the Grebes Nest Vein as indicated by fluid inclusion data (Collins, 1984; Collins and Strong, 1988).

Such decreases, followed by subsequent increases, in total-REE content have been attributed to recharge of the system by subsequent pulses of magmatic fluid (Strong et al., 1984). This is consistent with the framework proposed here, where periodic recharge, sometimes explosive, can affect the total REE concentration of the fluid, and consequently the REE concentration of the fluorite. However, the overall distribution of REE in the fluorite appears to be governed by factors which evolve continuously through the life of the hydrothermal system. The above observations (REE in fluorite) essentially outline the **'effect'**, therefore the next item to be addressed is the **'cause'**. In broad terms, such systematic REE behaviour must be related to either the systematic changes in LREE/HREE ratios in the evolving fluid or systematic changes in the content of other

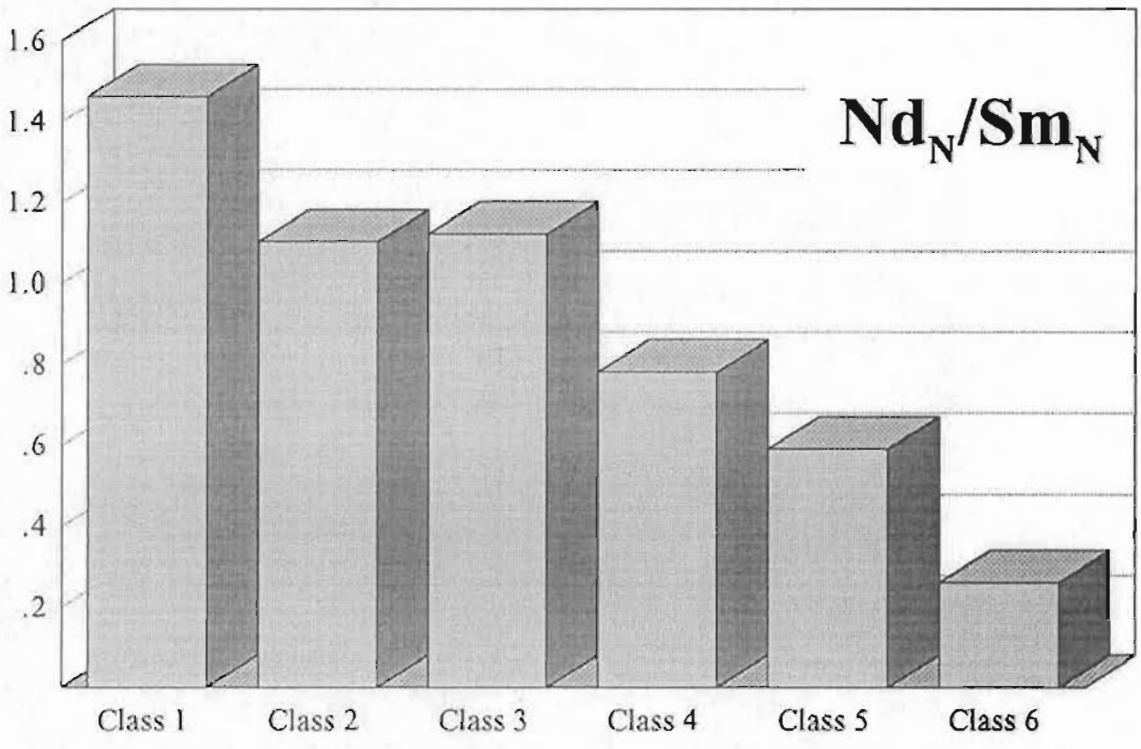

Figure 7.3.1 Schematic histogram showing the trend of Nd_N/Sm_N ratios throughout the genetic cycle 1 to 6, defined by the chondrite normalized REE distribution in fluorite.

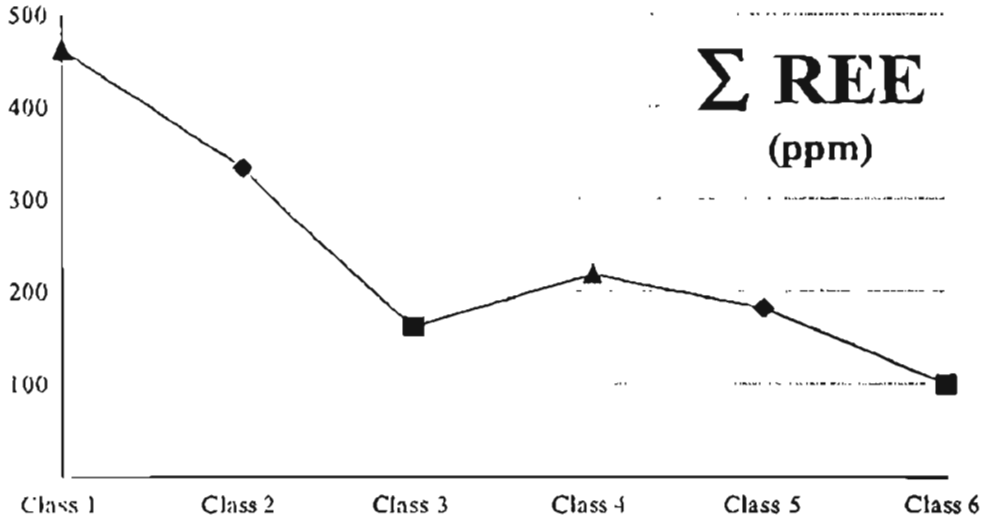

Figure 7.3.2 Graph showing decline in total-REE content (ppm) throughout successive genetic classes as defined by chondrite normalized REE patterns in fluorite.

elements (volatiles) in the evolving fluid which dramatically and systematically alter the concentration of REE ions which are available for co-precipitation with fluorite.

7.4 Application of Tb/Ca - Tb/La Abundance Ratios

Using a compilation of REE data for fluorite from a wide range of mineralizing environments, Schneider et al. (1975,1977) and Möller et al. (1976) suggested the use of Tb/Ca and Tb/La atomic abundance ratios as genetic indicators in fluorite. The Tb/Ca ratio is interpreted to reflect the chemical environment from which the fluorite was generated while the Tb/La ratio is related to the degree of fractionation during the mineralizing process. Möller et al. (1976) noted that the chondrite-normalized REE distributions in hydrothermal fluorite druse, from a mine in Germany, could be roughly characterized by:

A preferential concentration of the LREE in early crystallizing fluorite;

B relatively flat (chondritic) REE compositions in the intermediate stages of crystallization;

C preferential concentration of the HREE in late-stage fluorite mineralization.

This 3-fold characterization of chondrite-normalized REE distributions in German fluorites is similar to the overall REE evolution in the St. Lawrence fluorite. Möller et al. (1976) attribute such REE differentiation to two intimately associated geochemical processes:

1 complexation of REE in the ore-forming solutions

2 co-precipitation (in fluorite) in which only free (non-complexed) REE ions are incorporated into the crystal lattice of the mineral

Möller et al. (1976) suggested using a plot of Tb/Ca versus Tb/La as a synoptical representation to help classify fluorite into genetic groups. Using more than 150 samples from a wide variety of fluorspar deposits, they were able to define three fields on the plot, each of which represents a particular type of geochemical process. These fields were genetically classified based on the petrogenetic environments of the deposits concerned. These fields are defined as:

- **Pegmatitic (pneumatolytic)** characterized by higher Tb/Ca ratios for a given Tb/La ratio reflecting the higher total-REE contents of late-stage felsic differentiates
- **Hydrothermal** characterized by intermediate Tb/Ca ratios which increase with increasing Tb/La
- **Sedimentary** characterized by lower Tb/Ca ratios suggesting equilibrium with depleted "sedimentary-type" reservoirs

The fluorite samples from the St. Lawrence deposits were plotted on the Tb/Ca versus Tb/La diagram (figure 7.4.1) and sub-divided on the basis of assigned genetic

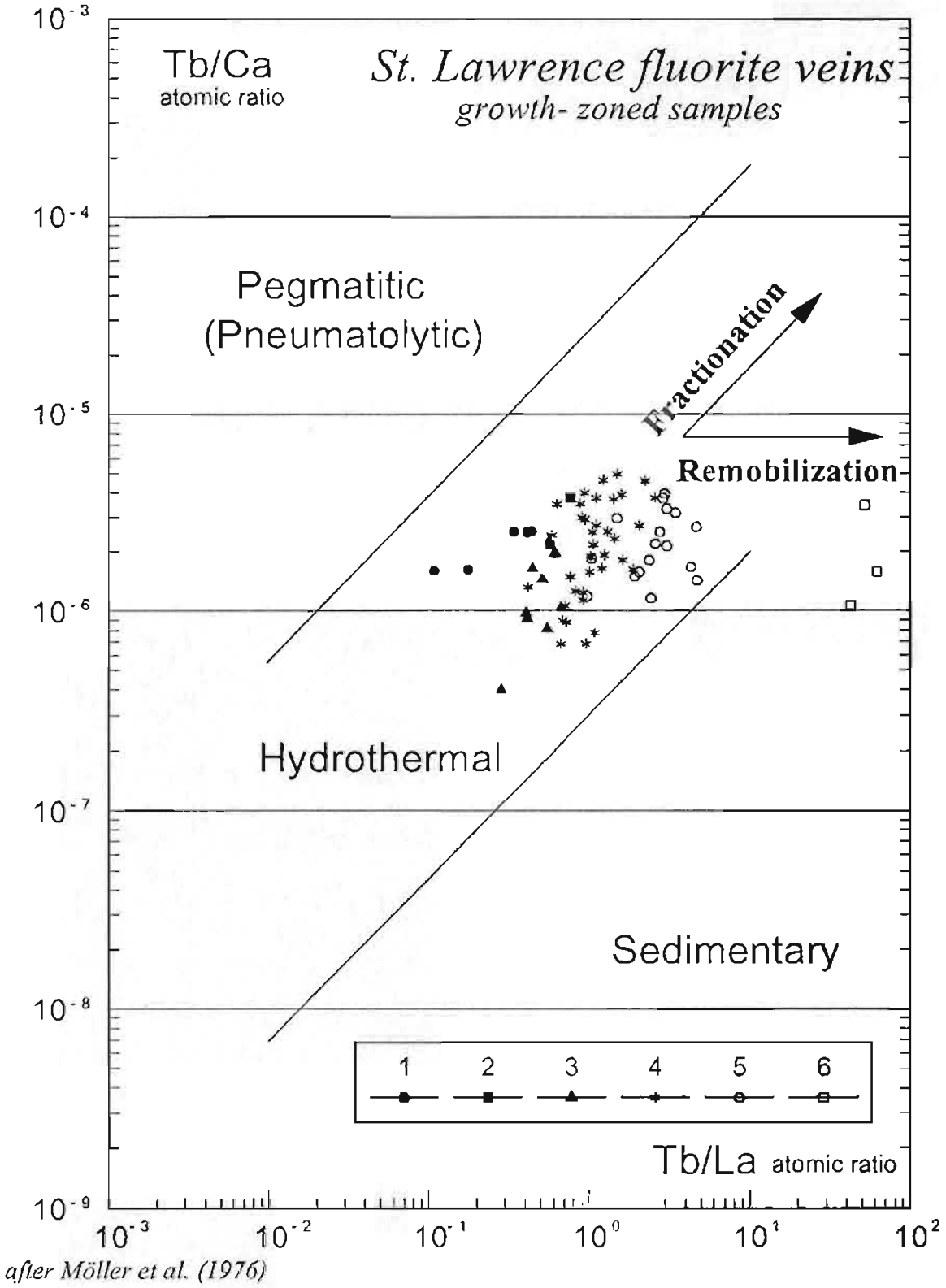

Figure 7.4.1 Plot of St. Lawrence fluorite samples on the Tb/Ca - Tb/La genetic discrimination diagram of Möller et al. (1976). The symbols represent the genetic classes (numbers) assigned to the fluorite samples based on their chondrite normalized REE patterns (section 7.1).

classes (section 7.1). Since Ca was not quantitatively analyzed for these samples, stoichiometric Ca (CaF_2) was assumed in calculating the Tb/Ca ratios. The diagram includes the trends (arrows) proposed by Möller et al. (1976) to represent 'normal' fractionation, with precipitation, and remobilization of previously precipitated fluorite. All the St. Lawrence fluorite samples, with the exception of the very late-stage fluorite, plot within the hydrothermal field. From this diagram it is apparent that the proposed classification scheme, based on the chondrite normalized plots is reflected in this diagram. From the earlier (1) to later (5) stages of mineralization the groups display a tendency to migrate along a trend parallel to the remobilization trend of Möller et al. (1976). The very-late stage samples are dramatically offset from the main group along this trend. It is apparent that samples within each individual group roughly follow the fractionation trend, whereas, between groups the trend roughly parallels that of the remobilization trend. Although remobilization may have been involved in the formation of the very late-stage fluorite, it is difficult to envisage such processes being dominant throughout the bulk of the mineralizing process. Therefore, there is a need to consider other potential explanations for the non-conformable but systematic trends displayed by the REE in the St. Lawrence fluorite.

8 Fluid Evolution and Fluorspar Deposition

8.1 Initial Magmatic Fluid

In summary, the St. Lawrence Granite is a relatively homogeneous pink, coarse grained, equigranular to megacrystic, high-silica, alkaline to peralkaline, granite. The apparent homogeneity of the granite may be partly due to limited sampling of the roof of the pluton, since the granite, showing little change in orientation since emplacement, is only exposed to shallow erosional levels. Geochemical, petrogenetic and field relationships indicate that the granite was emplaced to shallow levels (< 1 km) as a hot (> 800°C), relatively dry (< 2% H_2O), water-undersaturated, high-silica melt. Such granites are usually characterized by a protracted crystallization history (Whitney, 1988). Aplite and porphyry dykes, embayed and rounded quartz phenocrysts, and volcanic equivalents (Strong et al., 1978), suggests isothermal decompression in the water-vapour-undersaturated region, resulting from periodic venting to the surface or near-surface region.

From experimental studies, Whitney (1988) concluded that, for an alkaline granite composition similar to the St. Lawrence Granite (Cape Ann), if only 2% water is present (at 2 kb pressure), 75% of the melt would crystallize (between 720 and 685°C) before

vapour saturation is achieved. Following vapour saturation, the remaining melt would crystallize within 10°C as vapour is evolved (between 685 and 675°C). Since the pluton would cool and crystallize from the top and margins inward, this final vapour-saturated melt would be located within the core of the pluton. The closest equivalents of this late-stage melt, in the St. Lawrence Granite, are the aplitic and porphyritic dykes which cut the coarse grained 'roof-zone' granite.

Granitic magmas which initially have low water contents, but become water saturated as result of a high degree of crystallization, exhibit greater enrichments in F, and consequently, larger values for D_F (vapour/melt) at water saturation relative to magmas that contain high initial water contents (Webster, 1990). Webster and Holloway (1989) have shown that high-silica granite/rhyolite magmas may achieve extreme enrichments in F prior to fluid saturation. They calculate that, during the end stages of crystallization of a topaz rhyolite magma, initially containing 1 wt% F, the F concentration of the residual melt exceeds 10 wt% with as much as 10 wt% of the melt remaining. Using this analogy, the St. Lawrence Granite magma, which averages approximately 0.12 wt% F (where exposed), could be expected to achieve F concentrations to near 1 to 2 wt% at or near vapour saturation.

Experimental studies (Webster and Holloway, 1989) indicate that (at 2 kb and 800°C), in granitic melts containing < 7 wt% F, Cl partitions in favour of the fluid phase and F partitions strongly in favour of the melt. In granitic melts that contain ≥ 7 wt% F, Cl partitions in favour of the melt and F partitions in favour of the aqueous fluid (Webster and Holloway, 1989). They also concluded that F partitioning is relatively independent of Cl concentrations of either the fluid or the melt. This model suggests that,

unless F is more highly concentrated in the 'late-stage' granitic melt, the fluid evolved from the St. Lawrence Granite should be initially Cl dominated. With progressive crystallization and vapour evolution, the melt would become increasingly enriched in F, resulting in F dominance in extremely 'late-stage' fluids.

In response to lower water solubility in shallow levels of the crust (< 1000 bars), the melt may become progressively enriched in chlorine as vapour evolution proceeds (Candela, 1989). This results in dramatically different behaviour of Cl and Cl-complexed elements between low and high pressure regimes. In modelling Cl behaviour in magmatic vapour evolution, Candela (1989) demonstrated that, at depths of greater than 3-4 km, the concentration of Cl in the melt and the associated vapour phase display a monotonic decrease with progressive vapour evolution, as opposed to the same process at depths less than 3-4 km (shallow levels), in which increased Cl in the melt results in a gradual enrichment in Cl through most of the vapour evolution, with extreme Cl enrichment in 'late-stage' fluid.

The above results in a parabolic increase in Cl-complexed cations, including Cu, Pb and Zn, with progressive vapour evolution The "melt-compatible" elements like F, B and Mo are progressively enriched in both melt and vapour. This behaviour is schematically displayed in figure 8.1.1. Both F and Cl will become increasingly enriched in the melt and the fluid as vapour evolution proceeds (i.e. successive aliquots) and will be especially enriched in the 'late-stage' fluids. This indicates that Cu and other Cl-complexed cations will show marked changes in concentrations in 'late-stage' fluids, displaying extreme enrichment followed by extreme depletion. This is a result of the increasing Cl content of the fluid which causes increasing the 'effective partition

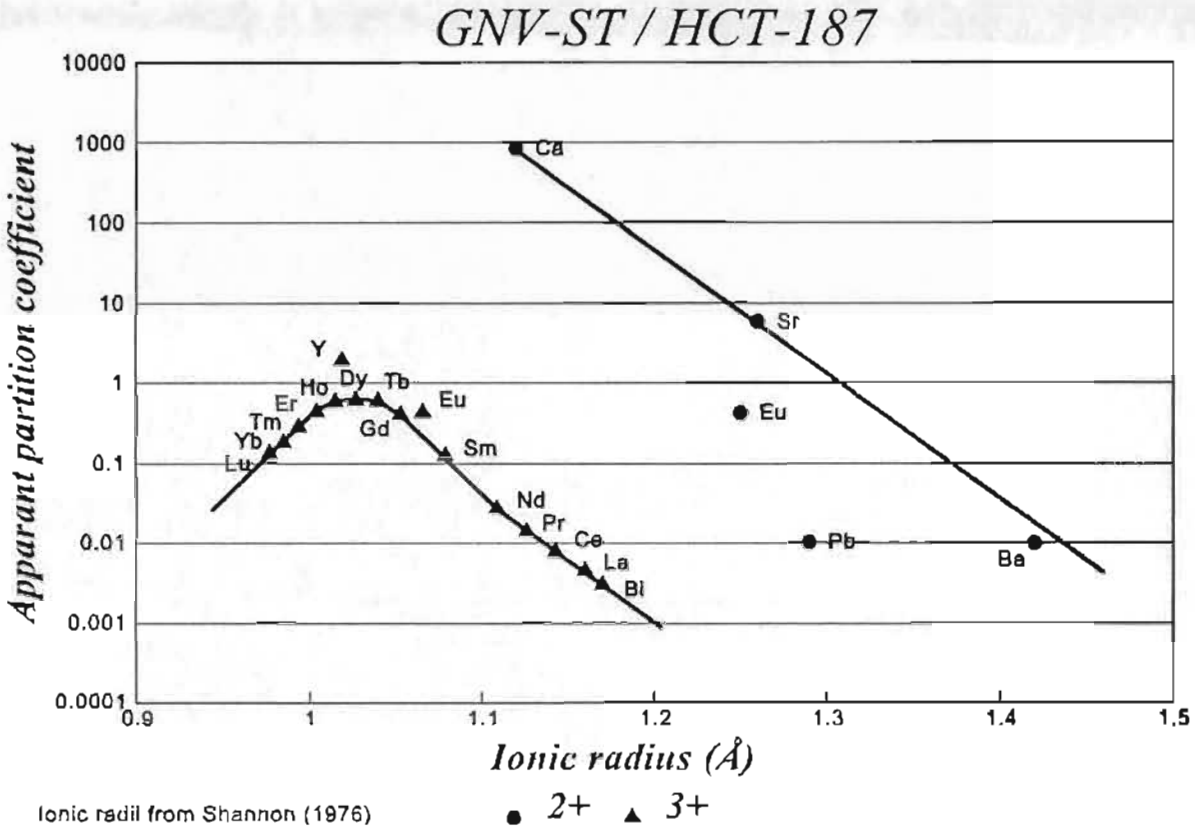

Figure 8.4.1 Plot of REE and selected element concentrations, normalized to St. Lawrence Granite model fluid composition, for fluorite sample GNV-ST, from the Grebe's Nest Vein. The diagram shows the relationship between apparent partition coefficient versus the ionic radius of the elements.

- the bulk of the mineralizing fluid in the system was originally evolved from the late-stage granite and if there was a meteoric component, it did not significantly change the REE balance of the fluid.
- the concentration of F in the fluid was reduced much more rapidly than the REE concentration due to fluorite precipitation.
- the late-stage fluorite was precipitated from a fluid with a much lower F activity, in which most of the REE fluoro-complexes would have decomposed and, therefore, it should be dominated by free-ion REE species and most closely reflect true fluorite/fluid partitioning relationships.

The apparent partition coefficients calculated from sample GNV-ST (figure 8.4.1) show a parabolic trend, for the trivalent elements, reminiscent of the type of partition relationships observed in crystal-melt studies (Onuma et al., 1968; Matsui et al., 1977).

is consistent with the continuous precipitation of fluorite throughout a wide range of fluid salinities in the St. Lawrence veins. The interpretation of the Cl systematics must take into account the fluid modification caused by boiling, separation of low salinity vapour and subsequent fluid mixing, within the conduit system, after initial vapour evolution. Whether related to decreased water solubility (Candela, 1989) or increased F content in the melt (Webster and Holloway, 1989) it would appear that both F and Cl should be enriched in 'late-stage' magmatic fluids. The concentration of F, and consequently Cl, in the 'early-stage' magmatic fluid depends on how effectively F was concentrated in the residual magma, prior to vapour saturation. Crystallization of F-bearing mineral phases prior to vapour saturation could reduce the F content of the residual melt, and consequently evolving an 'early-stage' fluid with lower F and higher Cl concentrations.

8.2 Partitioning of Trace Elements in Fluorite

The fluorite crystal structure consists of a calcium ion enclosed within a cube of fluorine anions, each of which is, in turn, coordinated tetrahedrally by four calcium ions (Jaffe, 1988). Therefore, the Ca^{2+} ions are in eight-fold coordination and the F^- ions are in four-fold coordination and their bonding is highly ionic. The REE and Y commonly replace Ca in the fluorite structure and their concentrations are influenced by the environment of formation (Fleischer, 1969). The degree of substitution of REE in fluorite is directly related to the concentration of uncomplexed REE^{3+} ions in the solution and the ionic radius of the substituting REE ion (Möller, 1983; Möller and Morteani, 1983).

The relationship between partition coefficients and ionic radius is well established for mineral/melt systems using crystal/melt relations. Onuma et al. (1968) presented plots of partition coefficients versus ionic radius for pyroxene phenocrysts from alkaline olivine basalts. They demonstrated that substitution of trace elements in crystal lattice sites is the main mechanism for trace element partitioning. These plots show parabolic curves with well defined peaks at or near the ionic radius of the major cation. The curves for individual valence states are roughly parallel, with the valence state of the major cation showing the strongest partitioning. They proposed the following relationship, based on the "isotropic elastic model of ionic crystals", proposed by Nagasawa (1966):

$$\ln D_q = A(r_n - r_0)^2 + B.$$

where D_q is the partition coefficient of the element; r_n and r_0 are the ionic radii of the trace element and the most favourable site size, respectively; A is a constant related to the elastic constants of the crystal and B is a constant introduced by the charge balance. With the refinement of more consistent values of ionic radius (Shannon, 1976) and improved trace element analytical techniques, these relationships were even more substantiated. Möller (1988) suggested the use of ionic volumes (i.e. r^3) and thermodynamic relations to better define the relationship between ionic radius and crystal-melt partitioning.

In a study of coprecipitation of radium and barium sulphates, Doerner and Hoskins (1925) conclude that the instantaneous trace/major ion ratio at the surface of a growing crystal is proportional to the ratio in the solution, reflecting the instantaneous distribution coefficient. If the instantaneous distribution coefficient is greater than unity, the trace component is enriched in the crystal and the crystal has the highest trace concentration at the centre. If it is less than unity, the trace component is enriched in the

solution and the crystal has the highest trace concentrations at the rim. The overall distribution between the mineral and solution can then be represented by the logarithmic distribution law such that:

$$\log (\text{final}/\text{initial})_{\text{tracer}} = \lambda \log (\text{final}/\text{initial})_{\text{carrier}}$$

where λ is the logarithmic distribution coefficient (constant for a given system), final and initial refer to concentrations in the solution and tracer and carrier refer to the trace cation and major cation, in the crystal, respectively (Doerner and Hoskins, 1925).

Matsui (1966) studied the coprecipitation of REE with calcium oxalate, showing that the distribution coefficients of the REE increased systematically from Ce to Lu, suggesting that ionic radius plays an important role in the process. He also recognized that the distribution coefficients of the REE increase with decreasing pH, but still follow the logarithmic law, and are relatively independent of ionic concentration.

In a study of the coprecipitation of the REE with synthesized calcite and aragonite, Terakado and Masuda (1988) concluded that the varying patterns of apparent partition coefficients is highly dependant on concentration levels of the REE in the solutions. They relate the extreme variance in partitioning to the strong control of REE-complexes and that crystal structure and ionic radius control is not a major factor. This extreme variation may have resulted from the effects of changing pH within the experiments, which range from ~6.3 at the beginning to ~(7.5 - 8.5) at the end, but the pH of the experiments are not reported individually. This pH range crosses the REE-carbonate complex dominance field of Wood (1990a, p. 177, fig. 15D) for 25°, who demonstrates (using Eu) that at a pH near 6 the dominant REE species changes from the free-ion to REE-carbonate complexed ions and by pH 7 the REE in the system would be

almost entirely carbonate complexed. The results of the short duration experiment (Fig. 1c [C3]) of Terakado and Masuda (1988) may best represent the partitioning of REE into calcite from weakly complexed solutions. This trend is parabolic, with a maximum at Sm, and suggestive of strong crystal structure and ionic radius control. It appears that the apparent partition coefficients in ionic (and other) crystals in natural systems is a function of the 'free-ion' concentration in the solution, which, itself, is a function of the 'bulk' chemical composition of the fluid and the physical conditions at the site of deposition.

There is no experimental work relating to the partitioning of elements between fluorite and solutions. In a study of the REE in natural barite, Guichard et al. (1979), attributes the observed REE distributions to crystallographic constraints on REE substitution, and to the complexing of REE in the mineralizing solutions. Morgan and Wandless (1980) studied REE distributions in natural barite, anhydrite, siderite and galena, concluding that, "...although complex formation may have an influence on the absolute values of partition coefficients, the relative REE pattern in a simple hydrothermal mineral is governed largely by the ionic radius of the major cation.".

The results of early work on the distribution of REE in fluorite and calcite, from a variety of European and Asian deposits, are extensively reviewed and interpreted in a paper by Möller and Morteani (1983). They concluded that "...the resulting fractionation of REE, as observed in fluorite and calcite, is the summation of REE shifts in all geochemical processes which are involved in the formation of the minerals; e.g. the generation of the solutions, the interaction of these solutions with the country rocks and crystallization from the altered solutions. Furthermore, remobilization and alterations of the minerals will add to the fractionation...". They attribute most of the fractionation

observed in fluorite and calcite to the effects of REE complexes, especially fluro-complexes. Using relationships documented in the Ca-REE-oxalate system (Matsui, 1966), Möller (1985) concluded that only uncomplexed REE^{3+} ions need to be considered in REE coprecipitation with Ca-minerals.

In considering precipitation of fluorite from a given volume (closed-system) of super-saturated solution, Möller and Morteani (1983) suggested that there would be more LREE available as free-ions, since the complex stabilities of the REE fluro-complexes increase from La to Lu, leading to the formation of LREE enriched fluorite at the beginning of precipitation. The continuous precipitation of fluorite results in an impoverishment in F^- ions in solution, causing the REE fluro-complexes to decompose, leading to more HREE available for coprecipitation and consequently HREE enriched fluorite in the final stages of precipitation. Möller and Morteani (1983) suggested that these results can be transferred to dynamic (open) hydrothermal systems where these early and late stage relationships relate to a given volume of fluid and can, therefore, be modified by factors such as periodic recharge and flow rate. They indicated that high degrees of fractionation of the REE in fluorite is characteristic of crystallization from a less productive hydrotherm (slow flow rate) and lesser degrees of fractionation are characteristic of crystallization from a more productive hydrotherm (fast flow rate). This relationship formed the basis of the Tb/Ca vs. Tb/La genetic discrimination diagram presented in Chapter 7 (fig. 7.4.1). These models provide a means of predicting the availability of REE ions in solution, which would be available for coprecipitation, but do not address the effects of crystal structure and ionic radius on the incorporation of the REE in fluorite and calcite.

8.3 REE Complexing in F-bearing Solutions

The stability constants of the low-temperature REE complexes have been determined experimentally by a number of workers and recently reviewed by Wood (1990a,b) who used the experimental results of Walker and Choppin (1967) to theoretically predict the stability of REE complexes in hydrothermal solutions to 350°C at saturation water vapor pressure. All studies conclude that the stability constants of REE fluoro-complexes increase from La to Lu but with some disagreement as to the nature of this increasing trend. The experimental results of Walker and Choppin (1967) suggest a monotonic increase in stability constants for REE monofluoro and difluoro complexes from La to Lu. Other studies (Bilal et al., 1979; Bilal and Becker, 1979; Bilal and Kaß, 1980) suggest a sygmoidal shaped trend for the REE monofluoro stability constants, which increase from La to Lu, with a maximum at Tb and local minima at Ce and Yb. They suggest a monotonic increase from La to Lu for the REE difluoro complexes. Bilal et al. (1979) conclude that REE monofluoro complexes will predominate at lower fluoride activities (up to 10^{-4} M) and with increasing fluoride activity (above 10^{-3} M) REE difluoro complexes will predominate. Bilal and Becker (1979) examined the stability of REE fluoro-complexes at various ionic strengths (I = 0.1, 0.5, 1.0 and 3.0 M) using a NaCl aqueous medium (at pH=3.6 and T=25°C), concluding that the highest degree of REE fractionation typical for fluorite is obtained if the salinity of the mineralization milieu was nearly corresponding to the ionic strength of I=0.5 M (5.85 eq. wt.% NaCl). Both the experimental results of Bilal and Langer (1987) and the theoretically determined results of Wood (1990b) attest to a dramatic increase in the stability of REE-fluoride complexes with increasing temperature up to 350°C.

In order to gain a deeper insight into the competition of the various complexes for trivalent REE in hydrothermal solutions, Wood (1990b) carried out equilibrium calculations at 100°C using Eu^{3+} as the representative for all the REE, owing to the completeness of the data set for that ion. He suggests that at higher fluoride concentration (10^{-3} M), the speciation is dominated by fluoride complexing over the entire pH region; at lower fluoride concentration (10^{-4} M), fluoride complexes predominate in the near-neutral region but chloride and carbonate complexes become important under relatively acidic and basic conditions, respectively; and at higher temperatures (>200°C), fluoride complexes predominate over other complexes throughout the entire pH range. The free fluoride activity of a hydrothermal fluid at 300°C in the presence of fluorite would be in the range 10^{-5} to 10^{-2} M (Wood, 1990b), and, at such fluoride activities and temperatures, fluoride complexes should predominate over all others in the pH range two to three units of acidic from neutral. Based on the predicted high fluorine activity in the St. Lawrence fluids, it appears that fluoro-complexes would be dominant throughout most of the precipitation history of the system.

8.4 Apparent Partitioning of REE in St. Lawrence Fluorites

In a study of REE distribution in hydrothermal minerals, Morgan and Wandless (1980) suggested that normalizing REE abundances to compositions that more closely resemble the hydrothermal fluids from which they were formed could provide more insight into apparent partition coefficients. In minerals from continental deposits, for example, they suggested normalizing to average REE abundances in continental igneous rocks and relating these values to atomic radius. From this type of plot, they suggested

that the relative REE patterns in hydrothermal minerals are strongly influenced by the respective sizes of major and trace cations.

To evaluate the influence of crystal structure and solution complexing in the St. Lawrence fluorites, the REE distributions from selected samples were normalized to a modified St. Lawrence Granite composition (HCT-187) and plotted versus ionic radius, along with Ca and other elements such as Y, Sr, Pb, Ba and Bi, which could substitute for Ca in fluorite. Weight proportions were converted to atomic proportions to better approximate the total number of trace ions replacing Ca ions in the fluorite lattice. The plots are based on the following assumptions:

- sample HCT-187 is a granitic porphyry dyke, interpreted to be latest (and least altered) granitic phase represented in samples from the St Lawrence area that has a complete set of reliable major and trace element data available. This composition should most closely approximate the composition of the late-stage granite melt from which the fluid evolved.
- the predicted composition of the fluid was calculated from the granite composition (HCT-187) using the vapour/melt partition coefficients (F-rich vapour) of Flynn and Burnham (1978) for the REE (~0.2). Since there is little data available on partitioning of other elements between a melt and fluorine-rich fluids, and Keppler and Wyllie (1991) indicate that the solubility of silicate components in an aqueous fluid can be very high in a fluorine-rich melt-fluid system, and the partition coefficient of Cu (a common Cl-complexed species) between a F-rich fluid and a haplogranite melt is in the order of 1-3 (2 kb, 750°C), the other elements (Ca, Sr and Ba) were assigned a partition coefficient of 1. The other element, which can have a 3+ valence state, Bi, was assigned the same partition coefficient as the REE.
- the normalized Ca value is calculated based on stoichiometric Ca contents of the fluorite.

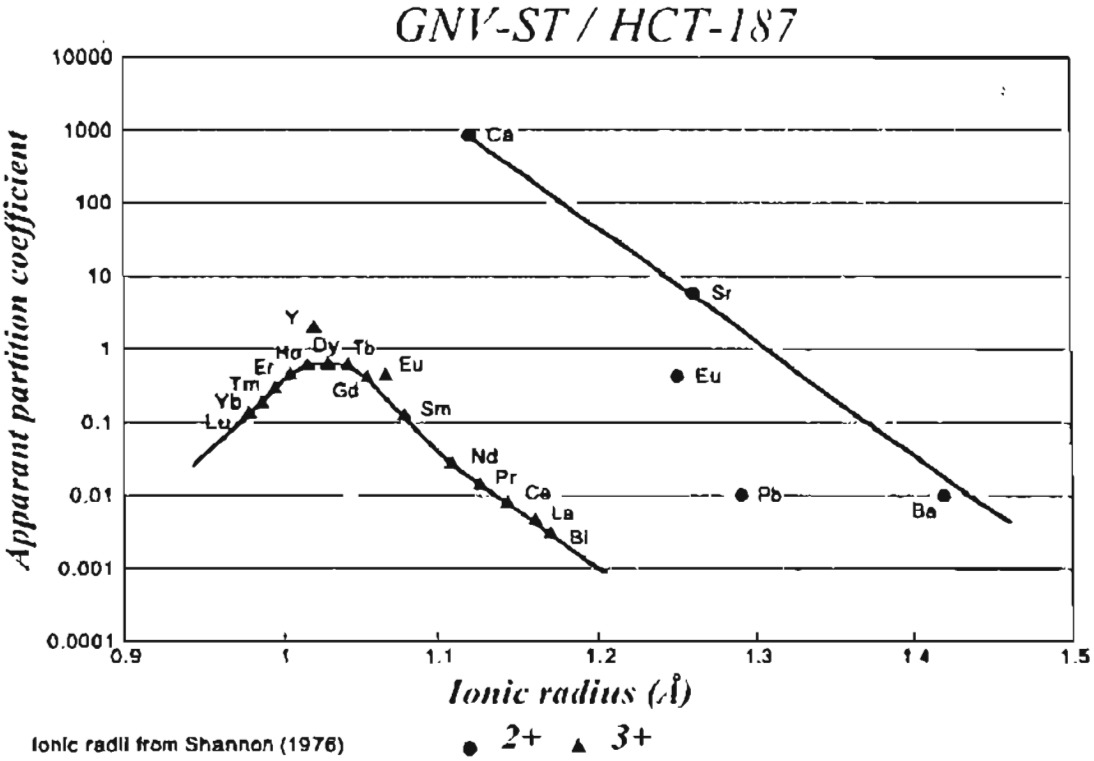

Figure 8.4.1 Plot of REE and selected element concentrations, normalized to St. Lawrence Granite model fluid composition, for fluorite sample GNV-ST, from the Grebe's Nest Vein. The diagram shows the relationship between apparent partition coefficient versus the ionic radius of the elements.

- the bulk of the mineralizing fluid in the system was originally evolved from the late-stage granite and if there was a meteoric component, it did not significantly change the REE balance of the fluid.
- the concentration of F in the fluid was reduced much more rapidly than the REE concentration due to fluorite precipitation.
- the late-stage fluorite was precipitated from a fluid with a much lower F activity, in which most of the REE fluoro-complexes would have decomposed and, therefore, it should be dominated by free-ion REE species and most closely reflect true fluorite/fluid partitioning relationships.

The apparent partition coefficients calculated from sample GNV-ST (figure 8.4.1) show a parabolic trend, for the trivalent elements, reminiscent of the type of partition relationships observed in crystal-melt studies (Onuma et al., 1968; Matsui et al., 1977).

This fluorite sample is a coarse grained fluorite displaying well developed crystal form (octahedral) with multiple small scale growth steps reflecting slow growth during late-stages of fluorite deposition. This fluorite is interpreted to have formed from a fluid in which the REE fluoro-complexes have broken down, as a result of decreasing F activity and/or decreasing temperature. Both of these factors contribute to a decreasing stability of REE fluoro-complexes (Wood, 1990a,b). This mechanism was also proposed by Strong et al. (1984) to explain similar behaviour of REE in fluorite from St. Lawrence.

Assuming that the apparent partition coefficient from sample GNV-ST resembles the true partitioning behaviour of free-ion or weakly complexed REE between fluorite and the hydrothermal fluid, several conclusions can be made:

1 fluorite has a partitioning maximum near the ionic radius of Dy (0.103 nm [1.03Å]) which may represent the most favourable site size. This would help to explain the anomalous behaviour of Y whose ionic radius (0.102 nm [1.02Å]) would be very close to optimum site size

2 the partitioning behaviour of the REE from La to Dy is parallel to the trend displayed by Ca and Sr, and also similar to partitioning trends noted in crystal/melt systems between trivalent and bivalent ions

3 Eu deviates from the trivalent trend suggesting the possibility that, at least some of the Eu was in the bivalent state. This is supported by spectral response in cathode-luminescence scans of Grebe's Nest fluorite.

The apparent partition coefficients for sample GNV-8-A are shown in figure 8.4.2. In this plot, the trends are similar to those of GNV-ST, except that the maximum has shifted to near Nd, with a flattening between Nd and Gd. This curve may reflect the extreme complexing of the REE in this high temperature, early-fluid, resulting in a suppression of the concentration of HREE available for substitution in the fluorite since

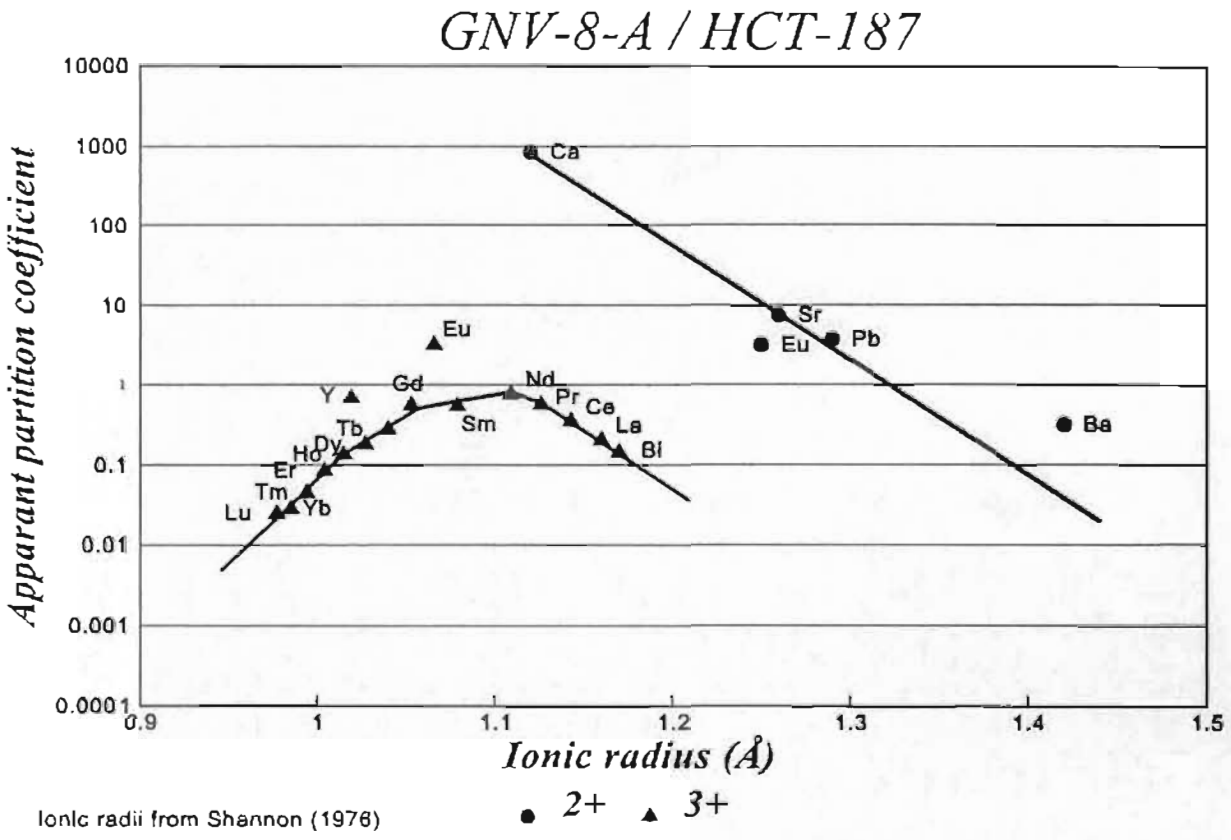

Figure 8.4.2 Plot of REE and selected element concentrations, normalized to St. Lawrence Granite model fluid composition, for fluorite sample GNV-8-A, from the Grebe's Nest Vein. The diagram shows the relationship between apparent partition coefficient versus the ionic radius of the elements.

the HREE fluoro-complexes are much more stable than those of the LREE. The lack of competition from the HREE, for the substitution site in fluorite, may account for the increased apparent partition coefficient of the LREE. In both these plots Bi appears to follow the same partitioning trend as La, suggesting the strong control of ionic radius and charge on trace element substitution.

The results of this study point to the need for experimental studies on the partitioning of trace elements between minerals and hydrothermal solutions. The high degree of systematic behaviour of trace elements in minerals could lead to an accurate means of 'fingerprinting' potential source(s) of mineralizing fluids by analyzing

associated minerals like fluorite or calcite, which are common gangue in a wide variety of ore deposits. With a comprehensive experimental database on low-temperature, fluid/mineral partitioning, fluid compositions could be more accurately monitored, leading to a better understanding of the processes involved in fluid evolution, and subsequent deposition of ores, in a wide range of mineral deposits.

9 Summary

The St. Lawrence Granite is high silica, alkaline A-type granite, emplaced to high crustal levels in the Early Devonian, in a post-tectonic extensional regime that followed a widespread Silurian orogenic event. The granite formed from a relatively hot, dry magma that underwent a protracted cooling history, during which progressive crystallization resulted in the concentration of volatiles (especially F) in late-stage residual magma at the core of the pluton. As this residual magma reached vapour saturation (after approximately 75-80% crystallization) it evolved a F-rich, relatively saline, supercritical magmatic fluid. This fluid, after varying degrees of unmixing to form a coexisting low salinity vapour and high salinity liquid, infiltrated into the conduit system already developed in structurally modified cooling cracks in the granite's 'roof-zone'.

The hot low salinity magmatic vapour reached the cooler upper levels of the conduit system much more rapidly than its denser liquid counterpart, there condensing to fill the conduit system with low salinity liquid. The hot, moderately saline magmatic fluid periodically broke through to low pressure (vented) regimes within the upper parts of the conduit system where it boiled and separated a low salinity vapour (steam), often with explosive force. Much of this low salinity fluid probably also condensed in the

upper regimes of the conduit system and variably mixed with condensed primary magmatic vapours as well as its more saline parent fluid that would eventually infiltrate into the upper levels of the system. Fluid inclusion evidence and breccia textures suggest that numerous episodes of boiling, and associated explosive activity, occurredin the conduit system. These explosive breccias probably formed as a result of the sealing of the conduit system by precipitating minerals and the subsequent development and violent release of overpressures caused by periodic recharge of the system by new pulses of hot magmatic fluid.

Apart from the effects of dilution and concentration, caused by boiling in the epithermal regime, the fluorite geochemistry suggests that the composition of the source fluid remained relatively constant throughout the mineralizing event. An exception is F, whose concentration appears to have decreased considerably in the later stages of mineralization. This probably reflects the transition from 'open system' to 'closed system' conditions caused by cessation of recharge by new magmatic fluid, either after complete vapour evolution and subsequent crystallization of the granite or after final sealing of the conduit system by precipitated minerals.

It appears that most of the REE variation in the fluorite can be related to changing stability of REE fluoro-complexes in response to higher temperatures in the early-stage fluids and declining F activity in the late-stage fluids. The fluids appear to have boiled periodically throughout most of the early and mid stages of the mineralizing event, with little effect on the chemical balance (especially the REE) of the fluid except for the localized effects of concentration and dilution. However, the boiling of the fluids may have contributed to the loss and/or redistribution of fluorine in the system.

In a study of solubility and deposition of fluorite in hydrothermal solutions, Richardson and Holland (1979a,b) concluded that the most likely mechanisms for fluorite deposition are: (1) simple cooling of ore fluids; (2) dilution of ore fluids with cool meteoric water; (3) mixing of two brines of different chemical composition; and (4) an increase in the pH of acid ore fluids. In the St. Lawrence veins, fluorite deposition consistently occurs during both increasing and decreasing temperature and salinity regimes which appears to rule out either of the first three mechanisms as the sole cause of fluorite deposition. Although the first three mechanisms may contribute indirectly, the main control on fluorite deposition, as suggested by Strong et al. (1984), appears to be an increase in the pH of initially acidic F-rich magmatic fluids, the fourth mechanism proposed by Richardson and Holland (1979b).

The specific mechanism responsible for such an increase in pH is not readily apparent but, as previously proposed by Strong et al. (1984), the boiling of fluids, incursion of higher pH meteoric water, and in particular the ebullition of carbon dioxide, possibly combined with the loss of acid as H_2CO_3, HCl or HF, could provide a means of increasing pH. Boiling removes gases (CO_2, H_2S, etc.) from solution accompanied by a decrease in the activity of H^+ (Henley et al., 1984) such as in the equilibrium reaction:

$$HCO_3^- + H^+ = CO_{2(g)} + H_2O$$

The incursion of high pH groundwater is a potential mechanism for increasing the pH of the ore forming solutions. Direct measurements of the fluid isotopic ($\delta^{18}O$) composition of decrepitated primary liquid fluid inclusions (Strong et al., 1984) ranged from -6 to -10 per mil. This was interpreted to indicate that a primary magmatic fluid underwent variable dilution and cooling by a reservoir of low temperature meteoric water which

episodically penetrated into the conduit system under appropriate hydraulic conditions. The sample (20) from which the inclusion fluids were extracted (Strong et al., 1984) displays chondrite normalized REE patterns which are characteristic of late-stage fluorite in the St. Lawrence deposits. Therefore, such incursions of meteoric waters appear to be most prevalent in the waning stages of the magmatic hydrothermal system as evidenced by the occurrence of goethite encrustations on late-stage fluorite in many of the St. Lawrence veins.

The most common means of increasing the pH of ore-forming fluids is by the reaction of the acidic solutions with wall rock to produce hydrous silicate minerals such as clays and micas. Although some zones of intense sericitic alteration of the granite have been observed, such zones are usually small and localized. Most of the fluorite bearing veins have sharp wall-rock contacts with little evidence of extensive alteration, suggesting that wall-rock alteration was not a significant factor in increasing the pH of the ore-forming solutions and promoting the deposition of the St. Lawrence Fluorspar Deposits.

10 References

Bailey, D.K., 1978, Continental rifting and mantle degassing: *In*, Neumann, E.R. and Ramberg, I.B., eds., Petrology and geochemistry of continental rifts: Reidel, Holland, *pp. 1-13.*

Bailey, J.C., 1977, Fluorine in granitic rocks and melts: a review: *Chem. Geol., V. 19, p.p. 1-42.*

Barker, F., Wones, D.R., Sharp, W.N. and Desborough, G.A., 1975, The Pike's Peak Batholith, Colorado Front Range, and a model for the origin of the gabbro-anorthosite-syenite-potassic granite suite: *Precambrian Res., V. 2, pp. 97-160.*

Batchelor, R.A. and Bowden, P., 1985, Petrogenetic interpretation of granitoid rock series using multicationic parameters: *Chem. Geol., V. 48, pp. 43-55.*

Bell, K., Blenkinsop, J. and Strong, D.F., 1977, The geochronology of some granitic bodies from eastern Newfoundland and its bearing on Appalachian Evolution: *Can. Jour. Earth Sci., V. 14, pp. 456-476.*

Bilal, B.A. and Becker, P., 1979, Complex formation of trace elements in geochemical systems - II. Stability of rare earths fluoro-complexes in fluorite bearing model systems at various ionic strengths: *Jour. Inorg. Nucl. Chem., V. 41, pp. 1607-1608.*

Bilal, B.A., Hermann, F. and Fleischer, W., 1979, Complex formation of trace elements in geochemical systems - I. Potentiometric study of fluoro-complexes of rare earth elements in fluorite bearing model systems: *Jour. Inorg. Nucl. Chem., V. 41, pp. 347-350.*

Bilal, B.A. and Koß, V., 1980, Complex formation of trace elements in geochemical systems - III. Studies on the distribution of fluoro-complexes of the rare earth elements in fluorite bearing model systems: : *Jour. Inorg. Nucl. Chem., V. 42, pp. 629-630.*

Bilal, B.A. and Langer, P., 1987, Complex formation of trace elements in geochemical systems: stability constants of fluoro-complexes of the lanthanides in a fluorite bearing model system up to 200°C and 1000 bars: *Inorg. Chim. Acta, V. 140, pp. 297-298.*

Black, R., Lameyre, J. and Bonin, B., 1985, The structural setting of alkaline complexes: *Jour. African Earth Sciences, V. 3, pp. 5-16.*

Blackwood, R.F. and O'Driscoll, C.F., 1976, The Gander - Avalon Zone boundary in southeastern Newfoundland: *Can. Jour. of Earth Sci., V. 13, pp. 1155-1159.*

Bodnar, R.J., 1983, A method of calculating fluid inclusion volumes based on vapor bubble diameters and P-V-T-X properties of inclusion fluids: *Econ. Geol., V. 78, pp. 535-542.*

Bowden, P. and Turner, D.C., 1974, Peralkaline and associated ring-complexes in the Nigeria-Niger province, West Africa: In, Sorensen, H., ed., The Alkaline Rocks, John Wiley & Sons, London, *pp. 330-351.*

Burnham, C.W., 1979, Magma and hydrothermal fluids: *In,* Barnes, H.L. ed., Geochemistry of Hydrothermal Ore Deposits: 2nd edition, John Wiley & Sons, New York, *pp. 71-136.*

Candela, P.A., 1989, Magmatic ore-forming fluids: thermodynamic and mass transfer calculations of metal concentrations: *In,* Whitney, J.A. and Naldrett, A.J., eds., Ore Deposition Associated With Magmas: Rev. Econ. Geol., V. 4, Econ. Geol. Publ. Co., El Paso, *pp. 203-221.*

Candela, P.A., 1990, Theoretical constraints on the chemistry of the magmatic aqueous phase: *In,* Stein, H.J. and Hannah, J.L., eds., Ore-bearing Granite Systems; Petrogenesis and Mineralizing Processes: Geol. Soc. Am. Spec. Pap. 246, Geol. Soc. Am. Inc., Boulder, *pp. 11-20.*

Candela, P.A. and Holland, H.D., 1986, A mass transfer model for copper and molybdenum in magmatic hydrothermal systems: the origin of porphyry-type copper ores: *Econ. Geol., V. 81, pp. 1-19.*

Chappell, B.W. and White, A.J.R., 1974, Two contrasting granite types: *Pacific Geology, V. 8, pp. 173-174.*

Clemens, J.D., Holloway, J.R. and White, A.J.R., 1986, Origin of A-type granites: Experimental constraints: *Am. Mineral., V. 71, pp. 317-324.*

Coleman, M., Cox, M. and Taylor, R., 1984, Isotopic evidence for the nature and extent of fluid involvement in metasomatism of the St. Lawrence Granite (Newfoundland, Canada): *Chem. Geol., V. 45, pp. 289-298.*

Collins, C.J., 1984a, Genesis of the St. Lawrence fluorite veins as indicated by fluid inclusion and trace element data from three selected veins: Unpubl. B.Sc. thesis, Memorial University of Newfoundland, St. John's, 103p.

Collins, C.J., 1984b, Genesis of the St. Lawrence fluorite deposits: *In* Mineral Deposits of Newfoundland - a 1984 perspective, compiled by Swinden, H.S., Newfoundland Department of Mines and Energy, Mineral Development Division, Report 84-3, *pp.* 164-170.

Collins, C.J., 1988a, Granite-hosted fluorspar deposits of the St. Lawrence area, Newfoundland: *In*, O'Driscoll, C.F., Collins, C.J. and Tuach, J. (leaders), Trip A5 - Volcanic-hosted, high-alumina, epithermal environments and the St. Lawrence fluorite deposit in the Avalon Zone, eastern Newfoundland: Field Trip Guidebook, GAC, MAC, CSPG Joint Annual Meeting, St. John's, *pp.* 51-76.

Collins, C.J., 1988b, Geology and Genesis of the St. Lawrence fluorspar deposits, Newfoundland: *In*, Program with Abstracts, GAC, MAC, CSPG Joint Annual Meeting, St. John's, V. 13, *p.* A23.

Collins, C.J. and Strong, D.F., 1985, The behaviour of fluorine in magmatic systems: a case study of Canada's largest fluorspar deposit: *In*, Taylor, R.P. and Strong, D.F., ed., Granite-related mineral deposits: Canadian Institute of Mining and Metallurgy Conference, Halifax, Extended Abstracts, *pp.* 66-71.

Collins, C.J. and Strong, D.F., 1988, A fluid inclusion and trace element study of fluorite veins associated with the peralkaline St. Lawrence Granite, Newfoundland: *In*, Taylor, R.P. and Strong, D.F., ed., Recent advances in granite-related mineral deposits: Canadian Institute of Mining and Metallurgy, Spec. Vol. 39, *pp.* 291-302.

Collins, C.J., and Strong, D.F., 1992, The distribution of REE in hydrothermal vein fluorite and calcite from the St. Lawrence Fluorspar District, Nfld.: *In*, Abstracts Volume, GAC/MAC Joint Annual Meeting, Wolfville, V. 17, *p. A19.*

Collins, W.J., Beams, S.D., White, A.J.R. and Chappell, B.W., 1982, Nature and origin of A-type granites with particular reference to southeastern Australia: *Contrib. Mineral. Petrol., V. 80, pp. 189-200.*

Cullers, R.L. and Graf, J.L., 1984, Rare earth elements in igneous rocks of the continental crust: intermediate and silicic rocks - ore petrogenesis: *In*, Henderson, P., ed., Rare Earth Element Geochemistry: Elsevier Scientific Publishers B.V., Amsterdam, *pp.* 275-316.

Currie, K.L., 1976, The alkaline rocks of Canada: Geol. Survey of Canada, Bull. 239.

Currie, K.L., Eby, G.N. and Gittins, J., 1986, The petrology of the Mount Saint Hilaire complex, southern Quebec: an alkaline gabbro-peralkaline syenite association: *Lithos, V. 19, pp. 67-83.*

de la Roche, H., Leterrier, J, Grand Claude, P. and Marchal, M., 1980, A classification of volcanic and plutonic rocks using R1-R2 diagrams and major element analysis - its relationships with current nomenclature: *Chem. Geol., V. 29, pp. 183-210.*

Deer, W.A., Howie, R.A. and Zussman, J., 1977, An Introduction to the Rock-Forming Minerals: 10th impression, Longman, Suffolk, *528p.*

Doerner, H.A. and Hoskins, W.M., 1925, Co-precipitation of radium and barium sulfates: *Amer. Chem Soc. Jour., V. 47, pp. 662-675.*

Dunning, G.R., O'Brien, S.J., Colman-Sadd, S.P., Blackwood, R.F., Dickson, W.L., O'Neill, P.P. and Krogh, T.E., 1990, Silurian orogeny in the Newfoundland Appalachians: *Jour. of Geol., V. 98, pp. 895-923.*

Ebadi, A. and Johannes, W., 1991, Beginning of melting and composition of first melts in the system Qz-Ab-Or-H_2O-CO_2: *Contrib. Mineral. Petrol., V. 106, pp. 286-295.*

Eby, G.N., 1990, The A-type granitoids: A review of theit occurrence and chemical characteristics and speculations on their petrogenesis: *Lithos, V. 26, pp. 115-134.*

Eby, G.N., 1992, Chemical subdivision of the A-type granitoids: Petrogenetic and tectonic implications: *Geology, V. 20, pp. 641-644.*

Elias, P. and Strong, D.F., 1982, Palaeozoic granitoid plutonism of southern Newfoundland: contrasts in timing, tectonic setting and level of emplacement: *Trans. Royal Soc. of Edinburgh: Earth Sciences, V. 73, pp. 43-57.*

Eppinger, R.G., Trace element and rare earth element variation in fluorites collected from skarn and epithermal mineral deposits in the Sierra Cuchillo area, south-central New Mexico: U.S.G.S., O.F. Rept. 88-566, Denver, *108p.*

Evans, A.M., ed., 1982, Metallization Associated with Acid Magmatism, John Wiley & Sons Ltd, Chichester, *385 p.*

Evans, J.L., 1977, Contact Metamorphism around the St. Lawrence Granite, Burin Peninsula, Newfoundland: B.Sc. (Hons.) Thesis, Memorial University of Nfld., St. John's, Newfoundland, *119 p.*

Farrell, H., 1967, Report of mining properties of the St. Lawrence Corporation: unpubl. report, Newfoundland Fluorspar Limited, St. Lawrence, *75 p.*

Fleischer, M., 1969, The lanthanide elements in fluorite: *The Indian Mineralogist, V. 10, pp. 36-39.*

Flynn, R.T. and Burnham, C.W., 1978, An experimental determination of rare earth partition coefficients between a chloride containing vapor phase and silicate melts: *Geochim. Cosmo. Acta, V. 42, pp. 685-701.*

Fryer, B.J., Kerr, A., Jenner, G.A. and Longstaffe, F.J., 1992, Probing the crust with plutons: regional isotopic geochemistry of granitoid intrusions across insular Newfoundland: *In*, Current Research, Nfld. Dept. of Mines and Energy, Geol. Survey Branch, Report 92-1, *pp. 119-139.*

Guichard, F., Church, T.M., Treuil, M. and Jaffrezic, H., 1979, Rare earths in barites: distribution and effects on aqueous partitioning: *Geochim. Cosmochim. Acta, V. 43, pp. 983-997.*

Harris, N.B.W. and Marriner, G.F., 1980, Geochemistry and petrogenesis of a peralkaline granite complex from the Midian Mountains, Saudi Arabia: *Lithos, V. 13, pp. 325-337.*

Henley, R.W., Truesdell, A.H., Barton Jr., P.B. and Whitney, J.A., 1984, Fluid-mineral equilibria in hydrothermal systems: Rev. Econ. Geol., V. 1, Econ. Geol. Publ. Co., El Paso, *267p.*

Hodge, B.L. and Partners, 1977, An appraisal of the ALCAN production operations based on the St. Lawrence fluorspar deposits, Newfoundland: Unpublished report for the Government of Newfoundland and Labrador, *20 p.*

Holland, H.D., 1972, Granites, solutions, and base metal deposits: *Econ. Geol., V. 67, pp. 281-301.*

Howley, J.P., 1917, Report on mineral statistics and mines of Newfoundland for the year 1900: Geological Survey of Newfoundland, Report, *35 p.*

Howse, A.F., and Collins, C.J., 1984, Barite evaluation in three areas of southeastern Newfoundland: *In*, Current Research: edited by Murray, M.J., Whelan, J.G. and Gibbons, R.V. , Mineral Development Division, Newfoundland Department of Mines and Energy, St. John's, Report 84-1, *pp.* 263-266.

Howse, A.F., and Collins, C.J., 1985, Industrial minerals survey - 1984: *In*, Current Research: edited by Brewer, K., Walsh, D. and Gibbons, R.V., Mineral Development Division, Newfoundland Department of Mines and Energy, St. John's, Report 85-1, *pp. 190-198*

Howse, A., Dean, P., Swinden, S., Kean B. and Morrissey, F., 1983, Fluorspar deposits of the St. Lawrence area, Newfoundland: geology and economic potential: Mineral Development Division, Newfoundland Department of Mines and Energy, St. John's, Report 83-9, *21 p.*

Ishihara, S. and Sasaki, A., 1991, Ore deposits related to granitic magmatism in Japan: a magmatic viewpoint: *Episodes, V. 14, pp. 286-292.*

Jaffe, H.W., 1988, Crystal chemistry and refractivity: Cambridge University Press, New York, *335 p.*

Jukes, J.B., 1843, General Report of the Geological Survey of Newfoundland for 1839 and 1840: London, *154 p.*

Kauffmann, R., 1936, Reconnaissance of the regional and economic geology of the St. Lawrence area, Newfoundland, with notes on fluorite: B.A. thesis, Princeton University, Princeton, New Jersey, *140 p.*

Keith, L.H., Crummett, W., Deegan, J.Jr., Libby, R.A., Taylor, J.K. and Wentler, G., 1983, Principles of environmental analysis: *Anal. Chem., V. 55, pp. 2210-2218.*

Keppler, H. and Wyllie, P.J., 1991, Partitioning of Cu, Sn, Mo, W, U and Th between melt and aqueous fluid in the systems haplogranite-H_2O-HCl and haplogranite-H_2O-HF: *Contrib. Mineral. Petrol., V. 109, pp. 139-150.*

Kerr, A., Dickson, L., Hayes, J. and Fryer, B., 1990, Geochemical Overview of late- and post-orogenic granites across Newfoundland: part of a long-term project to

integrate and interpret our large inventory of data: *In*, Hall, J., ed., LITHOPROBE EAST Transect Meeting, Report 13, Mem. Univ. of Nfld., St. John's, *pp. 117-135.*

Kerrich, R.R. and Fryer, B.J., 1979, Archean Precious metal hydrothermal systems, Dome Mine, Abitibi Greenstone Belt. II. REE and oxygen isotope studies: *Can. Jour. Earth Sci., V. 16, pp. 440-468.*

Kontak, D.J., Tuach, J., Strong, D.F., Archibald, D.A. and Farrar, E., 1988, Plutonic and hydrothermal events in the Ackley Granite, southeast Newfoundland, as indicated by total-fusion $^{40}Ar/^{39}Ar$ geochronology: *Can. Jour. Earth Sci., V. 25, pp. 1151-1160.*

Krogh, T.E., Strong, D.F., O'Brien, S.J., and Papezik, V.S., 1988, Precise U-Pb zircon dates from the Avalon Terrane in Newfoundland: *Can. Jour. of Earth Sci., V. 25, pp. 442-453.*

Kroner, A., 1980, Pan African crustal evolution: *Episodes, No. 2, pp. 3-8.*

Large, R.R., 1992, Australian volcanic-hosted massive sulfide deposits: features, styles, and genetic models: *Econ. Geol., V. 87, pp. 471-510.*

Loiselle, M.C. and Wones, D.R., 1979, Characteristics and origin of anorogenic granites: *Geol. Soc. Am. Abst. Prog., V. 11, p. 468.*

Longerich, H.P., Jenner, G.A., Fryer, B.J. and Jackson, S.E., 1990, Inductively coupled plasma-mass spectrometric analysis of geological samples: a critical evaluation based on case studies: *Chem. Geol., V. 83, pp. 105-118.*

Luth, W.C., Jahns, R.H. and Tuttle, O.F., 1964, The granite system at pressures of 4 to 10 kb: *Jour. Geophys. Res., V. 69, pp. 759-773.*

Maniar, P.D. and Piccoli, P.M., 1989, Tectonic discrimination of granitoids: *Geol. Soc. Am. Bull., V. 101, pp. 635-643.*

Manning, D.A.C., 1982, An experimental study of the effects of fluorine on the crystallization of granitic melts: *In*, Evans, A.M., ed., Metallization Associated with Acid Magmatism, John Wiley & Sons Ltd, Chichester, *pp. 191-203.*

Marshall, D.J., 1988, Cathodeluminescence of Geological Materials: Unwin Hyman, Boston, *146 p.*

Martin, W., 1983, St. Lawrence Town: its triumph and tragedy: In, Once Upon a Mine, Story of Pre-Confederation Mines on the Island of Newfoundland: C.I.M.M., spec. V. 26, Montreal, *pp. 66-72.*

Matsui, M., 1966, The coprecipitation behavior of rare earth elements with calcium oxalate upon precipitation from a homogeneous system: *Bull. Chem. Soc. Japan, V. 39, pp. 1114-1119.*

Matsui, Y., Onuma, N., Nagasawa, H., Higuchi, H. and Banno, S., 1977, Crystal structure control in trace element partition between crystal and magma: *Bull. Soc. fr. Minéral. Cristallogr., V. 100, pp. 315-324.*

Möller, P., 1983, Lanthanoids as a geochemical probe and problems in lanthanoid geochemistry - distribution and behaviour of lanthanoids in non-magmatic-phases: *In,* Sinha, ed., Systematics and the Properties of the Lanthanoids: D. Reidel Pub. Co., Dordrecht Lancaster, *pp. 561-616.*

Möller, P., 1988, The dependence of partition coefficients on differences of ionic volumes in crystal-melt systems: *Contrib. Mineral. Petrol., V. 99, pp. 62-69.*

Möller, P. and Morteani, G., 1983, On the geochemical fractionation of rare earth elements during the formation of Ca-minerals and its application to problems of the genesis of ore deposits: *In.* Augustithis, S.S., ed. The Significance of Trace Elements in Solving Petrogenetic Problems & Controversies: Theophrastus Pub., Athens, *pp. 747-791.*

Möller, P., Parekh, P.P. and Schneider, H.J., 1976, The application of Tb/Ca-Tb/La abundance ratios to problems of fluorspar genesis: *Mineral. Deposita, V. 11, pp. 111-116.*

Morgan, J.W. and Wandless, G.A., 1980, Rare earth element distribution in some hydrothermal minerals: evidence for crystallographic control: *Geochim. et Cosmochim. Acta, V. 44, pp. 973-980*

Murray, A. and Howley, J.P., 1881, Report of the Geological Survey of Newfoundland from 1864 to 1880: Geological Survey of Newfoundland, Publication, *536 p.*

Nagasawa, H, 1966, Trace element partition coefficient in ionic crystals: *Science, V. 152, pp. 767-769.*

Norman, D.I. and Landis, G.P., 1983, Source of mineralizing components in hydrothermal ore fluids as evidenced by $^{87}Sr/^{86}Sr$ and stable isotope data from the Pasto Bueno Deposit, Peru: *Econ. Geol., V. 78, pp. 451-465.*

O'Brien, S.J., Strong, P.G., and Evans, J.L., 1977, The geology of the Grand Bank (1M/4) and Lamaline (1L/13) map areas, Burin Peninsula, Newfoundland: Nfld. Dept. of Mines and Energy, Min. Dev. Div., Rept. 77-7, *16 p.*

O'Brien, S.J., Strong, D.F., Strong, P., Taylor, S.W., and Wilton, D.H., 1975, Geology of the Marystown - St. Lawrence area: Newfoundland Department of Mines and Energy, Mineral Development Division, Report 76-1, *pp. 64-70.*

Onuma, N., Higuchi, H, Wakita, H and Nagasawa, H., 1968, Trace element partition between two pyroxenes and the host lava: *Earth and Planetary Sci. Let., V. 5, pp. 47-51.*

Pearce, J.A., Harris, N.B.W. and Tindle, A.G., 1984, Tectonic interpretation of granitic rocks: *Jour. of Petrology, V. 24, part 4, pp. 956-983.*

Pitcher, W.S., 1983, Granite type and tectonic environment: In, Hsu, K. ed., Mountain Building Processes, Academic Press, London, *pp. 19-40.*

Richardson, C.K., and Holland, H D., 1979a, The solubility of fluorite in hydrothermal solutions, an experimental study: *Geochim. et Cosmochim. Acta, V. 43, pp. 1313-1325.*

Richardson, C.K., and Holland, H.D., 1979b, Fluorite deposition in hydrothermal systems: *Geochimica et Cosmochimica Acta, V. 43, pp. 1327-1335.*

Rock, N.M.S., 1988, Numerical Geology: Springer-Verlag, Berlin, *427p.*

Roedder, E., 1979, Fluid inclusions as samples of ore fluids: *In,* Barnes H.L., ed., Geochemistry of Hydrothermal Ore Deposits: 2nd ed., John Wiley and Sons, New York, *pp. 684-737.*

Roedder, E., 1984, Fluid inclusions: Reviews in Mineralogy, V. 12, Mineral. Soc. Am., Washington, *644p.*

Ruiz, J., Kesler, S.E. and Jones, L.M., 1985, Strontium isotope geochemistry of fluorite mineralization associated with fluorine-rich igneous rocks from the Sierra Madre Occidental, Mexico: possible exploration significance: *Econ. Geol., V. 80, pp. 33-42.*

Ruiz, J., Kesler, S.E., Jones, L.M. and Sutter, J.F., 1980, Geology and geochemistry of the Las Cuevas fluorite deposit, San Luis Potosi, Mexico: *Econ. Geol., V. 75, pp. 1200-1209.*

Schneider, H.J., Möller, P. and Parekh, P.P., 1975, Rare earth elements distribution in fluorites and carbonate sediments of the East-Alpine Mid-Triassic sequences in the Nördliche Kalakalpen: *Mineral. Deposita, V. 10, pp. 330-344.*

Schneider, H.J., Möller, P., Parekh, P.P. and Zimmer, E., 1977, Fluorine contents in carbonate sequences ond rare earth distribution in fluorites of Pb-Zn deposits in East-Alpine Mid-Triassic: *Mineral. Deposita, V. 12, pp. 22-36.*

Shannon, R.D., 1976, Revised effective ionic radii and systematic studies of interatomic distances in halides and chalcogenides: *Acta. Cryst., V. A32, pp. 751-767.*

Shibue, Y., 1991, Mixing diagrams for hydrothermal solutions: applications to interpretation of fluid inclusion data of hydrothermal ore deposits in Japan: *Geochem. Jour., V. 25, pp. 75-93.*

Smith, W.S., 1957, Fluorspar at St. Lawrence, Newfoundland: unpubl. open file report, Nfld. Dept. Mines & Energy, O.F. # 1L/14(16), *113p.*

Sourirajan, S. and Kennedy, C.C., 1962, The system H_2O-NaCl at elevated temperatures and pressures: *Am. Jour. Sci., V. 260, pp. 115-141.*

Stein, H.J. and Hannah, J.L., eds., 1990, Ore-bearing Granite Systems; Petrogenesis and Mineralizing Processes: Geol. Soc. Am. Spec. Pap. 246, Geol. Soc. Am. Inc., Boulder, *364 p.*

Strong, D.F., 1982, Carbothermal metasomatism of alaskitic granite, St. Lawrence, Newfoundland, Canada: *Chem. Geol., V. 35, pp. 97-114.*

Strong, D.F., Dickson, W.L., O'Driscoll, C.F. and Kean, B.F., 1974, Geochemistry of Eastern Newfoundland Granitoid Rocks: Mineral Development Division, Newfoundland Dept. Mines and Energy, Report 74-3, *140 p.*

Strong, D.F. and Dostal, J., 1980, Dynamic melting of Proterozoic upper mantle: evidence from rare earth elements in oceanic crust of eastern Newfoundland: *Contrib. Mineral. Petrol., V. 72, pp. 165-173.*

Strong, D.F., Fryer, B.J. and Kerrich, R., 1984, Genesis of the St. Lawrence fluorspar deposits, as indicated by fluid inclusion, rare earth elements and isotopic data: *Econ. Geol., V. 79, pp.1142-1158.*

Strong, D.F., O'Brien, S.J.F., Taylor, S.W., Strong, P.G. and Wilton, D.H., 1978, Geology of the Marystown (1M/3) and St. Lawrence (1L/14) map areas, Newfoundland: Nfld. Dept. Mines and Energy, Min. Dev. Div., Rept. 77-8, *81 p.*

Strong, P.G., 1976, Geology of the Lawn area, southeast Newfoundland. B.Sc. thesis (unpublished), Memorial University of Newfoundland, *68 p.*

Taylor, R.P. and Fryer, B.J., 1983, Rare earth element lithogeochemistry of granitoid mineral deposits: *C.I.M.M. Bull., V. 76, pp. 74-84.*

Taylor, R.P. and Strong, D.F., *eds.*, 1988, Recent Advances in the Geology of Granite-Related Mineral Deposits: C.I.M.M. Spec. Vol. 39, Geol. Div. C.I.M.M., Montreal, *445 p.*

Taylor, R.P., Strong, D.F. and Kean, B.F., 1980. The Topsails igneous complex: Silurian-Devonian peralkaline magmatism in western Newfoundland: *Can. Jour. Earth Sci., V. 17, pp. 425-439.*

Taylor, S.R. and McLennan, S.M., 1985, The Continental Crust: Its Composition and Evolution: Blackwell, Oxford, *312 p.*

Teng, H.C., 1974, A Lithogeochemical Study of the St. Lawrence Granite, Newfoundland: unpubl. M.Sc. thesis, Memorial University of Newfoundland, St. John's, *194 p.*

Teng, H.C. and Strong, D.F., 1976, Geology and geochemistry of the St. Lawrence peralkaline granite and associated fluorite deposits, southeastern Newfoundland: *Can. Jour. Earth Sci., V. 13, pp. 1374-1385.*

Terakado, Y. and Masuda, A., 1988, The coprecipitation of rere-earth elements with calcite and aragonite: *Chem. Geol., V. 69, pp. 103-110.*

Tilsley, J.E., 1984, Fluorspar Mines at St. Lawrence, Newfoundland: *In,* Guillet, G.R. and Martin, W., eds., The Geology of Industrial Minerals in Canada, CIMM Special Volume 29, CIMM, Montreal, *pp. 6-8.*

Tuttle O.F. and Bowen, N.L., 1958, Origin of granite in light of experimental studies in the system $NaAlSi_3O_8$-$KAlSi_3O_8$-SiO_2-H_2O: Geol. Soc. Am., Mem. 74, *153p.*

Urabe, T., 1985, Aluminous granite as a source magma of hydrothermal ore deposits: an experimental study: *Econ. Geol., V. 80, pp. 148-157.*

Urabe, T. and Marumo, K., 1991, A new model for Kuroko-type deposits of Japan: *Episodes, V. 14, pp. 246-251.*

Van Alstine, R.E., 1939, Summary field report, St. Lawrence area, Newfoundland: Nfld. Mineral Resources Division, unpub. internal Report, *9 p.*

Van Alstine, R.E., 1944, The fluorspar deposits of St. Lawrence, Newfoundland: *Econ. Geol., V. 39, No. 2, pp. 109-132.*

Van Alstine, R.E., 1948 , Geology and Mineral Deposits of the St. Lawrence Area, Burin Peninsula, Newfoundland: Geol. Surv. Nfld., Bull. 23, *64 p.*

Walker, J.B. and Choppin, G.R., 1967, Thermodynamic parameters of fluoride complexes of the lanthanides: *Adv. Chem., V. 71, pp. 127-140.*

Webster, J.D., 1990, Partitioning of F between H_2O and CO_2 fluids and topaz rhyolite melt: *Contrib. Mineral. Petrol., V. 104, pp. 424-428.*

Webster, J. D. and Holoway, J.R., 1989, Partitioning of F and Cl between magmatic-hydrothermal fluids and highly evolved granitic magmas: *In*, Stein, H.J. and Hannah, J.L. (eds.), Ore-bearing granite systems: petrogenesis and mineralizing processes: Geol. Soc. Am., Spec. Paper 246, *pp. 21-33.*

Whalen, J.B., 1985, Geochemistry of an island-arc plutonic suite: the Uasilau-Yau Yau intrusive complex, New Britain, PNG: *Jour. Petrol., V. 26, pp. 603-632.*

Whalen, J.B., Currie, K.L. and Chappell, B.W., 1987, A-type granites; geochemical characteristics and discrimination: *Contrib. to Min. and Pet., V. 87, pp. 420-436.*

White, A.J.R., 1979, Sources of granite magmas: *Geol. Soc. Am. Abst. Prog., V. 11, p. 539.*

Whitney, J.A., 1988, The origin of granite: The role and source of water in the evolution of granitic magmas: *Geol. Soc. Am. Bull., V. 100, pp. 1886-1897.*

Whitney, J.A. and Naldrett, A.J., *eds.*, 1989, Ore Deposition Associated With Magmas: Rev. Econ. Geol., V. 4, Econ. Geol. Publ. Co., El Poso, *250 p.*

Williams, H., 1964, The Appalachians in northeastern Newfoundland - A two-sided symmetrical system: *Amer. Jour. of Sci., V. 262, pp. 1137-1158.*

Williams, H., 1978, (compiler), Tectonic-Lithofacies Map of the Appalachian Orogen: Memorial University of Newfoundland, St. John's, Map No. 1.

Williams, H., 1979, Appalachian Orogen in Canada: *Can. Jour. of Earth Sci., V. 16, pp. 792-807*

Williams, H., Dickson, W.L., Currie, K.L., Hayes, J.P. and Tuach, J, 1989, Preliminary report on classification of Newfoundland granitic rocks and their relations to

tectonostratigraphic zoned and lower crustal blocks: *In*, Current Research, Geol. Survey of Canada, Paper 89-1-B, *pp. 47-53.*

Williams, H. and Hatcher, R.D., 1982, Suspect terranes and accretionary history of the Appalachian orogen: *Geology, V. 10, pp. 530-536.*

Williams, H., Kennedy, M.J. and Neale, E.R.W., 1972, The Appalachian structural province: *In* Price, R.A. and Douglas, R.J.W., ed., Variations in tectonic styles in Canada: Geol. Assoc. of Canada Spec. Paper 11, *pp. 181-261.*

Williams, H., Kennedy, M.J. and Neale, E.R.W., 1974, The northeastward termination of the Appalachian orogen, *In* Naim A.E.M and Stehli, F.G., ed., The Ocean Basins and Margins: Plenum Publishing Corporation, New York, , V. 2, *pp. 70-123.*

Williamson, D. H., 1956, The geology of the fluorspar district of St. Lawrence, Burin Peninsula, Newfoundland: Nfld. Mineral Res. Div., unpubl. internal rep., *126 p.*

Winkler, H.G.F., 1979, Petrogenesis of Metamorphic Rocks: 5th edition, Springer-Verlag, New York, *p. 348.*

Wood, S.A., 1990a, The aqueous geochemistry of the rare-earth elements and yttrium: 1. review of available low temperature data for inorganic complexes and the inorganic REE speciation of natural waters: *Chem. Geol., V. 82, pp. 159-186.*

Wood, S.A., 1990b, The aqueous geochemistry of the rare-earth elements and yttrium: 2. theoretical predictions of speciation in hydrothermal solutions to 350°C at saturation water vapor pressure: *Chem. Geol., V. 88, pp. 99-125.*

Appendix 1

Geochemistry

A. ICP-MS

The granite and related host rock samples discussed in Chapter 2 were analyzed for selected trace elements by ICP-MS and the analytical results are presented below. Two different dissolution methods, HF-HNO3 and Na_2O_2 (listed with the samples), were used in the preparation for analysis. The analytical procedures and the detection limits for the HF-HNO3 procedure were given by Jenner et al. (1990), and for the Na_2O_2 procedure by Longerich et al. (1990).

Trace elements in St. Lawrence Granite and related samples by ICP-MS

Sample #	BBS-84-64	CV-6	HCT-111	HCT-187	HCT-187	HCT-188	SDMS 4	SDMS 2-B	AZ-2	AZ-4
Rock type	tuffisite shale (hornf.)		granite	QF porphyry	QF porphyry	QF porphyry	granite	min. granite	alt. granite	alt. granite
Anal. Date	12-Jun-92	12-Jun-92	16-Sep-87	12-Jun-92	16-Sep-87	16-Sep-87	12-Jun-92	13-Mar-89	17-Jun-89	17-Jun-89
Dissolution	HF-HNO3	HF-HNO3	HF-HNO3	HF-HNO3	HF-HNO3	HF-HNO3	HF-HNO3	Na_2O_2 melt	Na_2O_2 melt	Na_2O_2 melt
Li	58	107	11	10	11	19	59			
Be	10.8	2.80		15.7			10.2			
Sc	ND (1.7)	22		ND (1.7)			ND (1.7)			
V	ND (1.3)	126	ND (1.3)	ND (1.3)	ND (1.3)	ND (1.3)	ND (1.3)			
Cr	4 (4)	126		ND (4)			ND (4)			
Cu	ND (31)	ND (31)		61 (31)			ND (31)			
Zn	40 (31)	255		67 (31)			56 (31)			
Rb	213	335	323	433	433	152	340			
Sr	12	47	12	12	15	24	5			
Y	122	36.6	121	117	129	95.5	46.4	75.4	62.9	91.6
Zr	334	94	364	279	280	262	314	128	234	231
Nb	30.1	17.9	ND (0.015)	65.2	ND (0.015)	ND (0.015)	60.5	54.3	37.1	23.9
Mo	1.5	1.0	ND (0.04)	9.5	ND (0.04)	ND (0.04)	6.1			
Cs	2.3	23	4.4	5.4	6.8	1.7	6.3			
Ba	83	906	48	53	60	85	48	530	778	581
La	63.3	46.9	61.8	66.2	47.0	28.3	25.3	41.7	64.9	113.4
Ce	136	93.7	131	93.5	93.7	59.4	54.7	75.5	129	227
Pr	16.1	10.8	17.5	11.0	10.6	7.16	6.39	8.72	15.5	27.1
Nd	65.7	40.3	66.3	39.0	36.8	26.5	22.8	29.0	57.9	101
Sm	15.6	7.46	16.8	10.5	9.04	7.91	5.63	7.56	10.4	18.9
Eu	0.377	1.42	0.405	0.230	0.222	0.650	0.079	NDD (DL)	0.430	0.727
Gd	16.8	6.87	16.3	11.7	10.6	8.16	5.18	7.34	7.75	14.5
Tb	2.76	0.975	3.33	2.42	2.46	2.12	1.05	1.73	1.35	2.28
Dy	17.8	6.00	22.4	18.2	17.5	15.4	8.27	12.7	7.61	11.6
Ho	3.84	1.24	4.72	4.11	3.97	3.42	1.93	2.83	1.58	2.29
Er	11.9	3.59	15.1	13.6	12.9	11.4	6.73	9.71	4.64	6.50
Tm	1.87	0.550	2.26	2.22	2.11	1.83	1.16	1.66	0.676	0.826
Yb	12.6	3.69	14.7	15.5	14.9	12.7	8.23	11.8	4.54	5.13
Lu	1.82	0.536	2.03	2.17	2.16	1.84	1.19	1.80	0.679	0.778
Hf	13	2.8	14	16	16	15	14	4.8	5.8	7.4
Ta	0.560	1.26	ND (0.084)	1.45	ND (0.084)	ND (0.084)	1.57	0.770	3.39	0.868
Tl	1.1	4.0	1.2	1.3	2.2	1.0	2.3			
Pb	16	35	27	60	67	141	49			
Bi	0.287	0.137	0.610	1.17	1.35	0.349	0.714			
Th	19.2	12.5	31.7	41.6	39.0	39.1	23.2	44.3	12.9	10.8
U	4.24	2.72	8.36	16.4	15.6	15.3	6.07			
$^{206}Pb/^{204}Pb$	1.22	1.19		1.25			1.21			
$^{208}Pb/^{204}Pb$	2.43	2.48		2.47			2.46			
$^{143}Nd/^{144}Nd$	0.1418	0.111		0.1163			0.147	0.157		
$^{87}Sr/^{86}Sr$	50.6	20.5		109			212			

Notes: blank spaces indicate that the element was not determined by the specified analytical method in the particular run that the sample was analyzed in. samples with determined values less than the limit of detection (LOD) are reported as ND(LOD).

In preparation for analysis by ICP-MS, the fluorite and calcite bearing vein samples were dissolved using a boric acid technique modified from Eppinger (1988). The boron cation (B^{+3}) forms extremely stable soluble complexes with fluorine, which results in rapid, total dissolution of fluorite and prevents the precipitation of insoluble fluorides, a problem that plagued fluorite analysis using standard HF-HNO_3 dissolution techniques. The common gangue minerals in the fluorite veins, barite and quartz, are relatively insoluble in this procedure, therefore in most mixed mineralogy samples, the analysis are almost entirely representative of the fluorite and/or calcite components of the samples.

The following procedure was used for fluorite dissolution:

1 weigh and record (S_w) approximately 0.1 grams of fluorite (and/or calcite) powder in a screw top Teflon bomb. If the sample contains barite or quartz the sample weight should be increased accordingly
2 add 0.5 ml of concentrated distilled HNO_3
3 add 1.0 ml of 5000 ppm boric acid solution (i.e. 2.85g H_3BO_3 in 100 g doubly distilled, Nanopure filtered, water) and cover
4 heat covered for 1 hour (90-100 °C)
5 remove from heat and let stand (covered) for 24 hours
6 add 1.0 ml of 500 ppm boric acid solution
7 cover and heat for an additional 2 hours (90-100 °C)
8 remove from heat and let cool
9 weigh, record, and label 1 dry, acid washed, 100 ml sample container (SC_w) and 1 dry, acid washed 50 ml centrifuge tube and cover (CT_o) for each sample
10 wash sample from Teflon bomb into centrifuge tube using ~30 ml of Nanopure distilled water, rinse the bomb and the cover several times
11 centrifuge for 10 minutes and decant liquid into sample container being careful not to decant any of the solid residue
12 use wash bottle (distilled water) to agitate residue (if any) to promote removal of absorbed sample, fill tube to ~30 ml and centrifuge again
13 repeat 12
14 weigh sample container (SC_f) and calculate sample solution weight (wt. SC_f - SC_w = sample sol. wt.) which should be ~90 g
15 place open centrifuge tube and its cover in drying over (overnight)
16 when dry, weigh the centrifuge tube and its cover (CT_f) to calculate sample residue weight (S_r) [i.e. $S_r = CT_f - CT_o$]

17 calculate weight of dissolved sample (S_d) [i.e. $S_d = S_o - S_i$]. This sample weight (S_d), is used to calculate elemental concentrations from the ICP-MS analysis. **(S_d primarily represents the weight of the fluorite and/or calcite components of the initial sample)**

The ICP-MS analysis of the fluorite-bearing vein minerals are presented in the following section along with the summaries and graphs of the analyses of calibration blanks, reagent blanks and fluorite control sample GNV-7. The control sample was analysed in duplicate in every dissolution run and most analytical runs. The replicate analytical results are consistent for most of the elements that occur in detectable concentrations. The REE are particularly reproducible, displaying relative standard deviations (RSD) of less than 10%.

ICP-MS boric-nitric dissolution procedure
Limits of Detection and Reagent Blanks (CLD normalized for a dilution of 0.500 g/kg)

Element	CLD (3 x std) (n = 54) (ppm)	CLQ (10 x std) (n = 54) (ppm)	MLD (3 x std) (n = 6) (ppm)	Mean Reagent Blank (ppm)	Maximum Reagent Blank (ppm)	Minimum Reagent Blank (ppm)	ELQ (ppm)	Blank Correction Factor (ppm)
Li	0.7	2	1.3	0.6	1.2	0.13	**2**	
Be	4	14	16	12	20	3	**14**	
Sc	6	20	6	3	6	0.000	**20**	
V	1.8	6	1.2	0.77	1.3	0.000	**6**	
Cr	26	85	52	8	47	0.000	**85**	
Cu	1.0	3	6	1.4	6	0.000	**3**	
Zn	4	12	7	3	7	0.4	**12**	
Rb	0.08	0.3	0.08	0.02	0.06	0.000	**0.3**	
Sr	0.2	0.7	4	0.9	3	0.000	**4**	-0.9
Y	0.006	0.02	0.07	0.04	0.07	0.007	**0.07**	-0.04
Zr	0.4	1.4	1.7	0.3	1.5	0.000	**1.4**	
Nb	0.010	0.03	0.013	0.004	0.012	0.000	**0.03**	
Mo	0.05	0.17	0.04	0.02	0.04	0.00	**0.17**	
Cs	0.012	0.04	0.4	0.06	0.3	0.000	**0.4**	-0.1
Ba	0.5	1.7	4	1.4	4	0.17	**1.7**	
La	0.008	0.03	0.7	0.11	0.6	0.000	**0.7**	-0.1
Ce	0.009	0.03	0.04	0.015	0.03	0.000	**0.03**	
Pr	0.005	0.018	0.6	0.10	0.6	0.001	**0.6**	-0.1
Nd	0.06	0.19	0.7	0.12	0.6	0.000	**0.19**	
Sm	0.03	0.11	0.7	0.12	0.6	0.004	**0.7**	-0.1
Eu	0.012	0.04	0.006	0.001	0.005	0.000	**0.04**	
Gd	0.04	0.14	0.07	0.016	0.07	0.000	**0.14**	
Tb	0.007	0.02	0.003	0.001	0.002	0.000	**0.02**	
Dy	0.02	0.08	0.010	0.004	0.010	0.000	**0.08**	
Ho	0.007	0.02	0.008	0.002	0.008	0.000	**0.02**	
Er	0.03	0.10	0.3	0.05	0.3	0.000	**0.10**	
Tm	0.007	0.02	0.4	0.05	0.3	0.000	**0.4**	-0.1
Yb	0.05	0.16	0.09	0.02	0.08	0.000	**0.16**	
Lu	0.009	0.03	0.008	0.002	0.006	0.000	**0.03**	
Hf	0.10	0.3	0.003	0.001	0.003	0.000	**0.3**	
Ta	0.011	0.04	0.008	0.003	0.006	0.000	**0.04**	
Tl	0.15	0.5	0.3	0.08	0.3	0.01	**0.5**	
Pb	0.3	0.9	3	0.8	3	0.018	**0.9**	
Bi	0.07	0.2	0.4	0.07	0.4	0.000	**0.2**	
Th	0.05	0.17	0.5	0.07	0.4	0.000	**0.17**	
U	0.04	0.12	0.6	0.09	0.5	0.000	**0.12**	

The calibration blank limit of detection (CLD) is based on the calibration blank (0.2 N HNO_3) standard deviation from 9 runs (6 blanks per run) between May 5, 1991 and January 18, 1992. The CLD is calculated as 3 times the standard deviation of the calibration blank while the limit of quantitation (CLQ) is calculated as 10 times the standard deviation of the calibration blank. The method limit of detection (MLD) is based on 5 analysis of reagent blanks within those 7 runs and calculated as 3 times the standard deviation of an individual determination. The effective limit of quantitation (ELQ) is equivalent to the calibration limit of quantitation (CLQ) except where the mean of the reagent blank is within the CLQ. In such cases, the MLD is used as the ELQ and a 'blank correction factor' is applied to the analytical value. These limits are applied to the analysis of fluorite (± barite, quartz & calcite) samples utilizing the dissolution proceedure described in the text.

Calibration Blank Limits of Detection (CLD) - ICP-MS Boric acid dissolution proceedure (normalized to a dilution of 0.500 g/kg)

Run #	417	458	460	463	464	467	472	474	475	Mean	s.d.	max.	min.
Dil. (g/kg)	1.014	0.578	0.619	0.549	0.629	0.402	0.726	0.583	0.584	0.632	0.157	1.014	0.402
Date	May 3, 1991	Aug 29, 1991	Sep 4 , 1991	Sep 23, 1991	Sep 25, 1991	Oct 23, 1991	Nov 22, 1991	Jan 12, 1992	Jan 18, 1992	0.500	g/kg normalized		(n = 54)
Li	0.134	0.097	0.484	0.390	0.598	4.068	0.157	0.201	0.266	0.711	1.198	4.068	0.097
Be	0.436	0.155	0.409	0.368	0.589	34.514	1.235	0.204	0.300	4.246	10.706	34.514	0.155
Sc	0.977	1.908	4.912	6.840	17.059	17.100	3.200	2.200	0.810	6.112	6.133	17.100	0.810
V	0.193	0.126	1.726	1.175	7.877	0.164	0.047	4.731	0.317	1.817	2.566	7.877	0.047
Cr	0.973	0.423	9.190	5.458	35.764	158.985	0.304	17.406	1.022	25.503	48.444	158.985	0.304
Cu	5.084	0.334	0.910	0.189	0.506	0.668	0.492	0.164	0.293	0.960	1.475	5.084	0.164
Zn	2.857	15.012	1.710	1.689	2.000	5.945	1.097	0.662	2.734	3.745	4.236	15.012	0.662
Rb	0.037	0.304	0.099	0.052	0.074	0.027	0.048	0.018	0.064	0.080	0.083	0.304	0.018
Sr	0.164	0.262	0.446	0.173	0.276	0.126	0.121	0.092	0.196	0.206	0.103	0.446	0.092
Y	0.004	0.008	0.007	0.005	0.009	0.007	0.007	0.002	0.002	0.006	0.003	0.009	0.002
Zr	0.047	1.188	0.734	0.377	0.657	0.089	0.556	0.084	0.162	0.435	0.362	1.188	0.047
Nb	0.004	0.006	0.018	0.006	0.014	0.005	0.023	0.012	0.002	0.010	0.007	0.023	0.002
Mo	0.016	0.057	0.103	0.049	0.075	0.032	0.089	0.011	0.029	0.051	0.030	0.103	0.011
Cs	0.010	0.010	0.016	0.013	0.011	0.010	0.021	0.003	0.015	0.012	0.005	0.021	0.003
Ba	0.353	0.074	0.173	0.063	0.199	3.520	0.232	0.031	0.042	0.521	1.065	3.520	0.031
La	0.002	0.007	0.012	0.009	0.013	0.013	0.012	0.001	0.003	0.008	0.005	0.013	0.001
Ce	0.002	0.008	0.016	0.005	0.009	0.020	0.010	0.005	0.004	0.009	0.005	0.020	0.002
Pr	0.002	0.002	0.009	0.004	0.004	0.014	0.004	0.009	0.001	0.005	0.004	0.014	0.001
Nd	0.022	0.042	0.036	0.047	0.083	0.130	0.075	0.034	0.029	0.056	0.033	0.130	0.022
Sm	0.020	0.027	0.061	0.044	0.033	0.048	0.040	0.018	0.017	0.034	0.014	0.061	0.017
Eu	0.008	0.006	0.017	0.009	0.016	0.032	0.013	0.007	0.004	0.012	0.008	0.032	0.004
Gd	0.022	0.027	0.059	0.029	0.039	0.095	0.055	0.008	0.016	0.042	0.030	0.095	0.008
Tb	0.004	0.003	0.014	0.005	0.007	0.018	0.004	0.002	0.002	0.007	0.005	0.018	0.002
Dy	0.010	0.011	0.019	0.011	0.025	0.094	0.045	0.003	0.002	0.025	0.028	0.094	0.002
Ho	0.002	0.005	0.006	0.008	0.009	0.020	0.013	0.001	0.002	0.007	0.006	0.020	0.001
Er	0.012	0.010	0.054	0.034	0.023	0.075	0.049	0.004	0.005	0.030	0.024	0.075	0.004
Tm	0.002	0.006	0.014	0.008	0.006	0.014	0.006	0.002	0.003	0.007	0.004	0.014	0.002
Yb	0.014	0.024	0.057	0.030	0.048	0.183	0.065	0.008	0.014	0.049	0.051	0.183	0.008
Lu	0.004	0.003	0.018	0.005	0.005	0.029	0.013	0.002	0.005	0.009	0.009	0.029	0.002
Hf	0.028	0.045	0.182	0.056	0.088	0.221	0.138	0.046	0.084	0.099	0.063	0.221	0.028
Ta	0.006	0.006	0.014	0.011	0.014	0.027	0.016	0.002	0.003	0.011	0.007	0.027	0.002
Tl	0.014	0.056	0.106	0.015	0.136	0.813	0.045	0.112	0.028	0.147	0.239	0.813	0.014
Pb	0.041	0.068	0.151	0.045	1.342	0.109	0.141	0.402	0.049	0.261	0.397	1.342	0.041
Bi	0.168	0.047	0.073	0.033	0.045	0.053	0.221	0.009	0.009	0.073	0.069	0.221	0.009
Th	0.020	0.107	0.054	0.036	0.050	0.109	0.066	0.006	0.013	0.051	0.035	0.109	0.006
U	0.008	0.066	0.037	0.028	0.030	0.113	0.031	0.004	0.005	0.036	0.033	0.113	0.004

Note: The calibration blank limit of detection (CLD) is calculated as three times the standard deviation of the analysis of the calibration blank (0.2N HNO3).
The calculated CLD, based on the blanks (6 per run), are presented for all 9 runs in which samples used in this study were analyzed (May 3, 1991 to Jan 18, 1992).
The original run CLD, calculated at the average run dilution, have been normalized to a dilution of 0.500 g/kg for comparison and statistical compilation.

Method Limit of Detection (MLD) - boric acid dissolution procedure

(calculated from reagent blanks)

Sample	BLANK (B1)	BLANK(B2)	BLANK(B4)	BLANK(B5)	BLANK(B6)	BLANK(B3)	mean	standard			MLD
Date	30-Aug-91	04-Sep-91	25-Sep-91	22-Oct-91	22-Nov-91	26-May-92	(n = 6)	deviation	maximum	minimum	(3 x sd)
Run	458	460	464	467	472	488	(ppm)	(ppm)	(ppm)	(ppm)	(ppm)
La	0.161	0.423	0.127	1.229	0.548	1.109	0.599	0.429	1.229	0.127	1.3
Be	3.176	35.612	20.403	10.586	8.852	13.095	11.954	5.395	20.403	3.176	16
Sc	4.043	2.853	2.759	-0.214	4.324	6.103	3.347	1.663	6.103	0.000	5
V	1.082	0.947	-0.505	0.612	0.688	1.289	0.770	0.413	1.289	0.000	1.2
Cr	-0.228	2.652	-4.331	47.318	0.054	0.669	8.454	17.406	47.318	0.000	52
Cu	5.744	1.881	0.253	-0.018	0.063	0.439	1.397	2.045	5.744	0.000	6
Zn	6.596	2.812	0.538	0.364	4.662	2.205	2.863	2.208	6.596	0.364	7
Rb	0.063	0.054	-0.017	-0.014	-0.035	-0.017	0.020	0.028	0.063	0.000	0.08
Sr	0.948	1.052	-0.115	-0.011	0.002	3.410	0.902	1.208	3.410	0.000	4
Y	0.034	0.049	0.007	0.008	0.069	0.050	0.036	0.023	0.069	0.007	0.07
Zr	-0.277	0.014	-0.099	-0.083	-0.315	1.493	0.251	0.555	1.493	0.000	1.7
Nb	0.007	0.002	0.000	0.003	-0.002	0.012	0.004	0.004	0.012	0.000	0.013
Mo	0.026	0.024	-0.024	0.024	0.038	-0.018	0.019	0.014	0.038	0.000	0.04
Cs	0.007	0.006	0.000	0.002	0.003	0.324	0.057	0.119	0.324	0.000	0.4
Ba	0.789	1.265	0.809	1.415	0.171	3.951	1.400	1.208	3.951	0.171	4
La	0.010	0.007	0.000	0.003	-0.002	0.633	0.109	0.234	0.633	0.000	0.7
Ce	0.022	0.027	0.000	0.007	0.002	0.031	0.015	0.012	0.031	0.000	0.04
Pr	0.003	0.003	0.001	0.004	0.001	0.583	0.099	0.216	0.583	0.001	0.6
Nd	0.004	0.042	-0.019	0.001	0.036	0.612	0.116	0.223	0.612	0.000	0.7
Sm	0.015	0.006	0.036	0.025	0.004	0.615	0.117	0.223	0.615	0.004	0.7
Eu	-0.005	0.003	-0.004	-0.004	0.005	-0.022	0.001	0.002	0.005	0.000	0.006
Gd	-0.005	0.016	0.002	-0.001	0.067	0.009	0.016	0.024	0.067	0.000	0.1
Tb	0.002	0.002	-0.001	-0.003	0.000	0.000	0.001	0.001	0.002	0.000	0.003
Dy	-0.001	0.010	0.004	0.006	-0.009	0.003	0.004	0.005	0.010	0.000	0.010
Ho	0.001	0.002	-0.004	0.008	0.002	-0.003	0.002	0.003	0.008	0.000	0.008
Er	-0.004	0.012	-0.007	0.015	0.002	0.297	0.054	0.109	0.297	0.000	0.3
Tm	0.001	0.001	-0.000	0.005	-0.002	0.322	0.055	0.119	0.322	0.000	0.4
Yb	0.003	0.006	-0.025	0.004	0.001	-0.011	0.016	0.031	0.084	0.000	0.09
Lu	0.000	0.001	0.006	0.006	-0.001	-0.016	0.002	0.003	0.006	0.000	0.008
Hf	-0.047	0.002	-0.009	0.003	-0.116	-0.045	0.001	0.001	0.003	0.000	0.003
Ta	0.000	0.006	-0.005	0.006	-0.001	0.003	0.003	0.003	0.006	0.000	0.008
Tl	0.064	0.033	0.022	0.053	0.007	0.301	0.080	0.101	0.301	0.007	0.3
Pb	0.967	0.402	3.135	0.067	0.053	0.018	0.774	1.106	3.135	0.018	3
Bi	-0.023	0.006	-0.022	0.025	-0.070	0.377	0.068	0.138	0.377	0.000	0.4
Th	-0.013	-0.002	-0.028	-0.002	-0.023	0.423	0.071	0.158	0.423	0.000	0.5
U	-0.003	0.012	0.009	0.019	0.011	0.519	0.095	0.190	0.519	0.000	0.6

Note: A single reagent blank was prepared with each dissolution run, using the same proportions of reagents as sample dissolutions.
In the statistical analysis, negative values were considered as zero concentration level (i.e. 0.000 ppm).

Fluorite Control Sample GNV-7

ICP-MS Analyses (boric acid dissolution)

Sample	GNV-7	GNV-7*	GNV-7 (B1)	GNV-7* (B1)	GNV-7* (B2)	GNV-7 (B2)	GNV-7 (B2x)	GNV-7* (B3)	GNV-7 (B4)	GNV-7 (B5A)	GNV-7 (B5)	GNV-7 (B6)	GNV-7* (B6)	GNV-7* (B6)	GNV-7* (B6)	Mean	Standard	Relative	Standard
Date	03-May-91	03-May-91	29-Aug-91	29-Aug-91	04-Sep-91	04-Sep-91	12-Jan-92	22-Oct-91	25-Sep-91	22-Oct-91	22-Oct-91	22-Nov-91	22-Nov-91	18-Jan-92	25-Jan-95	(n = 15)	Deviation	Standard	Error
Run #	437	437	458	458	460	460	474	467	464	467	467	472	472	475	569	(ppm)	(ppm)	Deviation	(2s)
Li	< 0.7	< 0.7	< 0.7	< 0.7	< 0.7	< 0.7	< 0.7	< 0.7	< 0.7	< 0.7	< 0.7	< 0.7	< 0.7	< 0.7	< 0.7	< 0.7	NA	NA	NA
Be	26	26	< 4	(6)	(8)	(8)	(7)	< 4	18	< 4	(6)	(8)	(11)	(8)		(10)	(6)	(77%)	(4)
Sc	(10)	(9)	< 6	< 6	< 6	< 6	< 6	< 6	< 6	(7)	< 6	< 6	< 6	< 6		< 6.1	NA	NA	NA
V	6.3	(5)	< 2	< 2	< 2	< 2	< 2	< 2	< 2	< 2	< 2	< 2	< 2	< 2		< 1.8	NA	NA	NA
Cr			< 26	< 26	< 26	< 26	< 26	< 26	< 26	< 26	(34)	< 26	< 26	< 26		< 25.5	NA	NA	NA
Cu			73	70	65	65	72	79	55	49	41	57	54	53		61	11	18%	6
Zn			(7)	(6)	(5)	(10)	(10)	(10)	(10)	< 4	(4)	25	24	(7)		(10)	(7)	(70%)	(4)
Rb	< 0.08	(0.11)	(0.16)	< 0.08	< 0.08	< 0.08	(0.10)	< 0.08	< 0.08	< 0.08	< 0.08	< 0.08	< 0.08	< 0.08	< 0.08	< 0.1	NA	NA	NA
Sr	73	72	65	65	61	66	66	67	72	68	65	70	66	71	69	68	3	5%	2
Y	712	708	677	632	601	654	671	651	754	659	659	688	635	736	734	679	42	6%	22
Zr	(1.3)	(1.4)	6	< 0.4	< 0.4	(1.4)	< 0.4	(0.5)	1.5	< 0.4	2	4	(0.5)	< 0.4	(1.4)	(1.4)	(1.5)	(112%)	(0.8)
Nb	0.237	0.191	0.264	0.099	0.034	0.071	0.080	0.070	0.490	0.069	0.045	0.078	0.088	0.055	0.060	0.102	0.068	66%	0.035
Mo	13	9.3	0.82	0.61	1.0	0.47	0.54	0.53	0.80	0.38	0.61	0.57	0.65	0.58	0.53	2.0	3.7	181%	1.9
Cs	(0.017)	(0.014)	(0.017)	(0.017)	< 0.012	(0.019)	(0.017)	(0.018)	(0.024)	(0.016)	(0.018)	(0.024)	(0.024)	(0.021)	< 0.012	(0.017)	(0.005)	(31%)	(0.003)
Ba	4	6	5	6	26	5	4	3	6	(1.6)	4	4	4	6	6	6	5	91%	3
La	24.2	24.0	21.5	21.6	22.3	22.6	22.4	22.2	24.9	22.5	22.5	23.5	21.8	24.1	24.2	22.9	1.1	5%	0.5
Ce	56.9	56.0	50.6	50.2	51.5	51.5	52.1	51.3	57.1	52.1	52.0	55.0	51.5	55.9	56.9	53.4	2.5	5%	1.3
Pr	7.60	7.59	6.73	6.69	6.86	6.86	6.88	6.97	7.48	7.10	6.99	7.31	6.90	7.48	7.46	7.13	0.31	4%	0.16
Nd	34.5	33.6	30.8	31.5	30.2	31.0	31.1	31.2	34.2	31.3	32.6	32.3	31.3	34.1	33.6	32.2	1.4	4%	0.7
Sm	9.66	9.48	8.66	8.95	8.50	8.59	8.72	8.42	9.65	8.92	9.26	9.18	8.77	9.79	9.87	9.12	0.46	5%	0.24
Eu	1.06	0.984	0.925	1.04	0.973	0.936	0.936	0.993	1.06	1.02	0.994	1.04	0.960	1.05	1.05	1.00	0.04	5%	0.02
Gd	16.0	16.7	14.4	17.3	15.5	13.5	15.0	15.1	17.8	16.1	15.3	17.1	15.0	16.8	18.4	16.0	1.3	8%	0.7
Tb	3.55	3.58	3.21	3.85	3.40	3.09	3.27	3.23	3.69	3.43	3.48	3.45	3.24	3.61	3.68	3.45	0.21	6%	0.11
Dy	29.1	29.4	25.8	32.8	26.7	25.3	26.7	26.6	31.0	28.0	28.9	27.9	26.8	30.0	29.7	28.3	2.0	7%	1.0
Ho	7.61	7.74	6.65	8.69	6.70	6.42	6.99	6.95	8.28	7.45	7.60	7.14	7.04	7.75	7.50	7.37	0.69	8%	0.31
Er	24.7	25.2	21.7	28.5	21.4	20.6	23.1	22.8	26.7	24.5	24.5	23.9	23.2	25.3	25.3	24.1	2.0	8%	1.0
Tm	3.34	3.34	3.00	3.73	2.89	2.77	3.12	3.10	3.71	3.24	3.39	3.22	3.10	3.46	3.34	3.25	0.26	8%	0.13
Yb	21.0	20.5	17.8	22.4	18.7	16.6	18.6	19.1	23.0	20.2	20.4	19.6	19.4	21.3	20.7	20.0	1.6	8%	0.8
Lu	2.78	2.77	2.46	3.04	2.20	2.03	2.57	2.60	3.12	2.88	2.62	2.69	2.55	2.81	2.76	2.66	0.28	10%	0.14
Total REE	242	241	214	240	218	212	221	221	252	229	231	233	222	243	245	231	12	5%	3
Hf	< 0.10	(0.16)	(0.24)	< 0.10	< 0.10	(0.10)	< 0.10	< 0.10	(0.20)	< 0.10	0.387	0.56	< 0.10	< 0.10	(0.28)	(0.16)	(0.15)	(96%)	(0.08)
Ta	0.106	0.117	0.156	0.138	0.050	0.091	0.109	0.175	0.122	0.167	0.243	0.172	0.144	0.090	0.121	0.133	0.044	33%	0.023
Tl	5.3	11	2.0	1.6	(0.37)	(0.20)	4.1	< 0.15	(0.45)	< 0.15	(0.42)	(0.23)	(0.29)	5.9	2.3	2.3	3.0	132%	1.6
Pb	7195	6421	6198	5563	5547	6547	6666	6251	6222	7005	7102	6798	6063	6671	6765	6468	484	7%	250
Bi	1.6	1.4	0.47	0.50	0.35	0.48	0.69	0.61	0.76	0.79	0.65	0.36	0.31	0.86	0.56	0.69	0.36	52%	0.18
Th	(0.07)	(0.06)	0.36	0.20	< 0.05	(0.10)	< 0.05	(0.05)	0.39	< 0.05	(0.16)	0.32	(0.11)	< 0.05	< 0.05	(0.13)	(0.12)	(95%)	(0.06)
U	0.16	(0.11)	(0.06)	(0.07)	(0.07)	(0.10)	(0.09)	(0.05)	(0.08)	< 0.04	0.12	(0.06)	(0.09)	(0.08)	(0.07)	(0.08)	(0.03)	(38%)	(0.02)
Pb-204/Pb-207	1.186	1.183	1.185	1.191	1.188	1.193	1.183	1.188	1.152	1.182	1.174	1.186	1.197	1.180	1.191	1.183	0.011	1%	0.006
Pb-206/Pb-207	2.418	2.419	2.429	2.431	2.425	2.409	2.429	2.431	2.400	2.421	2.425	2.428	2.445	2.425	2.444	2.430	0.018	1%	0.009
$^{206}Pb/^{204}Pb$	0.167	0.166	0.167	0.172	0.173	0.172	0.169	0.165	0.170	0.170	0.172	0.169	0.171	0.174	0.181	0.171	0.006	3%	0.002
$^{207}Pb/^{204}Pb$	0.082	0.083	0.083	0.083	0.083	0.083	0.083	0.083	0.083	0.083	0.083	0.083	0.083	0.083	0.083	0.083	0.000	0%	0.000

Notes: values less than the limit of detection (LOD) reported as < (LOD), in the statistical analysis such values less than LOD were assigned a value equal to ½(LOD).

values less than the "effective limit of quantitation" (ELQ) but greater than the LOD are reported to their value in parentheses, this range of values are considered semi-quantitative but were used in the statistical analysis.

values left blank indicate that the element(s) was not analyzed in that particular run.

ICP-MS Boric/Nitric Control Sample GNV-7

St. Lawrence fluorite analysis - 1992

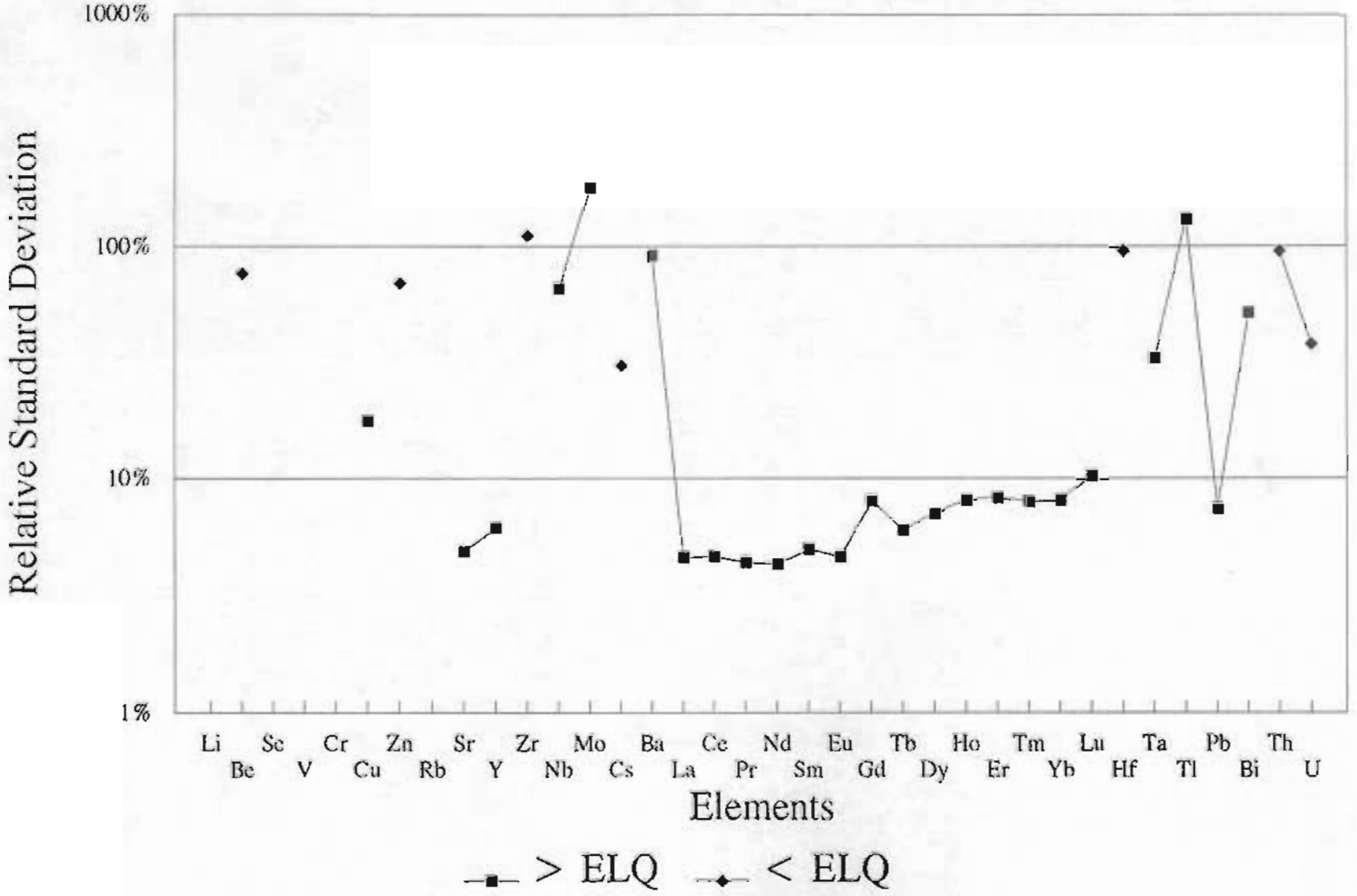

Sample #	2-10	2-2	2-4	2-8	AD-1-A	AZ-1	AZ-2	AZ-4	BB-84-11	BBS-84-64	BBS-84-D3C(	BBV-2-A	BBV-2-B	BBV-2-B*	BBV-2-C	BBV-2-D
Analysis date	12-Jan-92	27-Nov-91	22-Nov-91	12-Jan-92	22-Nov-91	27-Oct-91	17-Jan-89	17-Jan-89	16-Sep-87	12-Jan-92	22-Nov-91	04-Sep-91	04-Sep-91	04-Sep-91	26-Jul-90	03-May-91
Dissolution	Boric Acid	Boric Acid	Boric Acid	Boric Acid	Boric Acid	Boric Acid	Na2O2 Sint	Na2O2 Sint	HF/HNO3	HF/HNO3	Boric Acid	Boric Acid	Boric Acid	Boric Acid	HF/HNO3	Boric Acid
Li	(1.0)	3.5	< 0.7	< 0.7	< 0.7	3.4			< 0.3	58.0	< 0.7	< 0.7	< 0.7	< 0.7	< 0.3	< 0.7
Be	(8)	(11)	(10)	(7)	(8)	< 4				10.8	(8)	(12)	(9)	(9)	< 0.2	23
Sc	< 6	< 6	< 6	< 6	< 6	< 6				< 2	< 6	< 6	< 6	< 6	< 2	(7)
V	< 1.8	< 1.8	< 1.8	< 1.8	< 1.8	< 1.8				< 1.3	< 1.8	< 1.8	< 1.8	< 1.8	5	(5)
Cr	< 26	< 26	< 26	< 26	< 26	< 26			< 4	< 4	< 26	< 26	< 26	< 26	< 4	
Cu	28.8	45.4	18.7	17.7	6.6	206.9				< 31	(3)	220.7	280.9	276.3		
Zn	22	20	(8)	(5)	13	15				(40)	(7)	664	231	217		
Rb	0.48	0.39	(0.1)	(0.1)	(0.2)	6.90				213.5	< 0.08	(0.1)	(0.1)	< 0.08		0.27
Sr	25.9	105.9	94.5	64.7	103.7	38.2			89.4	12.3	111.6	38.3	39.5	40.6	24.9	137.4
Y	215.5	327.3	697.4	903.7	540.8	366.9	62.7	91.6	2051.4	122.1	878.5	575.9	428.5	433.0	443.5	1219.0
Zr	(0.5)	(1.3)	1.9	(1.1)	2.1	3.1	234.3	251.2	2.5	333.9	(0.5)	5.8	(0.6)	< 0.4	< 0.19	(1.4)
Nb	42.2	80.0	20.6	19.6	0.1	0.7	37.1	23.9		30.1	0.1	0.1	0.1	0.1	< 0.02	0.2
Mo	3.53	8.43	2.92	1.58	2.15	1.15				1.5	2.11	2.52	0.67	0.62	1.1	8.35
Cs	(0.06)	(0.07)	(0.05)	(0.02)	(0.03)	(0.10)			0.18	2.28	(0.01)	(0.03)	(0.02)	< 0.012	< 0.03	(0.03)
Ba	2.6	(1.3)	(1.2)	(1.0)	1831.3	235.5	778.2	581.4	2518.1	84.2	28.9	(1.7)	(1.3)	(1.4)	1.4	(0.7)
La	7.955	69.084	43.481	25.953	7.393	5.221	64.90	113.42	10.97	63.28	18.048	12.983	8.417	9.056	6.41	11.613
Ce	13.464	197.438	139.797	57.373	17.113	11.755	128.55	227.36	24.90	135.90	37.238	36.715	22.600	25.162	17.02	30.145
Pr	1.897	35.096	24.518	8.363	3.079	1.685	15.53	27.09	3.42	16.12	4.628	6.037	3.327	3.515	2.58	4.414
Nd	8.69	165.85	120.42	40.85	21.68	7.58	57.89	110.54	15.34	62.70	20.50	30.86	15.96	18.45	13.00	21.33
Sm	2.32	30.35	29.37	12.23	11.05	3.04	10.53	19.31	8.04	15.62	9.56	13.57	6.65	7.02	6.65	12.65
Eu	0.330	4.021	3.850	1.618	4.056	0.175	0.43	0.73	0.45	0.38	0.582	0.837	0.391	0.475	0.53	0.738
Gd	3.67	33.73	38.51	21.16	30.71	7.24	7.73	14.51	18.23	16.84	21.81	22.60	11.97	12.87	14.27	27.82
Tb	0.831	3.349	5.281	4.730	4.563	1.607	1.35	2.28	5.62	2.76	5.648	3.844	2.306	2.624	3.12	7.745
Dy	7.04	15.44	29.69	37.93	30.85	12.15	7.61	11.63	43.07	17.82	45.59	26.89	18.62	20.15	23.71	61.57
Ho	1.773	2.524	5.392	9.214	7.061	2.793	1.58	2.29	10.01	3.84	10.356	6.413	4.828	4.802	5.48	14.632
Er	5.86	4.69	11.87	27.04	19.04	7.75	4.64	6.50	28.44	11.87	28.98	20.61	16.48	16.84	17.51	46.45
Tm	0.781	0.371	1.076	3.170	2.078	1.000	0.68	0.83	3.48	1.87	3.586	3.193	2.662	2.703	2.54	6.566
Yb	4.93	1.55	4.88	17.16	11.58	6.08	4.54	5.13	17.23	12.62	18.17	23.21	21.26	19.08	18.50	44.73
Lu	0.654	0.203	0.576	2.162	1.363	0.754	0.68	0.78	2.11	1.82	2.114	3.417	3.156	2.937	2.49	5.698
Hf	< 0.10	(0.10)	0.48	(0.20)	0.57	< 0.10	5.84	7.41	0.37	12.53	< 0.10	(0.25)	(0.12)	< 0.10	< 0.04	(0.22)
Ta	35.2	20.0	22.4	20.6	0.086	0.115	3.39	0.87		0.56	0.064	0.121	0.123	0.109	0.02	0.137
Tl	< 0.15	< 0.15	< 0.15	< 0.15	< 0.15	0.61			< 0.13	1.1	< 0.15	0.71	(0.23)	< 0.15	11.1	7.04
Pb	35.4	14.6	4.9	21.9	42.8	25092.2			351.7	16.0	5.4	1229.2	1142.9	1117.7	356038.0	6508.7
Bi	0.37	1.08	0.58	1.18	< 0.07	5.81			0.31	0.29	< 0.07	(0.12)	(0.11)	(0.10)	10.86	0.93
Th	< 0.05	0.18	0.28	(0.06)	0.21	0.65	12.03	10.77	0.13	19.24	(0.15)	0.20	(0.07)	< 0.05	< 0.03	(0.06)
U	1.11	0.60	0.53	0.77	0.17	0.80			0.50	4.24	< 0.04	(0.05)	< 0.04	< 0.04	(0.05)	(0.07)
Pb206/Pb207	1.1882	1.1237	1.1906	1.1730	1.1852	2.4001				1.2204	1.1955	1.1868	1.1822	1.1906	0.5137	1.1971
Pb208/Pb207	2.4344	2.3624	2.4612	2.4235	2.4428	0.2359				2.4472	2.4234	2.4413	2.4405	2.4238	0.0822	2.4334
Sm147/Nd144	0.1699	0.1112	0.1468	0.1802	0.3059	0.5238				0.1478	0.2817	0.2676	0.2535	0.2262	0.3082	0.3477
Rb87/Sr86	0.0541	0.0108	0.0033	0.0060	0.0062	0.0083				50.4344	0.0016	0.0091	0.0083	0.0046	0.0106	0.0058

values less than limit of detection (LOD) - <LOD

values less than effective limit of quantitation (ELOQ or LOQ) - (value)

Sample #	BBV-2-D*	BBV-2-E	BBV-2-E	BBV-2-F	BBV-2-G	BBV-2-H	BBV-2-I	BLANK(1)	BLANK(2)	BLANK(3)	BLANK(4)	Blank(HF6)	BLANK(B1)	BLANK(B2)	BLANK(B3)	BLANK(B4)
Analysis date	03-May-91	04-Sep-91	26-Jul-90	04-Sep-91	04-Sep-91	25-Jul-90	04-Sep-91	16-Sep-87	25-Jul-90	25-Jul-90	26-Jul-90	12-Jan-92	30-Aug-91	04-Sep-91	26-May-92	25-Sep-91
Dissolution	Boric Acid	Boric Acid	HF/HNO3	Boric Acid	Boric Acid	HF/HNO3	Boric Acid	HF/HNO3	HF/HNO3	HF/HNO3	HF/HNO3	HF/HNO3	Boric Acid	Boric Acid	Boric Acid	Boric Acid
Li	< 0.7	< 0.7	< 0.3	< 0.7	(0.9)	(0.8)	(1.5)	< 0.3	< 0.3	< 0.3	< 0.3	< 0.3	< 0.7	< 0.7	(1.1)	< 0.7
Be	29	(12)	(0.3)	(11)	(8)	< 0.2	(7)		< 0.2	< 0.2	< 0.2	< 0.2	< 4	16	(13)	20
Sc	(11)	< 6	(3)	< 6	< 6	(5)	< 6		< 2	< 2	< 2	< 2	< 6	< 6	< 6	< 6
V	(6)	< 1.8	6	< 1.8	< 1.8	7	< 1.8		< 1.3	< 1.3	< 1.3	< 1.3	< 1.8	< 1.8	< 1.8	< 1.8
Cr		< 26	< 4	< 26	94	< 4	166	< 4	< 4	< 4	< 4	< 4	< 26	< 26	< 26	< 26
Cu		47.4		47.8	244.3		602.7					< 31	5.7	(21	< 1.0	< 1.0
Zn		14		472	< 4		< 4					< 31	(7)	< 4	< 4	< 4
Rb	(0.2)	(0.2)		(0.11	(0.1)		(0.3)					< 0.2	< 0.08	< 0.08	< 0.08	< 0.08
Sr	140.8	133.5	117.9	112.0	38.5	112.4	41.7	2.9	< 0.15	(0.2)	< 0.15	< 0.15	(1)	(1)	(3)	< 0.2
Y	1219.0	1086.1	1015.3	1031.7	452.3	958.1	379.4	0.0	(0.01)	(0.02)	(0.01)	< 0.006	(0.034)	(0.049)	(0.050)	(0.007)
Zr	(1.1)	2.0	(0.3)	< 0.4	< 0.4	1.0	< 0.4	0.9	< 0.19	(0.2)	< 0.19	< 0.19	< 0.4	< 0.4	1.5	< 0.4
Nb	0.2	0.1	0.5	0.1	0.5	0.2	0.7		< 0.02	< 0.02	< 0.02	< 0.02	< 0.010	< 0.010	(0.01)	< 0.010
Mo	11.04	0.45	0.9	1.27	4.09	4.3	4.34		0.7	< 0.06	< 0.06	< 0.06	< 0.05	< 0.05	< 0.05	< 0.05
Cs	(0.02)	(0.03)	< 0.03	(0.02)	(0.03)	< 0.03	(0.07)	< 0.03	< 0.03	< 0.03	< 0.03	< 0.03	< 0.012	< 0.012	(0.32)	< 0.012
Ba	(0.8)	(1.3)	2.5	2.4	2.2	10.1	4.8	6.3	1.2	(0.3)	0.9	< 0.17	(0.8)	(1.3)	4.0	(0.8)
La	11.406	9.818	9.08	11.942	6.540	8.07	4.105	(0.01)	< 0.008	0.04	(0.01)	< 0.008	(0.010)	< 0.008	(0.633)	< 0.008
Ce	29.954	25.147	23.04	31.590	17.350	20.74	10.938	(0.02)	< 0.009	0.04	(0.01)	< 0.009	(0.022)	(0.027)	0.031	< 0.009
Pr	4.449	3.691	3.34	4.693	2.612	3.04	1.575	< 0.006	< 0.006	(0.02)	< 0.006	< 0.006	< 0.005	< 0.005	(0.583)	< 0.005
Nd	21.96	18.22	15.38	23.26	13.17	14.34	7.41	< 0.03	< 0.03	(0.03)	< 0.03	< 0.03	< 0.06	< 0.06	0.61	< 0.06
Sm	12.78	10.53	9.39	13.44	7.18	8.66	4.34	< 0.02	< 0.02	< 0.02	< 0.02	< 0.02	< 0.03	< 0.03	(0.6)	(0.0)
Eu	0.726	0.544	0.45	0.932	0.592	0.47	0.299	< 0.008	< 0.008	< 0.008	< 0.008	< 0.008	< 0.012	< 0.012	< 0.012	< 0.012
Gd	28.39	22.91	21.37	30.42	15.78	18.98	8.62	< 0.03	< 0.03	< 0.03	< 0.03	< 0.03	< 0.04	< 0.04	< 0.04	< 0.04
Tb	7.790	6.880	5.85	8.202	3.768	5.26	2.412	< 0.005	< 0.005	< 0.005	< 0.005	< 0.005	< 0.007	< 0.007		< 0.007
Dy	62.46	55.78	47.96	64.48	29.91	41.94	18.53	< 0.018	< 0.018	< 0.018	< 0.018	< 0.018	< 0.02	< 0.02	< 0.02	< 0.02
Ho	14.839	13.143	11.32	15.485	7.249	9.91	4.537	< 0.005	< 0.005	< 0.005	< 0.005	< 0.005	< 0.007	< 0.007	< 0.007	< 0.007
Er	46.60	41.85	36.04	48.53	22.78	32.46	13.86	< 0.018	< 0.018	< 0.018	< 0.018	< 0.018	< 0.03	< 0.03	0.30	< 0.03
Tm	6.570	5.818	5.21	6.704	3.199	4.84	2.008	< 0.005	< 0.005	< 0.005	< 0.005	< 0.005	< 0.007	< 0.007	(0.322)	< 0.007
Yb	45.21	41.05	38.39	46.32	23.06	34.05	14.20	< 0.02	< 0.02	< 0.02	< 0.02	0.35	< 0.05	< 0.05	< 0.05	< 0.05
Lu	5.668	5.145	4.69	5.987	3.074	4.40	1.850	< 0.005	< 0.005	< 0.005	< 0.005	< 0.005	< 0.009	< 0.009	< 0.009	< 0.009
Hf	(0.17)	(0.22)	< 0.04	< 0.10	< 0.10	0.17	< 0.10	< 0.04	< 0.04	< 0.04	< 0.04	< 0.04	< 0.10	< 0.10	< 0.10	< 0.10
Ta	0.139	0.888	0.62	0.366	0.588	0.17	0.546		< 0.006	< 0.006	< 0.006	< 0.006	< 0.011	< 0.011	< 0.011	< 0.011
Tl	13.02	1.12	0.5	1.35	5.24	0.6	8.48	< 0.13	< 0.13	< 0.13	< 0.13	< 0.13	< 0.15	< 0.15	(0.30)	< 0.15
Pb	6627.0	6820.8	7713.2	16516.2	109779.4	4544.3	12346.4	7.0	(0.3)	(0.3)	< 0.10	< 0.10	1.0	(0.4)	< 0.3	3.1
Bi	0.94	(0.12)	(0.07)	0.35	4.90	0.12	0.80	< 0.03	< 0.03	< 0.03	< 0.03	< 0.03	< 0.07	< 0.07	0.38	< 0.07
Th	(0.05)	(0.14)	< 0.03	(0.08)	(0.08)	0.33	< 0.05	< 0.03	< 0.03	< 0.03	< 0.03	< 0.03	< 0.05	< 0.05	0.42	< 0.05
U	(0.07)	< 0.04	(0.06)	(0.07)	0.26	(0.03)	0.38	(0.02)	< 0.02	< 0.02	< 0.02	< 0.02	< 0.04	< 0.04	0.52	< 0.04
Pb206/Pb207	1.1819	1.1813	1.1844	1.1842	1.1834	1.1826	1.1964		1.2579	1.1514	0.0000	3.1404	1.2765	1.3391	0.0000	1.1751
Pb208/Pb207	2.4016	2.4099	2.4033	2.4046	2.2823	2.4269	2.4568		2.3529	2.2730	1.1297	10.4524	2.2304	2.1510	0.0000	2.3655
Sm147/Nd144	0.3445	0.3559	0.3623	0.3602	0.3275	0.3674	0.3568		0.0000	0.0444	0.0891	0.5904	2.5908	0.0800	0.6041	0.0000
Rb87/Sr86	0.0051	0.0051	0.0029	0.0025	0.0111	0.0072	0.0175		13.3672	0.0000	0.0000	0.0009	0.1936	0.1482	0.0000	0.4387

values less than limit of detection (LOD) - <LOD

values less than effective limit of quantitation (ELOQ or LOQ) - (value)

Sample #	BLANK(B5)	BLANK(B6)	BLANK(flour	BLANK(NIT)	BMWV-10-1	CPV-4-A	CPV-4-B	CPV-4-C	CPV-4-D	CPV-4-E	CPV-4-F	CPV-4-G	CV-6	GNV-7	GNV-7*	GNV-7 (B1)
Analysis date	22-Oct-91	22-Nov-91	03-May-91	25-Sep-91	22-Oct-91	25-Sep-91	25-Jul-90	25-Jul-90	26-Jul-90	23-Sep-91	23-Sep-91	23-Sep-91	12-Jan-92	03-May-91	03-May-91	30-Aug-91
Dissolution	Boric Acid	Boric Acid	Boric Acid	Boric Acid	Boric Acid	Boric Acid	HF/HNO3	HF/HNO3	HF/HNO3	Boric Acid	Boric Acid	Boric Acid	HF/HNO3	Boric Acid	Boric Acid	Boric Acid
Li	(1.2)	< 0.7	< 0.7	< 0.7	< 0.7	(0.9)	< 0.3	< 0.3	< 0.3	3.9	(1.1)	< 0.7	107.2	< 0.7	< 0.7	< 0.7
Be	(11)	(9)	15	< 4	< 4	(14)	< 0.2	(0.2)	< 0.2	21	(10)	(9)	7.8	26	26	< 4
Sc	< 6	< 6	(10)	< 6	< 6	(7)	(4)	(4)	< 2	< 6	< 6	< 6	22	(10)	(9)	< 6
V	< 1.8	< 1.8	< 1.8	< 1.8	< 1.8	< 1.8	7	7	7	(4)	< 1.8	< 1.8	126	6.3	(5)	< 1.8
Cr	(47)	< 26		< 26	< 26	(72)	< 4	< 4	< 4	737	< 26	< 26	126			< 26
Cu	< 1.0	< 1.0		< 1.0	577.2	8.2				42.9	3.8	4.6	< 31			72.9
Zn	< 4	(5)		< 4	26	14				33	(11)	17	255			(7)
Rb	< 0.08	< 0.08	< 0.08	< 0.08	(0.3)	9.44				168.86	11.07	1.72	334.5	< 0.08	(0.1)	(0.2)
Sr	< 0.2	< 0.2	< 0.2	< 0.2	239.2	131.8	90.9	68.7	64.3	60.2	63.4	71.2	47.3	73.1	71.9	65.2
Y	(0.008)	0.1	0.2	< 0.006	401.0	405.9	352.8	292.5	239.6	277.5	262.9	340.8	36.6	712.2	708.4	677.2
Zr	< 0.4	< 0.4	< 0.4	< 0.4	2.4	3.9	1.3	(0.6)	1.1	95.2	9.4	(1.0)	94.2	(1.3)	(1.4)	6.1
Nb	< 0.010	< 0.010	< 0.010	(0.01)	0.2	1.2	0.3	0.2	0.1	11.8	1.8	0.6	17.9	0.2	0.2	0.3
Mo	< 0.05	< 0.05	< 0.05	< 0.05	1.72	1.58	1.6	1.2	1.0	15.35	3.31	7.04	1.0	13.22	9.33	0.82
Cs	< 0.012	< 0.012	< 0.012	< 0.012	(0.05)	(0.19)	< 0.03	< 0.03	< 0.03	1.53	(0.18)	(0.07)	19.54	(0.02)	(0.01)	(0.02)
Ba	(1.4)	< 0.5	< 0.5	(1.1)	6795.0	6187.5	338.6	100.9	227.9	853.2	390.0	459.2	905.8	4.0	5.7	5.4
La	< 0.008	< 0.008	(0.012)	< 0.008	7.092	10.640	10.08	8.18	6.78	9.584	8.768	8.743	46.89	24.208	23.961	21.510
Ce	< 0.009	< 0.009	0.030	< 0.009	17.346	23.507	21.73	17.86	14.48	25.707	20.130	20.353	93.68	56.854	55.958	50.575
Pr	< 0.005	< 0.005	< 0.005	< 0.005	2.968	3.058	2.83	2.33	1.89	2.987	2.518	2.694	10.80	7.596	7.587	6.732
Nd	< 0.06	< 0.06	< 0.06	< 0.06	14.68	13.53	12.00	10.00	8.47	12.73	11.22	11.77	40.30	34.54	33.60	30.76
Sm	< 0.03	< 0.03	< 0.03	< 0.03	7.03	5.85	5.24	4.25	3.20	6.04	4.56	5.08	7.46	9.66	9.48	8.66
Eu	< 0.012	< 0.012	< 0.012	< 0.012	0.507	0.118	0.29	0.26	0.23	0.323	0.240	0.256	1.42	1.056	0.984	0.925
Gd	< 0.04	(0.07)	(0.06)	< 0.04	18.66	16.48	10.13	8.16	6.88	11.41	8.99	11.29	6.87	16.01	16.73	14.41
Tb	< 0.007	< 0.007	0.023	< 0.007	3.387	2.614	2.21	1.82	1.41	2.578	1.858	2.351	0.98	3.554	3.578	3.206
Dy	< 0.02	< 0.02	< 0.02	< 0.02	26.80	18.35	15.68	12.50	9.77	18.02	13.06	16.98	6.03	29.05	29.36	25.77
Ho	(0.008)	< 0.007	< 0.007	< 0.007	6.199	3.954	3.25	2.57	2.07	3.812	2.772	3.582	1.24	7.610	7.739	6.650
Er	< 0.03	< 0.03	< 0.03	< 0.03	19.63	10.47	8.31	6.84	5.22	10.76	7.39	9.44	3.59	24.73	25.24	21.73
Tm	< 0.007	< 0.007	< 0.007	< 0.007	2.791	1.246	0.96	0.80	0.63	1.423	0.868	1.129	0.55	3.339	3.340	3.000
Yb	(0.08)	< 0.05	< 0.05	< 0.05	18.35	6.29	5.09	3.93	3.39	7.81	4.73	6.12	3.69	21.04	20.54	17.82
Lu	< 0.009	< 0.009	< 0.009	< 0.009	2.374	0.841	0.62	0.51	0.41	1.045	0.585	0.753	0.54	2.784	2.773	2.464
Hf	< 0.10	< 0.10	< 0.10	< 0.10	(0.30)	(0.15)	< 0.04	(0.06)	< 0.04	3.83	0.38	< 0.10	2.81	< 0.10	(0.16)	(0.24)
Ta	< 0.011	< 0.011	< 0.011	< 0.011	0.115	0.254	0.07	0.06	0.12	0.128	0.873	0.675	1.26	0.106	0.117	0.156
Tl	< 0.15	< 0.15	< 0.15	< 0.15	1.81	(0.15)	< 0.13	< 0.13	< 0.13	1.09	< 0.15	< 0.15	4.0	5.26	11.08	1.97
Pb	< 0.3	< 0.3	1.0	< 0.3	57694.0	10.0	3.6	5.3	5.3	70.9	36.8	86.7	35.2	7194.5	6421.4	6197.7
Bi	< 0.07	< 0.07	< 0.07	< 0.07	5.92	(0.14)	(0.04)	(0.05)	< 0.03	1.19	0.32	0.31	0.14	1.63	1.36	0.47
Th	< 0.05	< 0.05	< 0.05	< 0.05	0.21	0.42	(0.09)	(0.05)	0.16	8.19	0.73	(0.15)	12.50	(0.07)	(0.06)	0.36
U	< 0.04	< 0.04	< 0.04	< 0.04	4.74	0.13	< 0.02	(0.03)	(0.04)	1.35	0.21	(0.12)	2.72	0.16	(0.11)	(0.06)
Pb206/Pb207	2.8512	4.6297	1.1988	0.2192	2.2854	1.1508	1.1042	1.1615	1.1902	1.1987	1.1995	1.1906	1.1946	1.1855	1.1831	1.1854
Pb208/Pb207	20.0313	8.8188	2.6162	0.5203	0.2807	2.4407	2.2993	2.5028	2.3510	2.4329	2.4581	2.4517	2.4837	2.4178	2.4188	2.4491
Sm147/Nd14-	3.6288	0.0686	0.0000	0.0000	0.0031	0.2590	0.2645	0.2585	0.2269	0.2862	0.2592	0.2618	0.1108	0.1672	0.1676	0.1670
Rb87/Sr86		0.0000	2.1022	0.6158		0.2079	0.0032	0.0080	0.0208	8.1047	0.5075	0.0705	20.5210	0.0021	0.0042	0.0071

values less than limit of detection (LOD) - <LOD

values less than effective limit of quantitation (ELOQ or LOQ) - (value)

Sample #	GNV-7* (B1)	GNV-7 (B2)	GNV-7*(B2)	GNV-7(B2a)	GNV-7*(B3)	GNV-7(B4)	GNV-7(B5A)	GNV-7(B5)	GNV-7(B6)	GNV-7**(B6)	GNV-7*(B6)	GNV-7***(B	GNV-7	GNV-7*	GNV-8-A	GNV-8-B
Analysis date	30-Aug-91	04-Sep-91	04-Sep-91	12-Jan-92	22-Oct-91	25-Sep-91	22-Oct-91	22-Oct-91	22-Nov-91	22-Nov-91	18-Jan-92	23-Jan-93	16-Sep-87	25-Jul-90	30-Aug-91	30-Aug-91
Dissolution	Boric Acid	Boric Acid	Boric Acid	Boric Acid	Boric Acid	Boric Acid	Boric Acid	Boric Acid	Boric Acid	Boric Acid	Boric Acid	Boric Acid	HF/HNO3	HF/HNO3	Boric Acid	Boric Acid
Li	< 0.7	< 0.7	< 0.7	< 0.7	< 0.7	< 0.7	< 0.7	< 0.7	< 0.7	< 0.7	< 0.7	< 0.7	< 0.3	< 0.3	2.4	< 0.7
Be	(6)	(8)	(8)	(7)	< 4	18	< 4	(6)	(8)	(11)	(8)			< 0.2	< 4	(7)
Sc	< 6	< 6	< 6	< 6	< 6	< 6	(7)	< 6	< 6	< 6	< 6			(2)	(7)	< 6
V	< 1.8	< 1.8	< 1.8	< 1.8	< 1.8	< 1.8	< 1.8	< 1.8	< 1.8	< 1.8	< 1.8			8	(3)	< 1.8
Cr	< 26	< 26	< 26	< 26	< 26	< 26	< 26	(34)	< 26	< 26	< 26		< 4	< 4	< 26	< 26
Cu	70.4	65.4	65.0	72.2	79.3	55.3	48.6	41.4	57.2	53.8	52.8				36.5	18.1
Zn	(6)	(10)	(5)	(10)	(10)	(10)	< 4	(4)	25	24	(7)				177	25
Rb	< 0.08	< 0.08	< 0.08	(0.1)	< 0.08	< 0.08	< 0.08	< 0.08	< 0.08	< 0.08	< 0.08	< 0.08			5.61	0.58
Sr	64.7	65.9	60.7	66.1	66.6	71.8	68.4	64.5	70.2	65.5	70.6	68.7	78.6	54.1	86.9	78.6
Y	632.1	654.4	601.1	671.3	651.3	754.0	658.8	658.9	687.8	634.8	736.2	734.2	733.1	565.4	398.0	743.5
Zr	< 0.4	(1.4)	< 0.4	< 0.4	(0.5)	1.5	< 0.4	2.2	3.5	(0.5)	< 0.4	(1.4)	0.6	< 0.19	2.9	(1.3)
Nb	0.1	0.1	0.0	0.1	0.1	0.1	0.1	0.0	0.1	0.1	0.1	0.1		(0.02)	1.2	0.2
Mo	0.61	0.47	1.00	0.54	0.53	0.80	0.38	0.61	0.57	0.65	0.58	0.53		1.0	0.69	0.26
Cs	(0.02)	(0.02)	< 0.012	(0.02)	(0.02)	(0.02)	(0.02)	(0.02)	(0.02)	(0.02)	(0.02)	< 0.012	< 0.03	< 0.03	0.83	(0.10)
Ba	6.0	4.7	25.8	4.4	2.8	6.1	(1.6)	4.1	3.9	3.6	5.7	5.6	4.1	5.1	17.2	3.1
La	21.597	22.604	22.250	22.365	22.172	24.861	22.451	22.513	23.515	21.780	24.138	24.238	24.23	18.66	47.135	35.547
Ce	50.187	51.502	51.481	52.066	51.309	57.139	52.100	52.044	55.049	51.482	55.862	56.903	55.01	42.92	173.389	110.450
Pr	6.689	6.860	6.858	6.880	6.974	7.482	7.096	6.991	7.307	6.899	7.476	7.462	7.42	5.75	30.917	18.880
Nd	31.50	31.00	30.18	31.10	31.15	34.19	31.30	32.55	32.30	31.29	34.13	33.56	33.04	25.75	146.80	94.04
Sm	8.95	8.59	8.90	8.72	8.42	9.65	8.92	9.26	9.18	8.77	9.79	9.87	9.53	7.60	28.62	25.42
Eu	1.043	0.936	0.973	0.936	0.993	1.062	1.015	0.994	1.044	0.960	1.047	1.053	1.08	0.78	3.677	3.204
Gd	17.28	13.53	15.46	14.99	15.13	17.75	16.08	15.28	17.15	14.99	16.84	18.36	15.09	12.95	32.34	35.13
Tb	3.852	3.087	3.401	3.268	3.231	3.693	3.430	3.480	3.449	3.236	3.610	3.680	3.64	2.71	3.382	5.292
Dy	32.84	25.26	26.67	26.75	26.61	30.99	28.04	28.95	27.89	26.83	30.00	29.73	28.33	21.79	16.30	30.97
Ho	8.695	6.421	6.695	6.992	6.945	8.278	7.447	7.604	7.143	7.036	7.752	7.500	7.43	5.76	2.751	6.131
Er	28.53	20.60	21.42	23.08	22.76	26.72	24.47	24.53	23.91	23.24	25.31	25.34	24.07	18.88	5.74	14.23
Tm	3.728	2.774	2.887	3.116	3.100	3.712	3.239	3.390	3.217	3.101	3.460	3.336	3.28	2.50	0.495	1.351
Yb	22.45	16.62	18.70	18.55	19.13	22.96	20.24	20.41	19.63	19.38	21.27	20.73	19.87	15.19	2.19	5.78
Lu	3.044	2.030	2.203	2.573	2.598	3.117	2.876	2.621	2.689	2.550	2.812	2.756	2.73	2.10	0.265	0.700
Hf	< 0.10	(0.10)	< 0.10	< 0.10	< 0.10	(0.20)	< 0.10	0.39	0.56	< 0.10	< 0.10	(0.28)	0.16	< 0.04	< 0.10	< 0.10
Ta	0.138	0.091	0.050	0.109	0.175	0.122	0.167	0.243	0.172	0.144	0.090	0.121		0.05	0.530	0.096
Tl	1.62	(0.20)	(0.37)	4.08	< 0.15	(0.45)	< 0.15	(0.42)	(0.23)	(0.29)	5.89	2.29	2.0	(0.3)	(0.25)	< 0.15
Pb	5563.4	6547.5	5547.0	6664.0	6251.2	6222.3	7005.1	7102.5	6797.9	6063.0	6671.0	6765.5	ERR	6172.6	224.0	33.9
Bi	0.50	0.48	0.35	0.69	0.61	0.76	0.79	0.65	0.36	0.31	0.86	0.56	0.59	0.57	0.83	0.31
Th	0.20	(0.10)	< 0.05	< 0.05	(0.05)	0.39	< 0.05	(0.16)	0.32	(0.11)	< 0.05	< 0.05	(0.06)	< 0.03	0.64	0.24
U	(0.07)	(0.10)	(0.07)	(0.09)	(0.05)	(0.08)	< 0.04	0.12	(0.06)	(0.09)	(0.08)	(0.07)	0.10	(0.05)	0.61	0.35
Pb206/Pb207	1.1911	1.1926	1.1880	1.1825	2.4310	1.1519	2.4209	2.4253	1.1657	1.1969	1.1800	1.1905		1.1861	1.1828	1.2003
Pb208/Pb207	2.4305	2.4087	2.4250	2.4289	0.1647	2.4001	0.1695	0.1721	2.4276	2.4455	2.4753	2.4442		2.4171	2.4529	2.4040
Sm147/Nd144	0.1719	0.1719	0.1733	0.1692	0.0028	0.1698	0.0007	0.0027	0.1690	0.1710	0.1744	0.1805		0.1783	0.1171	0.1660
Rb87/Sr86	0.0000	0.0034	0.0000	0.0044		0.0033			0.0015	0.0010	0.0026	0.0013		0.0000	0.1868	0.0214

values less than limit of detection (LOD) - < LOD

values less than effective limit of quantitation (ELOQ or LOQ) - (value)

Sample #	GNV-8-C	GNV-8-C*	GNV-8-D	GNV-8-E	GNV-8-F	GNV-8-G	GNV-8-H	GNV-8-I	GNV-8-I	GNV-8-J	GNV-8-K	GNV-8-K*	GNV-8-K*	GNV-8-L	GNV-8-M	GNV-8-N
Analysis date	30-Aug-91	30-Aug-91	30-Aug-91	30-Aug-91	30-Aug-91	30-Aug-91	30-Aug-91	22-Nov-91	16-Sep-87	30-Aug-91	03-May-91	04-Sep-91	03-May-91	30-Aug-91	30-Aug-91	30-Aug-91
Dissolution	Boric Acid	Boric Acid	Boric Acid	Boric Acid	Boric Acid	Boric Acid	Boric Acid	Boric Acid	HF/HNO3	Boric Acid	Boric Acid	Boric Acid	Boric Acid	Boric Acid	Boric Acid	Boric Acid
Li	< 0.7	< 0.7	< 0.7	< 0.7	< 0.7	< 0.7	< 0.7	< 0.7	< 0.3	< 0.7	< 0.7	< 0.7	< 0.7	< 0.7	< 0.7	< 0.7
Be	(6)	(9)	(8)	(5)	(6)	(7)	(7)	(9)		(6)	28	(9)	29	(6)	(6)	(6)
Sc	< 6	< 6	< 6	< 6	< 6	< 6	< 6	< 6		< 6	(9)	< 6	(11)	< 6	< 6	< 6
V	< 1.8	< 1.8	< 1.8	< 1.8	< 1.8	< 1.8	< 1.8	< 1.8		< 1.8	(6)	< 1.8	(6)	< 1.8	< 1.8	< 1.8
Cr	< 26	< 26	< 26	< 26	< 26	< 26	< 26	< 26	< 4	< 26		< 26		< 26	< 26	< 26
Co	15.0	12.3	23.8	16.7	18.5	17.1	44.5	12.2		53.5		19.0		45.1	75.3	291.4
Zn	(8)	(5)	(11)	(5)	(7)	(6)	(9)	(9)		(9)		(5)		(9)	17	92
Rb	0.30	(0.2)	(0.2)	< 0.08	< 0.08	< 0.08	< 0.08	< 0.08		(0.2)	< 0.08	< 0.08	< 0.08	< 0.08	< 0.08	0.66
Sr	80.0	75.2	80.4	60.3	54.2	56.5	48.5	54.1	56.9	47.1	60.6	53.0	62.8	58.7	41.9	47.7
Y	722.2	683.2	1183.1	598.3	729.4	653.7	317.2	587.7	548.9	349.8	543.7	462.1	542.7	505.9	338.3	728.4
Zr	3.4	(3.9)	(1.0)	< 0.4	(0.6)	< 0.4	< 0.4	(0.5)	< 0.19	2.0	(1.2)	(1.2)	(0.9)	11.6	1.9	(1.1)
Nb	0.2	0.1	0.2	0.1	0.4	0.1	0.4	0.2		0.1	0.2	0.1	0.2	0.3	0.3	0.1
Mo	0.35	0.25	0.49	0.25	0.56	0.47	0.51	0.38		0.45	10.76	0.23	11.21	0.79	0.51	0.88
Cs	(0.04)	(0.04)	(0.04)	(0.02)	(0.02)	(0.02)	(0.04)	< 0.012	< 0.03	(0.02)	< 0.012	< 0.012	(0.01)	(0.02)	(0.08)	(0.14)
Ba	(1.3)	(1.2)	7.4	(1.0)	(0.9)	(1.0)	(1.6)	< 0.5	1.1	(1.1)	< 0.5	(1.5)	< 0.5	(1.3)	3.4	4.9
La	37.993	36.195	33.419	24.338	21.025	21.015	13.547	17.920	18.87	9.469	10.830	9.392	10.879	14.540	5.091	2.988
Ce	120.058	116.210	95.636	62.521	49.305	49.314	30.144	40.251	40.69	20.152	23.574	20.614	23.794	30.122	12.118	8.921
Pr	20.568	19.761	15.843	9.804	7.027	6.971	4.067	5.407	5.61	2.718	3.223	2.770	3.247	3.923	1.660	1.480
Nd	103.52	99.52	88.25	50.07	35.23	34.81	18.62	25.38	25.86	12.40	15.56	13.89	15.81	17.81	8.07	8.50
Sm	26.23	25.30	25.63	14.18	10.30	10.34	4.97	6.91	7.20	3.71	5.28	4.60	5.15	4.80	3.10	5.09
Eu	3.475	3.450	3.591	2.095	1.429	1.494	0.868	1.109	1.09	0.770	1.023	0.754	1.034	0.837	0.657	1.037
Gd	36.89	36.14	44.05	24.59	19.38	19.03	9.16	13.17	11.71	7.91	9.89	8.94	10.40	8.69	6.97	13.28
Tb	5.243	5.229	7.780	4.490	4.102	4.023	1.910	3.012	3.05	1.687	2.240	1.943	2.308	2.026	1.416	2.979
Dy	30.54	31.36	51.51	30.39	33.53	32.04	14.77	24.02	25.58	13.24	17.74	15.21	18.12	17.95	10.60	21.76
Ho	5.921	6.185	10.870	6.445	8.274	7.511	3.471	6.142	6.51	3.363	4.624	3.795	4.744	4.903	2.521	4.813
Er	13.53	14.35	26.77	16.25	24.54	21.50	10.14	19.59	21.35	10.24	15.13	12.81	15.32	16.62	7.40	12.84
Tm	1.218	1.288	2.439	1.611	2.877	2.450	1.223	2.637	2.74	1.328	2.101	1.736	2.108	2.395	0.913	1.466
Yb	5.81	5.61	10.66	7.28	15.29	12.97	7.20	16.19	16.55	8.26	14.05	10.54	14.30	17.13	5.35	7.49
Lu	0.852	0.847	1.206	0.916	1.999	1.703	0.960	2.170	2.27	1.081	1.878	1.379	1.802	2.368	0.708	0.832
Hf	< 0.10	(0.19)	(0.16)	< 0.10	< 0.10	< 0.10	< 0.10	< 0.10	< 0.04	(0.14)	< 0.10	< 0.10	< 0.10	(0.28)	< 0.10	(0.14)
Ta	0.144	0.114	0.133	0.138	0.404	0.144	0.325	0.464		0.078	0.128	0.070	0.081	0.340	0.181	0.165
Tl	< 0.15	< 0.15	< 0.15	< 0.15	< 0.15	< 0.15	< 0.15	< 0.15	< 0.13	< 0.15	< 0.15	< 0.15	< 0.15	< 0.15	(0.18)	(0.32)
Pb	21.3	19.2	25.8	20.4	22.4	36.9	24.8	13.3	16.0	15.9	11.9	6.1	11.6	25.8	113.0	357.3
Bi	0.39	0.42	0.90	0.62	0.36	(0.23)	0.27	< 0.07	(0.04)	< 0.07	0.58	< 0.07	0.41	< 0.07	< 0.07	(0.08)
Th	(0.10)	(0.10)	(0.07)	(0.16)	(0.06)	0.31	(0.08)	0.18	(0.03)	0.21	(0.09)	(0.06)	(0.07)	(0.06)	(0.09)	0.17
U	0.46	0.57	0.63	0.80	0.51	0.53	0.86	0.31	0.35	0.96	0.35	0.32	0.39	0.67	1.09	3.09
$^{206}Pb/^{207}Pb$	1.0881	1.2331	1.1280	1.1849	1.1552	1.1944	1.1739	1.2231		1.2061	1.1732	1.1143	1.1825	1.1651	1.1502	1.1741
$^{208}Pb/^{207}Pb$	2.3698	2.3933	2.4126	2.4872	2.4892	2.5173	2.4071	2.4866		2.5143	2.5185	2.4507	2.4074	2.4296	2.4348	2.4584
$^{143}Nd/^{144}Nd$	0.1541	0.1515	0.1851	0.1724	0.1788	0.1821	0.1614	0.1624		0.1802	0.2003	0.1944	0.1960	0.1628	0.2340	0.3633
$^{87}Sr/^{86}Sr$	0.0110	0.0066	0.0082	0.0000	0.0000	0.0000	0.0000	0.0012		0.0135	0.0004	0.0000	0.0000	0.0004	0.0009	0.0400

values less than limit of detection (LOD) - <LOD

values less than effective limit of quantitation (ELOQ or LOQ) - (value)

ICP-MS analytical data

St. Lawrence fluorite and related samples

Sample #	GNV-8-O	GNV-8-O	GNV-8-P	GNV-ST	HCT-111	HCT-187	HCT-187	HCT-188	HEV-1-A	HEV-1-B	HEV-1-C	HEV-1-D	HEV-1-E	ISV-1-A	ISV-1-B	ISV-1-C
Analysis date	22-Nov-91	16-Sep-87	22-Oct-91	12-Jan-92	16-Sep-87	16-Sep-87	12-Jan-92	16-Sep-87	04-Sep-91	04-Sep-91	04-Sep-91	25-Sep-91	25-Sep-91	04-Sep-91	04-Sep-91	25-Jul-90
Dissolution	Boric Acid	HF/HNO3	Boric Acid	Boric Acid	HF-HNO3	HF/HNO3	HF/HNO3	HF/HNO3	Boric Acid	Boric Acid	Boric Acid	Boric Acid	Boric Acid	Boric Acid	Boric Acid	HF/HNO3
Li	(1.8)	1.1	30.0	< 0.7	11.0	10.7	10.3	19.0	27.2	< 0.7	< 0.7	< 0.7	< 0.7	5.0	34.1	13.1
Be	(9)		27	(8)			15.7		(8)	(7)	(7)	(7)	15	(7)	(7)	(0.4)
Sc	< 6		< 6	< 6			< 2		< 6	< 6	< 6	< 6	< 6	< 6	< 6	< 2
V	(2)		15.5	< 1.8			< 1.3		< 1.8	< 1.8	< 1.8	< 1.8	< 1.8	< 1.8	(2)	8
Cr	< 26	< 4	104	< 26	323	453	< 4	152	< 26	< 26	< 26	< 26	< 26	< 26	(41)	(4)
Cu	397.2		4430.5	6.7			(61)		22.7	45.2	168.4	607.4	238.4	53.4	47.6	
Zn	347		12537	(4)			(67)		31	29	15	666	1198	35	23	
Rb	3.50		40.33	(0.1)			433.2		18.42	(0.3)	< 0.08	0.51	0.60	2.73	4.26	
Sr	66.3	66.1	117.5	67.9	11.7	15.2	11.5	23.8	68.6	86.4	87.3	45.9	52.8	45.5	44.7	41.0
Y	825.1	762.4	820.6	1103.6	120.6	128.7	116.9	95.5	818.0	1442.9	1326.7	838.9	804.8	631.1	711.6	714.0
Zr	(1.3)	1.9	34.8	(0.6)	364.3	290.4	279.3	262.2	12.0	1.5	< 0.4	(0.6)	(0.8)	2.1	6.7	4.5
Nb	0.5		1.2	0.2			65.2		1.7	0.2	0.2	0.3	0.3	1.0	0.8	0.8
Mo	2.11		2.82	0.22			9.5		2.90	1.40	3.16	1.48	2.00	0.48	0.77	2.3
Cs	0.62	0.59	10.59	(0.02)	4.39	6.76	5.41	1.70	1.57	(0.05)	(0.02)	(0.11)	(0.12)	(0.18)	(0.30)	0.25
Ba	25.3	29.7	3340.7	(0.5)	47.8	59.7	53.5	85.0	41.7	11.8	55.9	8.6	31.4	232.4	122.5	124.7
La	6.301	6.50	29.674	1.053	61.78	47.00	46.24	28.26	14.685	17.361	20.038	12.450	15.507	13.313	11.622	8.90
Ce	16.389	15.87	85.101	3.856	130.78	93.65	99.47	59.40	36.926	44.282	49.673	30.887	42.260	32.337	26.855	21.63
Pr	2.740	2.68	11.373	0.768	17.54	10.59	11.02	7.16	5.210	5.947	6.515	4.280	6.354	4.157	3.489	2.81
Nd	14.84	14.18	52.25	5.18	66.27	36.75	38.96	26.52	24.22	27.75	28.38	20.01	32.39	17.36	14.61	12.23
Sm	9.27	8.16	18.00	6.48	16.84	9.94	10.50	7.91	10.97	13.32	12.25	9.45	16.95	7.48	6.37	5.56
Eu	1.473	1.34	2.083	0.490	0.40	0.22	0.23	0.65	0.555	0.642	0.522	0.369	0.714	0.420	0.422	0.35
Gd	22.22	17.30	28.00	23.64	16.29	10.55	11.69	8.16	21.27	28.79	25.19	19.60	32.11	14.63	14.75	13.42
Tb	4.434	4.11	6.259	7.120	3.33	2.46	2.42	2.12	5.236	9.498	7.657	4.818	6.152	3.907	4.003	3.77
Dy	30.16	27.20	45.60	54.76	22.42	17.55	18.16	15.39	40.29	83.24	68.24	38.30	43.45	31.73	34.17	32.50
Ho	6.365	5.76	10.528	11.811	4.72	3.97	4.11	3.42	9.738	21.107	17.512	9.444	10.083	7.403	8.364	8.02
Er	16.01	14.72	31.39	29.66	15.07	12.85	13.64	11.39	31.41	67.30	57.07	28.24	29.43	22.83	26.50	25.70
Tm	1.750	1.63	4.239	3.127	2.26	2.11	2.22	1.83	4.185	8.709	7.145	3.502	3.815	3.046	3.451	3.57
Yb	9.21	8.40	27.89	13.94	14.75	14.94	15.49	12.73	28.12	53.67	47.89	22.57	24.18	19.27	20.41	22.45
Lu	1.083	0.97	3.882	1.440	2.03	2.16	2.17	1.84	3.470	6.460	5.932	2.666	3.136	2.678	2.716	3.12
Hf	< 0.10	(0.13)	2.49	(0.15)	14.12	15.99	15.80	15.01	0.65	(0.12)	< 0.10	< 0.10	< 0.10	< 0.10	0.40	0.19
Ta	0.248		0.380	0.072			1.45		1.309	0.092	0.061	0.109	0.324	0.782	0.297	0.17
Tl	(0.24)	0.4	4.80	< 0.15	1.2	2.2	1.3	1.0	< 0.15	< 0.15	(0.35)	10.18	(0.43)	< 0.15	< 0.15	< 0.13
Pb	739.5	828.1	20930.2	(0.6)	26.9	67.5	60.2	141.4	720.8	853.3	8733.4	20131.0	19711.4	88.7	94.9	498.9
Bi	(0.21)	(0.07)	5.43	< 0.07	0.61	1.25	1.17	0.35	0.99	(0.19)	0.90	84.18	33.26	0.44	0.98	3.76
Th	0.41	0.34	7.66	0.18	31.73	39.03	41.65	39.14	1.72	(0.14)	< 0.05	(0.06)	(0.12)	0.39	0.61	0.21
U	4.28	4.13	179.06	< 0.04	8.36	15.59	16.38	15.29	0.88	0.44	1.66	0.89	1.65	0.51	1.11	2.75
Pb206/Pb207	1.1907		2.4357	1.1626			1.2319		1.2126	1.2109	1.2036	1.0598	1.1767	1.1976	1.1987	1.2141
Pb208/Pb207	2.4173		0.2101	2.6399			2.4710		2.4800	2.4611	2.4604	0.0000	2.3926	2.3883	2.3962	2.4846
Sm147/Nd144	0.3723		0.9921	0.7416			0.1628		0.2721	0.2986	0.2672	0.2855	0.3162	0.2597	0.2546	0.2774
Rb87/Sr86	0.1540			0.0055			108.7254		0.7735	0.0087	0.0018	0.0323	0.0327	0.1739	0.2760	0.3133

values less than limit of detection (LOD) - <LOD

values less than effective limit of quantitation (ELOQ or LOQ) - (value)

Sample #	ISV-1-D	ISV-1-E	ISV-1-F	ISV-1-G	ISV-1-G	ISV-1-G*	LBV-7-A	LBV-7-B	LBV-7-C	LBV-7-D	LBV-7-D*	LBV-7-E	LBV-7-F	LBV-7-G	LBV-7-G	LBV-7-H
Analysis date	26-Jul-90	30-Aug-91	04-Sep-91	03-May-91	16-Sep-87	03-May-91	25-Sep-91	22-Oct-91	25-Sep-91	25-Sep-91	25-Sep-91	04-Sep-91	22-Oct-91	22-Oct-91	26-Jul-90	22-Oct-91
Dissolution	HF/HNO3	Boric Acid	Boric Acid	Boric Acid	HF/HNO3	Boric Acid	Boric Acid	Boric Acid	Boric Acid	Boric Acid	Boric Acid	Boric Acid	Boric Acid	Boric Acid	HF/HNO3	Boric Acid
Li	1.2	< 0.7	(0.8)	< 0.7	< 0.3	< 0.7	3.5	3.2	2.4	4.2	4.2	< 0.7	(1.0)	30.7	< 0.3	3.2
Be	(0.3)	(6)	(5)	(14)		27	26	< 4	26	24	21	(5)	< 4	31	< 0.2	< 4
Sc	(3)	< 6	< 6	< 6		(9)	(14)	< 6	(7)	(7)	(8)	< 6	< 6	< 6	< 2	< 6
V	6	< 1.8	< 1.8	(4)		(5)	(5)	(5)	< 1.8	(3)	(3)	< 1.8	< 1.8	9.9	< 1.3	(3)
Cr	< 4	< 26	< 26		< 4		(32)	87	(82)	(71)	121	(29)	< 26	86	< 4	206
Cu		36.6	2962.6				259.4	316.8	663.2	723.7	1144.0	44.4	214.2	441.4		233.3
Zn		< 4	70				2319	1560	2179	2286	3320	< 4	32275	23440		656
Rb		< 0.08	< 0.08	< 0.08		< 0.08	59.40	24.00	11.27	11.52	12.76	1.41	3.58	16.48		5.36
Sr	77.4	129.8	32.0	28.2	34.5	29.1	953.6	2493.5	3030.5	2391.0	2742.5	685.7	754.9	4581.4	358.3	3119.9
Y	1093.8	1058.2	460.9	829.8	826.1	816.2	913.5	872.0	1055.7	988.6	980.5	310.0	566.6	336.8	16.4	774.3
Zr	1.9	< 0.4	< 0.4	2.4	5.6	(1.0)	9.3	10.2	3.6	3.1	4.1	< 0.4	1.5	5.6	< 0.19	1.5
Sb	0.4	0.1	0.1	0.2		0.2	0.8	4.8	2.0	1.4	1.3	0.1	0.6	0.5	(0.02)	2.2
Mo	0.3	0.26	1.15	8.22		9.77	1.22	2.88	3.55	3.03	3.31	0.83	0.97	5.39	0.7	7.17
Cs	< 0.03	< 0.012	< 0.012	< 0.012	< 0.03	< 0.012	23.69	8.85	5.53	4.47	4.60	0.92	1.76	6.31	0.24	2.76
Ba	85.3	12.7	292.0	64.7	56.1	51.9	8096.8	14691.4	8696.0	12720.8	7525.7	1529.5	8306.6	220927.3	3010.1	26706.5
La	8.46	12.587	6.401	(0.4371)	0.47	(0.3017)	36.443	23.359	30.125	24.956	24.681	8.705	14.868	19.274	0.56	22.055
Ce	21.99	30.567	16.656	1.330	1.31	1.215	85.224	56.711	76.567	64.414	62.530	22.206	37.338	25.159	1.03	53.645
Pr	3.30	4.267	2.387	(0.232)	0.24	(0.222)	12.708	8.086	11.204	9.500	9.449	3.378	5.548	3.678	0.15	7.806
Nd	16.17	20.24	12.21	1.34	1.52	1.27	58.60	37.98	51.80	46.46	46.14	15.73	28.00	17.53	0.68	36.87
Sm	10.60	11.19	6.65	1.80	1.88	1.63	21.68	15.60	21.45	20.14	19.80	7.17	12.29	7.69	0.38	15.36
Eu	0.62	0.726	0.341	0.164	0.18	0.126	4.246	2.499	3.525	2.901	2.989	0.804	1.591	0.048	0.75	2.478
Gd	25.33	29.24	16.06	10.13	9.90	8.11	41.61	34.01	46.76	38.92	42.13	14.04	26.22	13.46	0.61	38.10
Tb	6.57	7.793	3.288	3.628	3.61	2.948	7.256	6.197	8.243	7.957	7.579	2.610	4.501	2.744	0.11	6.057
Dy	51.02	61.86	23.96	31.03	30.90	25.29	50.34	45.06	58.56	54.70	53.44	16.63	29.35	18.50	0.73	42.06
Ho	11.79	14.268	5.312	7.187	7.39	5.829	10.517	9.739	12.216	11.503	11.268	3.377	6.097	3.861	0.16	8.939
Er	32.74	40.76	14.68	18.66	19.53	15.96	28.41	25.49	32.04	30.18	29.56	8.81	15.34	10.63	0.42	23.40
Tm	4.10	5.797	1.910	2.091	2.09	1.736	3.246	3.138	3.712	3.227	3.233	0.925	1.666	1.360	0.05	2.688
Yb	21.17	24.59	11.67	10.15	10.09	8.37	14.55	15.40	17.04	14.25	13.94	3.95	8.45	6.86	0.36	11.69
Lu	2.55	2.866	1.788	1.158	1.17	0.899	1.684	1.715	2.093	1.698	1.603	0.442	0.913	0.798	0.03	1.443
Hf	< 0.04	< 0.10	(0.12)	< 0.10	0.28	< 0.10	(0.29)	1.19	(0.27)	(0.12)	(0.24)	< 0.10	< 0.10	0.85	< 0.04	(0.12)
Ta	0.03	(0.09)	0.094	0.107		0.049	0.090	2.440	1.672	1.312	1.236	0.096	0.712	5.285	(0.01)	1.893
Tl	< 0.13	< 0.15	< 0.15	< 0.15	< 0.13	< 0.15	0.63	0.72	< 0.15	(0.48)	(0.46)	1.34	6.79	3.11	< 0.13	1.03
Pb	388.8	3.9	198.6	62.5	55.1	75.4	132.3	110.6	133.0	865.1	758.0	112.9	160518	22705.3	236.7	144.9
Bi	4.65	(0.13)	(0.12)	1.61	0.44	0.96	(0.14)	0.28	0.29	(0.24)	(0.21)	< 0.07	1.05	0.70	< 0.03	0.29
Th	0.22	< 0.05	< 0.05	(0.09)	(0.09)	(0.06)	0.51	1.00	0.21	0.31	0.33	< 0.05	(0.14)	0.39	< 0.03	(0.12)
U	11.56	0.75	4.30	1.24	1.03	1.26	0.22	0.20	0.31	0.21	0.25	(0.06)	(0.07)	1.08	(0.04)	0.16
Pb206/Pb207	1.2068	1.1681	1.2113	1.2249		1.1657	1.1681	2.4633	1.1528	1.1602	1.1731	1.1709	2.4081	2.4416	1.1884	2.4203
Pb208/Pb207	2.4805	2.4071	2.4058	2.5239		2.4567	2.4254	0.2521	2.4165	2.4365	2.4569	2.4225	0.2665	0.2667	2.4797	0.2527
Sm147/Nd144	0.3829	0.3326	0.3218	0.7928		0.7636	0.2217	0.0278	0.2481	0.2614	0.2575	0.2723	0.0138	0.0104	0.3353	0.0050
Rb87/Sr86	0.0128	0.0000	0.0019	0.0000		0.0000	0.1805		0.0107	0.0139	0.0135	0.0060			0.0072	

values less than limit of detection (LOD) - <LOD

values less than effective limit of quantitation (ELOQ or LOQ) - (value)

ICP-MS analytical data

St. Lawrence fluorite and related samples

Sample #	LC-1	LP-2-A	LP-2-B	LP-2-B*	LP-2-C	LP-2-D	LP-2-E	LP-2-F-H	LP-2-I	LP-2-J	LP-2-K	LP-2-L	NBS-79A(B4)	NBS-79A(B5)	NBS-79A(Be)	RHY-1
Analysis date	22-Nov-91	22-Oct-91	22-Oct-91	22-Oct-91	25-Sep-91	25-Sep-91	25-Sep-91	25-Sep-91	25-Sep-91	22-Oct-91	25-Sep-91	25-Sep-91	25-Sep-91	22-Oct-91	22-Nov-91	22-Nov-91
Dissolution	Boric Acid	Boric Acid	Boric Acid	Boric Acid	Boric Acid	Boric Acid	Boric Acid	Boric Acid	Boric Acid	Boric Acid	Boric Acid	Boric Acid	Boric Acid	Boric Acid	Boric Acid	Boric Acid
Li	< 0.7	3.0	6.3	3.8	(2.3)	(2.2)	(0.8)	(1.2)	(0.8)	5.0	2.7	< 0.7	< 0.7	< 0.7	< 0.7	< 0.7
Be	(8)	< 4	(7)	< 4	20	18	24	24	(13)	16	(12)	(12)	15	< 4	(11)	(7)
Sc	< 6	< 6	(8)	(13)	< 6	< 6	< 6	< 6	< 6	(9)	(7)	< 6	< 6	< 6	< 6	< 6
V	< 1.8	< 1.8	< 1.8	< 1.8	< 1.8	< 1.8	< 1.8	< 1.8	< 1.8	< 1.8	(3)	< 1.8	< 1.8	< 1.8	< 1.8	< 1.8
Cr	< 26	(41)	(37)	< 26	< 26	228	< 26	< 26	349	160	932	317	< 26	< 26	< 26	< 26
Cu	3.6	34.5	67.9	59.3	32.5	255.7	11.1	87.4	84.3	218.4	403.9	91.2	5.5	6.2	5.8	27.9
Zn	(10)	223	449	413	125	97	(10)	23	14	22	41	(9)	(9)	16	15	(9)
Rb	(0.1)	35.52	51.03	46.12	7.99	5.32	(0.2)	2.62	3.09	2.61	4.62	0.39	(0.2)	(0.2)	(0.2)	< 0.08
Sr	19.9	236.4	91.4	84.1	174.3	743.9	320.2	2944.5	515.0	388.0	179.5	148.2	287.2	267.6	349.5	82.1
Y	564.1	565.5	472.6	423.0	1272.2	547.4	1108.9	906.8	733.4	392.9	389.5	438.0	1.1	1.1	1.2	1031.6
Zr	4.5	7.3	18.6	14.7	2.6	(1.4)	1.7	(0.9)	< 0.4	3.6	< 0.4	(0.9)	< 0.4	< 0.4	< 0.4	(0.2)
Nb	0.1	3.1	3.3	2.7	0.6	1.6*	0.2	0.8	1.5	0.6	3.3	1.4	0.1	0.0	0.1	0.1
Mo	4.14	1.05	0.35	0.25	1.73	4.58	0.71	0.48	4.83	1.24	9.31	5.22	0.83	0.50	0.86	2.45
Cs	(0.03)	1.59	2.88	2.65	0.42	(0.30)	(0.02)	0.59	0.65	0.58	(0.35)	(0.07)	(0.02)	(0.03)	(0.02)	(0.01)
Ba	70.5	4826.2	1621.8	1423.8	4260.6	10922.0	8103.9	16927.8	4899.8	16107.8	4070.6	3708.5	150.1	161.2	195.5	89.8
La	(0.385)	48.918	43.352	38.777	25.784	26.877	19.382	28.267	27.989	13.323	11.297	10.204	(0.131)	(0.124)	(0.129)	5.613
Ce	0.998	113.464	102.333	91.867	61.635	63.305	45.288	65.095	66.655	31.085	26.660	26.595	0.281	0.251	0.271	15.160
Pr	(0.198)	13.326	12.469	11.056	8.364	8.292	6.421	8.949	9.021	4.352	4.019	3.934	(0.044)	(0.029)	(0.047)	2.433
Nd	1.03	50.78	48.48	43.90	39.99	35.91	30.41	39.75	40.89	20.41	19.09	18.23	(0.17)	(0.13)	0.25	13.09
Sm	1.27	16.94	14.89	13.44	20.72	14.37	16.65	20.40	16.99	7.93	7.30	7.72	(0.1)	< 0.03	(0.1)	8.36
Eu	0.123	1.393	1.140	1.061	2.678	1.693	2.203	2.016	1.660	0.813	1.183	0.970	(0.027)	(0.020)	(0.032)	0.558
Gd	6.60	25.95	20.69	19.15	41.49	30.04	36.54	46.37	34.92	20.87	18.21	19.26	0.25	0.21	0.46	22.20
Tb	2.217	6.004	4.935	4.153	10.260	5.034	8.105	9.605	7.268	3.095	3.272	3.411	(0.011)	(0.019)	(0.018)	5.541
Dy	19.43	46.87	37.40	32.22	85.00	35.60	63.52	76.01	54.54	23.18	23.76	25.76	0.12	(0.08)	0.14	41.80
Ho	4.453	11.233	9.051	7.579	19.974	7.716	14.298	18.152	12.928	5.355	5.652	5.833	(0.021)	(0.015)	0.027	9.275
Er	13.11	37.97	29.78	25.18	68.14	22.60	44.99	60.49	40.83	16.69	16.41	17.97	(0.04)	< 0.03	(0.10)	25.28
Tm	1.190	5.784	4.702	3.863	8.711	3.118	6.583	8.967	5.389	2.371	2.307	2.473	(0.012)	< 0.007	(0.008)	2.966
Yb	5.54	44.33	33.90	29.33	55.70	18.20	40.91	62.14	35.28	14.46	14.07	16.70	< 0.05	(0.06)	(0.07)	15.12
Lu	0.587	6.335	4.716	4.199	7.098	2.231	5.551	7.988	4.716	1.913	1.881	2.147	< 0.009	< 0.009	< 0.009	1.813
Hf	(0.30)	0.35	0.90	0.90	(0.26)	< 0.10	(0.17)	(0.13)	(0.23)	0.50	< 0.10	< 0.10	< 0.10	< 0.10	< 0.10	< 0.10
Ta	0.075	0.195	0.195	0.161	0.182	1.077	0.311	1.040	0.901	1.828	0.961	0.999	(0.029)	0.079	0.158	0.063
Tl	< 0.15	(0.41)	(0.40)	< 0.15	< 0.15	< 0.15	< 0.15	< 0.15	< 0.15	(0.24)	< 0.15	< 0.15	< 0.15	< 0.15	< 0.15	< 0.15
Pb	13.6	738.9	1140.9	973.4	1476.6	2541.4	609.3	185.6	147.1	679.7	1240.3	212.3	3.0	2.4	2.4	24.2
Bi	< 0.07	0.58	0.63	0.39	(0.20)	0.26	< 0.07	(0.08)	(0.12)	0.28	0.31	(0.13)	< 0.07	< 0.07	< 0.07	(0.11)
Th	(0.15)	1.71	3.29	3.08	0.36	0.37	(0.10)	(0.07)	< 0.05	0.23	< 0.05	< 0.05	0.24	(0.16)	0.37	(0.16)
U	2.41	1.76	1.88	1.39	0.46	1.00	0.18	2.86	0.89	2.03	1.43	0.35	0.13	(0.08)	0.17	0.14
Pb206/Pb207	1.4951	2.4506	2.4582	2.4633	1.1879	1.1927	1.1821	1.1909	1.1945	2.4695	1.1891	1.2040	1.2143	2.4633	1.3143	1.2215
Pb208/Pb207	2.3907	0.2001	0.1849	0.1861	2.4510	2.4538	2.4362	2.4377	2.4292	0.2287	2.4572	2.4766	2.5937	0.1529	2.4940	2.4764
Sm147/Nd144	0.7476	0.4355	1.6295	1.5892	0.3118	0.2395	0.3236	0.3052	0.2516	0.0194	0.2289	0.2522	0.2355	0.0017	0.2066	0.3873
Rb87/Sr86	0.0120				0.1329	0.0207	0.0022	0.0026	0.0174		0.0740	0.0076	0.0020		0.0012	0.0025

values less than limit of detection (LOD) - <LOD

values less than effective limit of quantitation (ELOQ or LOQ) - (value)

Sample #	SCVV(A)-A	SCVV(A)-B	SCVV(A)-C	SCVV(A)-C*	SDMS-2-A	SDMS-2-B	SDMS-4	SY-2 (B1)	SY-2(1)	SY-2(2)	SY-2(3)	SY-2(4)	SY-2(5)	SY-2(6)	SY-2(7)
Analysis date	22-Oct-91	22-Oct-91	25-Jul-90	25-Jul-90	15-Mar-89	15-Mar-89	12-Jan-92	30-Aug-91	16-Sep-87	25-Jul-90	26-Jul-90	15-Mar-89	15-Mar-89	18-Apr-89	19-Apr-89
Dissolution	Boric Acid	Boric Acid	HF/HNO3	HF/HNO3	Na2O2 Sint	Na2O2 Sint	HF/HNO3	Boric Acid	HF/HNO3	HF/HNO3	HF/HNO3	Na2O2 Sint	Na2O2 Sint	Na2O2 Sint	Na2O2 Sint
Li	< 0.7	< 0.7	2.2	2.0			59.0	24.9	[01.5	98.4	[05.6				
Be	< 4	< 4	(0.4)	(0.5)			18.2	(12)		24.5	24.2				
Sc	< 6	< 6	< 2	(2)			< 2	(6)		9	(7)				
V	< 1.8	< 1.8	7	6			< 1.3	14.9		51	51				
Cr	< 26	< 26	< 4	< 4			< 4	< 26	232	216	213				
Cu	27.8	49.6					< 31	5.4							
Zn	(6)	23					(56)	82							
Rb	< 0.08	< 0.08					340.0	7.39							
Sr	114.0	92.8	92.6	94.0			4.7	36.3	291.7	270.1	271.5				
Y	185.9	200.6	551.2	558.9	78.4	75.4	46.4	95.0	122.8	119.2	118.9	110.2	103.3	104.8	111.8
Zr	< 0.4	< 0.4	0.8	1.5	33.3	127.9	314.4	63.1	262.9	263.6	275.9	251.1	233.5	222.1	231.0
Nb	0.0	0.1	0.1	0.1	2.0	54.3	60.5	10.5		32.1	31.8	22.3	24.6	21.9	26.2
Mo	0.24	0.41	0.9	0.9			6.1	0.38		0.5	0.7				
Cs	(0.02)	(0.02)	< 0.03	< 0.03			6.27	(0.24)	2.64	2.69	2.68				
Ba	1161.1	5.8	4816.3	4869.4	234.6	530.3	48.2	22.0	434.3	454.2	458.6	434.9	419.2	423.0	434.9
La	31.866	23.161	3.73	3.77	137.14	41.70	25.34	61.575	66.64	70.52	70.70	66.90	63.63	64.32	67.58
Ce	84.723	58.682	8.64	8.64	210.76	75.47	54.68	143.485	150.73	164.89	165.68	151.19	148.32	148.33	151.63
Pr	10.053	7.096	1.44	1.48	18.58	8.73	6.39	17.115	18.83	20.39	20.46	19.30	18.72	18.77	19.34
Nd	36.36	26.34	7.17	7.36	49.03	29.02	22.80	64.65	70.65	76.05	75.38	71.34	68.53	67.88	71.69
Sm	8.96	5.85	5.04	4.96	9.75	7.56	5.63	13.01	14.91	15.87	16.28	15.36	14.68	14.00	15.28
Eu	0.258	0.283	0.64	0.81	0.11	< 0.003	0.08	2.031	2.29	2.46	2.45	2.28	2.19	2.20	2.19
Gd	9.73	6.99	13.89	14.14	7.75	7.34	5.18	14.74	14.59	18.02	18.87	14.02	13.00	13.05	13.49
Tb	1.675	1.313	3.50	3.45	2.14	1.73	1.05	2.428	2.73	2.97	2.96	2.88	2.75	2.72	2.85
Dy	11.82	9.46	24.28	24.30	16.47	12.70	8.27	16.51	19.29	20.01	20.21	19.64	18.62	18.59	19.05
Ho	2.767	2.474	5.18	5.19	3.80	2.83	1.93	3.699	4.33	4.59	4.57	4.57	4.29	4.22	4.36
Er	9.51	8.79	14.18	13.89	13.35	9.71	6.75	12.01	14.78	15.08	15.29	15.31	14.04	14.07	14.72
Tm	1.685	1.482	1.73	1.70	2.36	1.66	1.16	1.869	2.30	2.48	2.49	2.47	2.25	2.26	2.33
Yb	14.67	12.24	9.83	9.78	16.96	11.82	8.23	12.19	16.80	17.73	18.04	17.69	16.18	16.22	16.82
Lu	2.581	1.991	1.23	1.27	2.53	1.80	1.19	1.742	2.78	2.97	3.01	2.99	2.64	2.69	2.79
Hf	< 0.10	< 0.10	(0.13)	(0.08)	1.16	4.79	14.11	2.05	8.91	8.32	8.28	8.98	7.71	6.95	7.15
Ta	0.325	0.111	0.99	0.98	0.56	0.77	1.57	< 0.011		1.81	1.94	1.92	2.15	1.33	2.19
Tl	< 0.15	< 0.15	< 0.13	< 0.13			2.3	(0.15)	1.4	1.6	1.5				
Pb	22.5	70.6	48.6	48.6			48.6	80.7	59.0	95.9	94.3				
Bi	< 0.07	(0.08)	(0.04)	(0.07)			0.71	(0.10)	0.14	0.16	0.16				
Th	< 0.05	< 0.05	0.38	0.29	33.72	44.28	23.68	356.70	297.13	393.50	383.51	368.63	327.08	354.17	365.96
U	(0.08)	(0.06)	0.09	0.07			6.03	260.98	210.21	291.08	289.99				
Pb206/Pb207	2.5199	2.4930	1.2105	1.2176			1.2068	9.3725		7.7912	7.9755				
Pb208/Pb207	0.1488	0.1347	2.5006	2.4979			2.4598	4.4502		4.0323	4.0762				
Sm147/Nd144	0.0012	0.0008	0.4296	0.4045	0.1203	0.1575	0.1469	0.1208		0.1253	0.1290	0.1302	0.1294	0.1244	0.1286
RNF/Sr86			0.0058	0.0000			211.7200	0.5938		2.3145	2.2779				

values less than limit of detection (LOD) - < LOD

values less than effective limit of quantitation (ELOQ or LOQ) - (value)

B XRF

The vein and host rock samples were analyzed by XRF for selected trace and major (some semi-quantitative) elements using a pressed powder pellet technique. Samples SDMS-4, BBS-84-64 and CV-6 were analyzed for quantitative major elements using a fused bead XRF method. Two control samples were used to monitor the precision and accuracy (Ca and Si only) of the method for fluorite analysis. These samples were: (1) National Bureau of Standards (NBS) reference material 79a (acid-grade fluorspar concentrate); and (2) an internal control sample GNV-7 (coarsely crystalline fluorite) which was also extensively analyzed for trace elements by ICP-MS. An outline of the analytical method and tabulation of results from standards and samples are presented in the following section.

This brief outline of the analytical procedure and discussion of detection limits is taken primarily from Longerich (in press). The XRF data for the study was obtained using a FISONS/ARL 8420+ sequential wavelength dispersive X-ray spectrometer. It is equipped with one goniometer that is capable of holding 6 analyzing crystals. In this study 5 crystals were used, including a LiF200-H crystal, which is specially treated for enhanced heavy element sensitivity. All samples, including control samples and standards, were prepared as pressed pellets using the standard sample preparation procedure:

1 weigh 5.00 g (± 0.10 g) of sample powder into a clean 100 ml glass jar

2 add 0.70 g (± 0.10 g) of BRP-5933 Bakelite phenolic resin to the sample (add up to 0.05 g more or less for samples of lower or higher density than average silicate rocks)

3 mix powder well with spatula, add two clean 13 mm stainless steel ball bearing and firmly place a clean plastic lid on the jar

4 place the jar on a roller mixer for 10 minutes to thoroughly mix the powder and resin

5 carefully transfer the mixed sample into a cleaned Herzog pellet press (29 mm diameter mould) and press at a pressure of 20 tonne for 5 seconds

6 place pressed pellet on a flat stainless steel sheet and bake in an oven at 200°C for 15 minutes

7 label pellet on the side which was adjacent to the metal sheet and store in a clean container

The "Poisson" limit of detection (LOD), from Poisson counting statistics, is determined for each individual run. The value is reported as 3 times the Poisson standard deviation of the blanks of all pellets in the run. The LOD, presented in the table below, was compiled by Longerich (in press) from the means of 5 individual runs. He found a general agreement between the Poisson and Average rock (calculated from a SiO_2 blank pellet) indicating that the variation in the LOD is primarily due to counting statistics alone and other sources of error make only a small contribution to the total variance. The following Poisson LOD values (Longerich, in press) were used in the statistical analysis of the samples from this study. The limit of quantification (LOQ) was estimated as 10 times the Poisson standard deviation (or 3.33 times the LOD).

Poisson limits of detection for XRF analyses (pressed pellet)

Element	LOD	LOQ	Element	LOD	LOQ
SiO_2	.006%	.020%	Sc	6 ppm	20 ppm
TiO_2	.002%	.007%	V	6 ppm	20 ppm
Al_2O_3	.004%	.013%	Cr	7 ppm	23 ppm
Fe_2O_3	.002%	.007%	Ni	4 ppm	13 ppm
MnO	.001%	.003%	Cu	3 ppm	10 ppm
MgO	.010%	.03%	Zn	2 ppm	7 ppm
CaO	.002%	.007%	Ga	2 ppm	7 ppm
Na_2O	.010%	.03%	As	13 ppm	43 ppm
K_2O	.010%	.03%	Rb	0.7 ppm	2 ppm
P_2O_5	.003%	.01%	Sr	1.1 ppm	4 ppm
			Y	0.6 ppm	2 ppm
S	11 ppm	37 ppm	Zr	1.0 ppm	3 ppm
Cl	20 ppm	67 ppm	Nb	0.6 ppm	2 ppm
			Ba	18 ppm	60 ppm
			Ce	36 ppm	120 ppm
			Pb	4 ppm	13 ppm
			Th	3 ppm	10 ppm
			U	3 ppm	10 ppm

Fluorite Reference Material NBS-79a

XRF analysis (pressed pellet)

Replicate analyses n = 7

Run #	T930225T	T910827A	T911003T	T910818T	T910817T	T910910T	T910919T	mean	SD	RSD	2SL(m)
Major elements											
SiO2	1.15%	1.26%	(1.30%	1.29%	1.30%	1.31%	1.30%	1.27%	0.05%	4%	0.04%
TiO2	<0.002%	<0.002%	(0.002%)	(0.002%)	(0.004%)	(0.003%)	(0.003%)	(0.003%)	(0.002%	86%	(0.003)%
Al2O3	0.080%	0.140%	0.174%	0.169%	0.166%	0.174%	0.174%	0.158%	0.032%	21%	0.024%
Fe2O3	0.000%	0.020%	0.057%	0.054%	0.060%	0.056%	0.061%	0.054%	0.010%	19%	0.008%
MnO	<0.002%	<0.002%	(0.003%)	<0.002%	(0.002%)	<0.002%	(0.003%)	<0.002%	NA	NA	NA
MgO	<0.010%	<0.010%	<0.010%	<0.010%	<0.010%	<0.010%	<0.010%	<0.010%	NA	NA	NA
CaO	70.1%	70.3%	70.3%	70.4%	70.3%	70.0%	70.6%	70.3%	0.2%	0%	0.1%
Na2O	<0.010%	<0.010%	(0.025%)	<0.010%	<0.010%	<0.010%	(0.022%)	(0.010%)	0.008%	81%	0.006%
K2O	<0.002%	<0.002%	0.008%	0.007%	0.007%	0.007%	0.007%	(0.006%)	0.001%	33%	0.002%
P2O5	(0.003%)	<0.003%	(0.007%)	(0.006%)	(0.008%)	(0.006%)	(0.007%)	(0.006%)	0.003%	41%	0.002%
S ppm	305	562	760	626	604	626	664	593	131	22%	99
Cl ppm	100	(56)	146	134	121	127	171	128	40	31%	30
LOI			1.20%	1.40%				1.30%	0.10%	8%	0.14%
Trace elements											
Sc	29	45	46	45	46	29	50	43	10	23%	3
V	<6	<6	<6	<6	<6	(7)	(6)	<6	NA	NA	NA
Cr	<7	(14)	(15)	(16)	(12)	(11)	(15)	(12)	4	32%	3
Ni	<4	<4	<4	<4	(7)	(8)	<4	<4	NA	NA	NA
Cu	12	10	(8)	(10)	(9)	(9)	12	(10)	2	16%	1
Zn	(4)	<2	17	7	(5)	(6)	12	7	5	67%	4
Ga	<2	<2	(6)	<2	<2	<2	<2	<2	NA	NA	NA
As	(26)	(19)	68	(24)	<13	(21)	(18)	(26)	18	69%	14
Rb	<0.7	<0.7	<0.7	<0.7	<0.7	<0.7	<0.7	<0.7	NA	NA	NA
Sr	236	225	207	206	207	205	209	211	10	5%	8
Y	(1.6)	(1.9)	(1.8)	(1.7)	(1.9)	(1.7)	(1.6)	(1.8)	0.1	7%	0.1
Zr	<1.0	(3.0)	(2.8)	<1.0	(2.6)	(3.3)	<1.0	(1.9)	1.2	63%	0.9
Nb	<0.6	(0.7)	<0.6	<0.6	<0.6	<0.6	(0.9)	<0.6	NA	NA	NA
Ba	220	302	451	337	317	329	321	327	63	19%	46
Ce	<36	(45)	<36	<36	<36	(37)	<36	<36	NA	NA	NA
Pb	(6)	28	26	28	26	27	26	24	7	31%	6
Th	<3	<3	<3	<3	<3	<3	<3	<3	NA	NA	NA
U	<3	<3	<3	<3	<3	<3	<3	<3	NA	NA	NA

Calculated								mean	Accepted	Rel. diff. (%)[1]
CaF2	97.6%	97.8%	97.9%	97.9%	97.9%	97.5%	98.2%	97.8%	97.4%	0.3%
SiO2	1.15%	1.26%	1.30%	1.29%	1.30%	1.31%	1.30%	1.27%	0.67%	89.0%
CaF2[1]	97.2%	97.3%	97.5%	97.5%	97.4%	97.1%	97.8%	97.4%	97.3%	0.0%
SiO2[1]	0.61%	0.66%	0.68%	0.68%	0.68%	0.69%	0.69%	0.67%	0.67%	0.0%
BaSO4[2]	0.04%	0.05%	0.06%	0.06%	0.05%	0.06%	0.05%	0.06%		
SrSO4[2]	0.05%	0.04%	0.04%	0.04%	0.04%	0.04%	0.04%	0.04%		
Fe2O3	0.03%	0.06%	0.06%	0.05%	0.06%	0.06%	0.06%	0.05%		
Al2O3	0.08%	0.14%	0.17%	0.17%	0.17%	0.17%	0.17%	0.15%		
(REE,Y)F3[3]								0.03%		
PbS	0.00%	0.00%	0.00%	0.00%	0.00%	0.00%	0.00%	0.00%		
LOI	1.20%	1.40%						1.30%		
TOTALS	99.2%	99.7%	99.5%	99.5%	99.4%	99.1%	99.5%	99.7%		

Notes:
[1] Corrected to recommended value for NBS-79A
[2] All Ba and Sr assumed to occur as accessory sulphate phases
[3] All REE and Y assumed to occur as fluoride
Values less than the limit of detection (LOD) = <(LOD)
Values less than the limit of quantification (LOQ) = (value)

Fluorite Control Sample CNV-7

XRF analysis (pressed pellet) *Replicate analysis n = 7*

Run #	T9100919T	T9100918T	T9110903T	T9109077T	T9109110T	T9108826A	T9108829A	mean	SD	RSD	2SE(m)
Major elements											
SiO2	0.59%	0.56%	0.627%	0.575%	0.584%	0.689%	0.558%	0.600%	0.042%	7%	0.032%
TiO2	<0.002%	<0.002%	<0.002%	<0.002%	<0.002%	<0.002%	<0.002%	<0.002%	NA	NA	NA
Al2O3	0.018%	(0.008%)	0.020%	(0.008%)	(0.008%)	0.021%	(0.006%)	(0.013%)	0.006%	49%	0.005%
Fe2O3	0.033%	0.028%	0.027%	0.026%	0.026%	0.034%	0.025%	0.028%	0.003%	12%	0.003%
MnO	<0.002%	<0.002%	<0.002%	<0.002%	<0.002%	<0.002%	<0.002%	<0.002%	NA	NA	NA
MgO	<0.010%	<0.010%	<0.010%	<0.010%	<0.010%	<0.010%	<0.010%	<0.010%	NA	NA	NA
CaO	71.7%	71.5%	71.5%	71.0%	70.8%	73.4%	70.8%	71.5%	0.8%	1%	0.6%
Na2O	<0.010%	<0.010%	<0.010%	<0.010%	<0.010%	<0.010%	<0.010%	<0.010%	NA	NA	NA
K2O	<0.002%	<0.002%	<0.002%	<0.002%	<0.002%	<0.002%	<0.002%	<0.002%	NA	NA	NA
P2O5	<0.003%	<0.003%	<0.003%	<0.003%	<0.003%	<0.003%	<0.003%	<0.003%	NA	NA	NA
S ppm	1093	1068	1065	986	984	938	978	1018	56	5%	42
Cl ppm	88	(43)	102	(34)	(36)	(32)	(28)	(52)	28	54%	21
LOI			1.06%	1.20%				1.13%	0.07%	6%	0.10%
Trace elements											
Sc	55	45	60	57	36	46	43	46	7	15%	5
V	<6	<6	<6	<6	<6	(7)	<6	<6	NA	NA	NA
Cr	<7	(11)	(13)	(14)	<7	(16)	(9)	(10)	5	46%	4
Ni	<4	<4	<4	<4	<4	<4	<4	<4	NA	NA	NA
Cu	78	75	77	81	77	83	77	78	3	3%	2
Zn	12	<2	21	<2	<2	<2	<2	(5)	7	136%	6
Ga	18	22	25	9	(6)	9	13	14	7	47%	5
As	<13	<13	(38)	<13	<13	<13	<13	<13	NA	NA	NA
Rb	<0.7	<0.7	<0.7	<0.7	<0.7	<0.7	(1.4)	<0.7	NA	NA	NA
Sr	65	65	64	66	68	66	65	66	1.2	2%	0.9
Y	812	813	777	780	782	778	778	789	15	2%	12
Zr	<1.0	<1.0	<1.0	<1.0	<1.0	<1.0	<1.0	<1.0	NA	NA	NA
Nb	<0.6	<0.6	(1.9)	(1.6)	2	(1.4)	(1.2)	(1.3)	0.7	53%	0.5
Ba	150	152	153	182	169	<18	185	140	56	40%	43
Ce	<36	<36	<36	<36	<36	<36	<36	<36	NA	NA	NA
Pb	5253	5075	5120	5154	5258	5211	5252	5189	68	1%	51
Th	<3	<3	(3)	<3	<3	<3	(5)	<3	NA	NA	NA
U	<3	<3	<3	<3	<3	(5)	<3	<3	NA	NA	NA
Calculated								mean	SD	RSD	2SE(m)
CaF2	91.8%	90.6%	90.6%	98.8%	98.6%	102.2%	98.6%	99.6%	1.2%	1%	0.4%
SiO2	0.598%	0.568%	0.627%	0.575%	0.584%	0.689%	0.558%	0.600%	0.042%	7%	0.016%
CaF2	90.3%	90.1%	90.1%	98.4%	98.2%	101.8%	98.1%	99.1%	1.2%	1%	0.4%
SiO2	0.315%	0.299%	0.330%	0.303%	0.307%	0.363%	0.294%	0.316%	0.022%	7%	0.008%
BaSO4	0.022%	0.026%	0.026%	0.031%	0.029%	0.030%	0.032%	0.028%	0.010%	42%	0.004%
SrSO4	0.014%	0.014%	0.013%	0.014%	0.014%	0.014%	0.014%	0.014%	0.000%	2%	0.000%
Fe2O3	0.033%	0.028%	0.027%	0.026%	0.026%	0.034%	0.025%	0.028%	0.003%	12%	0.001%
Al2O3	0.018%	(0.008%)	0.020%	(0.008%)	(0.008%)	0.021%	(0.006%)	(0.013%)	NA	NA	NA
(REE,Y)F3								0.14%	NA	NA	NA
19F	0.607%	0.586%	0.591%	0.595%	0.607%	0.602%	0.606%	0.599%	0.008%	1%	0.003%
LOI	1.20%	1.12%	1.06%	1.20%	1.05%			1.11%	0.06%	6%	0.029%
TOTALS	101%	101%	101%	101%	101%	103%	99%	101%	1.0%	1%	0.4%

Notes
[1] Corrected to recommended value for NBS-79A
[2] All Ba and Sr assumed to occur as accessory sulphate phases
[3] All REE and Y assumed to occur as fluoride
Values less than the limit of detection (LOD) = <LOD
Values less than the limit of quantification (LOQ) = (value)

St. Lawrence fluorite - XRF (pressed pellet) analytical data

subscripts: value is average of (1) duplicate; (2) triplicate; or (3) more than 3 analyses

Sample	AZ-2	AZ-4	BB-84-11	BBS-84-64	BBV-2-A	BBV-2-B	BBV-2-C	BBV-2-D	BBV-2-E	BBV-2-F	BBV-2-G	BBV-2-H
MUN #	M1631	M1632	M1633	M2000	M1544	M1545	M1634	M567	M1546	M1547	M1548	M1635
Majors (%)												
SiO2	74.670	67.096	3.266	82.109	0.183	0 158	0.528	0.197	0.211	0.356	12.380	1.982
TiO2	0.229	0.132	0.019	0.082	< 0.002	< 0.002	< 0.002	< 0.002	< 0.002	< 0.002	< 0.002	< 0.002
Al2O3	10.904	7.268	0.183	8.046	< 0.004	< 0.004	0.018	0.041	(0.013)	0.017	0.067	0.020
Fe2O3	1.910	1.266	0.341	1.776	0.052	0.055	0.290	0.105	0.011	0.007	0.121	0.076
MnO	0.055	0.095	0.023	0.010	< 0.002	< 0.002	< 0.002	< 0.002	< 0.002	< 0.002	< 0.002	(0.003)
MgO	< 0.010	< 0.010	< 0.010	(0.019)	< 0.010	< 0.010	< 0.010	< 0.010	< 0.010	< 0.010	< 0.010	< 0.010
CaO	4.546	17.510	67.068	0.660	74.604	76.172	32.942	73.142	71.984	71.485	43.230	71.706
Na2O	2.351	< 0.010	< 0.010	2.379	< 0.010	< 0.010	< 0.010	< 0.010	< 0.010	< 0.010	1.393	0 087
K2O	5.212	5.829	0.042	3.544	< 0.002	< 0.002	< 0.002	< 0.002	< 0.002	< 0.002	0 021	< 0.002
P2O5	0.015	0.013	0.013	< 0.003	(0.005)	(0.008)	(0.008)	< 0.003	(0.006)	(0.010)	0.012	0.012
Traces (ppm)												
V	< 6	< 6	(6)	< 6	< 6	< 6	< 6	< 6	< 6	< 6	< 6	(6)
Cr	(8)	< 7	(8)	(13)	(7)	< 7	(12)	< 7	(11)	< 7	225	114
Ni	< 4	< 4	< 4	< 4	< 4	< 4	< 4	< 4	< 4	< 4	172	25
Cu	442	1508	90	(4)	277	279	9795	601	38	41	488	40
Zn	427	193	13	20	2246	216	1775	26	< 2	432	160481	6211
Ga	50	(3)	< 2	18	< 2	< 2	6250	12	27	104	1480	(7)
As	(14)	< 13	< 13	< 13	< 13	< 13	< 13	< 13	< 13	< 13	< 13	< 13
Rb	284.6	282.7	3.2	199.6	< 0.7	< 0.7	< 0.7	< 0.7	(0.7)	(1.3)	< 0.7	< 0.7
Sr	28.5	26.0	69.1	11.3	35.6	40.0	32.7	132.0	144.8	116.8	44.4	119.1
Y	66 8	97.5	1014.5	129.8	662.2	521.7	492.2	1371.0	1426.1	1294.4	611.9	1205.3
Zr	291.2	246.9	(2.9)	341.6	< 1.0	(1.1)	< 1.0	< 1.0	< 1.0	< 1.0	< 1.0	< 1.0
Nb	42.0	28.5	< 0.6	51.2	(1.3)	(1.8)	8.2	2 9	3.2	2.3	5.0	< 0.6
Ba	1231	821	3338	84	< 18	126	< 18	(21)	< 18	< 18	< 18	(22)
Ce	(73)	252	< 36	135	(38)	(44)	< 36	< 36	< 36	< 36	< 36	< 36
Pb	5065	866	208	16	1158	1205	709380	6553	8672	20984	182558	3751
Th	(7)	10	< 3	20	< 3	< 3	< 3	(4)	< 3	(7)	71	< 3
U	(4)	(4)	< 3	(6)	< 3	< 3	91	< 3	< 3	< 3	23	< 3

values less than the limit of detection (LOD) - <LOD

values less than limit of quantitation (LOQ) - (value)

St. Lawrence fluorite - XRF (pressed pellet) analytical data

subscripts: value is average of (1) duplicate; (2) triplicate; or (3) more than 3 analyses

Sample MUN #	CPV-4-A M1550	CPV-4-B M1636	CPV-4-C M1637	CPV-4-D M1638	CPV-4-E M1551	CPV-4-F M1552	CPV-4-G M1553	CV-6 M1998	GNV-7[3] AVERAGE	GNV-8-A M1554	GNV-8-B M1555	GNV-8-C M1556
Majors (%)												
SiO2	10.859	1.085	2.694	3.248	64.037	26.838	16.914	58.931	0.600	2.493	0.360	0.161
TiO2	(0.004)	< 0.002	< 0.002	< 0.002	0.024	< 0.002	< 0.002	1.015	< 0.002	0.022	< 0.002	< 0.002
Al2O3	0.192	0.032	0.104	0.059	1.678	0.242	0.088	22.906	(0.013)	0.624	0.071	(0.006)
Fe2O3	0.208	0.053	0.054	0.032	0.715	0.183	0.181	8.133	0.028	0.255	0.057	0.033
MnO	0.009	< 0.002	< 0.002	(0.003)	0.008	(0.004)	(0.003)	0.069	< 0.002	0.012	(0.003)	< 0.002
MgO	< 0.010	< 0.010	< 0.010	< 0.010	< 0.010	< 0.010	< 0.010	2.257	< 0.010	< 0.010	< 0.010	< 0.010
CaO	66.067	74.527	73.329	75.264	32.584	60.200	66.328	0.785	71.538	72.865	75.458	76.194
Na2O	< 0.010	0.076	0.303	< 0.010	< 0.010	< 0.010	< 0.010	0.694	< 0.010	0.142	< 0.010	< 0.010
K2O	0.099	(0.005)	0.046	0.012	1.216	0.136	0.025	5.386	< 0.002	0.128	0.007	< 0.002
P2O5	< 0.003	< 0.003	(0.005)	< 0.003	< 0.003	< 0.003	< 0.003	0.120	< 0.003	0.012	< 0.003	< 0.003
Traces (ppm)												
V	< 6	< 6	< 6	< 6	< 6	< 6	< 6	145	< 6	< 6	< 6	< 6
Cr	151	55	47	< 7	723	(15)	(9)	138	(10)	(20)	(14)	(8)
Ni	32	(8)	(10)	< 4	184	< 4	< 4	51	< 4	< 4	< 4	< 4
Cu	(7)	(8)	(9)	(3)	14	< 3	(6)	(10)	78	38	13	(8)
Zn	< 2	< 2	< 2	< 2	< 2	< 2	< 2	227	(3)	210	12	< 2
Ga	< 2	< 2	< 2	< 2	< 2	< 2	< 2	33	14	< 2	< 2	< 2
As	< 13	< 13	< 13	< 13	< 13	< 13	(19)	< 13	< 13	< 13	< 13	< 13
Rb	8.2	(0.7)	< 0.7	< 0.7	85.3	10.1	(1.8)	313.1	< 0.7	6.2	< 0.7	< 0.7
Sr	183.7	106.7	76.9	79.2	31.4	54.1	65.8	47.3	65.6	87.5	78.1	77.8
Y	365.7	486.4	390.9	355.4	147.1	247.7	357.3	43.0	788.6	451.5	926.3	857.5
Zr	11.1	< 1.0	< 1.0	< 1.0	86.2	10.3	(2.6)	147.2	< 1.0	6.1	(1.7)	< 1.0
Nb	3.2	< 0.6	< 0.6	< 0.6	14.4	3.0	(1.7)	17.1	< 0.6	2.3	(1.7)	(1.6)
Ba	20055	457	137	341	425	388	746	989	134	366	(27)	< 18
Ce	< 36	(82)	(51)	(84)	(50)	(57)	(55)	123	< 36	257	186	187
Pb	19	18	23	(12)	51	44	105	39	5189	267	49	30
Th	< 3	< 3	< 3	< 3	(4)	< 3	(4)	13	< 3	(3)	< 3	< 3
U	< 3	< 3	< 3	< 3	(3)	< 3	< 3	(4)	< 3	< 3	< 3	(4)

values less than the limit of detection (LOD) - <LOD

values less than limit of quantitation (LOQ) - (value)

St. Lawrence fluorite - XRF (pressed pellet) analytical data

subscripts: value is average of (1) duplicate; (2) triplicate; or (3) more than 3 analyses

Sample	GNV-8-D	GNV-8-E	GNV-8-F	GNV-8-G	GNV-8-H	GNV-8-I	GNV-8-J	GNV-8-K	GNV-8-L	GNV-8-M	GNV-8-N	GNV-8-O
MUN #	M1557	M1558	M1559	M1560	M1561	M1639	M1562	M568	M1563	M1564	M1565	M1640
Majors (%)												
SiO2	0.321	0.175	0.155	0.081	0.371	0.327	0.070	0.072	0.269	0.123	0.282	1.747
TiO2	< 0.002	< 0.002	< 0.002	< 0.002	(0.005)	(0.002)	< 0.002	< 0.002	< 0.002	< 0.002	< 0.002	0.014
Al2O3	(0.008)	(0.005)	0.039	< 0.004	0.072	0.088	< 0.004	< 0.004	0.072	0.030	0.083	0.571
Fe2O3	0.055	0.028	0.027	0.020	0.063	0.036	0.064	0.029	0.103	2.534	3.938	6.455
MnO	< 0.002	< 0.002	< 0.002	< 0.002	< 0.002	(0.003)	< 0.002	< 0.002	(0.002)	0.012	0.027	0.048
MgO	< 0.010	< 0.010	< 0.010	< 0.010	< 0.010	< 0.010	< 0.010	< 0.010	< 0.010	< 0.010	< 0.010	< 0.010
CaO	74.186	75.744	74.198	75.556	74.567	75.583	74.188	75.853	74.738	72.408	72.607	66.084
Na2O	< 0.010	< 0.010	< 0.010	< 0.010	0.122	0.244	< 0.010	< 0.010	0.038	< 0.010	< 0.010	< 0.010
K2O	< 0.002	< 0.002	< 0.002	< 0.002	0.017	0.026	< 0.002	< 0.002	0.016	< 0.002	(0.003)	0.076
P2O5	(0.006)	< 0.003	(0.003)	(0.004)	(0.005)	(0.009)	(0.006)	(0.007)	(0.005)	(0.005)	0.020	0.015
Traces (ppm)												
V	< 6	< 6	< 6	< 6	< 6	< 6	< 6	< 6	< 6	< 6	< 6	< 6
Cr	(10)	< 7	(12)	(8)	(13)	< 7	(9)	(9)	(18)	(13)	(7)	23
Ni	< 4	< 4	< 4	< 4	< 4	< 4	< 4	< 4	< 4	< 4	< 4	< 4
Cu	14	14	(8)	(9)	44	15	58	22	37	86	220	330
Zn	< 2	< 2	< 2	< 2	< 2	< 2	< 2	< 2	< 2	< 2	75	447
Ga	< 2	< 2	< 2	< 2	< 2	< 2	< 2	< 2	< 2	< 2	< 2	< 2
As	< 13	< 13	< 13	< 13	< 13	< 13	< 13	< 13	< 13	< 13	(26)	102
Rb	< 0.7	< 0.7	< 0.7	< 0.7	< 0.7	< 0.7	< 0.7	< 0.7	< 0.7	(1.0)	(0.7)	4.1
Sr	81.9	58.9	52.9	51.0	45.8	47.7	44.9	55.5	56.1	39.0	43.5	56.7
Y	1467.4	713.4	889.8	742.8	383.6	672.9	421.1	591.8	595.2	395.3	848.1	902.5
Zr	(1.2)	(1.0)	< 1.0	< 1.0	(1.4)	< 1.0	< 1.0	< 1.0	< 1.0	< 1.0	< 1.0	< 1.0
Nb	3.2	(1.3)	2.2	(1.5)	(1.6)	< 0.6	(1.2)	(1.5)	(1.4)	(1.2)	(1.9)	< 0.6
Ba	(28)	< 18	< 18	< 18	91	104	< 18	87	(24)	< 18	(21)	289
Ce	205	(120)	141	(85)	(48)	(80)	(54)	(39)	(84)	< 36	(53)	(51)
Pb	34	26	27	38	31	20	22	19	30	125	383	665
Th	(3)	< 3	< 3	< 3	< 3	< 3	< 3	< 3	< 3	< 3	< 3	< 3
U	< 3	< 3	< 3	< 3	< 3	< 3	< 3	< 3	< 3	< 3	(6)	< 3

values less than the limit of detection (LOD) - <LOD

values less than limit of quantitation (LOQ) - (value)

St. Lawrence fluorite - XRF (pressed pellet) analytical data

subscripts: value is average of (1) duplicate; (2) triplicate; or (3) more than 3 analyses

Sample	GNV-8-P	HCT-111	HCT-187	HCT-188	HEV-1-A	HEV-1-B	HEV-1-C	HEV-1-D	HEV-1-E	ISV-1-A	ISV-1-B	ISV-1-C
MUN #	M1641	M1642	M1643	M1644	M1566	M1567	M1568	M1569	M1570	M1571	M1572	M1645
Majors (%)												
SiO2	7.167	80.339	79.615	75.700	11.539	0.287	0.328	1.384	1.321	5.320	5.359	2.152
TiO2	0.045	0.125	0.055	0.055	0.012	< 0.002	< 0.002	< 0.002	< 0.002	< 0.002	0.014	0.016
Al2O3	1.578	11.984	12.488	12.383	0.583	0.022	0.049	(0.011)	0.019	0.192	0.462	0.288
Fe2O3	80.905	2.256	1.280	0.964	0.110	0.068	0.166	0.044	0.117	0.208	0.178	0.346
MnO	0.278	(0.006)	0.027	0.040	< 0.002	< 0.002	< 0.002	< 0.002	(0.002)	0.214	0.106	0.123
MgO	< 0.010	< 0.010	< 0.010	< 0.010	< 0.010	< 0.010	< 0.010	< 0.010	< 0.010	< 0.010	< 0.010	< 0.010
CaO	4.949	0.506	0.151	1.795	67.424	74.331	72.273	24.998	68.652	70.657	70.508	71.862
Na2O	0.082	3.786	4.114	5.820	< 0.010	< 0.010	0.098	< 0.010	< 0.010	(0.015)	0.195	< 0.010
K2O	0.314	4.791	4.653	2.310	0.247	< 0.002	(0.006)	< 0.002	< 0.002	0.039	0.104	0.051
P2O5	0.081	(0.004)	(0.004)	(0.005)	(0.009)	0.012	0.017	(0.009)	(0.009)	0.023	0.031	0.027
Traces (ppm)												
V	(10)	< 6	< 6	< 6	< 6	< 6	< 6	< 6	< 6	< 6	< 6	< 6
Cr	101	< 7	< 7	< 7	< 7	38	38	(14)	(8)	32	65	(13)
Ni	31	< 4	< 4	< 4	< 4	< 4	< 4	< 4	< 4	< 4	19	20
Cu	2118	< 3	46	164	15	26	152	2421	156	45	60	145
Zn	7049	< 2	22	23	< 2	12	< 2	2799	1368	26	25	43
Ga	56	30	29	31	< 2	< 2	25	6669	136	< 2	< 2	< 2
As	918	(23)	(14)	< 13	< 13	< 13	< 13	< 13	< 13	< 13	< 13	< 13
Rb	17.5	301.5	408.0	141.8	20.9	< 0.7	< 0.7	< 0.7	(2.2)	3.5	4.7	5.3
Sr	23.9	8.8	11.7	19.6	69.4	93.4	95.8	55.3	48.5	46.2	42.8	42.6
Y	268.5	128.5	125.1	99.7	980.7	1803.4	1728.9	319.3	919.6	806.3	905.4	1050.4
Zr	7.5	544.0	280.4	264.3	41.2	(1.2)	< 1.0	< 1.0	< 1.0	6.4	13.3	5.5
Nb	2.3	111.2	109.9	101.4	8.5	4.3	3.9	37.1	(1.7)	4.2	3.7	< 0.6
Ba	765	(41)	(55)	92	154	(55)	75	98	93	1076	409	283
Ce	(63)	169	(110)	(88)	(79)	(70)	< 36	< 36	< 36	(39)	(41)	< 36
Pb	8654	19	64	143	861	946	9003	908657	23534	106	103	510
Th	< 3	35	45	40	< 3	< 3	(4)	< 3	26	< 3	< 3	(4)
U	30	11	19	18	< 3	< 3	< 3	231	< 3	< 3	< 3	(5)

values less than the limit of detection (LOD) - <LOD

values less than limit of quantitation (LOQ) - (value)

St. Lawrence fluorite - XRF (pressed pellet) analytical data

subscripts: value is average of (1) duplicate; (2) triplicate; or (3) more than 3 analyses

Sample MUN #	ISV-1-D M1646	ISV-1-E M1573	ISV-1-F M1574	ISV-1-G M565	LBV-7-A M1575	LBV-7-B M1576	LBV-7-C AVERAGE	LBV-7-D M1578	LBV-7-E M1579	LBV-7-F M1580	LBV-7-G M1647	LP-2-A M1648
Majors (%)												
SiO2	0.842	0.078	0.308	0.080	10.757	9.825	7.187	7.375	1.443	0.369	0.594	21.761
TiO2	0.020	< 0.002	< 0.002	< 0.002	0.055	0.022	0.009	0.021	0.008	< 0.002	0.043	0.009
Al2O3	0.212	< 0.004	0.033	(0.005)	1.205	0.355	0.137	0.131	0.095	0.126	0.215	0.983
Fe2O3	0.807	0.043	0.503	0.248	0.524	0.227	< 0.002	< 0.002	< 0.002	< 0.002	< 0.002	0.081
MnO	0.014	(0.004)	(0.004)	(0.003)	0.024	< 0.002	< 0.002	< 0.002	< 0.002	< 0.002	< 0.002	0.312
MgO	< 0.010	< 0.010	< 0.010	< 0.010	< 0.010	< 0.010	< 0.010	< 0.010	< 0.010	< 0.010	< 0.010	< 0.010
CaO	70.112	71.278	72.518	72.490	33.115	28.459	7.759	10.812	35.777	32.805	1.874	58.632
Na2O	< 0.010	< 0.010	< 0.010	< 0.010	< 0.010	< 0.010	< 0.010	< 0.010	< 0.010	0.180	< 0.010	(0.017)
K2O	0.021	< 0.002	< 0.002	< 0.002	0.489	0.117	0.035	0.037	0.019	0.030	0.058	0.590
P2O5	0.028	(0.005)	(0.005)	< 0.003	(0.010)	(0.006)	< 0.003	< 0.003	(0.005)	(0.005)	0.010	(0.007)
Traces (ppm)												
V	< 6	< 6	< 6	< 6	< 6	< 6	< 6	< 6	< 6	< 6	< 6	< 6
Cr	39	(12)	(13)	< 7	208	236	443	487	229	228	668	(15)
Ni	< 4	< 4	< 4	< 4	38	19	49	52	20	(9)	19	< 4
Cu	946	48	1435	797	126	156	150	176	77	147	113	31
Zn	57	< 2	77	(6)	1165	732	278	441	2488	26560	1844	208
Ga	< 2	< 2	< 2	< 2	< 2	< 2	< 2	< 2	< 2	< 2	< 2	< 2
As	< 13	< 13	< 13	< 13	< 13	< 13	< 13	< 13	(21)	169	(21)	< 13
Rb	(1.6)	< 0.7	< 0.7	< 0.7	42.9	11.6	2.5	4.7	2.6	5.4	3.5	37.2
Sr	89.4	133.9	30.7	24.1	3076.3	4875.7	8376.4	7841.0	4129.1	4311.7	6407.1	572.6
Y	1798.6	1308.5	578.5	880.4	491.1	457.8	134.7	171.4	417.2	330.2	22.7	595.8
Zr	< 1.0	< 1.0	(1.7)	< 1.0	33.4	40.0	58.8	55.5	31.4	27.3	< 1.0	5.2
Nb	< 0.6	2.8	(1.5)	2.2	2.8	3.4	(1.5)	(1.2)	2.4	2.3	2.2	(1.7)
Ba	369	(46)	510	506	292478	367848	539917	534416	388063	416486	666963	19611
Ce	(59)	(75)	< 36	< 36	< 36	< 36	< 36	< 36	< 36	< 36	< 36	(78)
Pb	497	(9)	194	57	(12)	< 4	< 4	48	135	11537	579	1193
Th	< 3	< 3	< 3	< 3	< 3	< 3	< 3	< 3	< 3	< 3	< 3	< 3
U	(6)	< 3	(5)	< 3	(7)	(3)	< 3	< 3	(4)	< 3	11	< 3

values less than the limit of detection (LOD) - <LOD

values less than limit of quantitation (LOQ) - (value)

St. Lawrence fluorite - XRF (pressed pellet) analytical data

subscripts: value is average of (1) duplicate; (2) triplicate; or (3) more than 3 analyses

Sample MUN #	LP-2-B M1649	LP-2-C M1582	LP-2-D M1650	LP-2-E M1583	LP-2-F-H M1584	LP-2-J M1651	NBS-79A[3] AVERAGE	SCVV(A)-A M1653	SCVV(A)-B M1654	SCVV(A)-C M1587	SDMS-2-A M1655	SDMS-2-B M1656
Majors (%)												
SiO2	20.409	4.703	27.594	2.898	11.572	75.286	1.300	4.255	12.888	0.526	102.166	79.443
TiO2	0.013	< 0.002	(0.004)	< 0.002	0.016	< 0.002	(0.004)	< 0.002	< 0.002	< 0.002	0.010	0.063
Al2O3	1.408	0.216	0.126	(0.009)	0.055	0.173	0.171	0 026	0.061	0.021	4.390	12.859
Fe2O3	0.121	0.042	0.095	< 0.002	< 0.002	0.025	0.058	0.061	0.112	0.088	0.242	1.446
MnO	0.251	0.034	< 0.002	< 0.002	< 0.002	< 0.002	< 0.002	0.715	0.487	0.011	(0.004)	0.019
MgO	< 0.010	< 0.010	< 0.010	< 0.010	< 0.010	< 0.010	< 0.010	< 0.010	< 0.010	< 0.010	< 0.010	< 0.010
CaO	58.769	71.431	43.676	71.247	23.289	25.486	70.317	70.906	65.659	75.284	0.863	0.299
Na2O	(0.033)	< 0.010	< 0.010	< 0.010	< 0.010	< 0.010	< 0.010	< 0 010	< 0.010	< 0.010	0.645	4.408
K2O	0.840	0.094	0.041	< 0.002	0.007	0.035	0.007	< 0.002	(0.004)	< 0.002	2.447	4.437
P2O5	(0.005)	(0.004)	(0.007)	< 0.003	< 0.003	(0.004)	(0.008)	< 0 003	(0.004)	0.010	0.015	(0.006)
Traces (ppm)												
V	< 6	< 6	< 6	< 6	< 6	< 6	< 6	< 6	< 6	< 6	< 6	< 6
Cr	(12)	52	323	(15)	215	< 7	(14)	(7)	29	< 7	(7)	< 7
Ni	< 4	(5)	81	< 4	15	< 4	< 4	< 4	< 4	< 4	< 4	< 4
Cu	56	15	158	< 3	72	80	(9)	19	47	134	12	< 3
Zn	403	110	43	< 2	< 2	< 2	9	< 2	24	< 2	12	36
Ga	< 2	< 2	< 2	< 2	< 2	(6)	< 2	< 2	< 2	< 2	< 2	28
As	< 13	< 13	< 13	< 13	< 13	54	(28)	< 13	< 13	< 13	< 13	< 13
Rb	60.1	8.8	4.0	< 0.7	(1.9)	2.7	< 0.7	< 0.7	< 0.7	< 0.7	183.3	378.6
Sr	73.4	165.5	2534.1	496.0	7846.4	192.3	206.8	100.2	81.2	95.1	12.7	5.6
Y	464.3	1332.7	376.5	1132.9	325.8	144.6	(1.8)	198.4	209.6	649.5	81.5	80.5
Zr	30.3	4.8	< 1.0	4.9	52.9	(2.5)	(1.1)	< 1.0	< 1.0	(1.2)	31.4	318.2
Nb	4.5	3.8	< 0.6	2.5	2.0	(1.3)	< 0.6	< 0.6	< 0.6	(1.7)	12.8	104.0
Ba	1707	6656	118161	30839	416379	9457	351	142	213	12156	316	596
Ce	129	< 36	< 36	< 36	< 36	< 36	< 36	200	(69)	< 36	121	(103)
Pb	920	1298	1252	547	< 4	225	27	31	158	64	796	48
Th	< 3	< 3	< 3	< 3	< 3	< 3	< 3	< 3	< 3	< 3	63	55
U	< 3	< 3	(5)	< 3	(4)	< 3	< 3	< 3	< 3	< 3	(4)	16

values less than the limit of detection (LOD) - <LOD

values less than limit of quantitation (LOQ) - (value)

St. Lawrence fluorite - XRF (pressed pellet) analytical data

subscripts: value is average of (1) duplicate; (2) triplicate; or (3) more than 3 analyses

Sample MUN #	SDMS-4 M1999
Majors (%)	
SiO2	77.555
TiO2	0.058
Al2O3	11.391
Fe2O3	1.506
MnO	0.016
MgO	< 0.010
CaO	0.047
Na2O	3.726
K2O	4.527
P2O5	< 0.003
Traces (ppm)	
V	< 6
Cr	(11)
Ni	< 4
Cu	(8)
Zn	45
Ga	28
As	< 13
Rb	322.9
Sr	4.7
Y	50.1
Zr	270.1
Nb	71.4
Ba	(48)
Ce	(59)
Pb	52
Th	25
U	(7)

values less than the limit of detection (LOD) - < LOD

values less than limit of quantitation (LOQ) - (value)

Appendix 2

Fluid inclusion Data

Samples for fluid inclusion analysis were cut into thin slabs to separate individual growth zones within hand samples of vein material. A water cooled diamond saw was used to cut the samples. The fluorite and carbonate samples were relatively soft, so overheating during cutting was not a problem. Extra care was taken not to overheat the harder silica rich samples. The thin slabs were ground and polished to produce doubly polished wafers on which the microthermometric measurements were made.

The fluid inclusion study was conducted using a modified USGS heating and freezing stage. Since most of the inclusions homogenised at relatively low temperatures, heating experiments were carried out first, followed by freezing experiments. It was considered that expansion on freezing would have a higher potential for stretching the inclusions than expansion involved in the low temperature heating measurements. Reproducibility of both temperature and salinity measurements indicate that stretching was not a problem in most of the samples studied.

Calibration was periodically conducted using both reagent standards and synthetic fluid inclusions. Early work, calibrated with reagent standards and distilled water indicated less than 1 degree variance between 250°C and 0°C and a correction factor of only plus 2°C at 400°C. Later calibrations, using a wide range of synthetic fluid inclusions indicate deviations of less than 1°C up to 375°C and as low as -56°C. Distilled water consistently indicated ice melting temperatures near 0°C.

The fluid inclusion data are listed in the following section. For sample descriptions and vein locations, see text.

Sample	Mineral	Tm(eut)	Tm(hyd)	Tm(ice)	NaCl eq%	ThL	ThV
AD 8 A	Fluorite	-25.1		-25.1	25.1	109.0	
AD-8 A	Fluorite		-12.4		24.0	112.2	
AD-8 A	Fluorite	-24.4		-24.4	24.9	84.6	
AD 8-A	Fluorite	-27.8		-27.8	26.2	49.8	
AD 8 A	Fluorite	-30.3		-30.3	26.3	170.5	
AD-8-A	Fluorite	-30.8		-24.4	25.0	137.0	
AD-8 A	Fluorite			-2.4	4.0	90.4	
AD 8-A	Fluorite			-4.6	7.3	95.2	
AD 8 B	Fluorite			-10.0	14.0	132.0	
AD 8 B	Fluorite	-24.5		-24.5	25.0	83.3	
AD 8-B	Fluorite	-32.2		-22.9	24.9	100.0	
AZ-1-A	Fluorite	-25.0	-12.1		24.0	87.4	
AZ-1-A	Fluorite	-25.6	-9.5		24.7	75.7	
AZ-1-A	Fluorite			-5.0	7.8	93.8	
AZ-1 A	Fluorite			-3.7	5.1	96.3	
AZ-1-A	Fluorite			-7.2	10.8	93.2	
AZ-1-A	Fluorite			-11.2	15.2	73.5	
AZ-1-A	Fluorite			-5.7	8.0	72.1	
AZ-1-A	Fluorite			-5.4	7.6	75.9	
AZ 1-A	Fluorite			-2.8	3.7	105.7	
AZ-1-A	Fluorite			-6.1	8.5	69.5	
AZ-1 B	Fluorite			-3.8	6.1	111.8	
AZ 1 B	Fluorite			-4.5	7.2	106.5	
AZ 1 B	Fluorite			-8.9	12.8	117.5	
AZ-1 B	Fluorite			-3.4	5.5	100.2	
AZ-1 B	Fluorite	-25.0	-12.0		24.0	97.3	
AZ 1-B	Fluorite			-10.2	13.5	113.5	
AZ-1 B	Fluorite			-9.4	13.3	101.8	
AZ-1 B	Fluorite			-6.1	9.4	90.4	
AZ-1 B	Fluorite			-6.9	10.4	66.6	
AZ 1-B	Fluorite			-6.2	9.5	71.5	
AZ-1-C	Fluorite			-4.1	6.6	101.2	
AZ-1-C	Fluorite			-5.0	7.8	95.5	
AZ-1-C	Fluorite			-9.8	13.8	100.0	
AZ-1-C	Fluorite			-9.4	13.3	110.8	
AZ-1-C	Fluorite			-13.7	17.6	92.5	
AZ-1-C	Fluorite			-7.4	11.0	94.3	
AZ-1-C	Fluorite			-11.2	15.2	166.5	
AZ-1-C	Fluorite			-12.1	16.1	184.4	
AZ-1-C	Fluorite			-3.4	5.6	100.3	
AZ-1-C	Fluorite			-8.9	12.8	115.2	
AZ 3 B	Fluorite			-19.5	22.3	80.7	
AZ-3-B	Fluorite			-18.1	21.3	83.3	
AZ-3-B	Fluorite			-4.6	7.3	98.5	
AZ-3-B	Fluorite			-4.8	7.6	98.0	
AZ-3-B	Fluorite			-13.5	17.4	107.2	
AZ-3 B	Fluorite			-8.0	11.7	92.0	
AZ-3-B	Fluorite			-9.0	12.9	77.2	
AZ-3 B	Fluorite			-17.9	21.1	76.2	
AZ-3-B	Fluorite			-18.4	21.5	90.3	
AZ-3-B	Fluorite	-24.2	-12.8		23.9	108.4	
D2C(30')	Fluorite			-9.4	13.3	105.4	

Sample	Mineral	Tm(eut)	Tm(hyd)	Tm(ice)	NaCl eq%	ThL	ThV
D2C(30')	Fluorite			-9.3	13.2	102.3	
D2C(30')	Fluorite			-8.6	12.4	110.6	
D2C(30')	Fluorite		-7.3		25.0	74.8	
D2C(30')	Fluorite			-22.4	24.1	104.2	
D2C(30')	Fluorite			-10.3	14.3	98.7	
D2C(30')	Fluorite			-2.3	3.8	84.6	
D2C(30')	Fluorite			-20.8	23.3	85.6	
D2C(30')	Fluorite			-4.4	7.0	98.5	
D2C(30')	Fluorite			-4.8	7.6	103.7	
D3C(79')	Fluorite		-7.0		25.0	62.8	
D3C(79')	Fluorite			-28.1	26.3	91.3	
D3C(79')	Fluorite			-12.6	16.6	97.9	
D3C(79')	Fluorite			-15.1	18.8	96.6	
D3C(79')	Fluorite			-27.6	26.2	97.4	
D3C(79')	Fluorite			-7.3	10.9	89.5	
D3C(79')	Fluorite			-12.3	16.3	107.0	
D3C(79')	Fluorite			-25.3	25.3	74.5	
D3C(79')	Fluorite			-9.0	12.9	113.5	
D3C(79')	Fluorite			-2.6	4.3	118.9	
D3C(140')	Fluorite			-7.2	10.8	136.0	
D3C(140')	Fluorite			-6.9	10.4	119.0	
D3C(140')	Fluorite			-6.8	10.3	134.0	
D3C(140')	Fluorite			-7.6	11.2	138.5	
D3C(140')	Fluorite			-6.2	9.5	122.8	
D3C(140')	Fluorite			-3.8	6.1	114.1	
D3C(140')	Fluorite			-8.1	11.8	148.0	
D3C(140')	Fluorite			-7.6	11.2	140.5	
D3C(140')	Fluorite			-7.1	10.6	140.0	
D3C(140')	Fluorite			-7.3	10.9	163.3	
BBV-2-A	Fluorite			-10.8	14.8	378.5	
BBV-2-A	Fluorite			-10.9	14.9	383.8	
BBV-2-A	Fluorite			-6.6	10.0	127.0	
BBV-2-A	Fluorite			-7.3	10.9	129.2	
BBV-2-A	Fluorite			-1.6	2.7	127.9	
BBV-2-A	Fluorite			-7.2	10.8	125.0	
BBV-2-A	Fluorite			-7.2	10.8	127.0	
BBV-2-A	Fluorite	-28.0		-7.4	11.0	126.4	
BBV-2-A	Fluorite	-40.0		-7.2	10.8	127.3	
BBV-2-A	Fluorite	-30.0		-2.4	4.0	126.5	
BBV-2-B	Fluorite	-28.0		-2.0	3.3	125.0	
BBV-2-B	Fluorite	-40.0		-5.2	8.2	122.8	
BBV-2-B	Fluorite	-30.0		-0.5	0.8	125.0	
BBV-2-B	Fluorite	-31.0		-6.0	9.2	121.4	
BBV-2-B	Fluorite	-31.0		-0.5	0.8	121.2	
BBV-2-C	Fluorite	-30.0		-4.9	7.7	127.1	
BBV-2-C	Fluorite	-30.0		-1.5	2.5	131.3	
BBV-2-C	Fluorite	-35.0		-5.3	8.3	132.2	
BBV-2-C	Fluorite	-35.0		0.6	0.0	119.2	
BBV-2-C	Fluorite	-35.0		-5.6	8.7	123.5	
BBV-2-C	Fluorite	-30.0		-5.3	8.3	188.3	
BBV-2-C	Fluorite	-35.0		-5.2	8.2	131.6	
BBV-2-C	Fluorite	-35.0		0.8	0.0	126.2	

Sample	Mineral	Tm(eut)	Tm(hyd)	Tm(ice)	NaCl eq%	ThL	ThV
BBV-2-D	Fluorite			-12.4	16.4	99.0	
BBV-2-D	Fluorite			-12.1	16.1	99.0	
BBV-2-D	Fluorite			-7.4	11.0	57.5	
BBV-2-D	Fluorite			-4.7	7.5	72.5	
BBV-2-D	Fluorite	-32.7		-0.6	1.0	114.1	
BBV-2-D	Fluorite	-21.5		-13.4	17.4	79.4	
BBV-2-D	Fluorite	-21.7		-21.7	23.7	92.7	
BBV-2-D	Fluorite	-21.5		-21.5	23.5	84.4	
BBV-2-D	Fluorite	-21.2		-21.2	23.4	86.3	
BBV-2-D	Fluorite			-0.2	0.4	122.1	
BBV-2-E	Fluorite			-6.3	9.6	114.8	
BBV-2-E	Fluorite			-1.0	1.7	113.2	
BBV-2-E	Fluorite			-5.7	8.8	92.1	
BBV-2-E	Fluorite			-5.6	8.7	86.3	
BBV-2-E	Fluorite			-6.7	10.1	105.3	
BBV-2-E	Fluorite			-6.6	10.0	96.5	
BBV-2-E	Fluorite			-10.1	14.1	99.7	
BBV-2-E	Fluorite			-5.3	8.3	91.6	
BBV-2-E	Fluorite			-1.1	1.9	114.4	
BBV-2-E	Fluorite			-4.1	6.6	96.5	
BBV-2-F	Fluorite	-21.9		-21.9	23.8	88.3	
BBV-2-F	Fluorite	-21.8		-21.8	23.7	87.3	
BBV-2-F	Fluorite			-7.5	11.1	135.1	
BBV-2-F	Fluorite			-7.0	10.5	119.2	
BBV-2-F	Fluorite			-3.2	5.2	92.2	
BBV-2-F	Fluorite			-5.0	7.9	111.5	
BBV-2-F	Fluorite			-7.0	10.5	112.7	
BBV-2-F	Fluorite			-3.5	5.7	112.7	
BBV-2-F	Fluorite	-32.7		-6.4	9.8	108.7	
BBV-2-F	Fluorite			-2.4	4.0	111.6	
BBV-2-G	Quartz			-9.8	13.8	109.8	
BBV-2-G	Quartz			-9.0	12.9	110.4	
BBV-2-G	Quartz	-22.1		-22.1	24.0	85.1	
BBV-2-G	Fluorite			-8.7	12.6	107.8	
BBV-2-G	Fluorite			-3.9	6.3	107.5	
BBV-2-G	Fluorite			-3.5	5.7	109.4	
BBV-2-G	Fluorite			-10.8	14.8	88.6	
BBV-2-G	Fluorite	-23.4	-19.4		23.4	86.9	
BBV-2-G	Fluorite			-10.3	14.3	101.5	
BBV-2-G	Fluorite			-6.0	9.2	113.0	
BBV-2-H	Fluorite			-5.0	7.8	111.5	
BBV-2-H	Fluorite			-10.2	14.2	99.0	
BBV-2-H	Fluorite			-10.1	14.1	111.0	
BBV-2-H	Fluorite			-3.9	6.3	101.5	
BBV-2-H	Fluorite			-9.6	13.6	107.4	
BBV-2-H	Fluorite			-2.8	4.6	131.0	
BBV-2-H	Fluorite			-7.3	10.9	120.2	
BBV-2-H	Fluorite			-6.6	10.0	121.6	
BBV-2-H	Fluorite			-9.0	12.9	106.6	
BBV-2-H	Fluorite			-15.7	19.4	91.2	
BMWV-1-A	Fluorite			-1.2	2.0	84.2	
BMWV-1-A	Fluorite			-0.6	1.0	100.2	

Sample	Mineral	Tm(eut)	Tm(hyd)	Tm(ice)	NaCl eq%	Th L.	Th V
BMWV-1-A	Quartz			-13.0	17.0	150.0	
BMWV-1-B	Fluorite			-32.5	26.3	83.6	
BMWV-1-B	Fluorite			-12.7	16.7	106.7	
BMWV-1-B	Fluorite	-26.2	0.3		26.3	85.4	
BMWV-1-B	Fluorite	-45.0		-26.2	25.3	88.8	
BMWV-1-B	Fluorite	-47.0		-30.0	26.3	86.7	
BMWV-1-B	Fluorite	-26.0	-3.6		25.2	80.2	
BMWV-1-B	Fluorite	-25.0	-10.4		24.2	92.0	
BMWV-1-B	Fluorite	-40.0	-5.4		25.3	81.2	
BMWV-1-B	Fluorite	-34.0		-1.1	1.9	93.7	
BMWV-1-C	Barite			-5.8	8.9	162.5	
BMWV-1-C	Fluorite			-2.2	3.7	80.1	
BMWV-1-C	Fluorite			-2.6	4.3	86.5	
BMWV-1-C	Fluorite			-10.9	14.9	106.9	
BMWV-1-C	Fluorite	-31.1		-31.1	26.3	89.2	
BMWV-1-C	Fluorite	-31.1		-31.1	26.3	87.3	
BMWV-1-E	Fluorite	-38.0		-6.2	9.5	112.7	
BMWV-1-E	Fluorite	-38.0		-6.4	9.8	95.6	
BMWV-1-E	Fluorite	-50.0		-4.0	6.5	83.6	
BMWV-1-E	Fluorite	-45.0		0.7	0.0	92.1	
BMWV-1-E	Fluorite	-45.0		-4.0	6.5	102.6	
BMWV-1-E	Fluorite	-50.0		-28.7	26.3	89.6	
BMWV-1-E	Fluorite	-50.0	-8.6		24.2	90.0	
BMWV-1-E	Fluorite	-50.0		-29.6	26.3	86.1	
BMWV-1-E	Fluorite	-35.0		-4.8	7.6	107.3	
BMWV-1-E	Fluorite	-35.0		-0.2	0.4	84.3	
BMWV-1-F	Fluorite		-5.5		25.2	80.8	
BMWV-1-F	Fluorite			-4.9	7.7	99.3	
BMWV-1-F	Fluorite		-21.0	-4.8	7.6	97.1	
BMWV-1-F	Fluorite			-11.1	15.1	117.5	
BMWV-1-F	Fluorite			-11.1	15.1	115.9	
BMWV-1-F	Fluorite			-11.0	15.0	112.1	
BMWV-1-F	Barite			-0.1	0.1	250.0	
BMWV-1-F	Fluorite	-30.0		-2.3	3.9	83.5	
BMWV-1-F	Fluorite			-2.8	4.6	80.4	
BMWV-1-F	Fluorite			-10.2	14.2	109.2	
BMWV-1-G	Fluorite			-6.2	9.5	123.5	
BMWV-1-G	Fluorite			-3.5	5.7	88.3	
BMWV-1-G	Fluorite			-1.4	2.4	97.1	
BMWV-1-G	Fluorite			-10.7	14.7	107.2	
BMWV-1-G	Fluorite			-10.7	14.7	109.6	
BMWV-1-G	Fluorite			-28.0	26.3	90.0	
BMWV-1-G	Fluorite			-6.9	10.4	96.8	
BMWV-1-G	Fluorite			-2.4	4.0	91.6	
BMWV-1-G	Fluorite			-1.9	3.1	89.2	
BMWV-1-G	Fluorite			-1.9	3.1	89.0	
BMWV-1-H	Fluorite	-45.0	-4.6		25.4	86.4	
BMWV-1-H	Fluorite	-45.0	-4.6		25.4	86.6	
BMWV-1-H	Fluorite	-45.0		-32.0	26.3	86.2	
BMWV-1-H	Fluorite	-45.0	-5.7		25.3	80.5	
BMWV-1-H	Fluorite	-50.0		-19.0	22.4	95.7	
BMWV-1-H	Fluorite	-50.0		-18.8	22.3	95.8	
BMWV-1-H	Fluorite	-50.0	-7.3		25.0	80.2	

Sample	Mineral	Tm(eut)	Tm(hyd)	Tm(ice)	NaCl eq%	ThL	ThV
BMWV10 1B	Fluorite	-30.9		-17.1	23.5	93.0	
BMWV10 1B	Fluorite			-10.2	14.2	113.8	
BMWV10 1B	Fluorite			-2.1	3.5	166.8	
BMWV10-1B	Fluorite		2.7		26.6	56.1	
BMWV10-1B	Quartz			-5.0	7.9	108.2	
BMWV10 1B	Quartz			-11.5	15.5	113.0	
BMWV10 1B	Fluorite			-1.7	2.8	92.8	
BMWV10-1B	Fluorite			-1.0	1.7	112.0	
BMWV10-1B	Fluorite			-10.8	14.8	95.2	
BMWV10-1B	Fluorite			-6.6	10.0	97.3	
BMWV10-3	Quartz			-11.3	15.3	284.5	
BMWV10-3	Quartz			-14.1	18.0		500.0
BMWV10-3	Quartz			-3.8	6.1	100.0	
BMWV10-3	Quartz			-1.4	2.4	302.7	
BMWV10 3	Quartz			-1.6	2.7	374.3	
BMWV10-3	Fluorite			-10.8	14 8	121 7	
BMWV10 3	Fluorite			-10.8	14.8	112.4	
BMWV10 3	Quartz			-2.1	3.5	265.0	
CPV-4-A	Fluorite			-2.7	4.5	59.7	
CPV-4-A	Fluorite			-7.2	10.8	69.2	
CPV-4-A	Fluorite			-4.1	6.6	75.5	
CPV-4-A	Fluorite	-25.3	-9.6		24.4	83.7	
CPV-4 A	Fluorite	-24.4	-9.6		24.4	76.5	
CPV-4 A	Fluorite			-7.2	10.8	68.6	
CPV-4 A	Fluorite	-26.7		-13.5	16.8	57.1	
CPV-4-A	Fluorite	-48.7		-6.1	8 5	58.4	
CPV-4 A	Fluorite	-25.3	-8.1		24.7	73.8	
CPV-4-A	Fluorite			-7.8	11.5	58.0	
CPV-4 B	Fluorite	-50 0		-8.4	12.2	78.1	
CPV-4 B	Fluorite	-50.0		-19.7	22.5	72.4	
CPV-4 B	Fluorite	-50.0	-10.9		24.0	68.7	
CPV-4 B	Fluorite	-50.0		-4.2	6.7	77.6	
CPV-4 B	Fluorite			-8.9	12.8	90.9	
CPV-4 B	Fluorite			-4.9	7.7	97.8	
CPV-4-B	Fluorite			-1.7	2 8	98.6	
CPV-4-B	Fluorite	-45.0		-2.4	4.0	80.9	
CPV-4-B	Fluorite	-45.0		-4.1	6.6	72.0	
CPV-4 C	Fluorite			-4.7	7.4	72.2	
CPV-4-C	Fluorite			-3.9	6.3	74.5	
CPV 4 C	Fluorite			-3 4	5.6	80.4	
CPV-4-C	Fluorite	-23.3		-23 3	24.7	72.1	
CPV-4-C	Fluorite			-4.0	6.5	84.6	
CPV-4 C	Fluorite	-22.1		-22.1	24.0	68.7	
CPV-4 C	Fluorite			-3.3	5.4	81.8	
CPV-4-C	Fluorite			-19.7	22.6	60.5	
CPV-4 C	Fluorite			-7.7	11.4	100.6	
CPV-4-C	Fluorite			-2.6	4.3	100.5	
CPV-4-D	Quartz	-30.0		-20.2	22.8	95.6	
CPV-4-D	Fluorite	-30.0		-8.7	12.5	73.5	
CPV-4 D	Fluorite	-30.0		-11.9	15.9	84.1	
CPV-4-D	Fluorite			-8.6	12.4	110.0	

Sample	Mineral	Tm(eut)	Tm(hyd)	Tm(ice)	NaCl eq%	ThL	ThV
CPV-4-D	Fluorite	-38.0	-9.2		24.7	79.8	
CPV-4-D	Fluorite			-8.1	11.9	103.1	
CPV-4-D	Fluorite			-12.8	16.8	65.3	
CPV-4-D	Fluorite	-40.0	-4.8		25.4	77.8	
CPV-4-D	Fluorite			-10.1	14.1	88.0	
CPV-4-D	Fluorite			-9.2	13.1	86.5	
CPV-4-G	Fluorite	-45.0		-11.5	15.5	92.1	
CPV-4-G	Fluorite	-45.0		-3.1	5.1	103.5	
CPV-4-G	Fluorite	-45.0		-6.6	10.0	98.0	
CPV-4-G	Fluorite	-45.0		-6.8	10.3	94.5	
CPV-4-G	Fluorite	-45.0		-6.3	9.6	100.4	
CPV-4-G	Fluorite	-45.0		-6.9	10.4	104.7	
CPV-4-G	Fluorite	-45.0	-2.6		26.0	90.3	
CPV-4-G	Quartz			-7.5	11.1	89.4	
CPV-4-G	Quartz			-0.9	1.5	108.0	
CPV-4-G	Fluorite			-0.6	1.0	79.8	
CPV-4-G	Fluorite			-5.1	8.0	66.8	
GNV-8-A	Fluorite	-27.0		-6.5	9.9	126.0	
GNV-8-A	Fluorite			-7.2	10.7	126.8	
GNV-8-A	Fluorite			-6.6	10.0	146.3	
GNV-8-A	Fluorite	-39.0		-18.6	21.6	146.0	
GNV-8-A	Fluorite			-6.8	10.3	110.2	
GNV-8-A	Fluorite			-3.7	6.0	128.0	
GNV-8-B	Fluorite	-28.7		-7.6	11.2	179.6	
GNV-8-B	Fluorite			-5.9	9.1	125.5	
GNV-8-B	Fluorite			-8.7	12.6	261.0	
GNV-8-B	Fluorite			-7.6	11.2	215.8	
GNV-8-B	Fluorite	-28.7		-10.3	14.3	372.5	
GNV-8-B	Fluorite	-23.8		-8.3	12.1	321.6	
GNV-8-B	Fluorite			-7.1	10.6	117.0	
GNV-8-B	Fluorite	-28.7		-9.6	13.6	311.6	
GNV-8-C	Fluorite	-29.4		-7.6	11.3	259.2	
GNV-8-C	Fluorite			-7.7	11.4	289.2	
GNV-8-C	Fluorite			-7.1	10.6	128.2	
GNV-8-C	Fluorite	-28.0		-8.8	12.7	265.0	
GNV-8-C	Fluorite	-23.8		-9.3	13.2	307.1	
GNV-8-C	Fluorite			-10.5	14.5	366.5	
GNV-8-D	Fluorite	-28.9		-7.3	10.9	132.2	
GNV-8-D	Fluorite	-22.7		-1.6	2.7	113.0	
GNV-8-D	Fluorite	-20.9		-2.1	3.5	122.0	
GNV-8-D	Fluorite	-24.1		-6.6	10.0	131.5	
GNV-8-D	Fluorite	-23.2		-7.9	11.6	181.9	
GNV-8-D	Fluorite	-28.7		-9.7	13.7	135.0	
GNV-8-D	Fluorite	-29.3		7.3	10.9	126.4	
GNV-8-E	Fluorite	-28.2	-7.5		11.1	194.4	
GNV-8-E	Fluorite	-29.4		4.3	6.8	104.8	
GNV-8-E	Fluorite	-29.1		-7.0	10.5	182.8	
GNV-8-E	Fluorite	-58.5		6.6	10.0	148.6	
GNV-8-E	Fluorite	-29.2		-7.3	10.9	141.8	
GNV-8-E	Fluorite	-28.9		-7.3	10.9	137.1	
GNV8-F+G	Fluorite			-7.5	11.1	173.9	
GNV8-F+G	Fluorite	-25.8		-7.5	11.1	161.8	

Sample	Mineral	Tm(ext)	Tm(hyd)	Tm(ice)	NaCl eq%	ThL	ThV
GNV8-F + G	Fluorite	-58.2		-7.6	11.3	161.7	
GNV8-F + G	Fluorite			-7.4	11.0	141.9	
GNV8-F + G	Fluorite			-7.3	10.9	139.9	
GNV8-F + G	Fluorite			-7.5	11.1	134.8	
GNV-8 G	Fluorite	-29.0		-7.8	11.5	140.0	
GNV-8-G	Fluorite	-27.2		-6.6	10.0	205.0	
GNV-8-G	Fluorite	-27.4		-7.5	11.1	145.0	
GNV-8-G	Fluorite	-21.3		-6.6	10.0	146.2	
GNV-8-G	Fluorite	-26.7		-6.1	9.4	254.7	
GNV-8-G	Fluorite	-27.0		-6.8	10.2	138.1	
GNV-8-G	Fluorite	-23.2		-6.9	10.4	129.0	
GNV-8 G	Fluorite	-28.7	-7.6		11.3	135.0	
GNV-8 G	Fluorite			-6.7	10.1	130.0	
GNV-8-H	Fluorite			-7.6	11.2	217.2	
GNV-8-H	Fluorite	-19.7		-7.0	10.5	151.8	
GNV-8-H	Fluorite	-28.0		-7.4	11.0	207.9	
GNV-8 H	Fluorite	-25.0	-6.9		25.0	87.1	
GNV-8 H	Fluorite	-29 9		-29.9	26.3	86.9	
GNV-8 H	Fluorite	-25.7		-24.7	25.0	87.2	
GNV 8 H	Fluorite	-27.5		-25.2	25.2	84.5	
GNV-8 H	Fluorite	-24.7	-7.6		24.9	88.0	
GNV-8 I	Fluorite	-26 7		-6.7	10.1	116.2	
GNV-8-I	Fluorite	-29.1		-1.4	2.4	117.2	
GNV-8 I	Fluorite	-58.5		-7.0	10.5	130.7	
GNV-8 I	Fluorite	-29.2		-7.3	10.9	119.4	
GNV-8-I	Fluorite			-7.4	11.0	135.8	
GNV-8-I	Fluorite			-7.5	11.1	136.6	
GNV-8-J	Fluorite	-28.7		-7.6	11.2	159.3	
GNV-8 J	Fluorite	-28.2		-7.6	11.2	153.3	
GNV-8 J	Fluorite	-27.2		-7 6	11.2	156.8	
GNV-8-J	Fluorite	-27.8		-7.6	11.2	174.8	
GNV-8-J	Fluorite	-29.6		-7.3	10.9	125.8	
GNV-8 J	Fluorite	-28.5		-1.5	2 6	155.4	
GNV-8-J	Fluorite			-7.1	10.6	164.5	
GNV8-K + L	Fluorite	-25.8		-1.3	2.2	216.5	
GNV8-K + L	Fluorite	-58.2		-4.0	6.4	116.7	
GNV8-K + L	Fluorite			-7.8	11.5	120.7	
GNV8 K + L	Fluorite			-8.1	11.8	118.5	
GNV8-K + L	Fluorite			-8.0	11.7	134.3	
GNV8 K + L	Fluorite			-7.9	11.6	118.6	
GNV-8-M	Fluorite			-2.8	4.6	114.4	
GNV-8-M	Fluorite			-3.1	5.1	110.3	
GNV-8 M	Fluorite	-29.1		-7.6	12.0	118.0	
GNV-8 M	Fluorite			-4.5	7.1	115.2	
GNV-8-M	Fluorite	-29.2		-8.2	12.0	114.6	
GNV-8-M	Fluorite			-8.2	12.0	156.2	
GNV-8-N	Fluorite			-4.8	7.6	94.7	
GNV-8-N	Fluorite			-3.8	6.2	109.0	
GNV-8-N	Fluorite			-6.3	9.6	96.4	
GNV 8-N	Fluorite			-5.6	8.7	96.7	

Sample	Mineral	Tm(eut)	Tm(hyd)	Tm(ice)	NaCl eq%	Th L	Th V
GNV-8-N	Fluorite	-25.2		-5.0	7.8	85.7	
GNV-8-N	Fluorite	-30.3		-30.3	26.3	85.7	
GNV-8-O	Fluorite	-24.2		-21.1	23.3	86.2	
GNV-8-O	Fluorite		-1.0		26.2	359.8	
GNV-8-O	Fluorite			-22.0	24.0	89.5	
GNV-8-O	Fluorite	-23.5		-19.5	22.3	89.1	
GNV-8-O	Fluorite	-23.0		-19.6	22.4	98.0	
GNV-8-O	Fluorite			-21.2	23.5	94.5	
GNV-8-O	Fluorite			-21.2	23.5	94.3	
HEV-1-A	Fluorite			-5.0	7.8	72.1	
HEV-1-A	Fluorite			-6.0	9.2	66.8	
HEV-1-A	Fluorite			-7.0	10.5	97.7	
HEV-1-A	Fluorite			-5.0	7.8	84.0	
HEV-1-A	Fluorite			-4.8	7.6	58.0	
HEV-1-A	Fluorite			-8.3	12.1	73.7	
HEV-1-A	Fluorite			-9.3	13.2	80.1	
HEV-1-A	Fluorite			-6.2	9.5	98.5	
HEV-1-A	Fluorite			-4.8	7.6	105.8	
HEV-1-A	Fluorite			-10.2	14.2	92.3	
HEV-1-B	Fluorite			-13.2	17.2	72.0	
HEV-1-B	Fluorite	-21.9		-21.9	23.8	88.7	
HEV-1-B	Fluorite	-29.5		-29.5	26.3	79.2	
HEV-1-B	Fluorite	-25.3	-11.5	-13.5	24.2	78.5	
HEV-1-B	Fluorite	-25.5	-11.9	-12.5	24.1	75.6	
HEV-1-B	Fluorite	-25.4		-1.2	2.1	121.6	
HEV-1-B	Fluorite	-21.8		-21.8	23.7	62.6	
HEV-1-B	Fluorite	-25.5	-5.8		9.9	80.7	
HEV-1-B	Fluorite	-21.1		-8.9	12.8	97.0	
HEV-1-B	Fluorite	-20.8		-3.0	4.9	110.4	
HEV-1-C	Fluorite	-22.2	-13.5	-22.8	23.8	63.9	
HEV-1-C	Fluorite	-24.4	-12.5	-17.7	24.0	73.1	
HEV-1-C	Fluorite	-25.4		-25.4	25.4	80.1	
HEV-1-C	Fluorite			-2.2	3.6	116.3	
HEV-1-C	Fluorite	-25.5	-8.0	5.3	24.9	69.0	
HEV-1-C	Fluorite	-21.1		-21.1	23.4	79.9	
HEV-1-C	Fluorite	-20.8		-20.8	23.3	95.0	
HEV-1-C	Fluorite	-28.6		-28.6	26.3	78.3	
HEV-1-C	Fluorite	-25.3	-12.0	-9.5	24.0	64.8	
HEV-1-C	Fluorite	-28.1		-28.1	26.3	70.4	
HEV-1-D	Fluorite	-24.2		-24.2	25.0	96.0	
HEV-1-D	Fluorite	-29.1		-29.1	26.3	78.7	
HEV-1-D	Fluorite	-25.5	-13.2		23.8	81.8	
HEV-1-D	Fluorite	-21.8		-21.8	23.8	96.2	
HEV-1-D	Fluorite	-22.8		22.8	24.2	94.3	
HEV-1-D	Fluorite	-25.1	-17.7		23.5	84.0	
HEV-1-D	Fluorite			-9.4	13.0	145.3	
HEV-1-D	Fluorite			-3.8	6.1	93.5	
HEV-1-D	Fluorite			-5.3	8.3	97.3	
HEV-1-D	Fluorite			-3.7	6.0	100.2	
HEV-1-E	Fluorite			-5.0	7.8	52.4	
HEV-1-E	Fluorite	-27.7		-27.7	26.2	74.2	

Sample	Mineral	Tm(eut)	Tm(hyd)	Tm(ice)	NaCl eq%	ThL	ThV
HEV-1-E	Sphalerite			-9.5	13.4	123.9	
HEV-1-E	Sphalerite			-2.4	4.0	115.2	
HEV-1-E	Fluorite			-8.0	11.7	109.0	
HEV-1-E	Fluorite			-2.7	4.5	89.5	
HEV-1-E	Fluorite			-4.9	7.7	82.6	
HEV-1-E	Fluorite			-6.8	10.2	225.0	
HEV-1-E	Fluorite			-8.5	12.3	120.8	
HEV-1-E	Fluorite	-25.7	-1.8		25.7	73.4	
ISV-1-A	Fluorite	-30.6		-25.1	25.7	85.5	
ISV-1-A	Fluorite			-21.7	23.8	85.8	
ISV-1-A	Fluorite		-23.4	-16.5	20.0	106.3	
ISV-1-A	Fluorite	-28.3	-24.7	-16.7	20.2	85.7	
ISV-1-A	Fluorite		-25.3	-17.7	21.0	86.5	
ISV-1-A	Fluorite		-27.5	-15.9	19.5		280.4
ISV-1-A	Fluorite			-15.9	19.5	106.5	
ISV-1-A	Fluorite	-30.7	-24.7	-17.7	21.0	84.4	
ISV-1-B	Fluorite	-28.8	-23.4	-17.2	21.1	96.2	
ISV-1-B	Fluorite	-27.8	-27.8		26.3	83.0	
ISV-1-B	Quartz			-17.5	20.8	88.0	
ISV-1-B	Fluorite			-15.0	18.8	103.0	
ISV-1-B	Fluorite	-27.2		-27.2	26.0	84.1	
ISV-1-B	Fluorite		-22.4	-13.6	18.2	84.1	
ISV-1-C	Fluorite			-16.9	20.3	98.2	
ISV-1-C	Fluorite			-18.6	21.6	98.7	
ISV-1-C	Fluorite	-24.7		-11.7	16.3	90.2	
ISV-1-C	Fluorite	-29.1		-16.5	20.6	97.3	
ISV-1-D	Fluorite	-20.3		-18.0	21.2	87.0	
ISV-1-D	Fluorite			-9.6	14.2	121.0	
ISV-1-D	Fluorite			-7.7	11.4	122.1	
ISV-1-D	Fluorite			-9.4	13.3	107.6	
ISV-1-D	Fluorite			-11.0	15.0	113.6	
ISV-1-D	Fluorite	-21.1		-5.0	7.9	103.6	
ISV-1-E	Fluorite			-8.1	11.9	113.5	
ISV-1-E	Fluorite	-28.8		-23.9	24.5	82.5	
ISV-1-E	Fluorite	-28.7		-16.2	19.8	94.8	
ISV-1-E	Fluorite			-14.7	18.5	82.5	
ISV-1-E	Fluorite			-22.5	24.0	92.8	
ISV-1-E	Fluorite			-9.6	13.5	104.9	
ISV-1-F	Fluorite	-29.2		-7.6	11.3	122.0	
ISV-1-F	Fluorite			-4.3	6.9	115.0	
ISV-1-F	Fluorite	-29.6		-6.9	10.4	139.8	
ISV-1-F	Fluorite			-6.7	10.1	138.4	
ISV-1-F	Fluorite			-1.6	2.7	114.7	
ISV-1-F	Fluorite			-6.2	9.5	135.4	
ISV-1-G	Fluorite	-22.3		-8.3	12.8	109.7	
ISV-1-G	Fluorite			-3.7	6.0	106.0	
ISV-1-G	Fluorite			-3.5	5.7	105.8	
ISV-1-G	Fluorite			-9.1	13.0	109.6	
LP-2-E	Fluorite	-45.0		-2.2	3.7	74.8	
LP-2-E	Fluorite	-45.0		-0.8	1.4	102.4	

Sample	Mineral	Tm(eut)	Tm(hyd)	Tm(ice)	NaCl eq%	Th L	Th V
LP-2-E	Fluorite	-45.0		-3 0	4 9	78.9	
LP-2-E	Fluorite	-50.0		-14.9	18.7	97.6	
LP-2-E	Fluorite	-50.0		-15.0	18.8	92.6	
LP-2-E	Fluorite	-50.0		-9.1	13.0	109.3	
SCVV-A-A	Fluorite			-6 6	10.0	143.2	
SCVV-A-A	Fluorite			-6 6	10.0	145.8	
SCVV-A-A	Calcite			-8.0	11 7	126 1	
SCVV-A-A	Calcite	-26.0	-2.6	-2.6	25.9	92.4	
SCVV-A-A	Calcite			-6.8	10.2	144 0	
SCVV-A-A	Calcite			-7.2	10.8	109.5	
SCVV-A-A	Calcite			-7.2	10.8	112.0	
SCVV-A-A	Calcite			-1 6	2.7	105.6	
SCVV-A-A	Calcite			-6.8	10 3	142 8	
SCVV-A-A	Calcite			-6 9	10 4	141 0	
SCVV-A-C	Fluorite			-8 0	11.7	114.4	
SCVV-A-C	Fluorite	-25.7	-25.7		25.5	84.3	
SCVV-A-C	Fluorite	-25 6	-10.9		14.9	109.8	
SCVV-A-C	Fluorite	-22.0		-22 0	23.7	86.7	
SCVV-A-C	Fluorite		-6.7	-10 9	14.9	116.5	
SCVV-A-C	Fluorite	-24.8	-15 9		23.5	70 9	
SCVV-A-C	Fluorite	-31.0		-11 0	15.0	67 6	
SCVV-A-C	Fluorite		-25.7	-6.8	10.2	101.3	
SCVV-A-C	Fluorite	-25.2	-13.3		24 2	85 0	
SCVV-A-C	Fluorite	-25.6	-11.6		24 3	112.0	
SDMS-1-A	Quartz					262 1	
SDMS-1-A	Quartz					88.3	
SDMS-1-A	Quartz					96 6	
SDMS-1-A	Quartz					323 5	
SDMS-1-A	Quartz					180 0	
SDMS-1-A	Quartz					316.0	
SDMS-1-A	Quartz					328.0	
SDMS-3-A	Quartz			-4.4	7.0	94.5	
SDMS-3-A	Quartz			-0.2	0.4	210.0	
SDMS-3-A	Quartz			1.4	0.0		200.0
SDMS-3-A	Quartz			0.1	0.0	245.0	
SDMS-3-A	Quartz			0 2	0 0	294 0	
SDMS-3-A	Quartz			0.7	0 0	238 0	
SDMS-3-A	Quartz			-2.2	3.7		250 0
SDMS-3-A	Quartz			-1.0	1.7	150 0	
SDMS-3-A	Quartz			-14.4	18.2	275.0	

Appendix 3

Statistical Analysis

of

REE Genetic Classes

Earliest Fluorite - Genetic Class 1

(n = 5)

	Mean	Std. dev.	Maximum	Minimum
Boric Acid Dissolution				
% undissol	0.100	0.100	0.200	0.000
% dissol.*	99.9	0.1	100	99.8
Calculated from XRF				
CaF2(c)*	104	2	106	101
BaSO4(c)	0.023	0.028	0.062	0.002
SiO2(c)	0.521	0.547	1.29	0.083
PbS(c)	0.013	0.012	0.031	0.003
ZnS(c)	0.011	0.014	0.031	0.000
CuFeS2(c)	0.001	0.000	0.001	0.000
Total	104			
XRF Majors				
SiO2	1.00	1.06	2.49	0.161
TiO2	(0.008)	0.009	0.022	< 0.003
Al2O3	0.233	0.278	0.624	< 0.006
Fe2O3	0.115	0.099	0.255	0.033
MnO	(0.005)	0.005	0.012	< 0.002
MgO	< 0.02	NA	< 0.020	< 0.020
CaO*	74.8	1.4	76.2	72.9
Na2O	0.052	0.064	0.142	< 0.014
K2O	0.045	0.058	0.128	< 0.002
P2O5	(0.005)	0.005	0.012	< 0.003
LOI	1.07	0.53	1.82	0.69
XRF Trace				
S	298	255	658	107
Cl	161	185	422	(24)
Sc*	39	3	43	36
V	< 7	NA	< 7	< 7
Cr	(14)	5	(20)	(8)
Ni	< 4	NA	< 4	< 4
Cu	19	13	38	(8)
Zn	74	96	210	< 3
Ga	< 4	NA	< 4	< 4
Rb	(2.3)	2.8	6.2	< 0.7
Sr*	81	4.3	88	78
Y	643	181	799	390
Zr	(2.8)	2.4	6.1	< 1.0
Nb*	(1.91	0.3	2.3	(1.6)
Ba	135	164	366	< 23
Ce*	210	33	257	186
Pb	115	108	267	30
Th	< 3	NA	(3)	< 3
U	< 4	NA	< 4	< 4

	Mean	Std. dev.	Maximum	Minimum
ICP-MS Trace				
Li	1.4	1.1	3.5	< 0.1
Be	(8.0)	2.5	(10.8)	(3.9)
Sc	(5)	2	(7)	< 4
V	< 2	NA	(3)	< 2
Cr	(8)	6	(18)	< 8
Cu	26	12	45	14
Zn	47	65	177	(6)
Rb	1.39	2.12	5.61	(0.11)
Sr*	88.7	10.6	105.9	77.6
Y	574	175	744	357
Zr	1.9	0.6	2.9	(1.3)
Nb	20.4	30.8	80.0	0.140
Mo	2.52	3.11	8.43	0.26
Cs	0.219	0.304	0.826	0.041
Ba	4.8	6.2	17	(1.2)
Hf	(0.17)	0.18	0.48	< 0.07
Ta	8.65	10.3	22.4	0.096
Tl	(0.07)	0.09	0.25	< 0.06
Pb	59.5	82.8	224	4.85
Bi	0.761	0.498	1.68	0.315
Th	0.29	0.19	0.64	(0.10)
U*	0.52	0.09	0.61	0.35
ICP-MS REE				
La	46.5	12.1	69.1	35.5
Ce	148	33	197	110
Pr	25.9	6.2	35.1	18.9
Nd	126	27	166	94
Sm*	27.9	2.0	30.4	25.4
Eu*	3.64	0.29	4.02	3.20
Gd*	35.2	2.1	38.5	32.1
Tb	4.51	0.93	5.29	3.15
Dy	24.7	7.2	31.0	15.4
Ho	4.57	1.60	6.13	2.52
Er	10.1	4.1	14.2	4.69
Tm	0.909	0.403	1.35	0.471
Yb	4.02	1.80	5.78	1.55
Lu	0.479	0.205	0.700	0.203
Total REE*	462	63	564	387
ICP-MS Ratios				
Pb206/Pb207	1.172	0.027	1.200	1.134
Pb208/Pb207	2.412	0.039	2.461	2.362
Sm147/Nd144	0.119	0.012	0.166	0.111
Rb87/Sr86	0.0486	0.071	0.187	0.0033

Note: all elements with RSD < or = 20% denoted by (*)

values less than limit of detection (LOD) - <LOD

values less than limit of quantification (LOQ) - (value)

Early Fluorite - Genetic Class 2

n 2

	Mean	Std dev.	Maximum	Minimum
Boric Acid Dissolution				
% undissol	NA	NA	NA	NA
% dissol.	NA	NA	NA	NA
Calculated from XRF				
CaF2(c)*	104	1	105	103
BaSO4(c)	0.003	0.001	0.005	0.002
SiO2(c)	0.128	0.038	0.17	0.090
PbS(c)*	0.003	0.000	0.004	0.003
ZnS(c)	0.000	0.000	0.000	0.000
CuFeS2(c)	0.000	0.000	0.000	0.000
Total	104			
XRF Majors				
SiO2	0.248	0.073	0.321	0.175
TiO2	< 0.003	NA	< 0.003	< 0.003
Al2O3	< 0.006	NA	(0.008)	< 0.006
Fe2O3	0.041	0.014	0.055	0.028
MnO	< 0.002	NA	< 0.002	< 0.002
MgO	< 0.02	NA	< 0.020	< 0.020
CaO*	75.0	0.8	75.7	74.2
Na2O	< 0.014	NA	< 0.014	< 0.014
K2O	< 0.002	NA	< 0.002	< 0.002
P2O5	(0.004)	0.002	(0.006)	< 0.003
LOI*	0.645	0.085	0.730	0.560
XRF Traces				
S	(107	31	140)	74
Cl*	33	6	39	(27)
Sc*	42	3	45	38
V	< 7	NA	< 7	< 7
Cr	(6)	3	(10)	< 6
Ni	< 4	NA	< 4	< 4
Cu*	14	0	14	14
Zn	< 3	NA	< 3	< 3
Ga	< 4	NA	< 4	< 4
Rb	< 0.7	NA	< 0.7	< 0.7
Sr*	70	11	82	59
Y	941	325	1266	616
Zr*	(1.1)	0.1	(1.2)	(1.0)
Nb	2.3	0.9	3.2	(1.3)
Ba	< 23	NA	(28)	< 23
Ce	163	41	205	120
Pb*	30	4	34	26
Th	< 3	NA	(3)	< 3
U	< 4	NA	< 4	< 4

	Mean	Std. dev.	Maximum	Minimum
ICP-MS Traces				
Li	< 0.3	NA	< 0.3	< 0.3
Be	(6.5)	1.5	(8.0)	(5.0)
Sc	< 4	NA	(4)	< 4
V	< 2	NA	< 2	< 2
Cr	< 8	NA	< 8	< 8
Cu*	20	4	24	17
Zn	(8)	3	11	(5)
Rb	(0.13)	0.09	(0.23)	< 0.08
Sr*	70.4	10.0	80.4	60.3
Y	891	292	1183	598
Zr	(0.6)	0.4	(1.0)	< 0.4
Nb	0.173	0.041	0.214	0.132
Mo	0.368	0.122	0.490	0.246
Cs	0.031	0.012	0.043	(0.019)
Ba	4.2	3.2	7.4	(1.0)
Hf	(0.10)	0.06	(0.16)	< 0.07
Ta*	0.135	0.003	0.138	0.133
Tl	< 0.06	NA	< 0.06	< 0.06
Pb*	23.1	2.74	25.8	20.4
Bi*	0.760	0.140	0.900	0.620
Th	(0.11)	0.04	0.16	(0.07)
U*	0.71	0.09	0.80	0.63
ICP-MS REE				
La*	28.9	4.5	33.4	24.3
Ce	79.1	16.6	95.6	62.5
Pr	12.8	3.0	15.8	9.80
Nd	67.2	17.1	84.2	50.1
Sm	19.9	5.7	25.6	14.2
Eu	2.84	0.75	3.59	2.10
Gd	34.3	9.7	44.0	24.6
Tb	6.13	1.65	7.78	4.49
Dy	40.9	10.6	51.5	30.4
Ho	8.66	2.21	10.9	6.44
Er	21.5	5.3	26.8	16.2
Tm	2.03	0.41	2.44	1.61
Yb*	8.97	1.69	10.7	7.28
Lu*	1.06	0.15	1.21	0.916
Total REE	334	79	414	255
ICP-MS Ratios				
146Nd/144Nd	1.156	0.028	1.185	1.128
150Nd/144Nd	2.450	0.037	2.487	2.413
147Sm/144Nd	0.179	0.006	0.185	0.172
87Sr/86Sr	0.002	0.006	0.008	-0.003

Note: all elements with RSD < or = 20% denoted by (*)

values less than limit of detection (LOD) - <LOD

values less than limit of quantification (LOQ) - (value)

Middle Fluorite - Genetic Class 3

(n = 10)

	Mean	Std. dev.	Maximum	Minimum
Boric Acid Dissolution				
% undissol	0.000	0.000	0.000	0.000
% dissol.	100	0	100	100
Calculated from XRF				
CaF2(c)*	103	2	105	99.1
BaSO4(c)	0.010	0.008	0.023	0.002
SiO2(c)	0.126	0.091	0.31	0.036
PbS(c)	0.078	0.197	0.599	0.002
ZnS(c)	0.000	0.000	0.000	0.000
CuFeS2(c)	0.001	0.001	0.003	0.000
Total	103			
XRF Majors				
SiO2	0.24	0.17	0.60	0.070
TiO2	< 0.003	NA	(0.005)	< 0.003
Al2O3	0.037	0.034	0.088	< 0.006
Fe2O3	0.046	0.027	0.103	0.020
MnO	< 0.002	NA	(0.003)	< 0.002
MgO*	< 0.02	NA	< 0.020	< 0.020
CaO*	74.5	1.3	75.9	71.5
Na2O	0.055	0.081	0.244	< 0.014
K2O	0.008	0.009	0.026	< 0.002
P2O5	(0.005)	0.002	(0.009)	< 0.003
LOI	0.625	0.202	1.11	0.410
XRF Traces				
S	320	289	1018	77
Cl	185	216	658	(21)
Sc*	42	6	54	31
V	< 7	NA	< 7	< 7
Cr	(10)	4	(18)	< 6
Ni	< 4	NA	< 4	< 4
Cu	34	23	78	18
Zn	< 3	NA	< 3	< 3
Ga	< 4	NA	14	< 4
Rb*	< 0.7	NA	< 0.7	< 0.7
Sr*	52	6	66	45
Y	439	253	768	< 0.6
Zr	< 1.0	NA	(1.4)	< 1.0
Nb	(1.3)	0.6	2.2	< 0.6
Ba	(59)	47	134	< 23
Ce	(68)	36	141	< 32
Pb	672	1707	5189	19
Th	< 3	NA	< 3	< 3
U	< 4	NA	< 4	< 4

	Mean	Std. dev.	Maximum	Minimum
ICP-MS Traces				
Li	< 0.3	NA	(1.0)	< 0.3
Be	(8.5)	4.5	21.8	(5.6)
Sc	< 4	NA	(8)	< 4
V	< 2	NA	(4)	< 2
Cr	< 8	NA	(15)	< 8
Cu	32	17	61	12
Zn	(9)	5	22	(3)
Rb	(0.11)	0.14	0.48	< 0.08
Sr	53.2	10.7	67.5	25.9
Y	545	198	904	216
Zr	1.9	3.3	12	< 0.4
Nb	6.36	13.3	42.2	0.105
Mo	1.78	2.63	7.40	0.377
Cs	(0.022)	0.014	0.055	< 0.010
Ba	1.7	1.5	6.0	(0.4)
Hf	(0.09)	0.08	0.28	< 0.07
Ta	5.77	11.5	35.2	0.078
Tl	0.27	0.66	2.25	< 0.06
Pb	685	1927	6446	9.89
Bi	0.355	0.336	1.18	< 0.05
Th	(0.12)	0.08	0.33	(0.04)
U	0.62	0.30	1.1	0.08
ICP-MS REE				
La	16.5	5.9	26.0	7.95
Ce	36.6	14.6	57.4	13.5
Pr	5.06	2.11	8.06	1.98
Nd	24.1	10.5	40.8	8.7
Sm	6.96	3.15	12.2	2.42
Eu	1.04	0.37	1.62	0.340
Gd	12.8	5.6	21.2	3.67
Tb	2.79	1.19	4.73	0.841
Dy	22.6	9.6	37.9	7.04
Ho	5.64	2.31	9.21	1.77
Er	17.4	6.8	27.0	5.86
Tm	2.21	0.81	3.24	0.781
Yb	13.2	4.7	19.9	4.93
Lu	1.94	0.62	2.65	0.654
Total REE	169	66	269	60
ICP-MS Ratios				
146Nd/146Nd	1.182	0.021	1.224	1.155
146Sm/146Nd	2.459	0.038	2.517	2.403
Sm147/Sm149	0.174	0.011	0.197	0.161
86Sr/88Sr	0.007	0.046	0.054	-0.054

Note: all elements with RSD < or = 20% denoted by [*]

values less than limit of detection (LOD) - <LOD

values less than limit of quantification (LOQ) - (value)

Middle-Late Fluorite - Genetic Class 4

(n = 36)

	Mean	Std. dev.	Maximum	Minimum
Boric Acid Dissolution				
% undissol.	46.2	29.6	96.1	0.740
% dissol.	53.5	29.9	99.3	3.92
Calculated from XRF				
CaF2(c)	71.5	32.9	104	2.60
BaSO4(c)	22.4	35.3	113	0.002
SiO2(c)	7.94	17.3	75.3	0.041
PbS(c)	3.73	19.1	105	0.000
ZnS(c)	0.188	0.721	3.96	0.000
CuFeS2(c)	0.005	0.015	0.084	0.000
Total	106			
XRF Majors				
SiO2	10.9	17.6	75.3	0.078
TiO2	0.010	0.013	0.055	< 0.003
Al2O3	0.243	0.358	1.68	< 0.006
Fe2O3	0.220	0.468	2.53	< 0.002
MnO	0.020	0.047	0.214	< 0.002
MgO	< 0.02	NA	< 0.020	< 0.020
CaO	51.6	23.8	75.3	1.87
Na2O	(0.033)	0.070	0.303	< 0.014
K2O	0.103	0.231	1.22	< 0.002
P2O5	(0.008)	0.008	0.031	< 0.003
LOI	3.26	2.15	7.72	0.300
XRF Traces				
S	23196	32032	87063	134
Cl	192	207	974	(28)
Sc	30	20	60	< 7
V	< 7	NA	< 7	< 7
Cr	150	199	723	< 6
Ni	21	36	184	< 4
Cu	152	433	2421	< 3
Zn	1262	4838	26560	< 3
Ga	233	1216	6669	< 4
Rb	8.2	16.8	85.3	< 0.7
Sr	1777	2744	8376	31
Y	536	411	1556	20
Zr	17	23	86	< 1.0
Nb	4	7	37	< 0.6
Ba	131578	207914	666963	< 23
Ce	(34)	24	(84)	< 32
Pb	32291	165638	908657	< 4
Th	< 3	NA	(4)	< 3
U	(11)	42	231	< 4

	Mean	Std. dev.	Maximum	Minimum
ICP-MS Traces				
Li	4.4	8.3	34	< 0.3
Be	(10.5)	9.1	31	< 0.4
Sc	< 4	NA	(14)	< 4
V	(2)	2	10	< 2
Cr	97	200	932	< 8
Cu	173	223	934	< 0.3
Zn	1945	6430	32275	< 3
Rb	11.0	28.7	169	< 0.08
Sr	720	1148	4581	38.2
Y	713	396	2051	240
Zr	5.5	13	95	< 0.4
Nb	1.25	2.03	11.8	< 0.009
Mo	2.87	3.00	15.35	< 0.05
Cs	1.75	4.22	23.7	< 0.010
Ba	10788	36042	220927	3.4
Hf	0.31	0.65	3.8	< 0.07
Ta	0.734	0.991	5.29	< 0.007
Tl	0.86	2.0	10	< 0.06
Pb	4500	11177	57694	3.64
Bi	3.06	13.8	84.2	< 0.05
Th	0.50	1.3	8.2	< 0.04
U	0.82	0.97	4.7	< 0.02
ICP-MS REE				
La	15.9	7.8	36.4	5.09
Ce	37.5	19.1	85.2	11.8
Pr	5.22	2.78	12.7	1.66
Nd	24.0	13.1	58.6	7.58
Sm	10.6	5.7	21.7	3.04
Eu	1.12	1.06	4.25	0.048
Gd	23.2	12.0	46.8	6.88
Tb	4.92	2.53	10.3	1.41
Dy	37.5	20.8	85.0	9.77
Ho	8.59	5.06	21.1	2.07
Er	25.5	16.5	67.3	5.22
Tm	3.28	2.26	8.97	0.632
Yb	19.3	15.2	62.1	3.39
Lu	2.43	1.95	7.99	0.413
Total REE	219	112	454	65
ICP-MS Ratios				
Pb206/Pb207	1.146	0.196	1.214	0.000
Pb208/Pb207			2.503	
Sm147/Nd 44	0.257	0.051	0.333	0.000
Rb87/Sr86	0.322	1.327	8.105	-0.001

Notes: all elements with RSD < or = 20% denoted by [*]

values less than limit of detection (LOD) - <LOD

values less than limit of quantification (LOQ) - (value)

Late Fluorite - Genetic Class 5

(n = 17)

	Mean	Std. dev.	Maximum	Minimum
Boric Acid Dissolution				
% undissol	1.11	1.46	3.18	0.000
% dissol.*	98.9	1.5	100	96.8
Calculated from XRF				
CaF2(c)*	93.1	17.1	106	45.6
BaSO4(c)	0.165	0.528	2.066	0.002
SiO2(c)	0.778	1.59	6.41	0.082
PbS(c)	7.91	21.2	85.9	0.007
ZnS(c)	1.85	6.13	23.9	0.000
CuFeS2(c)	0.037	0.085	0.339	0.001
Total	104			
XRF Majors				
SiO2	1.50	3.07	12.4	0.158
TiO2	(0.004)	0.005	0.020	< 0.003
Al2O3	0.080	0.146	0.571	< 0.006
Fe2O3	0.902	1.83	6.46	0.007
MnO	0.008	0.013	0.048	< 0.002
MgO*	< 0.02	NA	< 0.020	< 0.020
CaO*	67.2	12.3	76.2	32.9
Na2O	0.112	0.356	1.39	< 0.014
K2O	0.009	0.020	0.076	< 0.002
P2O5	(0.011)	0.007	0.028	< 0.003
LOI	1.15	0.57	2.06	0.560
XRF Traces				
S	6890	12803	48720	99
Cl	123	110	386	(24)
Sc	47	13	73	(20)
V	< 7	NA	< 7	< 7
Cr	34	60	225	< 6
Ni	16	44	172	< 4
Cu	1056	2453	9795	38
Zn	12387	41106	160481	< 3
Ga	573	1619	6250	< 4
Rb	(1.0)	1.0	4.1	< 0.7
Sr	74	39.5	145	31
Y	819	337	1552	425
Zr	< 1.0	NA	(1.7)	< 1.0
Nb	2.3	2.0	8.2	< 0.6
Ba	974	3105	12156	< 23
Ce	< 32	NA	(59)	< 32
Pb	68543	183596	709380	64
Th	(9)	18	71	< 3
U	(11)	23	91	< 4

	Mean	Std. dev.	Maximum	Minimum
ICP-MS Traces				
La	(0.8)	0.5	2.1	< 0.3
Be	(8.0)	6.2	26	< 0.4
Sc	< 4	NA	(9)	< 4
V	(1)	2	7	< 2
Cr	(18)	43	166	< 8
Cu	116	688	2963	< 0.3
Zn	608	1359	5768	< 3
Rb	0.418	0.790	3.30	< 0.08
Sr	72.7	36.1	139	24.9
Y	742	274	1219	379
Zr	(1.2)	1.3	5.8	< 0.4
Nb	0.223	0.182	0.694	< 0.039
Mo	2.38	2.22	9.69	0.42
Cs	0.069	0.142	0.617	< 0.010
Ba	423	1182	4841	(0.8)
Hf	(0.12)	0.13	0.47	< 0.07
Ta	0.29	0.3	1.0	0.024
Tl	2.1	2.7	11	< 0.06
Pb	12909	26198	109779	24.2
Bi	3.35	7.98	33.1	< 0.05
Th	0.15	0.12	0.41	< 0.04
U	1.5	2.9	12	(0.03)
ICP-MS REE				
La	8.03	3.32	15.5	2.99
Ce	21.2	9.2	42.3	8.64
Pr	3.25	1.39	6.35	1.46
Nd	16.8	7.1	32.4	7.27
Sm	9.23	3.42	16.9	4.14
Eu	0.876	0.841	4.06	0.299
Gd	20.6	6.9	32.1	8.62
Tb	4.75	1.78	8.20	2.41
Dy	35.9	14.6	64.5	18.5
Ho	8.33	3.52	15.5	4.54
Er	25.0	11.4	48.5	12.8
Tm	3.37	1.65	6.70	1.47
Yb	22.1	12.1	46.1	7.49
Lu	2.88	1.56	5.99	0.812
Total REE	182	68	312	93
ICP-MS Ratios				
206/204	1.152	0.169	1.221	0.514
208/207	2.250	0.554	2.502	0.082
147/143	0.341	0.043	0.417	0.240
88/86	0.019	0.015	0.154	0.000

Note: all elements with RSD < or = 20% denoted by [*]

values less than limit of detection (LOD) - <LOD

values less than limit of quantification (LOQ) - (value)

Late Fluorite - Genetic Class 6

(n = 3)

	Mean	Std. dev.	Maximum	Minimum
Boric Acid Dissolution				
% undissol	0.835	0.835	1.67	0.000
% dissol *	99.2	0.8	100	98.3
Calculated from XRF				
CaF2(c)	100	0	100	100
BaSO4(c)	0.086	0.000	0.086	0.086
SiO2(c)	0.042	0.000	0.042	0.042
PbS(c)	0.007	0.000	0.007	0.007
ZnS(c)	0.001	0.000	0.001	0.001
CuFeS2(c)	0.028	0.000	0.028	0.028
Total	101			
XRF Majors				
SiO2	0.080	0.000	0.080	0.080
TiO2	< 0.003	NA	< 0.003	< 0.003
Al2O3	< 0.006	NA	< 0.006	< 0.006
Fe2O3	0.248	0.000	0.248	0.248
MnO	(0.003)	0.000	(0.003)	(0.003)
MgO	< 0.02	NA	< 0.020	< 0.020
CaO	72.5	0.0	72.5	72.5
Na2O	< 0.014	NA	< 0.014	< 0.014
K2O	< 0.002	NA	< 0.002	< 0.002
P2O5	< 0.003	NA	< 0.003	< 0.003
LOI	0.56	0.00	0.56	0.56
XRF Traces				
S	1156	0	1156	1156
Cl	31	0	31	31
Sc	30	0	30	30
V	< 7	NA	< 7	< 7
Cr	< 6	NA	< 6	< 6
Ni	< 4	NA	< 4	< 4
Cu	797	0	797	797
Zn	(6)	0	(6)	(6)
Ga	< 4	NA	< 4	< 4
Rb	< 0.7	NA	< 0.7	< 0.7
Sr	24	0	24	24
Y	760	0	760	760
Zr	< 1.0	NA	< 1.0	< 1.0
Nb	2.2	0.0	2.2	2.2
Ba	506	0	506	506
Ce	< 32	NA	< 32	< 32
Pb	57	0	57	57
Th	< 3	NA	< 3	< 3
U	< 4	NA	< 4	< 4

	Mean	Std. dev.	Maximum	Minimum
ICP-MS Traces				
Li	(0.3)	0.2	(0.6)	< 0.3
Be	(12.4)	5.6	20	(8.4)
Sc	< 4	NA	(7)	< 4
V	(2)	2	(5)	< 2
Cr	< 8	NA	< 8	< 8
Cu	(3.4)	3	(6.7)	< 0.3
Zn	(5)	4	10	< 3
Rb	(0.08)	0.04	(0.13)	< 0.08
Sr	38.8	20.9	67.9	19.9
Y	830	220	1104	564
Zr	2.3	1.6	4.5	(0.6)
Nb	0.180	0.059	0.228	0.097
Mo	4.45	3.59	9.00	0.22
Cs	(0.016)	0.008	(0.025)	< 0.010
Ba	43.1	30.5	70.5	(0.5)
Hf	(0.16)	0.11	0.30	< 0.07
Ta*	0.075	0.002	0.078	0.072
Tl	< 0.06	NA	(0.08)	< 0.06
Pb	27.7	29.6	69	(0.6)
Bi	0.445	0.595	1.29	< 0.05
Th	0.13	0.04	0.18	(0.07)
U	1.2	1.0	2.4	(0.02)
ICP-MS REE				
La	0.620	0.307	1.05	0.383
Ce	2.04	1.29	3.86	1.00
Pr	0.398	0.262	0.768	0.198
Nd	2.50	1.90	5.18	1.03
Sm	3.15	2.36	6.48	1.27
Eu	0.253	0.168	0.490	0.123
Gd	13.1	7.5	23.6	6.60
Tb	4.21	2.10	7.12	2.22
Dy	34.1	15.0	54.8	19.4
Ho	7.59	3.10	11.8	4.45
Er	19.4	7.7	29.7	11.1
Tm	2.08	0.80	3.13	1.19
Yb	9.58	3.44	13.9	5.54
Lu	1.02	0.35	1.44	0.587
Total REE	100	46	163	55
ICP-MS Ratios				
Pb206/Pb207	1.284	0.150	1.495	1.163
Pb208/Pb207	2.507	0.102	2.640	2.391
Sm147/Nd144	0.756	0.016	0.778	0.742
Rb87/Sr86	0.005	0.005	0.012	-0.001

Note: all elements with RSD < or = 20% denoted by [*]

values less than limit of detection (LOD) - <LOD

values less than limit of quantification (LOQ) - (value)

Middle Fluorite - Genetic Class 3 (NMP)

(n = 9)

	Mean	Std. dev.	Maximum	Minimum
Boric Acid Dissolution				
% undissol	0.000	0.000	0.000	0.000
% dissol.	100	0	100	100
Calculated from XRF				
CaF2(c)*	104	1	105	103
BaSO4(c)	0.008	0.007	0.018	0.002
SiO2(c)	0.100	0.062	0.19	0.036
PbS(c)	0.003	0.001	0.004	0.002
ZnS(c)	0.000	0.000	0.000	0.000
CuFeS2(c)	0.001	0.001	0.002	0.000
Total	104			
XRF Majors				
SiO2	0.192	0.119	0.371	0.070
TiO2	< 0.003	NA	(0.005)	< 0.003
Al2O3	0.040	0.035	0.088	< 0.006
Fe2O3	0.049	0.027	0.103	0.020
MnO	< 0.002	NA	(0.003)	< 0.002
MgO*	< 0.02	NA	< 0.020	< 0.020
CaO*	75.0	0.6	75.9	74.2
Na2O	0.062	0.084	0.244	< 0.014
K2O	0.009	0.010	0.026	< 0.002
P2O5	(0.005)	0.002	(0.009)	< 0.003
LOI*	0.56	0.09	0.67	0.41
XRF Traces				
S	221	126	427	77
Cl	204	224	658	(21)
Sc*	42	6	54	31
V	< 7	NA	< 7	< 7
Cr	(10)	4	(18)	< 6
Ni	< 4	NA	< 4	< 4
Cu	28	18	58	(8)
Zn	< 3	NA	< 3	< 3
Ga	< 4	NA	< 4	< 4
Rb*	< 0.7	NA	< 0.7	< 0.7
Sr*	51	4.2	56	45
Y	530	141	768	331
Zr	< 1.0	NA	(1.4)	< 1.0
Nb	(1.4)	0.5	2.2	< 0.6
Ba	(49)	40	104	< 23
Ce	(76)	32	141	(39)
Pb	27	6	38	19
Th	< 3	NA	< 3	< 3
U	< 4	NA	< 4	< 4

	Mean	Std. dev.	Maximum	Minimum
ICP-MS Traces				
Li	< 0.3	NA	(1.0)	< 0.3
Be	(8.5)	4.8	22	(5.6)
Sc	< 4	NA	(8)	< 4
V	< 2	NA	(4)	< 2
Cr	< 8	NA	(15)	< 8
Cu	28	14	54	12
Zn	(9)	5	22	(5)
Rb	(0.12)	0.142	0.483	< 0.08
Sr*	51.6	10.1	60.7	25.9
Y	531	204	904	216
Zr	2.0	3.5	12	< 0.4
Nb	7.06	13.8	42.2	0.115
Mo	1.74	2.22	7.40	0.377
Cs	(0.023)	0.014	0.055	< 0.010
Ba	(1.2)	0.591	2.60	(0.4)
Hf	(0.09)	0.09	0.28	< 0.07
Ta	6.40	12.0	35.2	0.078
Tl	< 0.06	NA	(0.08)	< 0.06
Pb	22.9	8.7	36.9	9.89
Bi	0.316	0.332	1.18	< 0.08
Th	(0.12)	0.09	0.31	(0.04)
U	0.67	0.26	1.1	0.31
ICP-MS REE				
La	15.8	5.8	26.0	7.95
Ce	34.8	14.2	57.4	13.5
Pr	4.83	2.10	8.36	1.93
Nd	23.2	10.7	40.8	8.69
Sm	6.73	3.24	12.2	2.32
Eu	1.04	0.39	1.62	0.383
Gd	12.4	5.8	21.2	3.67
Tb	2.72	1.24	4.73	0.831
Dy	21.9	9.9	37.9	7.04
Ho	5.45	2.36	9.21	1.77
Er	16.7	6.7	27.0	5.86
Tm	2.09	0.77	3.17	0.781
Yb	12.5	4.1	17.2	4.93
Lu	1.64	0.57	2.47	0.654
Total REE	162	66	269	60
ICP-MS Ratios				
Pb206/Pb207	1.182	0.022	1.223	1.155
Pb208/Pb207	2.462	0.039	2.517	2.407
Sm147/Nd144	0.174	0.012	0.197	0.161
Rb87/Sr86	0.007	0.017	0.054	-0.004

Note: all elements with RSD < or = 20% denoted by (*)
NMP - no minor phases (i.e. primarily fluorite)

values less than limit of detection (LOD) - <LOD

values less than limit of quantification (LOQ) - (value)

References Cited in Appendix

Eppinger, R.G. III, 1988, Trace element and rare earth element variation in fluorites collected from skarn and epithermal mineral deposits in the Sierra Cuchillo area, south-central New Mexico: U.S. Geological Survey, Open-File Report 88-566, Denver, *108 p.*

Jenner, G.A., Longerich, H.P., Jackson, S.E. and Fryer, B.J., 1990, ICP-MS - A powerful tool for high-precision trace-element analysis in Earth sciences: Evidence from analysis of selected U.S.G.S. reference samples: *Chem. Geol., V. 83, pp. 133-148.*

Longerich, H.P., (in press), The analysis of geological samples prepared as pressed pellets using wavelength dispersive X-ray fluorescence spectrometry:

Longerich, H.P., Jenner, G.A., Fryer, B.J. and Jackson, S.E., 1990, Inductively coupled plasma-mass spectrometric analysis of geological samples: A critical evaluation based on case studies: *Chem. Geol., V. 83, pp. 105-118.*